Universitat Politècnica de València
Departamento de Máquinas y Motores Térmicos

Control-oriented modelling and diagnostics of diesel after-treatment catalysts

PhD Dissertation
Presented by
D. Javier Mora Pérez
Advised by
Dr. Carlos Guardiola

Valencia, November 2018

Resumen. Esta tesis doctoral abarca el desarrollo de algoritmos orientados a mejorar el sistema de control de emisiones en motores Diesel. Para este propósito, la inclusión en el vehículo de sensores embarcados como los de temperatura, los de NO_x o el de NH_3 permite realizar diagnóstico a bordo de los sistemas de post-tratamiento foco de este trabajo, los cuales son el DOC y el SCR. Así pues, el objetivo es el de satisfacer las normativas de diagnóstico a bordo para mantener las emisiones por debajo del umbral permitido por la normativa a lo largo del tiempo.

Los tests experimentales, incluyendo las medidas con analizador de gases, permiten tener una visión más amplia de las especies en la línea de escape. Complementariamente, se utilizan unidades nuevas y envejecidas para tener el efecto experimental del envejecimiento en los catalizadores. De esta manera, se analiza el efecto de la temperatura, el gasto de escape, las concentraciones de las especies y el envejecimiento en el DOC y en el SCR, así como la evaluación de algunas de las medidas relevantes realizadas por los sensores.

Las temperaturas tienen una influencia destacada en el funcionamiento de los catalizadores, por lo que se requiere la evaluación de las medidas de los sensores de temperatura, junto con el desarrollo de modelos de transmisión de calor, para alimentar las funciones a continuación desarrolladas. En este sentido, la medida lenta del sensor aguas arriba del DOC se mejora en condiciones transitorias mediante una técnica de fusión de la información basada en un filtro de Kalman. Luego, se presenta un modelo de transmisión de calor 1D y un modelo agrupado 0D, en los cuales se evalúan las entradas aguas arriba según el uso del modelo. Por otra parte, se presenta una técnica para estimar el incremento de temperatura debido a la oxidación de los pulsos de post-inyección en el DOC.

Se proponen modelos para ambos DOC y SCR para estimar el efecto del envejecimiento en las emisiones, en los cuales el factor de envejecimiento es modelado como un parámetro sintonizable que permite variar desde estados nuevos a envejecidos. Por una parte, un modelo agrupado 0D es desarrollado para el DOC con el propósito de estimar el desliz de HC y CO, el cual es validado en un WLTC para después ser usado en simulación. Por otra parte, un modelo 1D y un modelo 0D se desarrollan para el SCR, los cuales se usan a continuación para alimentar la estrategia de diagnóstico y para simulación.

Finalmente, las estrategias de diagnóstico se presentan para fallo total o retirada de DOC, así como para la estimación de la eficiencia en DOC y SCR. Por una parte, la primera estrategia se divide en pasiva y activa, en la que se usan post-inyecciones en la activa para excitar el sistema y confirmar el fallo total si es el caso. A continuación, la eficiencia del DOC se estima a través de una técnica indirecta en la que la temperatura de activación se detecta y se relaciona con el incremento de emisiones a través del modelo. Por otra parte, se desarrolla un observador para estimar el estado de envejecimiento del SCR, el cual está basado en un filtro de Kalman extendido. Sin embargo, para evitar asociar baja eficiencia del catalizador debido a pobre calidad de la urea inyectada, a envejecimiento del SCR, un indicador de la calidad de la urea se ejecuta en paralelo.

Resum. Esta tesi doctoral abasta el desenvolupament d'algoritmes orientats a millor el sistema de control d'emissions en motors Diesel. Per a este propòsit, la inclusió en el vehicle de sensor embarcats com els de temperatura, els de NO_x o el d'NH_3 permet realitzar el diagnòstic a bord dels sistemes de post-tractament focus d'este treball, els quals són el DOC i el SCR. Així doncs, l'objectiu és el de satisfer les normatives de diagnòstic a bord per a mantindre les emissions per baix de l'umbral permés per la normativa al llarg del temps.

Els tests experimentals, incloent les mesures amb analitzador de gasos, permeten obtindre una visió més àmplia de les espècies en la línia d'escapament. Complementàriament, s'utilitzen unitats noves i envellildes per tal de tindre l'efecte experimental de l'envelliment en els catalitzadors. D'aquesta manera, s'analitza l'efecte de la temperatura, la despesa d'escapament, les concentracions de les espècies i l'envelliment en el DOC i en el SCR, així com l'avaluació d'algunes mesures relevants realitzades pels sensors.

Les temperatures tenen una influència destacada en el funcionament dels catalitzadors, pel que es requerix l'avaluació de les mesures dels sensors de temperatura, junt amb el desenvolupament de models de transmissió de calor, per a alimentar les funcions a continuació desenvolupades. En este sentit, la mesura lenta del sensor a l'entrada del DOC es millora en condicions transitòries mitjançant una tècnica de fusió de la informació basada en un filtre de Kalman. Després, es presenta un model de transmissió de calor 1D i un model agrupat 0D, en els quals s'avaluen les entrades a l'entrada segons l'ús del model. Per altra banda, es presenta una tècnica per a estimar l'increment de temperatura degut a l'oxidació dels pulsos de post-injecció en el DOC.

Es proposen models per a DOC i SCR per a estimar l'efecte de l'envelliment en les emissions, en els quals es modela el factor d'envelliment com un paràmetre sintonizable, que permet variar des d'estats nous a envellits. Per altra banda, un model agrupat 0D és desenvolupat per al DOC amb el propòsit d'estimar la relliscada de HC i CO, el qual és validat en un WLTC per a després ser usat en simulació. Per altra banda, un model 1D i un model 0D es desenvolupen per al SCR, els quals s'usen a continuació per a alimentar l'estratègia de diagnòstic i per a simulació.

Finalment, les estratègies de diagnòstic es presenten per a la fallada total o retirada del DOC, així com per a l'estimació de l'eficiència en DOC i SCR. Per altra banda, la primera estratègia es divideix en passiva i activa, en la que s'utilitzen post-injeccions en la activa per a excitar el sistema i confirmar la fallada total si es dona el cas. A continuació, l'eficiència del DOC s'estima a través d'una tècnica indirecta en la que la temperatura d'activació es detecta i es relaciona amb l'increment d'emissions a través del model. Per altra banda, es desenvolupa un observador per a estimar l'estat d'envelliment del SCR, el qual està basat en un filtre de Kalman extès. No obstant això, per a evitar associar baixa eficiència degut a pobre qualitat de l'urea injectada a l'envelliment del SCR, un indicador de la qualitat de l'urea s'executa en paral·lel.

Abstract. This dissertation covers the development of algorithms oriented to improve the emission control system of Diesel engines. For this purpose, the inclusion of on-board sensors like temperature, NO_x and NH_3 sensors allows performing on-board diagnostics to the after-treatment systems focus of this work, which are the DOC and the SCR system. Then, the target is to meet on-board diagnostics regulations in order to keep emissions below a regulation threshold over time.

Experimental tests, including gas analyzer measurements, allow having a wider view of the species in the exhaust line. Complementary, new and aged units are used in order to have the experimental effect of ageing on the catalysts. Then, the effect of temperature, exhaust mass flow, species concentrations and ageing is analyzed for DOC and SCR, in combination with the assessment of some relevant sensors measurements. As a result, the characteristics, opportunities and limitations extracted from experimental data are used as the basis for the development of models and diagnostics techniques.

The assessment of temperature sensors measurements, along with the development of heat transfer models is required to feed temperature dependent functions. In this sense, the slow measurement of the DOC upstream temperature sensor is improved in transient conditions by means of a data fusion technique, based on a fast model and a Kalman filter. Then, a 1D and a 0D lumped heat transfer models are presented, in which the upstream inputs are assessed in relation to its use. On the other hand, a technique to estimate the temperature increase due to post-injection pulses oxidation is also presented.

Both DOC and SCR models are proposed in order to estimate the effect of ageing on emissions, in which an ageing factor is modelled as a tunable parameter that allows varying from new to aged states. On the one hand, a 0D lumped model is developed for DOC in order to estimate the HC and CO species slip, which is validated in a WLTC and is then used for simulation. On the other hand, a 1D and a 0D models are developed for SCR, which are then used to feed the diagnostics strategy and for simulation.

Finally, diagnostics strategies are presented for total failure or removal of DOC, as well as for efficiency estimation of DOC and SCR. On the one hand, the former strategy is separated into passive and active diagnostics, in which post-injections are used in active diagnostics in order to excite the system and confirm a total failure, in case. Then, the DOC efficiency estimation is done by means of an indirect technique in which the light-off temperature is detected and an emissions increase is related by means of the DOC ageing model. On the other hand, an observer to estimate the SCR ageing state is developed, which is based on an extended Kalman filter. However, in order to avoid associating low SCR efficiency to ageing, an indicator of the injected urea quality is developed to run in parallel.

Quan surts per fer el viatge cap a Ítaca,
has de pregar que el camí sigui llarg,
ple d'aventures, ple de coneixences.

Has de pregar que el camí sigui llarg,
que siguin moltes les matinades
que entraràs en un port que els teus ulls ignoraven,
i vagis a ciutats per aprendre dels que saben.

Tingues sempre al cor la idea d'Ítaca.
Has d'arribar-hi, és el teu destí,
però no forcis gens la travessia.

És preferible que duri molts anys,
que siguis vell quan fondegis l'illa,
ric de tot el que hauràs guanyat fent el camí,
sense esperar que et doni més riqueses.

Ítaca t'ha donat el bell viatge,
sense ella no hauries sortit.

I si la trobes pobra, no és que Ítaca
t'hagi enganyat. Savi, com bé t'has fet,
sabràs el que volen dir les Ítaques.

— *Lluís Llach, 1975. Adaptació de Constantino Cavafis, 1911.* —

Agradecimientos

Todavía me acuerdo como si fuese ayer de la asignatura de motores de combustión interna alternativos con Carlos Guardiola. Su lenguaje cercano y la manera en la que era capaz de simplificar los sistemas más complejos me hizo despertar el interés por profundizar en el abismo de complejidad que se esconde detrás de los motores. Por estos motivos, siempre quise trabajar con él y así poder aprender de una de las mejores mentes que he conocido. Casi sin darme cuenta, de eso han pasado ya seis años, en los que no solo se ha convertido en mi director de tesis, sino que ha sabido enseñarme a enfocar los problemas y la vida. Gracias por llevarme a *Ítaca* y darme la oportunidad de eSCRibir esta tesis DOCtoral.

Mención especial merece Benjamín Pla, que durante los primeros años tuvo conmigo la paciencia necesaria para enseñarme cómo resolver los problemas que se iban presentando. Gracias a su ayuda mis torpes líneas de código iniciales son ahora elegantes scripts.

I switch to English to acknowledge the time I spent in Eindhoven with Professors Willems and Seykens. I really appreciate the opportunity you gave to me, the time you dedicated to me, and our discussions about SCR diagnosis and life in general. I have to recognise that I spent a good time, barbaques were superb.

Quiero agradecer de una manera especial a todos los compañeros de despacho, por todos los buenos momentos que hemos pasado, dentro y fuera de él. A Alberto, por haber sido más un amigo que un compañero y por compartir tantas horas de deporte. A Pau, por ser como es y estar siempre dispuesto a sacar una sonrisa. A Marcelo, Alvin y Varun por ser compañeros de batalla. Y en definitiva, a todas las personas que han pasado por el despacho y de los que me llevo un recuerdo y una amistad: Vicent, Iván, Sergio, Nando, Jaime, Juanfran, Vero, Josep, Jose, Loïc, Brice, Abhinav, etc.

También quiero agradecer a toda la gente del departamento que de una manera u otra me ha ayudado a desarrollar mi trabajo: a la dirección, a toda la secretaría, a los profesores, al resto de doctorandos y a los técnicos. De estos últimos, especialmente a Vicentón. Es díficil de explicar todas las cosas por las que hemos pasado juntos trabajando codo con codo.

Canvie al valencià per agraïr el recolzament incondicional de la meua família. Als meus pares, Miguel i Maria Luisa, que sempre m'han donat totes les facilitats al seu abast, sempre disposats a ajudar en tot allò possible. Agraïr també a Miguel, el meu germà, per ser un far en la distància, i del que sempre es pot aprendre alguna cosa.

Finalment, és moment d'emprendre nous camins cap a *Ítaca*, i de segur que els recorreré amb tu, Clara.

Valencia, a 13 de Septiembre de 2018

Contents

Nomenclature

Acronyms

A	Area
ANR	Ammonia to NO_x ratio
ATS	After-treatment system
CDPF	Catalyzed DPF
CF	Conformity factor
CFD	Computational fluid dynamics
CI	Compression ignition
CIDI	Compression ignition Diesel engine
CO	Carbon monoxide
CO2	Carbon dioxide
DF	Data fusion
DOC	Diesel oxidation catalyst
DPF	Diesel particulate filter
ECU	Electronic control unit
EGO	Exhaust gas oxygen
EGR	Exhaust gas recirculation
EKF	Extended Kalman filter
EMF	Electro magnetic field
ETK	Emulation task kopf
EV	Electric vehicle
FFT	Fast Fourier transform
FTIR	Fourier-transform infrared spectroscopy
FTP	Fewderal test procedure
GA	Gas analyzer
GDP	Gross domestic product
H2O	Water
HC	Hydrocarbons
HCCI	Homogeneous charge compression ignition
HDV	Heavy duty vehicle
HEV	Hybrid electric vehicle
HFID	Heated vacuum-type flame ionization detector

HIL	Hardware-in-the-loop
HPEGR	High pressure EGR
ICE	Internal combustion engine
IE	Integral error
IUPR	In-use performance ratio
KF	Kalman filter
LDV	Light duty vehicle
LNT	Lean NO_x trap
LOT	Light-off temperature
LPEGR	Low pressure EGR
LTC	Low temperature combustion
MIL	Malfunction indicator light
MVEM	Mean value engine model
NDIR	Non-dispersive infrared sensor
NEDC	New European driving cycle
NMHC	Non-methane hydrocarbons
NO	Nitric oxide
NO_2	Nitric dioxide
NO_x	Nitrogen oxides
NSR	NH_3 storage ratio
NTC	Negative temperature constant
OBD	On-board diagnostics
PCCI	Premixed Charge Compression Ignition
PEMS	Portable emissions measurement system
PI	Post-injection
PM	Particulate matter
PNA	Passive NO_x adsorber
PSD	Power spectral density
PWM	Pulse-width modulation
RCCI	Reactivity Controlled Compression Ignition
RDE	Real driving emissions
RLS	Road load simulation
RMSE	Root mean squared error
RPS	Rapid prototyping system
SCR	Selective catalytic reduction system
SCRF	Selective catalytic reduction system filter
SOF	Solid organic fraction
SOI	Start of injection
SUV	Sport utility vehicle
SV	Spatial velocity
TCH	Turbocharger
TC	Thermocouple
TDC	Top dead center
THC	Total hydrocarbons

TWC	Three way catalyst
UEGO	Universal exhaust gas oxygen
VGT	Variable geometry turbine
WG	Waste-gate
WHTC	World harmonized heavy-duty test procedure
WLTC	World harmonized light-duty test procedure

Abbreviations

0D	0 dimensional
1D	1 dimensional
3D	3 dimensional
$\mathbf{A}$	State transition matrix
a	Air
A_{eff}	Effective area
A_f	Ammonia factor
acc	Accumulated
act	Actual
AD	high diagnostics threshold
amb	ambient
avg	Average
$\mathbf{B}$	Inputs matrix
$\mathbf{C}$	Measurements matrix
C	Species concentration
c_p	Specific heat
Δ	Increment
D	Bore
ds	Downstream
E	Activation energy
ϵ	Error
η	Efficiency
eff	Efficiency
exh	Exhaust
exp	Experimental
$\mathbf{F}$	Linearized state transition matrix
f	Fuel
fst	Fast
Γ	Correction factor
γ	Urea quality indicator
$\hat{}$	Estimated value
$\mathbf{H}$	Linearized measurements matrix
h	Convection factor
H_f	Fuel lower heating value
I	Inhibition term
i	Species
in	inlet
int	Intake

$\mathbf{K}$	Kalman gain matrix
k	Time step
k_x	Constant for x
k_i	Pre-exponential factor
m	Mass
$\dot{m}_f$	Mass flow
max	Maximum
min	Minimum
mod	Modelled
N	Number of sections
n	Engine speed
$_n$	Axial section
ν	Measurement noise
nom	Nominal
Ω	NH_3 accumulation capacity of the SCR
Ω_A	Ageing factor of SCR
out	outlet
ϕ	Emissions percentage
$\mathbf{P}$	covariance matrix
P	Pressure
PD	Low diagnostics threshold
pos	Position
ppm	Particles per million
$\mathbf{Q}$	Process noise matrix
$\mathbf{R}$	Measurements noise matrix
R	Ideal gas constant
r	Reaction rate
ref	Reference
σ^2	Variance
S	Stroke
slw	Slow
std	Standard
str	stroke
τ	Delay
T	Temperature
t	Time
θ	Bias
θ_{NH_3}	NH_3 storage in the SCR
Θ	Look-up table
Ts	Sampling period
u	input
us	Upstream
virt	Virtual
w	Process noise

W	Engine work
ξ	Ageing factor of DOC
$\boldsymbol{x}$	States matrix
y	Measurement
z	Shape factor

Chapter 1

Introduction

Contents

1.1 Background

Moving is a must for all people in our society nowadays, and road transportation is the most used means of transport. Passenger cars offer a degree of flexibility that have become indispensable in developed countries, since the cars fleet increases in development countries while the gross domestic product per capita (GDP) increases, as seen in Figure 1.1 [1]. In this Figure, a plateau in cars / people is appreciated once the GDP is sufficient, around 30000$. In this sense, the developed countries of Europe and North America do not expect an important growth of new vehicles for the next years, but China is instead found in the boom phase and a growth of 500% is expected from 2010 to 2025.

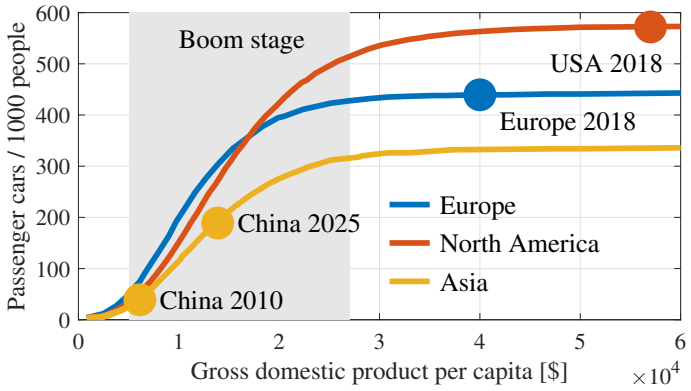

Figure 1.1. *Motorization trends in Europe, North America and Asia from 2010 to 2025. Adapted from [1].*

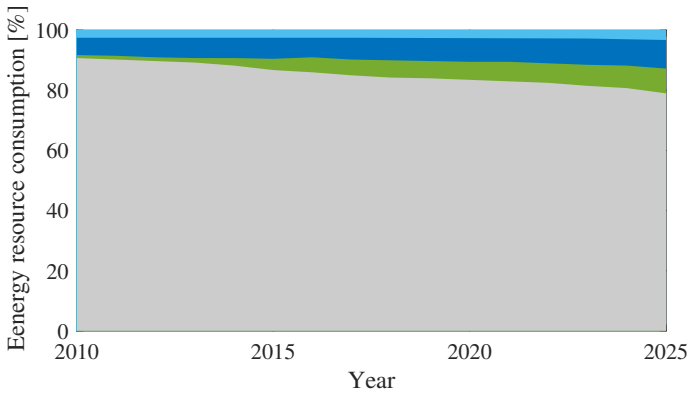

Figure 1.2. *Pattern of energy resource consumption in the transportation sector. Adapted from [1].* ■ *Electricity* ■ *Gas* ■ *Others* ■ *Oil.*

Trends in automotive propulsion systems The distribution of the car fleet revealed a 92% of fossil fuel powered vehicles in 2010 and predicts an 83% by 2025, as shown in Figure 1.2. On the other hand, the predictions of global oil consumption announce that oil reserves will be able to provide fossil fuel during at least the next decades [2], while the total oil consumption will slightly increase due to the decrease in the average fuel consumption [3]. In this scenario, internal combustion engines (ICE) will still be the main propulsion system used during next decades.

The undeniable growth of alternative technologies in the automotive sector has still a low percentage of 3% in the total transportation sector, as shown

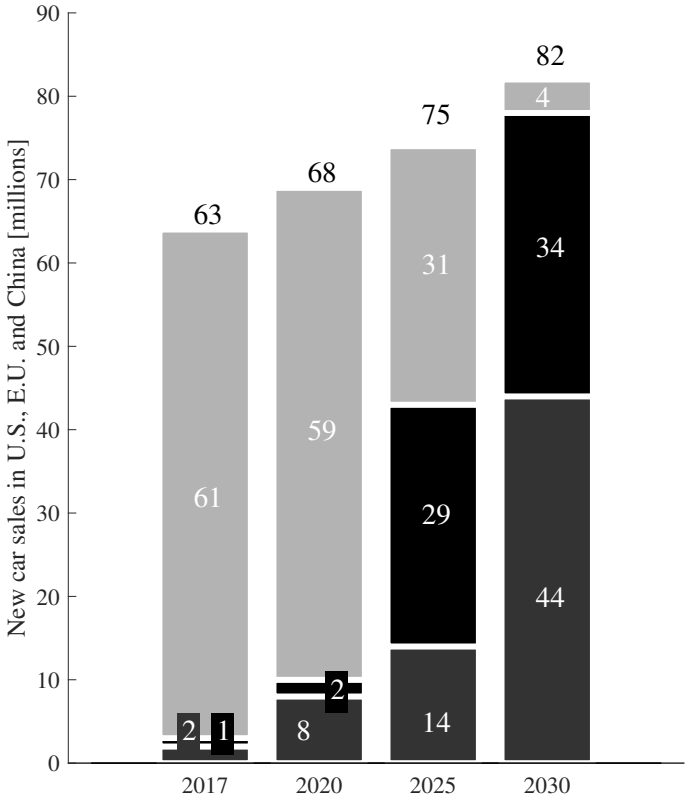

Figure 1.3. *Fleet distribution of new cars among ■ combustion ■ hybrid and ■ electric. Adapted from [4].*

in Figure 1.2. However, several technologies are being used or under investigation in order to reduce the dependency of fossil fuels in ICEs and to reduce the emissions of CO_2 from well to wheel. Specifically, electricity-based technologies will take progressive leadership until they cope the market by 2030, in which combustion engines mixed with electric compounds will still play an important role of 34% in new car sales, as shown in Figure 1.3.

Some of the most relevant technologies under production or investigation are described next.

- New low temperature combustion (LTC) modes, usually diluted with high EGR rates, are being developed to increase combustion performance and reduce emissions, such as the homogeneous charge compression ignition (HCCI) [5–7], the partially pre-mixed compression ig-

nition (PCCI) [8, 9] or the reactivity controlled compression ignition (RCCI) [10].

- Hybrid electric vehicles (HEV) are a current technology that reduce fuel consumption and emissions [11–13], which has been used since the 90s. In fact, several HEV technologies like range extender [14] and plug-in [15] hybrid electric vehicles are used, while batteries management are a focus of investigation nowadays [16–18].

- New biofuels are being investigated [19, 20] from their plant production to the vehicle combustion [21]. As ICEs are proven to be a robust and mature technology, biofuels can take progressive leadership as partial surrogates of fossil fuels [22, 23]. However, the cost of diesel production of 0.45 €/l over the cost of biodiesel of 0.84 €/l imply that biofuels are not a real competent force against fossil fuels [1].

- Electric vehicles (EV) will have an upgrowth of 400% between 2010 and 2025. Note that new small electric vehicles could not be considered here for being still out of regulation in many countries, whose use is not meant to replace automobiles, but they will be used instead for short journeys. In any case, for LDV or HDV, the source of electricity is still nowadays dependent on fossil fuels, so that the change in emissions is local, but not global [24].

- In the future, hydrogen is pointed to be the energetic vector between energy sources and road transportation, but its technology is still far to be achieved [18].

Research and development of ICEs has had an exhaustive activity during the last decades, which is still being carried on nowadays [25]. In this sense, it is relevant to mention the importance of control evolution [10, 26], in part due to the growth of on-board computational resources [27].

As a result of this progress, the solution to the pollution problem of the old vehicles is not to remove alternative combustion engines from the road, but the solution is instead found in the recent and coming technology. In the end, costumers will have diversity of choices and means of transport will suit

more to the individuals needs.

Diesel engines emissions Combustion engines emissions play an important role in the environment pollution problems worlwide [28]. Some relevant characteristics of the pollutant emissions from Diesel engines are next described:

- Nitrogen oxides (NO_x) are formed at high temperatures and lean conditions in the combustion chamber [29]. NO_x are composed of NO and NO_2 species, whose proportion is generally dominated by NO in a 70% to 90% proportion [30]. NO_x species are responsible of evident causes of air pollution like acid rain and smog [31]. Furthermore, [32] evidences the health effects of human exposure to NO_2 gases on the long term, supported by studies since 2004 that documented epidemiological respiratory symptoms.
- Particulate matter (PM) may be originated from the agglomeration of very small particles, whose typical composition is 41% carbon, 7% of unburned fuel, 25% unburned lube oil, 13% ash and other components, and 14% sulfates and water [33] [34]. The diameter of more than 90% of PM are smaller than 1 μm, being 14-55 nm a common value. These emissions are documented to cause important health problems and are responsible for the pollution of air, water and soil [35].
- Carbon monoxide (CO) is a result of incomplete combustion, mainly at local rich mixtures inside the combustion chamber [36], which take place during strong accelerations. It is an odorless anc colorless gas, and it is more important in SI than in CI. The effect that CO has on humans is that it inhibits the capacity to transfer oxygen of the hemoglobin [37].
- Hydrocarbons (HC) are mainly composed of unburnt fuel due to insufficient temperature, so they usually occur in Diesel engines at light loads. Hydrocarbons are composed of thousands of species as a result of fuel cracking [38], but regulation differentiates between non-methane hydrocarbons (NMHC) and total hydrocarbons (THC).

Carbon dioxide (CO_2) has the largest rate in greenhouse gases emissions so that it is the main actor in the global warming. It is directly related to fuel consumption in combustion engines. Transportation is the second-largest sector in the production of global CO_2 emissions with a range of 22% [39] [40].

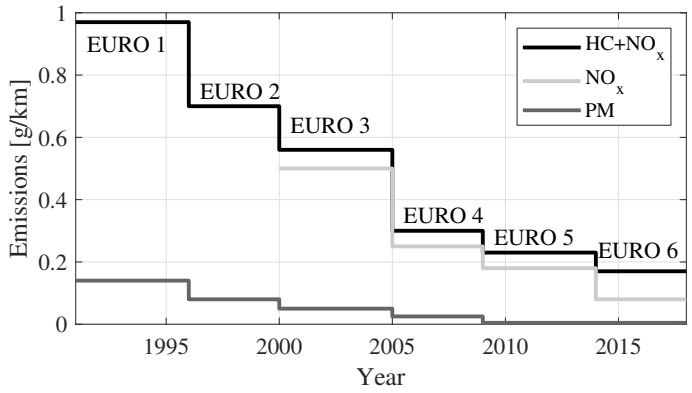

Figure 1.4. *European emissions regulations tendency for HC+NO_x, NO_x and PM.*

Unfortunately, the emissions reduction systems like the EGR penalize the reduction of fuel consumption and therefore of the CO_2 emissions [41]. Even so, both fuel consumption and emissions have been reduced over the last decades.

1.2 The need for after-treatment systems

Despite the most recent technologies with high and low pressure exhaust gas recirculation (EGR) loops [41], improved combustion efficiency, new combustion chamber designs, etc. engine raw emissions are still too high to comply with regulation [42]. Therefore, vehicles are equipped with emission control systems to meet the actual emissions standards requirements [43].

The emissions regulation in diesel engines Emissions standards for combustion engines have been tightened over the past decades for both SI and CI engines. The first implementations of regulations appeared in Europe, North America and Japan around the 90s decade [44], while emissions standards became common in China, South America, India, Japan, Australia and other countries during the first decade of the 21^{st} century.

Specifically, the European regulation has lowered the limits for type-approval vehicles over the years, as shown in Figure 1.4 for NO_x and PM. The first Euro 1 and Euro 2 had a regulation for NO_x emissions in company with HC, while

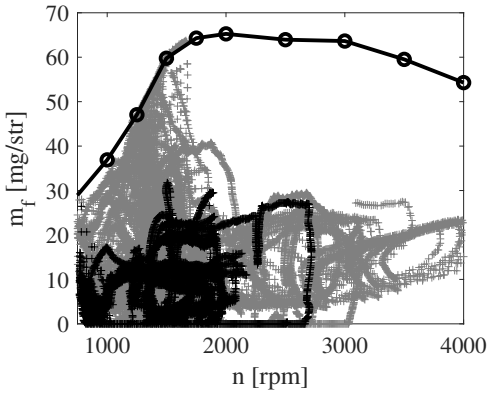

Figure 1.5. *Comparison of the NEDC, black crosses, and WLTC, gray crosses, regulation cycles with the range of engine operation. In the full load line, black, circles stand for experimental measurements.*

the first NO_x isolated regulation appeared in the Euro 3 with a limit of 500 mg/km. Then, the Euro 4 and Euro 5 regulations decreased these limits to 250 and 180 mg/km, respectively. The PM emissions regulations were introduced from the first Euro 1 and have also decreased over the years. Several modifications to the Euro 6 limits have appeared from the first publication in 2007 to the latest Euro 6d of 80 mg/km of NO_x and 4.5 mg/km of PM [45–47].

The progressive emissions reduction of regulations has not been accompanied by an analogic real reduction of the pollutant species in real life conditions. When the vehicles are out of the regulation conditions, their emissions overcome the allowed thresholds [48,49]. In fact, the Euro 6 regulation explicitly recognises real driving emissions (RDE) problems. Several reasons have splitted type-approval limits from their RDE, mainly regarding NO_x emissions, whose relation is represented by the conformity factors (CF) [50] in the regulation. The real CF have increased with the appearance of tightener regulations [51]. To avoid this issue, the regulation foresees the use of portable exhaust measurement systems (PEMS) to measure the RDE of vehicles [52,53].

Up to recent times, vehicles emissions were approved by means of standarized tests. The New european driving cycle (NEDC) was the test used in Europe from the Euro 3 regulation until september 2017 under the Euro 6 regulation [45], when it was replaced by the more realistic in terms of dynamics and power demand, as it can be seen in Figure 1.5 and Table 1.1, Worldwide harmonised light-duty vehicles test procedures (WLTP) [54]. Even

Table 1.1. *NEDC and WLTC characteristics.*

	NEDC	WLTC
Time (s)	1.180	1800
Length (km)	11.007	23.26
Idle time (%)	21.8	13
V_{max} (km/h)	120	131.6
$V_{average}$ (km/h)	33.6	46.3
$Accel_{max}$ (m/s^2)	1	1.6

so, the discrepancy between WLTP CO_2 emissions and reality is forecasted to lie between 20% and 30% [51], since these tests are still predefined and do not represent RDE. Other regulations use similar procedures, like the Federal Test Procedure (FTP) in the US and California. For this reason, the main purpose of the PEMS is to effectively control emissions over the large majority of in-use operating conditions, not just those covered by the test cycle. [55] [56].

On-board diagnostics On-board diagnostics (OBD) functions are responsible for controlling emissions, ensuring a proper operation of the emissions control system, so that vehicles can meet emissions limits during their lifespan [57–61]. Identifiying the system failures in controlled laboratory conditions previously, the algorithms of the OBD functions then have to use the available on-board signals to monitor the system's condition [62–67].

The application of the regulation to aged parts once the vehicle do not allow using the gas analysers and the normalized cycle conditions of the brand new procedure [68,69]. In this line, monitoring the performance of each of the after-treatment systems separately allows maintaining emission levels below the OBD threshold. The regulations consider an emissions threshold for OBD with a margin for ageing with regards to new vehicles, as can be seen in Table 1.2 for the case of the European regulation [70,71]. Thus, a pollutant emissions increase is foreseen due to the effect of engine, sensors and after-treatment ageing [72, 73].

When a malfunction is detected in a system that could potentially lead to high emissions, the driver is alerted with a malfunction indicator light (MIL). However, prior to activate a MIL, the OBD system must have a series of verification steps in order to ensure that it corresponds to a real malfunction and not to spurious circumstances.

Table 1.2. *Regulation thresholds for Euro 6-d [74].*

	Euro 6-d	Euro 6-d OBD
NO_x (mg/km)	80	140
HC+NOx (mg/km)	170	-
NMHC (mg/km)	-	290
CO (mg/km)	500	1750
PM (mg/km)	4.5	12

Both U.S. and European regulations have adopted in-use performance ratios (IUPR) that require a minimum frequency of monitoring events per duty cycle, where a duty cycle consists of an engine startup and engine shut-off, which can alternatively be defined as key-on key-off for start and stop engines. The IUPR is specific to each monitor, M in equation (1.1), and it is defined as follows:

$$IUPR = \frac{Numerator_M}{Denumerator_M} \tag{1.1}$$

where the numerator is a counter measuring the number of times a vehicle has been operated such that all monitoring conditions necessary for the specific monitor to detect a malfunction are given. On the other hand, the denominator is to provide a counter indicating the number of vehicle driving events, taking into account special conditions for a specific monitor. For DOC and DPF OBD, the denumerator must be incremented at the last time after 500 miles or 800km. Both the numerator and the denumerator increase unit by unit. Apart from an IUPR of 0.336 for the after-treatment system (ATS), DPFs and DOCs have an additional requirement from regulations which stands for detection of total failure or removal.

The on-board measurements limitation problem Efficient control and monitoring of the emissions control system requires on-board measurements, which feed of information to the electronic control unit (ECU) [75]. The sensors in an exhaust line are limited, since they suppose an extra economic weight [69, 76, 77]. In this sense, the after-treatment blocks suppose also a considerable increment of price, mainly due to its impregnation with precious materials.

Although all vehicles must accomplish with regulation requirements, the economic weight of the after-treatment system is not equal for any kind of vehicle. For instance, the relative economic impact of a NO_x sensor for a small light duty vehicle (LDV) of segment C is bigger than for a sport utility vehicle (SUV) or a heavy duty vehicle (HDV) [78].

1.3 Scope of the work

The scope of this work is to develop control-oriented models and diagnostics strategies that can improve the performance of the emissions control system, with focus on diesel catalysts, i.e. DOC and SCR. To this aim, the development of the proposed methods considers the availability of on-board measurements, while laboratory tests and measurements allow having a more detailed view of the processes occurring to the sensors and catalysts.

Despite the fact that DPF is a fundamental part of the diesel ATS, its modelling and diagnostics is out of the scope of this dissertation, since its physical structure, its operation principles and its focused sensors are different than those of a catalyst. On the other hand, several works are available in literature in terms of patents and articles for DPF operation and diagnostics [79–84]. In this sense, DOC and SCR are the diesel catalysts focus of this work.

In some cases, the on-board sensors measurements might not represent the value that they are supposed to provide. Therefore, the emissions control system must deal with their accuracy, precision, dynamic response, offset, cross-correlations and ageing. As a result, these phenomena are relevant and influence the decision to adopt the proper diagnostics strategies. In particular, the measurements provided by the temperature sensor and the λ measurement of the NO_x sensor are assessed by means of test bench thermocouples and gas analyzers, which provide a wider view.

An initial experimentation phase is proposed prior to develop models and algorithms, which combines RDE tests and test bench tests. Dynamic cycles, which include regulation cycles, are used for several purposes, which comprises the identification of potential use cases, the application of a model, the application of a diagnostics method, etc. As well, specific tests are also done to

analyze or characterize a particular matter of catalysts or sensors operation in detail. Then, the possibilities and limitations for on-board purposes can be outlined.

Since catalysts operation is highly dependent on thermal conditions, species-focused models require temperatures as inputs, whose estimation is proposed with a novel lumped 0D model and a literature-based 1D model. On the other hand, a fast estimation is proposed for the DOC upstream temperature by means of a data fusion technique based on a Kalman filter (KF). Then, the slow but reliable value that the sensor provides is improved in transient conditions with a fast but non necessarily precise model. Besides, a methodology to estimate the temperature peak due to post-injection pulses oxidation is also proposed.

Modelling is relevant for OBD purposes, since a model estimation can be compared with a sensor measurement, it can be used to feed an observer or it can be used to perform simulations. In this sense, models can provide measurable and non-measurable states, like species storage in the last case. Then, models including an ageing factor are proposed for both DOC and SCR, being a novel control-oriented lumped approach for the former and literature-based 1D and 0D approaches for the later.

Finally, diagnostics techniques are proposed for both DOC and SCR, whose approach is based on sensors measurements, which might be then part of a model or an observer. Total failure or removal detection algorithms are developed for DOC, as the the regulation requires, as well as the catalyst efficiency estimation, whose indirect algorithm is based on the on-board light-off temperature (LOT) estimation. Then, the LOT needs to be related to an ageing state and an emissions level increase. On the other hand, a 5 state observer is proposed to estimate the ageing level of an SCR, expanding observability of algorithms available literautre, while an indicator of the urea quality is proposed to run in parallel.

1.4 Objectives

The aim of the present work is to propose a framework to detect the Diesel engine catalysts ageing, taking into account the on-board sensors characteris-

tics and limitations. Specifically, the following items may be identified as the main objectives:

- The experimental characterization of the catalysts behaviour and their ageing, analyzing those deterioration modes that can be detected through the on-board sensors, whose temperature and λ measurements are also assessed (Chapter 4).
- The development of thermal models and temperature estimations to feed methods and strategies with their required inputs. (Chapter 5).
- The development of models, including an ageing state, to simulate ageing conditions and to feed diagnostics functions (Chapter 6).
- The design of OBD functions to estimate the ageing state of DOC and SCR catalysts, as well as its possible removal by the end user (Chapter 7).

1.4.1 Methodology

The present section contains the general structure followed in this work, divided into the existent chapters.

Chapter 2 contains the description of the current available after-treatment systems in the market, considering both after-treatment blocks and on-board sensors. The main characteristics, advantages and limitations of each device are assessed, being DOC and SCR, the after-treatment blocks focus of this dissertation, analyzed with more detail. In this sense, details of modelling approaches are given for the relevant catalysts in this work.

Chapter 3 is focused on the experimental set-up, describing the use of Diesel engines as gas generators, the rapid prototyping system to perform the by-pass and hardware-in-the-loop tests, the available measurements, the on-board sensors and the catalysts with different deterioration modes. The kind of different tests performed are also explained in this section.

Chapter 4 is dedicated to observe the experimental behaviours of the different catalysts, assessing some relevant sensors measurements. First, the main characteristics of catalyst operation is shown. Then, specific tests are repeated in case of DOC for parts with different ageing levels. Finally, dynamic tests are

applied to each catalyst and the effect that ageing has on their performance is analyzed.

Chapter 5 focus is on the DOC inlet temperature, the heat transfer along the catalysts and the temperature increase estimation due to post-injection pulses during steady engine operation conditions. On the one hand, a data fusion technique is applied to the upstream temperature sensor to improve its dynamic response. On the other hand, a 1D model and a 0D lumped models of heat transfer are presented, both including a downstream temperature sensor model.

Chapter 6 is focused on a 0D lumped model for DOC and both 1D and 0D models for SCR, including an ageing factor in all cases. On the one hand, the DOC model is based on the experiments shown in Chapter 4, where the ageing factor relates the LOT increase, the HC and CO slip increase and the HC accumulation capacity decrease. On the other hand, the ageing factor of the SCR models represents the decrease in NH_3 storage capacity.

Chapter 7 contains the main work of this dissertation. In this sense, the previous chapters constitute the the basis to develop the OBD algorithms, where the characteristics and limitations of each catalyst and the on-board measurements are assessed.

The total failure or removal diagnostics strategy for DOC is separated into passive and active diagnostics, where the active diagnostics makes use of fuel late post-injections to excite the system and decide if the part is completely faulty. On the other hand, the regulation also states an OBD limit for the pollutant species to which the DOC has effect. As a direct evaluation of the ageing state is not possible due to the on-board sensors limitation, an indirect method is presented, based on the estimation of the light-off temperature. Then, by means of the model, the LOT increase is related to an emissions increase.

The SCR ageing is detected by means of an extended Kalman filter (EKF) based observer. However, poor quality urea injected could lead to the association of low SCR efficiency to ageing, for what a urea quality indicator is developed, which can be run in parallel to the observer for SCR ageing. Then, when poor urea is detected, the SCR ageing estimator is frozen.

1.A Publications

Some of the contents have been published in international journals. Thus, the publications that are directly linked with the dissertation are listed below. In addition, the chapter which contains the publication information is pointed out in brackets.

Journal papers

1. Guardiola, C., Pla, B., Piqueras, P., Mora, J., and Lefebvre, D. (2017). Model-based passive and active diagnostics strategies for diesel oxidation catalysts. *Applied Thermal Engineering*, 110, 962-971. [Chapters 5, 6 and 7]
2. Guardiola C., Dolz V., Pla B. and Mora J. (2016) Fast estimation of diesel oxidation catalysts inlet gas temperature Control Engineering Practice, *Control Engineering Practice*. [Chapters 2, 4 and 5]
3. Guardiola C., Pla B., Mora J. and Lefebvre D. (2018) Experimental determination and modelling of the DOC ageing effects, *Proceedings of the Institution of Mechanical Engineers, Part D: Journal of Automobile Engineering* . [Chapters 4 and 6]
4. Guardiola C., Pla B., Bares P. and Mora J. (2018) An on-board method to estimate the light-off temperature of diesel oxidation catalysts, *International Journal of Engine Research*. [Chapters 4 and 7]

Conference papers

1. Guardiola C., Pla B., Mora J. and Lefebvre D. Control Oriented Model for Diesel Oxidation Catalyst Diagnosis *IFAC-PapersOnLine*. [Chapter 5]
2. Mora J., Willems F., Seykens X. and Guardiola C. An OBD strategy to estimate SCR ageing and avoid urea injection faults *IFAC-PapersOnLine*. [Chapter 7]

References

[1] Lukoil. "Global trends in oil and gas markets to 2025". Technical report, Lukoil, 2013. (cited in pp. 1, 2, and 4)

[2] Lukoil. "Major trends global oil market to 2030". Technical report, Lukoil, 2015. (cited in p. 2)

[3] Mock P, Kuehlwein J, Tietge U, Franco V, bandivadekar A and German J. "The WLTP: How a new test procedure for cars will affect fuel consumption values in the EU". Technical report, The international council on clean trasnportation, 2014. (cited in p. 2)

[4] PwC. "Projected vehicle sales in China, the U.S. and the EU between 2017 and 2030.", 2017. (cited in p. 3)

[5] Chiang C-J, Stefanopoulou A G and Jankovic M. "Nonlinear observer-based control of load transitions in homogeneous charge compression ignition engines". *IEEE Transactions on Control Systems Technology*, Vol. 15 n^o 3, pp. 438–448, 2007. (cited in pp. 3 and 36)

[6] Lu X, Han D and Huang Z. "Fuel design and management for the control of advanced compression-ignition combustion modes". *Progress in Energy and Combustion Science*, Vol. 37 n^o 6, pp. 741 – 783, 2011. (cited in p. 3)

[7] Stanglmaier Rudolf H. and Roberts Charles E. "Homogeneous Charge Compression Ignition (HCCI): Benefits, Compromises, and Future Engine Applications". In *International Fuels and Lubricants Meeting and Exposition 1999-01-3682*. SAE International, oct 1999. (cited in p. 3)

[8] Zehni A, Saray R K and Poorghasemi K. "Numerical comparison of PCCI combustion and emission of diesel and biodiesel fuels at low load conditions using 3D-CFD models coupled with chemical kinetics". *Applied Thermal Engineering*, Vol. 110, pp. 1483 – 1499, 2017. (cited in p. 4)

[9] Lee J, Chu S, Cha J, Choi H and Min K. "Effect of the diesel injection strategy on the combustion and emissions of propane/diesel dual fuel premixed charge compression ignition engines". Vol. 93, pp. 1041–1052, 12 2015. (cited in p. 4)

[10] Payri F, Luján José M, Guardiola Carlos and Pla B. "A challenging future for the ic engine: new technologies and the control role". *Oil & Gas Science and Technology–Revue d´IFP Energies nouvelles*, Vol. 70 n^o 1, pp. 15–30, 2015. (cited in p. 4)

[11] Nuesch T, Ott T, Ebbesen S and Guzzella L. "Cost and fuel-optimal selection of HEV topologies using particle swarm optimization and dynamic programming". In *American Control Conference (ACC), 2012*, pp. 1302–1307. IEEE, 2012. (cited in p. 4)

[12] Chan CC, Wong YS, Bouscayrol Alain and Chen Keyu. "Powering sustainable mobility: roadmaps of electric, hybrid, and fuel cell vehicles". *Proceedings of the IEEE*, Vol. 97 n^o 4, pp. 603–607, 2009. (cited in p. 4)

[13] Chan C Chue. "The state of the art of electric, hybrid, and fuel cell vehicles". *Proceedings of the IEEE*, Vol. 95 n^o 4, pp. 704–718, 2007. (cited in p. 4)

[14] Millo F, Rolando L, Mallamo F and Fuso R. "Development of an optimal strategy for the energy management of a range-extended electric vehicle with additional noise, vibration and harshness constraints". *Proceedings of the Institution of Mechanical Engineers, Part D: Journal of Automobile Engineering*, Vol. 227 n^o 1, pp. 4–16, 2013. (cited in p. 4)

[15] Jason S Moura, Fathy H K, Callaway D S and Stein J L. "A stochastic optimal control approach for power management in plug-in hybrid electric vehicles". *IEEE Transactions on control systems technology*, Vol. 19 n^o 3, pp. 545–555, 2011. (cited in p. 4)

[16] Johannesson L, Murgovski N, Ebbesen S, Egardt B, Gelso E R and Hellgren J. "Including a battery state of health model in the HEV component sizing and optimal control problem". In *IFAC Advances in Automotive Control*, volume 7, pp. 398–403, 2013. (cited in p. 4)

[17] Serrao L, Onori S, Sciarretta A, Guezennec Y and Rizzoni G. "Optimal energy management of hybrid electric vehicles including battery aging". In *American Control Conference (ACC), 2011*, pp. 2125–2130. IEEE, 2011. (cited in p. 4)

[18] Thomas C.E. Sandy. "Transportation options in a carbon-constrained world: Hybrids, plug-in hybrids, biofuels, fuel cell electric vehicles, and battery electric vehicles". *International Journal of Hydrogen Energy*, Vol. 34 n^o 23, pp. 9279 – 9296, 2009. (cited in p. 4)

[19] Heuser B. "Tailor-Made Fuels from Biomass". Technical report, RWTH - Aachen, 2016. (cited in p. 4)

[20] Graziano B, Heuser B, Kremer F, Pischinger S and Rohs H. "The Oxidation Potential Number: An Index to Evaluate Inherent Soot Reduction in D.I. Diesel Spray Plumes". *SAE International Journal of Engines 2015-01-1934*, Vol. 9 n^o 1, pp. 222–236, sep 2015. (cited in p. 4)

[21] Graziano B, Perez J Mora, Kremer F, Pischinger S, Reddemann MA, Kneer R, Heufer KA and Rohs H. "Virtual Fuel Approach: a new simulative methodology to analyse effects of fuel properties on mixture formation in compression igni-tion combustion". In *THIESEL Conference*, 2014. (cited in p. 4)

[22] Hoppe F, Heuser B, Thewes M, Kremer F, Pischinger S, Dahmen M, Hechinger M and Marquardt W. "Tailor-made fuels for future engine concepts". *International Journal of Engine Research*, Vol. 17 n^o 1, pp. 16–27, 2016. (cited in p. 4)

[23] Thomas C.E. "Fuel cell and battery electric vehicles compared". *International Journal of Hydrogen Energy*, Vol. 34 n^o 15, pp. 6005 – 6020, 2009. (cited in p. 4)

[24] Thomas C.E. Sandy. "How green are electric vehicles?". *International Journal of Hydrogen Energy*, Vol. 37 n^o 7, pp. 6053 – 6062, 2012. XII International Symposium on Polymer Electrolytes: New Materials for Application in Proton Exchange Membrane Fuel Cells. (cited in p. 4)

[25] Desantes J M and Payri F. *Motores de combustión interna alternativos*. 2011. (cited in p. 4)

[26] Kang M, Wu Y and Shen T. "Logical control approach to fuel efficiency optimization for commuting vehicles". *International Journal of Automotive Technology*, Vol. 18 n^o 3, pp. 535–546, Jun 2017. (cited in p. 4)

[27] Xie H, Stobart R, Tunestal P, Eriksson L, Huang Y and Leteinturier P. "Future Engine Control Enabling Environment Friendly Vehicle". In *SAE 2011 World Congress & Exhibition 2011-01-0697*. SAE International, apr 2011. (cited in p. 4)

[28] Reşitoğlu İbrahim A, Altinişik K and Keskin A. "The pollutant emissions from diesel-engine vehicles and exhaust aftertreatment systems". *Clean Technologies and Environmental Policy*, Vol. 17 n^o 1, pp. 15–27, 2015. (cited in p. 5)

[29] Heywood JB and others. *Internal combustion engine fundamentals*. Mcgraw-hill New York, 1988. (cited in pp. 5 and 22)

[30] López Hernández L. *Desarrollo de una metodología para la predicción y optimización de emisiones contaminantes y consumo en motores Diesel de automoción mediante redes neuronales artificiales*. PhD Thesis, 2004. (cited in p. 5)

[31] Grewe V, Dahlmann K, Matthes S and Steinbrecht W. "Attributing ozone to NOx emissions: Implications for climate mitigation measures". *Atmospheric Environment*, Vol. 59, pp. 102 – 107, 2012. (cited in p. 5)

[32] Organization World Health. "Review of evidence on health aspects of air pollution". Technical report, Regional office for Europe, 2013. (cited in p. 5)

[33] Maricq M. Matti. "Chemical characterization of particulate emissions from diesel engines: A review". *Journal of Aerosol Science*, Vol. 38 n^o 11, pp. 1079 – 1118, 2007. (cited in p. 5)

[34] Kittelson DB. "Engines and nanoparticles: a review". *Journal of Aerosol Science*, Vol. 29 n^o 5, pp. 575 – 588, 1998. (cited in p. 5)

[35] Englert N. "Fine particles and human health: a review of epidemiological studies". *Toxicology Letters*, Vol. 149 n^o 1, pp. 235 – 242, 2004. (cited in p. 5)

[36] Wu C-W, Chen R-H, Pu J-Y and Lin T-Hui. "The influence of air-fuel ratio on engine performance and pollutant emission of an SI engine using ethanol-gasoline-blended fuels". *Atmospheric Environment*, Vol. 38 n^o 40, pp. 7093 – 7100, 2004. (cited in p. 5)

[37] Kampa M and Castanas E. "Human health effects of air pollution". *Environmental Pollution*, Vol. 151 n^o 2, pp. 362 – 367, 2008. (cited in p. 5)

[38] Yamada H, Misawa K, Suzuki D, Tanaka K, Matsumoto J, Fujii M and Tanaka K. "Detailed analysis of diesel vehicle exhaust emissions: Nitrogen oxides, hydrocarbons and particulate size distributions". *Proceedings of the Combustion Institute*, Vol. 33 n^o 2, pp. 2895 – 2902, 2011. (cited in p. 5)

[39] Agency International Energy. "CO2 emissions from fuel Combustion". Technical report, OECD, 2017. (cited in p. 5)

[40] Davis S., Diegel S. and Boundy R. *Transportation energy data book*. 2007. (cited in p. 5)

[41] Pla B. *Análisis del Proceso de la Recirculación de los Gases de Escape de Baja Presión en Motores Diesel Sobrealimentados*. PhD thesis. Riunet, 2009. (cited in pp. 6 and 23)

[42] Johnson T V. "Diesel Emission Control in Review". In *SAE technical paper 2007-01-0233*. SAE International, 2007. (cited in pp. 6 and 28)

[43] Alkemade U G. and Schumann B. "Engines and exhaust after treatment systems for future automotive applications". *Solid State Ionics*, Vol. 177 n^o 26-32, pp. 2291 – 2296, 2006. (cited in pp. 6 and 41)

[44] Johnson TV. "Diesel Emission Control in Review". In *SAE 2001 World Congress 2001-01-0184*. SAE International, mar 2001. (cited in pp. 6 and 29)

[45] Regulation EU Comission. *No 715/2007*. Official Journal of the European Union, 2007. (cited in p. 7)

[46] Regulation EU Comission. *No 692/2008*. Official Journal of the European Union, 2008. (cited in pp. 7 and 179)

[47] Regulation EU Comission. *No 459/2012*. Official Journal of the European Union, 2012. (cited in p. 7)

[48] Naber D, Kufferath A, Krüger M, Maier R, Scherer S and Schumacher H. "Measures to fulfill real driving emission (RDE) with Diesel passenger cars". pp. 423–446, 2017. (cited in p. 7)

[49] Weiss Martin, Bonnel Pierre, KÃ¼hlwein JÃ¶rg, Provenza Alessio, Lambrecht Udo, Alessandrini Stefano, Carriero Massimo, Colombo Rinaldo, Forni Fausto, Lanappe Gaston, Lijour Philippe Le, Manfredi Urbano, Montigny Francois and Sculati Mirco. "Will Euro 6 reduce the NOx emissions of new diesel cars? - Insights from on-road tests with Portable Emissions Measurement Systems (PEMS)". *Atmospheric Environment*, Vol. 62, pp. 657 – 665, 2012. (cited in p. 7)

[50] Hooftman N, Messagie M, Mierlo J Van and Coosemans T. "A review of the European passenger car regulations - Real driving emissions vs local air quality". *Renewable and Sustainable Energy Reviews*, Vol. 86, pp. 1 – 21, 2018. (cited in p. 7)

[51] Mock P. "2020–2030 CO2 standards for new cars and light-commercial vehicles in the European Union". In *ICCT*, pp. 1–19, 2017. (cited in pp. 7 and 8)

[52] Regulation EU Comission. *No 2016/427*. Official Journal of the European Union, 2016. (cited in p. 7)

[53] Daham B, Li H, Andrews G E., Ropkins K, Tate J E. and Bell M C. "Comparison of real world emissions in urban driving for EURO 1-4 vehicles using a PEMS". Technical report, SAE Technical Paper 2009-01-0941, 2009. (cited in p. 7)

[54] Regulation EU Comission. *No 2017/1151*. Official Journal of the European Union, 2017. (cited in p. 7)

[55] Franco V, Sánchez F P, German J and Mock P. "Real-world exhaust emissions from modern diesel cars". *communications*, Vol. 49 n^o 30, pp. 847129–102, 2014. (cited in p. 8)

[56] Johnson T and Joshi A. "Review of Vehicle Engine Efficiency and Emissions". In *WCX 17: SAE World Congress Experience 2017-01-0907*. SAE International, mar 2017. (cited in p. 8)

[57] Herman A, Wu M-C, Cabush D and Shost M. "Model Based Control of SCR Dosing and OBD Strategies with Feedback from NH3 Sensors". *SAE International Journal of Fuels and Lubricants 2009-01-0911*, Vol. 2 n^o 1, pp. 375–385, apr 2009. (cited in pp. 8 and 33)

[58] P Jones James C. and Muske Kenneth R. "Model-based OBD for Three-Way Catalyst Systems". In *2004-01-0639*. SAE International, 2004. (cited in p. 8)

[59] Vitale G, Siebenbrunner P, Halser H, Bachler J and Pfahl U. "OBD Algorithms: Model-based Development and Calibration". In *SAE Technical Paper 2007-01-4222*. SAE International, 2007. (cited in pp. 8, 26, and 175)

[60] Arsie I, Flauti G, Pianese C, Rizzo G, Barberio C, Flora R, Serra G and Siviero C. "On-board diagnosis of SI engine catalyst efficiency: a confidence level analysis". In *International Workshop on Diagnostics in Automotive Engines and Vehicles, Fisciano, Italy*, 2002. (cited in p. 8)

[61] Boatas A, Agnes M, Peltier D and Dubuisson B. "OBD Using Statistical Pattern Recognition". In *SAE Technical Paper 2000-01-3104*. SAE International, 2000. (cited in pp. 8 and 26)

[62] Matsumoto A, Furui K, Ogiso M and Kidokoro T. "Model-Based OBD Logic Utilizing Adsorption and Desorption Model of NH3 in SCR Catalyst". In *SAE Technical Paper 2016-01-0960*. SAE International, 04 2016. (cited in pp. 8, 33, and 151)

[63] Sahner K, Fleischer M, Magori E, Meixner H, Deerberg J and Moos R. "HC-sensor for exhaust gases based on semiconducting doped SrTiO3 for On-Board Diagnosis". *Sensors and Actuators B: Chemical*, Vol. 114 n^o 2, pp. 861 – 868, 2006. (cited in pp. 8 and 39)

[64] Ochs T, Schittenhelm H, Genssle A and Kamp B. "Particulate Matter Sensor for On Board Diagnostics (OBD) of Diesel Particulate Filters (DPF)". *SAE International Journal of Fuels and Lubricants 2010-01-0307*, Vol. 3 n^o 1, pp. 61–69, apr 2010. (cited in pp. 8 and 29)

[65] Hoepfner A and Roduner C A. "PM Sensor Based On-Board Diagnosis of Particulate Filter Efficiency". In *SAE Technical Paper 10.4271/*. SAE International, 2013. (cited in pp. 8, 29, and 39)

[66] Hagen G, Burger K, Wiegaertner S, Schoe Kamin D and Moos R. "A mixed potential based sensor that measures directly catalyst conversion a novel approach for catalyst on-board diagnostics". *Sensors and Actuators B: Chemical*, Vol. 217, pp. 158–164, 2015. (cited in pp. 8 and 39)

[67] Kamimoto T. "A review of soot sensors considered for on-board diagnostics application". *International Journal of Engine Research*, 2016. (cited in pp. 8 and 39)

[68] Delphi. "Worldwide emission standards". Technical report, Delphi, 2017. (cited in pp. 8 and 32)

[69] Riegel J, Neumann H and Wiedenmann H-M. "Exhaust gas sensors for automotive emission control". *Solid State Ionics*, Vol. 152, pp. 783–800, 2002. (cited in pp. 8, 9, 34, and 138)

[70] Eijnden E v d, Cloudt R, Willems F and Heijden P v d. "Automated Model Fit Tool for SCR Control and OBD Development". In *SAE Technical Paper Series 2009-01-1285*. SAE International, apr 2009. (cited in pp. 8, 66, and 152)

[71] Willems F, Cloudt R, van den Eijnden E, van Genderen M, Verbeek R, de Jager B, Boomsma W and van den Heuvel I. "Is Closed-Loop SCR Control Required to Meet Future Emission Targets?". In *SAE Technical Paper Series 2007-01-1574*. SAE International, apr 2007. (cited in pp. 8, 33, 34, 37, and 99)

[72] Ruetten O, Pischinger S, Kuepper C, Weinowski R, Gian D, Ignatov D, Betton W and Bahn M. "Catalyst Aging Method for Future Emissions Standard Requirements". In *SAE Technical Paper 2010-01-1272*. SAE International, 2010. (cited in pp. 8 and 26)

[73] Li J, Szailer T, Watts A, Currier N and Yezerets A. "Investigation of the Impact of Real-World Aging on Diesel Oxidation Catalysts". *SAE Int. J. Engines 2012-01-1094*, Vol. 5, pp. 985–994, 04 2012. (cited in pp. 8, 26, and 87)

[74] Regulation EU Comission. *No 136/2014*. Official Journal of the European Union, 2014. (cited in p. 9)

[75] Wang D Y, Yao S, Shost M, Yoo J-H, Cabush D, Racine D, Cloudt R and Willems F. "Ammonia Sensor for Closed-Loop SCR Control". *SAE International Journal of Passenger Cars - Electronic and Electrical Systems 2008-01-0919*, Vol. 1, pp. 323–333, apr 2008. (cited in pp. 9, 38, 99, and 138)

[76] Tobias P, Martensson P, Goeras A, Lundstroem I and Spetz AL. "Moving gas outlets for the evaluation of fast gas sensors". *Sensors and Actuators B: Chemical*, Vol. 58 n^o 1, pp. 389 – 393, 1999. (cited in p. 9)

[77] Moos R. "A brief overview on automotive exhaust gas sensors based on electroceramics". *International Journal of Applied Ceramic Technology*, Vol. 2 n^o 5, pp. 401–413, 2005. (cited in pp. 9 and 36)

[78] Blanco-Rodriguez D., Vagnoni G. and Holderbaum B. "EU6 C-Segment Diesel vehicles, a challenging segment to meet RDE and WLTP requirements". *IFAC-PapersOnLine*, Vol. 49 n^o 11, pp. 649 – 656, 2016. 8th IFAC Symposium on Advances in Automotive Control AAC 2016. (cited in pp. 10 and 39)

[79] Van Nieuwstadt M. "Pressure sensor diagnosis via a computer". 2005. US Patent 6,947,831. (cited in p. 10)

[80] Emi M and Miura M. "Deterioration diagnosis of diesel particulate filter". 2007. US Patent 7,281,369. (cited in p. 10)

[81] Piqueras P. *Contribucion al modelado termofluidodinamico de filtros de particulas diesel de flujo de pared*. PhD Thesis, Universitat Politecnica de Valencia, 2005. (cited in p. 10)

[82] Van Nieuwstadt MJ and Trudell DF. "Diagnostics for diesel particulate filters". *SAE Technical Papers 2004-01-1422*, 2004. (cited in p. 10)

[83] Haralampous O. A., Kandylas I. P., Koltsakis G. C. and Samaras Z. C. "Diesel particulate filter pressure drop Part 1: Modelling and experimental validation". *International Journal of Engine Research*, Vol. 5 n^o 2, pp. 149–162, 2004. (cited in p. 10)

[84] Haralampous O. A., Kandylas I. P., Koltsakis G. C. and Samaras Z. C. "Diesel particulate filter pressure drop Part 2: On-board calculation of soot loading". *International Journal of Engine Research*, Vol. 5 n^o 2, pp. 163–173, 2004. (cited in p. 10)

Chapter 2

Emission control system in Diesel engines

Contents

2.1 Introduction

Emission control system of a Diesel engine must guarantee the correct operation of its components in order to keep tail-pipe emissions under the

regulation threshold. For this purpose, the components of CI engines like the fuel injection, the EGR and the VGT as engine subsystems, and the after-treatment system, must be controlled and monitored. The ATS, focus of this dissertation, is composed of after-treatment blocks and on-board sensors, located at the turbine downstream. In a diesel exhaust line, different architectures of ATS can be found, and the main blocks, the relevant sensors and their combinations in the more common applications are reviewed in this chapter.

In order to analyze, control and monitor the exhaust line devices, it is necessary the use of models that are able to represent their behaviour. As after-treatment systems are a reality from the 90s, several works have already been done in this sense, from which the main conclusions are outlined at the end of the chapter for DOC and SCR.

2.2 Diesel engine subsystems

The necessary after-treatment is dependent on the vehicle and its engine. In this sense, curent Diesel engines share basic elements in the fuel and air paths, which are described next [1].

2.2.1 The fuel path system

The physical part of the fuel injection system in traditional CI engines is composed of the common-rail system and the injectors. In a common-rail system, the low pressure side feeds the high pressure side through the pump and the control valves, while devolves the fuel excess through the return line. Then, the common-rail piece acts as an accumulator and the control holds the pressure in correspondence to the engine operating point. Finally, the ECU commands the duration of the signal to the injector as a function of the rail pressure and the desired injected fuel mass, $\dot{m}_f$. The start of injection (SOI), measured with respect to the TDC, is determined by a calibrated look-up table that depends on the engine operating condition, i.e. engine speed and injected fuel. The afore-mentioned mechanism is calibrated in steady-state points, so in case of strong transient phases and in order to avoid high HC and soot emissions, the smoke limiter function limits $\dot{m}_f$ until the air path is able to provide the required air mass $\dot{m}_a$ for the combustion.

2.2.2 The air path system

A typical air path of a commercial CI engine is composed of an air filter, a hot film flow meter that measures the intake flow ($\dot{m}_{int}$, a compressor, which is part of the turbocharger (TCH), an intercooler, the intake manifold, the combustion chamber, the exhaust manifold, the high and/or low pressure EGR loops, and the turbine, which is the other relevant element of the TCH. The ATS are however considered apart.

- The air filter cleans the air from undesired particles, provoking a reduced pressure drop in the line.
- The technology of a state-of-the-art TCH system is the variable geometry system (VGT) and the waste-gaste (WG). The VGT varies the nozzles of the turbine depending on the pressure and exhaust flow, while the WG bypasses the flow minimizing the exhaust flow through the turbine. These technologies are to solve the major problem of the TCH, which is the turbolag, associated with the inertial response of the turbo shaft [2].
- The EGR is spread into Diesel engines as the most common active NO_x reduction system since the 90s. Its operation fundamentals lay on adding inert gases, resulting from the combustion, again into to the combustion chamber, provoking the use of fuel energy to heat these inert gases and therefore decrease the flame adiabatic temperature, responsible for NO_x formation. A deep study of the effect of EGR on emission can be found in the *Ladommatos et. al* work [3–10]. The EGR air flow ($\dot{m}_a$) follows the following equations:

$$\dot{m}_{int} = \dot{m}_a + \dot{m}_{EGR} \tag{2.1}$$

$$EGR = \frac{\dot{m}_{EGR}}{\dot{m}_{int}} \tag{2.2}$$

  Several architecutures exist with regards to EGR, in which high pressure EGR (HPEGR) and low pressure EGR (LPEGR) are the two main groups. The HPEGR has the air loop between the combustion chamber and the TCH upstream, while the LPEGR has the air loop between the combustion chamber the TCH downstream, being common the EGR valve after the DPF [11].

The correct operation of the elements of the Diesel engine subsystems, with special focus on the EGR, is responsibility of the emissions control system, in order to guarantee fuel consumption and emissions limitations.

2.2.3 Control of fuel and air paths

The control of the fuel path has been traditionally done by look-up table depending on the engine operating conditions, calibrated in steady-state conditions, while transient operation is validated without the necessity of feedback from the exhaust. In this sense, only the air path is controlled in closed-loop. The problem of transients is rooted on the different dynamics present in an engine. Despite the fact that some authors have proposed the joint control of the air and fuel paths for optimized transient operation with real time measurements [12,13], manufacturers are still reluctant. With respect to the effect of the ATS on engine control, [14] demonstrated that the inclusion of an SCR in combination with an EGR system can reduce fuel consumption up to a 2% and keep emissions under Euro VI regulations.

2.3 After-treatment systems

The available after-treatment blocks for Diesel engines are described in this section. Their relevant characteristics, their function in the exhaust line, their composition, their control, if any, and the main ageing mechanisms are outlined for DOC, DPF, lean NO_x trap (LNT) or PNA, SCR and ammonia oxidation catalyst (AMOX).

2.3.1 Diesel oxidation catalysts

Diesel Oxidation catalysts were the first catalysts to appear on vehicles in the 70s on US cars, and they are now the heart of the diesel ATS, due to the different roles they play [15], i.e. the oxidation of unburned HC and CO species, the creation of exothermic heat to regenerate the DPF, the NO conversion into NO_2 that affects the SCR performance [16–18], as described in eq. (2.3) to eq. (2.5) and the oxidation of the solid organic fraction (SOF) from liquid hydrocarbons. For these reasons, the DOC is the first after-treatment system placed in an exhaust line. A scheme of the DOC efect on the species concentrations in shown in Figure 2.1.

$$CO + \frac{1}{2}O_2 \rightarrow CO_2 \tag{2.3}$$

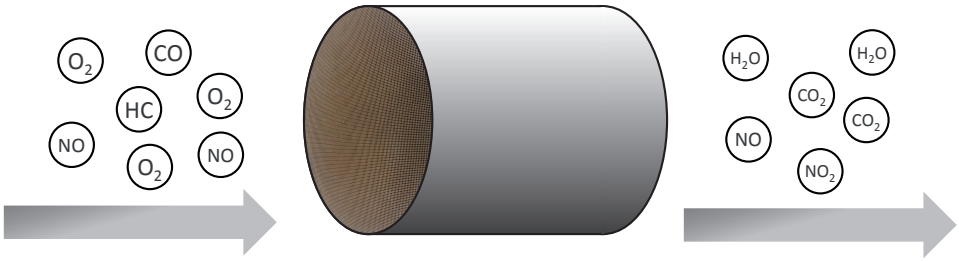

Figure 2.1. *DOC effect over the relevant species concentrations.*

$$C_xH_y + O_2 \rightarrow CO_2 + H_2O \tag{2.4}$$

$$NO + O_2 \rightleftharpoons NO_2 \tag{2.5}$$

The HC oxidation reaction is complex due to the presence of large variety of HC chains in the engine raw emissions, which difficult its measurement and therefore its modelling. For the purpose of simplifying this problematic, authors like [19, 20] reduce this expression to fixed HC.

The impregnation layer of the DOC monolith is mainly composed of a mixture of Pt and Pd, which show good oxidation performance along with good thermal durability [21]. The addition of Pd to a base of Pt increases the resistance to ageing with respect to Pt-only catalysts in terms of light-off temperature [22, 23]. However, the increase of Pd decreases the NO_2 production [24], so that a ratio of 3:1 showed the best rate of substitution [25].

The operation of DOCs is mainly dominated by the exhaust gas temperature, the exhaust gas concentrations and the exhaust gas velocity or exhaust mass flow. Some of the main characteristics are described next. The light-off temperature is a relevant characteristic to consider with regards to its operation, since it represents the threshold over which the DOC is able to oxidize the already mentioned species [26]. Regarding the LOT of the different species, it is higher for HC than for the CO and the NO into NO_2 converison [27]. In this sense, new LTC processes will challenge oxidation catalysts [15]. The oxidation of species may present cross interferences, thorugh which the presence of high HC concentrations limit the NO to NO_2 conversion [28]. Apart from

oxidation capacities, other relevant phenomena of DOCs is the accumulation capacity of HC and NO at low temperatures [29], which follows an adsorption/desorption phenomena [30].

After an experiment with several DOCs ordenated in series, in which high temperatures from engine exhaust gas were applied, permanent ageing damages appeared. The front catalysts were aged primarily due to ash contamination, while the back catalysts are generally thermally aged [31]. The light-off characteristics deteriorate due to both effects as the mileage increases [16]. However, as a mileage ageing would be too time and resources consuming to analyze in laboratory conditions, the exposure to high temperatures is considered as a valid ageing method for regulation validations [32].

While the presence of a downstream sensor is a must to perform diagnosis to any after-treatment system, the use of models is widely used to perform diagnostics in the automotive industry [33, 34]. In this sense, model estimations are compared with downstream measurements, which in the case of DOCs is an NTC temperature sensor. However, sensors accuracy and tight thresholds make diagnostics difficult for DOCs, as stated in [35]. For this reason, the use of non model based techniques becomes an alternative to estimate the ageing of a DOC through indirect techniques [36], since neither HC, CO nor NO or NO_2 sensors are available. For this purpose, special engine operation conditions like idle may be useful for diagnostics [37]. For instance, [38] proposes a technique to estimate the LOT, although it is not applicable on-board.

Ageing of DOCs is a critical phenomenon that can impact the HC and CO emissions, the DPF regeneration process, and the SCR performance through the NO to NO_2 conversion efficiency [16]. Due to the damaging atmosphere in which DOCs are located, DOCs are subjected to several permanent and temporary deactivation mechanisms [39]. Main permanent causes are excessive temperatures above 600°C, induced by generating exotherm on the catalyst, and exposure to various inorganic species like sulfur poisoning [40], contained in the engine exhaust fluids [31]. As an example of a permanent DOC damage, light-off temperature is increased due to an exposure to excessive temperature [41, 42]. The oxidation capacity decrease of DOCs is also appreciated at high HC concentrations, as described in [43]. In this line, the NO to NO_2 conversion efficiency is also affected by ageing, as it is experimentally described in [44]. On the other hand, reversible deactivation mechanisms are analyzed

in [39], althouth they strongly depend on the catalyst composition.

Several DOC models can be found in literature, whose approach is based on its target application. For instance, the works in [45], [19] and [20] are focused on the identification of the reaction kinetics, so a set of experiments is presented in a flow bench to fit the reaction rates to a Pt catalyst with C_3H_6 as inlet concentration in a first step, and the calibration of a commercial DOC with C_3H_6 and C_10H_22 in a second step. Analogically, the work in [46] was done in an engine bench in order to validate the terms of constants and activation energies of the Arrhenius equations available in literature.

The works presented in [47] and [48] analyzed the inhibition terms among HC, CO, NO, NO_2 and N_2O, considering C_3H_6 as representative of the HC species. In this line, a synthetic gas bench study for HC, CO and NO, NO_2 and N_2O reactions in steady state space velocity is found in [49], in which the genetic algorithm of GT-Power is used to calibrate the rection rates, and analyze the interaction of the different species. As described before, these models approaches require the use controlled conditions in terms of species presence to characterize in detail the reaction rates.

Models for DPF regeneration are focused on matching the DOC outlet temperature during high levels of inlet HC [50]. In this sense, [51] presented its model results during a steady flow, while [52] presented a more dynamic validation during a transient cycle. However, in the case of the model presented in [52], calibrated in steady state points, the dynamic results are shown for the resultant controlled temperature, not for the model results. In both cases, the models presented a strong component of heat transmission. In [53], the authors used a model taking into account reaction rates for HC and CO oxidation and NO to NO_2 conversion in steady state for DPF regeneration at one operating point, which was then used in [54] to estimate the NO_2 concentration at the DOC outlet during dynamic conditions. Finally, as a method for strong simplification, [55] proposes a delayed first order model of the injected HC with the temperature increase at the DOC outlet.

The experiments performed are also relevant for the model approach [56]. In this sense, the model for calibration and control presented in [57] is based on maps obtained through engine bench characterization tests, which represents the complexity of reaction rates characterization. Then, in other models like [34] and [58], the target is to estimate the DOC outlet temperature, which

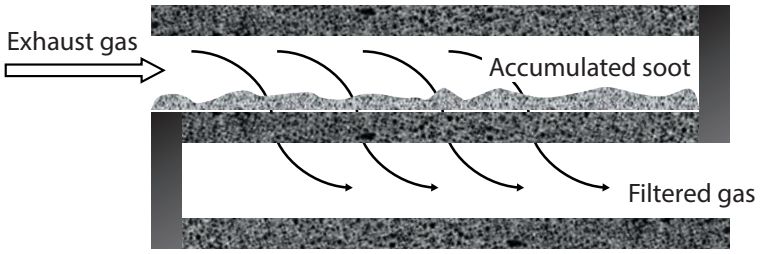

Figure 2.2. *Scheme of the exhaust flow and the accumulated soot in a channel of a DPF.*

require the use of dynamic tests for its validation. In conclusion, the large variety of modelling approaches highlights the complexity of the catalyst processes.

In the work presented in this dissertation in Chapter 6, the DOC control-oriented model is focused on capturing the effect of ageing on HC and CO emissions during dynamic conditions, as well as a dynamic validation of the heat transmission that leads to the outlet temperature.

2.3.2 Diesel particulate filter

Diesel particulate filters are spread into Diesel engine vehicles nowadays. The cause of this is rooted on the fact that from the Euro 5 implementation of the european regulation in 2009, the allowed PM emissions were reduced to a 20% from the first PM regulation in the Euro 3 in the year 2000. In this sense, the function of the filter is to accumulate PM, as shown in Figure 2.2, until they are burned by means of a regeneration process, which can be induced by the ECU when necessary and in accordance with the differential pressure measurement [59]. The main focus of investigations take place in the ceramic structure, the DPF regeneration process and the on-board diagnostics.

The DPF is a ceramic-based reactor usually composed of cordierite or silicon, in which numerous channels are present in the monolith. These channels are alternatively blocked at the end, but are related to the adjacent channels by porous walls. Therefore, the exhaust gases are forced to flow through the walls, which act as filters for the particulate filter, as depicted in Figure 2.2 [60].

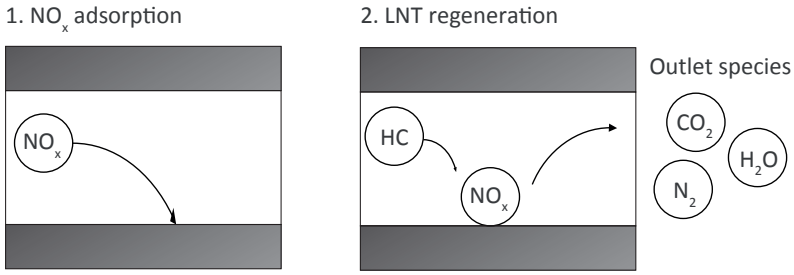

Figure 2.3. *Scheme of the NO_x adsorption and the regeneration process at rich conditions of an LNT.*

Once the DPF requires active regeneration [61], the filter temperature needs to raise until 600°C, which is usually done through late fuel post-injections that are burned in the DOC [55]. The active DPF regeneration is complex due to the control of the exothermic heat generated in the DOC and the unexpected driving conditions, whose process was already used in the early 90s and it still a focus of investigation nowadays [52, 62]. However, fuel post-injection does not only have impact on DPF regeneration, since [63] analyzed the cross effect that they can have on SCR performance due to oxidation in the DOC.

The DPF diagnosis is commonly based on the measured differential pressure. With this signal, and the use of an appropiate model like [64], the strategy can determine if the filter is trapping enough soot or not. In this sense, the inclusion of direct PM measurements would increase the accuracy of the DPF ageing state [65–67].

2.3.3 Lean NO_x trap

Lean NO_x traps are part of the family of technologies for exhaust pipe NO_x emissions reduction, which has been a focus of activity since the 70s [68, 69]. This catalyst, in comparison with the SCR, does not require the addition of an ammonia-based solution, although requires extra fuel consumption. At low temperatures, its performance is more suitable than the SCR, although in the rest of cases its performance is lower than that of the SCR, taking into account the range of operating conditions and temperatures of an engine. For these reasons, the typical applications of LNT is for vehicles with engine displacements below 2 liters or combined with an SCR system [70].

The LNT stores NO_x species during lean conditions, while it then can release them or reduce if rich mode conditions are achieved, process which is shown in Figure 2.3. In this last case, the reduction of NO_x is done at the expense of fuel post-injections, with the incrase of fuel consumption that it supposes. Passive NO_x adsorbers are similar to LNT, however, their operation does not allow the regeneration of the adsorbed NO_x, so that NO_x are released either when the PNA saturates or when the temperature increases enough [71].

The LNT optimization problem on minimizing the exhaust NO_x emissions with a minimal fuel cost is attracting attention in recent investigations [72–74]. During LNT regeneration a certain amount of ammonia is produced, which can be then used by a downstream SCR for additional NO_x reduction. Such systems are reliable and they have been introduced into series production on some diesel NO_x reduction systems [75]. In case of high NO_x emissions, which usually take place at peaks during urban driving conditions and high loads, the LNT may not be able to reduce NO_x as much as necessary [70]. In this, case, the SCR enters to scene.

In a control-oriented model for LNTs, the main variables taken into account for the accumulation capacity of the trap are the temperature, the space velocity and the storage fraction. In this, a model of the catalyst bed temperature becomes necessary to have a 1D distribution of temperatures [76].

The direct measurement of NO_x from an NO_x sensor, as the main species for LNT, allows generating several diagnostics possibilities. In this sense, control-oriented models like [77, 78] enable the application of observers that estimate the ageing state through the NO_x emissions increase [79, 80].

2.3.4 Selective catalytic reduction system

The SCR is one of the most efficient ATS available nowadays for NO_x reduction. It was first implemented for HDV [81] and it has become popular among them since the Euro IV, and it is becoming popular in passenger cars under the last Euro 6 regulation [82,83]. However, it requires costly additional hardware such as a tank to store the urea, a urea injector, a complex control system, and depending of the vehicle considered, NO_x sensors, NH_3 sensors and an ammonia oxidation catalyst [84]. In this catalyst, the injected urea is converted into ammonia and adsorbed by the catalyst surface, which is then used to reduce the NO_x species, whose reactions are described next and it is

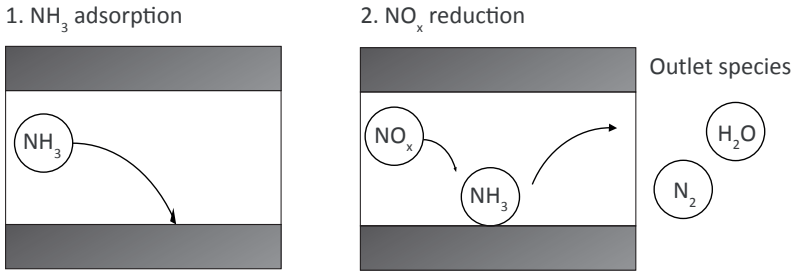

Figure 2.4. *Scheme of the SCR operation principle, in which NH_3 is adsorbed and NO_x species are then reduced.*

shown in Figure 2.4.

- Urea decomposition: urea thermolysis and HNCO hydrolysis. These processes may limit the urea adsorption into the catalyst surface, since NH_3 needs to be formed before adsorption [85]. Its reactions are, respectively:

$$H_4N_2CO \rightarrow NH_3 + HNCO \tag{2.6}$$

$$HNCO + H_2O \rightarrow NH_3 + CO_2 \tag{2.7}$$

- Standard, fast and slow SCR reactions, respectively:

$$4NH_3 + 4NO + O_2 \rightarrow 4N_2 + 6H_2O \tag{2.8}$$

$$2NH_3 + NO + NO_2 \rightarrow 2N_2 + 3H_2O \tag{2.9}$$

$$8NH_3 + 6NO_2 \rightarrow 7N_2 + 12H_20 \tag{2.10}$$

- N_2O formation:

$$2NH_3 + 2NO_2 \rightarrow N_2O + N_2 + 3H_2O \tag{2.11}$$

$$4NH_3 + 4NO + 3O_2 \rightarrow 4N_2O + 6H_2O \tag{2.12}$$

$$2NH_3 + 3N_2O \rightarrow 4N_2 + 3H_2O \tag{2.13}$$

- NH_3 oxidation, which takes place at high temperatures:

$$4NH_3 + 5O_2 \rightarrow 4NO + 6H_2O \tag{2.14}$$

$$4NH_3 + 3O_2 \rightarrow N_2 + 6H_2O \tag{2.15}$$

Nova and *Tronconi* [86] published a comprehensive review of the relevant technologies developed to the date with regards to available technologies for SCR, catalysts composition, reaction kinetics for modelling, modelling, control-oriented modelling, control and ammonia supply. The main groups of SCR are classified accordingly to its composition, i.e. Vanadia based, Fe-Zeolite based and Cu-Zeolite based, which have different stability against temperatures and NO_x reduction efficiencies [87, 88]. The catalyst composition is selected depending on the vehicle use. While Vanadia-based catalysts are more appropiate for HDV due to its temperature range of operation, the efficiency window of Zeolite based catalysts is more suitable for passenger cars [89].

The supply of a urea solution, diluted in a 32.5 % in water, is required upstream the SCR for NO_x reduction [90]. A compressor pressurizes the line that contains the urea from the urea tank to the injector, which is opened by the ECU [91, 92]. There exist several kind of injectors, which include water refrigerated and non-refrigerated, where the non-refrigerated by water can use the own urea to be refrigerated. The signal to the injector is commanded with a pulse width modulation (PWM) signal, whose value needs to take into account the instantaneous pressure in the line, given by the compressor [93]. Then, the injected urea solution is converted by thermolysis and hydrolisis into ammonia [94], which is mixed with the exhaust gases and is accumulated in the SCR [95].

The effect of the SCR on the exhaust gas concentrations is mainly dominated by the inlet gas species concentrations, the temperatures and the space velocity [96, 97]. The complex processes occuring inside the SCR, with several elements influencing its operation and one direct actuator (the urea injection), are the cause that have made SCR control a hot spot of investigation during the last years [98–101]. The necessary control level has evoluted with the restriction of the NO_x emissions regulations [102], which require maximal NO_x conversion, performance at low temperatures and meeting of in-use complliance requirements. The open-loop control [103, 104] has evolved to

adaptive [105] and closed-loop control, necessary to comply with Euro 6 regulations, and to which more on-board sensors are necessary than for open-loop control [106–109]. In addition, the sensors measurements are also used for performance monitoring and on-board diagnostics [110, 111].

SCR modelling and control have been a focus of activity during last years. With regards to modelling, and depending on the application, several model approaches exist. A detailed model allows a better representation of the system by sufficient space dimensionalization and the complete set of reaction rates present in the SCR processes. On the other hand, control-oriented models have evolved following ECU computation burden limitations and the necessity for linearization, reducing the space dimensionalization and limiting the model to the relevant reactions [112]. In this sense, the performance of 0D and 1D control-oriented models including ageing are presented in Chapter 6.

The SCR ageing affects mainly to the ammonia storage capacity, as [113] assesses for Vanadia, Cu-Zeolite and Fe-Zeolite SCR aged catalysts by means of thermal deactivation from 2 to 16 hours at high temperatures. [114] analyzed explicitly the effect of hydrothermal ageing on NO_x conversion, where NO_x conversion was significantly reduced over the Cu-based SCR tested and the Fe-based SCR had more resistance to loss of NO_x conversion decrease. In this sense, the estimation of ageing may be done in open-loop from the time of the DPF regeneration events due to the high temperatures achieved [115]. Sulfur ageing also has negative effect, although the efficiency can be recovered after sulfur removal [116]. The migration of Pt as a result of high temperature decomposition also has negative impact on SCR performance [117].

SCR diagnostics is based on the NO_x and, in case, NH_3 measurements. [118] contains one of the first algorithms to estimate the SCR ageing state through an EKF observer, whose required model is based on [119], for which both NO_x and NH_3 signals are required. Then, later algorithms like [101, 106, 120, 121] are based on [118] and [119] works. However, a simpler and common technique is to run models with different SCR ageing states in parallel and associate the SCR ageing to the one that better fits the measured emissions [122]. On the other hand, [122] presented an OBD strategy by means of a model that estimates the NH_3 slip through the Langmuir approach.

In any case, the accuracy of the sensors is fundamental for detection algorithms [123], as well as the correct estimation of urea dosing [124]. For the case of urea injection, [125] and [93] present techniques to detect urea injector

faults in terms of flow through the available signals in the urea injection system, although poor dilution of urea with respect to commercial AdBlue could bypass the strategy.

2.3.5 Ammonia oxidation catalyst

An ammonia oxidation catalyst can be placed downstream of the SCR in order to guarantee negligible NH_3 slip, i.e., the NH_3 slip would be conserved below the 10ppm that regulations stablish for this species. However, the addition of this catalyst supposes several drawbacks. It supposes the addition of an additional block, whose cost may be justified in a HDV, but it might not be assumed in a LDV. Morevoer, the NH_3 conversion and selectivity of state-of-the-art AMOX catalysts needs to be improved to make this an attractive option for future systems [109].

2.3.6 On-board sensors for control and diagnostics

The introduction of stringent regulations and OBD requirements make necessary the presence of sensors in the exhaust line of Diesel engines [126]. Negative temperature constant temperature sensors, pressure differential sensors, λ sensors, NO_x sensors and NH_3 sensors can be already found in a Diesel exhaust line, while other sensors like the soot sensor and the HC sensor are not planned to be present [127].

On the other hand, on-board sensors need to be reliable to the harsh environment present in an exhaust line, in which solid particles and water are present, the exhaust gas achieves high temperatures and thermal shocks occur, among other circumstances. In this line, the sensors need to be as reliable over time, as precise and as accurate as possible.

Accuracy and dynamic response are two of the most problematic issues on sensors. I.e. a couple of up- and downstream sensors may not exactly measure the same concentration in steady-state conditions of a determined exhaust gas. On the other hand, the dynamic response of sensors is usually slower than the order of magnitude of engine dynamics [128], although this problem may be solved through data fusion techniques, which allow combining sensors measurement with the fast dynamics of a model [129, 130]. The dynamic problem is illustrated in Figure 2.5 with the signal of the NTC sensor measurement, while the accuracy problem is shown with the λ measurement of a couple of NO_x sensor sensors in Figure 3.8.

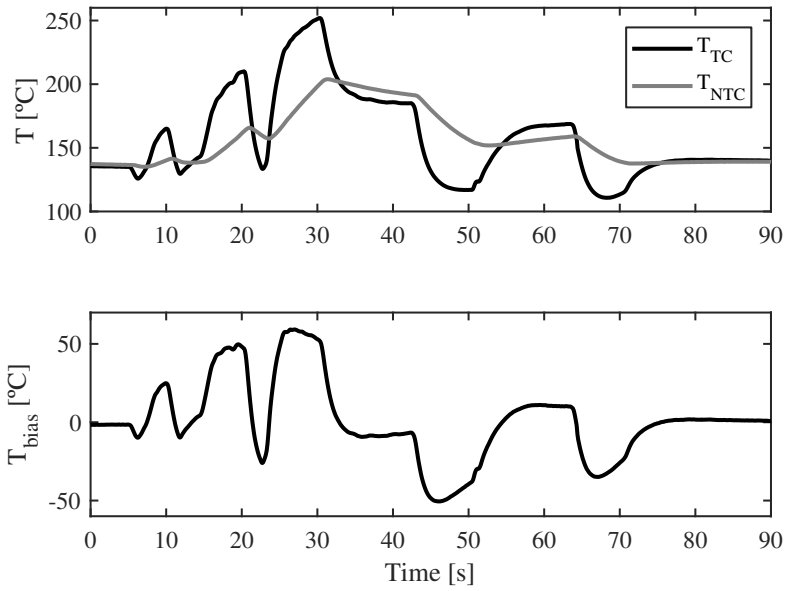

Figure 2.5. *Dynamic problem shown for the NTC temperature sensor during a transient phase. The T_{TC} measurement corresponds to a thin thermocouple, while the T_{NTC} measurement corresponds to an on-board temperature sensor. Bottom plot: T_{TC}-T_{NTC} during the time window..*

2.3.6.1 NTC sensor

Thermistors, or NTC sensors, have been used for automotive applications to measure exhaust gas temperature since 1940s. These sensors are used to measure the inlet temperature of DPFs, with special focus on DPF regeneration control, and also to perform DOC diagnostics. The robustness requirements required for surviving in the exhaust environment are satisfied by an increased sensor mass, whose thermal inertia implies filtering the exhaust gas temperature measurements. In this line, their operation characteristics allow measuring temperatures in a range of 40°C to 1000°C [131].

The dynamic problem of the NTC sensor is represented in Figure 2.5, in which a comparison of the two measurements from a fast thin thermocouple and an NTC on-board sensor is done. As it can be appreciated, the NTC measurement is not able to get the transients as the thermocouple does, so its signal is significantly filtered. The bottom plot quantitatively represents this difference, in which a bias up to 50°C takes place. Due to this problem, models using the temperature sensor measurements as an input could have a

deficient total energy measurement, and operation characteristics of the DOC, like LOT, that strongly depend on temperature could not be observed.

2.3.6.2 λ sensor

Exhaust gas oxygen (EGO) sensors were first implemented to control the three way catalyst (TWC) on SI engines in 1968 [132]. However, EGO sensors were replaced by universal exhaust gas oxygen (UEGO) sensors for SI and CI engines in the 90s, which represent a linear resolution of the oxygen concentration and therefore are named wide-band [133]. In traditional CI engines, λ sensors are used to control and monitor the AFR, as well as the performance of AT catalysts, while λ sensors are fundamental for the control of new LTC modes [134].

The oxygen concentration is measured by means of the so-called λ sensor. Its measurement, the λ signal, represents the air excess factor with respect to the stoichiometric air-to-fuel ratio, through which the oxygen concentration can be obtained. Its equation is the following:

$$\lambda = \frac{\dot{m}_a}{\dot{m}_f} \frac{1}{14.5} \tag{2.16}$$

where $\dot{m}_a$ is the air mass flow, $\dot{m}_f$ is the fuel mass flow and 14.5 is the approximate stoichiometric air-to-fuel ratio in Diesel engines. Typically, the λ signal is used instead as λ^{-1}. In this way, an infinite value does not appear, since the sensor signal at ambient air is 0 and not infinite:

- Lean conditions: $\lambda > 1$
- Stoichiometric conditions: $\lambda = 1$
- Rich conditions: $\lambda < 1$
- Ambient air: $\lambda = 0$

2.3.6.3 NO_x sensor

Current NO_x sensors are manufactured using the planar ZrO_2 multilayer technology [135], and this kind of sensors simultaneously provide the λ signal

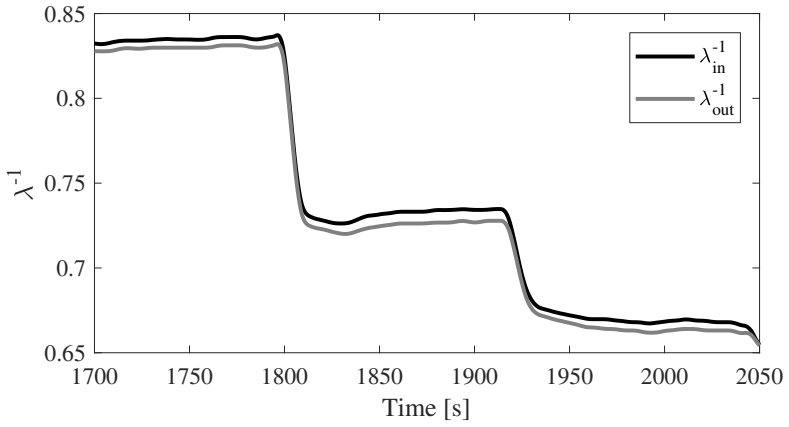

Figure 2.6. *Accuracy problem shown with λ signals, whose measurements are done with a couple of NO_x sensors up- and downstream the DOC without oxidation..*

and NO_x concentration [136]. The implementation of an NO_x sensor in an exhaust line allows controlling and monitoring NO_x dedicated systems like the LNT or the SCR [124], apart from the functions that require a λ signal, which the sensor is also able to measure. Therefore, an NO_x sensor should be placed at the end of an AT with NO_x reduction catalysts. However, NO_x sensors are cross-sensitive to NH_3 that may slip from the SCR, which complicates the use in closed-loop SCR control strategies [109].

The problem of sensors accuracy is represented in Figure 3.8 with the λ measurements of the NO_x sensors. The pair of sensors is located up- and downstream the DOC, whose measurement differ from one another, even though no oxidation is occurring in the DOC. Despite the differences between both measurements are contained in a $\pm 5\%$ band, this inaccuracy could be problematic for some applications.

2.3.6.4 NH_3 sensor

The NH_3 sensor, or ammonia sensor, is manufactured with a monolithic thick film multi layer composite substrate, which is mainly composed of an Alumina / Zirconia composite. Its measurement range, from 0 to 1000 ppm, has a tolerance of ± 5 at 10 ppm, its temperature range of operation is included between 200°C and 450°C, and its time response is 3s for a 60% and 5s for a 90%. The presence of O_2 and H_2O in the diesel exhaust compensate the crossed

effect that each one have over the ammonia measurement, as the following equation shows:

$$EMF \approx \frac{kT}{3e} Ln(P_{NH_3}) - \frac{kT}{4e} Ln(P_{O_2}) - \frac{kT}{2e} Ln(P_{H_2O}) \tag{2.17}$$

where EMF si the resulting mV singal of the sensor, k is a calibrable constant and P_i is the parcial pressure of the i species. However, for a more representative measurement, the following correction formula is suggested [137]:

$$NH_{3,cor} = NH_{3,meas}\Big(\big(\frac{O_2}{O_{2,ref}}\big)^{O_{2,exp}} \big(\frac{H_2O}{H_2O_{ref}}\big)^{H_2O_{exp}} \big(\frac{P}{P_{ref}}\big)^{P_{exp}} \Big) \tag{2.18}$$

where NH_3 $_{,cor}$ stands for the corrected NH_3 measurements, NH_3 $_{,meas}$,O_2, H_2O and P correspond to signals, x_{ref} correspond to reference values and x^{exp} correspond to the exponential factors.

The ammonia sensor is located downstream the SCR, although in case there is an AMOX catalyst and the sensor is still required, it should be placed upstream this catalyst [102]. It is designed for closed-loop control and diagnostics of the SCR, which allows reducing the NO_x emissions in comparison with the use of an NO_x sensor [138]. However, the NH_3 sensor feedback is limited to high temperature operating conditions, while NO_x sensors can operate in all operating conditions [139].

2.3.6.5 Differential pressure sensor

The differential pressure (ΔP) sensor is a piezo-resisitive element that is present in the exhaut line to estimate the DPF soot load from the pressure drop measurement [85], so that it is integrated up- and downstream the DPF system. With the ΔP signal, an active regeneration can be performed when necessary to keep the engine performance and comply with regulations [140].

2.3.6.6 Other sensors

Some sensors are being designed for emissions reduction through control or OBD, but they do not play a role in the exhaust line of a series Diesel engine [60]. In this sense, the problematic of pollutant species emissions sensors

is resolved having in mind production cost and reliability, so that market forces will resist added costs without tangible benefits. These sensors are next described.

HC First studies for HC sensors in [141] presented a sensing concept composed of a single-layer alumina substrate for ease of hand build and for proof of the concept. Then, the multilayer resistive sensor based on catalytically activated and non-activated SrTiO3 presented in [142] show consistent results with the hydrocarbons concentration and its measured signal. However, the oxygen concentration needs to be compensated for a correct lecture of the measurements, which could be done by means of a λ measurement. On the other hand, the sensor measurement is also dependent on the heating state of the sensor [143].

In order to have a performance monitoring or OBD sensor, [144] proposes to use this HC sensor as analogically to the differential pressure sensor DPFs. In this sense, the differential concentration in HC would be an indicator of the health state of the DOC.

Soot Soot sensors are designed to measure the particles passing through the DPF and to estimate the cumulative particle flow. Note that in this case, the term 'soot' is used to include a full range of PM, and not only the carbonaceous fractions [66,145] to which the actual term soot makes reference. These resistive sensors measure in cycles, in which a sample is collected and the PM is detected, while a regeneration is then required to oxidize and remove the collected material.

The soot sensor was tested in comparison with laboratory measurements, whose result showed good correlation for a range of 1 to 25 mg/m^3, with a good dynamic correlation also comparing the accumulated values [146]. In fact, and despite the two steps measurement process, [65] tested the sensor in an NEDC test, in which the accumulated measurements showed results with a deviation of a 1%. However, the PM sensor still needs an improved accuracy for low soot concentrations [147].

2.3.7 Diesel exhaust layouts

The increasing emissions standards for Diesel engines make manufacturers struggle to find an after-treatment system configuration that optimizes the trade-off between low cost, low emissions, low fuel consumption and robustness [15]. Therefore, the layout of the ATS is dependent on the vehicle, in

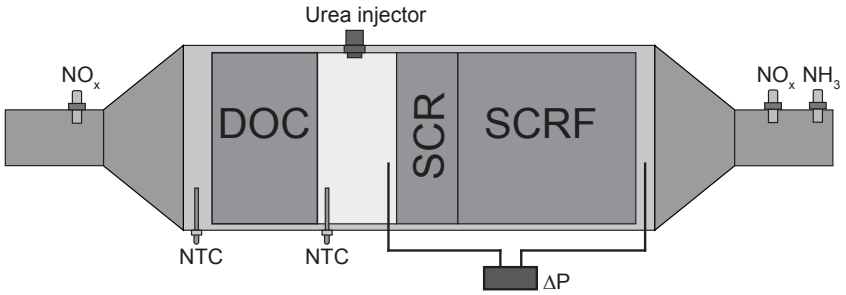

Figure 2.7. *Example of ATS layout to comply with Euro 6 regulations.*

which the budget and the applied regulation have a special relevance [148]. Different configurations can be seen also for LDV and HDV [149]. Here, the available technology for ATS in terms of packaging and feasible Euro 6 exhaust lines are described, including the preferred positions for on-board sensors. An example is shown in Figure 2.7

The tendency is to compact the ATS blocks into single components, since it reduces its cost, its weight, its effective space [150], and also improves the warm-up time, which is a must for LTC engines. As a consequence, the DPF technology has evolved to integrate the DOC functions, which results in the catalyzed DPF (CPDF) [150, 151], or the SCR, which results in the SCR filter (SCRF). However, current technology does not allow integrating both DOC and SCR into de DPF, so the preferred option is the integration of the DPF in the SCR. However, as the main metal for the NO_x adsorption is the platinum, deNO_x systems like the LNT or PNA can be integrated into the DOC [152].

Tourlonias et. al. [153] assessed that the best configuration taking into account fuel consumption, capacity to regenerate the DPF and the proper restriction for Euro 6 pollutant emissions limits is a DOC-SCR-SCRF. The inclusion of PNA upstream the SCR improves the low temperature NO_x reduction [151]. Morevoer, SCR catalysts can use ammonia the generated during its regeneration [89]. Therefore, the DOC could be substituted by a combined PNA substrate, which was not considered in [153]. In case only one deNO_x system could be chosen, the NO_x reduction performance for LNT is lower than for SCR, although other aspects like low temperature activity, resistance to ageing and complexity are better for LNT [154], so LNT would be the preferred option for small cars [155] and the SCR would be the preferred option for higher NO_x conversion rates.

An AT solution for improved NO_x conversion, is the use of two SCR blocks in series, with the NO_x sensor in the middle [156]. The target of this layout is to keep the first catalyst loaded with excess of NH_3, which results in higher storage ratio and therefore in higher NO_x conversion, while leaving the second catalyst to adsorb the excess of NH_3 slip [16].

On-board sensors distribution over the exhaust line Exhaust sensors are necessary to perform control and diagnostics of the ATS. However, due to the afore mentioned economic costs that they imply, its inclusion is restricted to the minimum possible. Morevoer, sensors need to be exhaustly tested and proved to survive in the harsh environment, and their manufacturing malfunctions, offsets, bias, ageing and dynamic response must be suitable for the application [157]. The following items present a state-of-the-art scenario of sensors for each catalyst:

- Two NTC surround the DOC in order to perform control during DPF regenerations and diagnose the catalyst. NO_x signals from a pair of up- and downstream NO_x sensors measurements does not provide relevant information, unless it has PNA capacities, since DOCs have impact over the NO and NO_2 concentrations but they do not have impact in principle over the total NO_x. Nevertheless, the λ signals can be used for diagnostics.
- A pair of up- and downstream NO_x sensors are useful for the LNT control and diagnostics, since the NO_x sensors measurements allow tracking the stored NO_x, and allow the estimation of the piece performance.
- The differential pressure sensor is the traditional sensor used for soot loading estimation and allows deciding when an active regeneration is necessary.
- The SCR system can operate in open-loop for former regulations, although an NO_x sensor is required downstream the catalyst for closed-loop control and diagnostics. Moreover, an NO_x sensor located upstream can improve the overall performance of the piece. Unfortunately, no sensor exist for the differentiation of NO and NO_2, although on-board models are used to track the concentration of these species, taking into account also the effect of the DOC.
- An NH_3 sensor may be located at the SCR downstream, in order to have a better control over the SCR system and the urea dosing, as well as to

account for its performance and also for diagnostics purposes. In case there is presence of an AMOX catalyst, the NH_3 sensor must be located upstream this catalyst, in order to have the NH_3 measurement before it is consumed by the catalyst.

A λ measurement is at least required after the turbine in order to perform combustion diagnostics, as well as to improve the performance and diagnose the ATS. The NO_x signal upstream the catalyst can come either from an NO_x sensor or from a model [158, 159], depending on the application.

2.4 Conclusions

The state of the art of the emissions control system has been presented in this chapter. For this purpose, the Diesel engine subsystems has been explained as responsible for the gas generation that feed the ATS. Then, a review of the catalysts history, composition, relevant characteristics, its function in the exhaust line, the operation behaviour, the relevant sensors, its control, the ageing mechanisms and its effects has been assessed. In this sense, the on-board sensors present in the exhaust line for control and diagnostics have been also presented, in combination with their combination in a current ATS layout for Euro 6 regulations. Finally, the main problematics of the on-board sensors measurements have been as well presented.

References

[1] Heywood JB and others. *Internal combustion engine fundamentals*. Mcgraw-hill New York, 1988. (cited in pp. 5 and 22)

[2] Park S, Matsumoto T and Oda N. "Numerical Analysis of Turbocharger Response Delay Mechanism". In *SAE 2010 World Congress & Exhibition 2010-01-1226*. SAE International, apr 2010. (cited in p. 23)

[3] Ladommatos N, M. Abdelhalim S and Zhao H. "The Effects of Exhaust Gas Recirculation on Diesel Combustion and Emissions". Vol. 1, pp. 107–126, 02 2000. (cited in p. 23)

[4] Ladommatos N, M. Abdelhalim S and Zhao H. "The Effects of Exhaust Gas Recirculation on Diesel Combustion and Emissions". Vol. 1, pp. 107–126, 02 2000. (cited in p. 23)

[5] Ladommatos N, M Adelhalim S, Zhao Hua and Hu Z. "The effects of carbon dioxide in exhaust gas recirculation on diesel engine emissions". Vol. 212, pp. 25–42, 01 1998. (cited in p. 23)

[6] Ladommatos N, Abdelhalim S and Zhao H. "Control of oxides of nitrogen from diesel engines using diluents while minimising the impact on particulate pollutants". *Applied Thermal Engineering*, Vol. 18 n^o 11, pp. 963 – 980, 1998. (cited in p. 23)

[7] Ladommatos N, Abdelhalim SM, Zhao Hua and Hu Z. "The dilution, chemical, and thermal effects of exhaust gas recirculation on diesel engine emissions-part 1: Effect of reducing inlet charge oxygen". Technical report, SAE Technical Paper 961165, 1996. (cited in p. 23)

[8] Ladommatos N, Abdelhalim SM, Zhao Hua and Hu Z. "The dilution, chemical, and thermal effects of exhaust gas recirculation on diesel engine emissions-part 2: Effects of Carbon Dioxide". Technical report, SAE Technical Paper 961167, 1996. (cited in p. 23)

[9] Ladommatos N, Abdelhalim SM, Zhao Hua and Hu Z. "The dilution, chemical, and thermal effects of exhaust gas recirculation on diesel engine emissions-part 3: Effects of water vapour". Technical report, SAE Technical Paper 971659, 1997. (cited in p. 23)

[10] Ladommatos N, Abdelhalim SM, Zhao Hua and Hu Z. "The dilution, chemical, and thermal effects of exhaust gas recirculation on diesel engine emissions-part 4: Eects of Carbon Dioxide and Water Vapour". Technical report, SAE Technical Paper 971660, 1997. (cited in p. 23)

[11] Pla B. *Análisis del Proceso de la Recirculación de los Gases de Escape de Baja Presión en Motores Diesel Sobrealimentados*. PhD thesis. Riunet, 2009. (cited in pp. 6 and 23)

[12] Tschanz F, Amstutz A, Onder C H. and Guzzella L. "Feedback control of particulate matter and nitrogen oxide emissions in diesel engines". *Control Engineering Practice*, Vol. 21 n^o 12, pp. 1809 – 1820, 2013. (cited in p. 24)

[13] Zhao D, Liu C, Stobart R, Deng J, Winward E and Dong G. "An explicit model predictive control framework for turbocharged diesel engines". *IEEE Transactions on Industrial Electronics*, Vol. 61 n^o 7, pp. 3540–3552, 2014. (cited in p. 24)

[14] Willems F, Mentink P, Kupper F and Van den Eijnden E. "Integrated emission management for cost optimal EGR-SCR balancing in diesels". *IFAC Proceedings Volumes*, Vol. 46 n^o 21, pp. 711–716, 2013. (cited in pp. 24 and 66)

[15] Johnson T. "Vehicular Emissions in Review". *SAE Int. J. Engines 2014-01-1491*, Vol. 7, pp. 1207–1227, 2014. (cited in pp. 24, 25, and 39)

[16] Johnson T. "Vehicular Emissions in Review". *SAE International Journal of Engines 2013-01-0538*, Vol. 6 n^o 2, pp. 699–715, apr 2013. (cited in pp. 24, 26, and 41)

[17] Stadlbauer S, Waschl H and del Re L. "NO/NO2 Ratio based NH3 Control of a SCR". In *SAE Technical Paper 2014-01-1565*. SAE International, apr 2014. (cited in p. 24)

[18] Chen P and Wang J. "Nonlinear and adaptive control of NO/NO 2 ratio for improving selective catalytic reduction system performance". *Journal of the Franklin Institute*, Vol. 350 n^o 8, pp. 1992–2012, 2013. (cited in p. 24)

[19] Sampara C S, Bissett E J and Chmielewski M. "Global kinetics for a commercial diesel oxidation catalyst with two exhaust hydrocarbons". *Industrial & Engineering Chemistry Research*, Vol. 47 n^o 2, pp. 311–322, 2008. (cited in pp. 25, 27, and 138)

[20] Sampara C S, Bissett E J, Chmielewski M and Assanis D. "Global kinetics for platinum diesel oxidation catalysts". *Industrial & Engineering Chemistry Research*, Vol. 46 n^o 24, pp. 7993–8003, 2007. (cited in pp. 25, 27, and 138)

[21] Russell April and Epling William S. "Diesel Oxidation Catalysts". *Catalysis Reviews*, Vol. 53 n^o 4, pp. 337–423, 2011. (cited in p. 25)

[22] Johansen K, Dahl S, Mogensen G, Pehrson S, Schramm Je and Ivarsson A. "Novel base metal-palladium catalytic diesel filter coating with NO2 reducing properties". Technical report, SAE Technical Paper 2007-01-1921, 2007. (cited in p. 25)

[23] Cavataio G, Jen H-W, Girard J W, Dobson D, Warner J R and Lambert C K. "Impact and prevention of ultra-low contamination of platinum group metals on SCR catalysts due to DOC design". *SAE International Journal of Fuels and Lubricants 2009-01-0627*, Vol. 2, pp. 204–216, 2009. (cited in p. 25)

[24] Johnson T V. "Diesel Emission Control in Review". *SAE Int. J. Fuels Lubr. 2008-01-0069*, pp. 68–81, 2008. (cited in p. 25)

[25] A Morlang, U Neuhausen, K Klementiev and F Sc. "Bimetallic Pt Pd diesel oxidation catalysts: Structural characterisation and catalytic behaviour". *Applied Catalysis B: Environmental*, Vol. 60 n^o 3-4, pp. 191 – 199, 2005. (cited in p. 25)

[26] Bartley G J. "Identifying Limiters to Low Temperature Catalyst Activity". In *SAE Technical Paper 2015-01-1025*. SAE International, 2015. (cited in pp. 25, 87, and 139)

[27] Ye S, Yap Y H., Kolaczkowski S T., Robinson K and Lukyanov D. "Catalyst light-off experiments on a diesel oxidation catalyst connected to a diesel engine-methodology and techniques". *Chemical Engineering Research and Design*, Vol. 90 n^o 6, pp. 834 – 845, 2012. (cited in pp. 25, 84, 87, and 146)

[28] Henry C, Currier N, Ottinger N, Yezerets A, Castagnola M, Chen H-Y and Hess H. "Decoupling the Interactions of Hydrocarbons and Oxides of Nitrogen Over Diesel Oxidation Catalysts". In *SAE 2011 World Congress & Exhibition 2011-01-1137*. SAE International, 2011. (cited in pp. 25 and 139)

[29] Sampara C S., Bissett E J. and Assanis D. "Hydrocarbon storage modeling for diesel oxidation catalysts". *Chemical Engineering Science*, Vol. 63, pp. 5179–5192, 2008. (cited in pp. 26, 88, and 140)

[30] Kryl D, Kocí P, Kubícek M, Marek M, Maunula T and Härkönen M. "Catalytic converters for automobile diesel engines with adsorption of hydrocarbons on zeolites". *Industrial & engineering chemistry research*, Vol. 44 n^o 25, pp. 9524–9534, 2005. (cited in pp. 26 and 138)

[31] Li J, Szailer T, Watts A, Currier N and Yezerets A. "Investigation of the Impact of Real-World Aging on Diesel Oxidation Catalysts". *SAE Int. J. Engines 2012-01-1094*, Vol. 5, pp. 985–994, 04 2012. (cited in pp. 8, 26, and 87)

[32] Ruetten O, Pischinger S, Kuepper C, Weinowski R, Gian D, Ignatov D, Betton W and Bahn M. "Catalyst Aging Method for Future Emissions Standard Requirements". In *SAE Technical Paper 2010-01-1272*. SAE International, 2010. (cited in pp. 8 and 26)

[33] Guardiola C, Pla B, Piqueras P, Mora J and Lefebvre D. "Model-based passive and active diagnostics strategies for diesel oxidation catalysts". *Applied Thermal Engineering*, Vol. 110, pp. 962–971, 2017. (cited in pp. 26 and 188)

[34] Guardiola C., Pla B., Mora J. and Lefebvre D. "Control Oriented Model for Diesel Oxidation Catalyst Diagnosis". *IFAC-PapersOnLine*, Vol. 48 n^o 15, pp. 427 – 433, 2015. (cited in pp. 26, 27, 138, and 146)

[35] Nieuwstadt M Van, Upadhyay D and Yuan F. "Diagnostics for Diesel Oxidation Catalysts". In *SAE Technical Paper 2005-01-3602*. SAE International, 2005. (cited in pp. 26, 64, and 164)

[36] Vitale G, Siebenbrunner P, Halser H, Bachler J and Pfahl U. "OBD Algorithms: Model-based Development and Calibration". In *SAE Technical Paper 2007-01-4222*. SAE International, 2007. (cited in pp. 8, 26, and 175)

[37] Boatas A, Agnes M, Peltier D and Dubuisson B. "OBD Using Statistical Pattern Recognition". In *SAE Technical Paper 2000-01-3104*. SAE International, 2000. (cited in pp. 8 and 26)

[38] Sutjiono R, Tayal P, Zhou K and Meckl P. "Real-Time On-Board Indirect Light-Off Temperature Estimation as a Detection Technique of Diesel Oxidation Catalyst Effectiveness Level". In *SAE Technical Paper 2013-01-1517*. SAE International, 04 2013. (cited in pp. 26, 87, 138, and 175)

[39] Ahari H, Zammit M, Cattani L, Jacques J and Pauly T. "Cause and Effect of Reversible Deactivation of Diesel Oxidation Catalysts". In *SAE Technical Paper 2014-01-1518*. SAE International, 2014. (cited in pp. 26 and 27)

[40] Cabello Galisteo F., Larese C., Mariscal R., López Granados M., Fierro J. L. G., Fernández-Ruiz R. and Furió M. "Deactivation on vehicle-aged diesel oxidation catalysts". *Topics in Catalysis*, Vol. 30 n^o 1, pp. 451–456, Jul 2004. (cited in p. 26)

[41] Schultz R and Meckl P H. "Light-Off Temperature Shift for Catalyzed Diesel Particulate Filter On-Board Diagnostics". In *SAE Technical Paper 2012-01-1248*. SAE International, 04 2012. (cited in pp. 26 and 176)

[42] Wiebenga M H., Kim C Hwan, Schmieg S J., Oh S H., Brown D B., Kim D Heui, Lee J-H and Peden C H.F. "Deactivation mechanisms of Pt/Pd-based diesel oxidation catalysts". *Catalysis Today*, Vol. 184 n^o 1, pp. 197 – 204, 2012. Catalytic Control of Lean-Burn Engine Exhaust Emissions. (cited in p. 26)

[43] Nakane T., Ikeda M., Hori M., Bailey O. and Mussmann L. "Investigation of the Aging Behavior of Oxidation Catalysts Developed for Active DPF Regeneration Systems". In *SAE Technical Paper 2005-01-1759*. SAE International, 2005. (cited in p. 26)

[44] Katare S R., Patterson J E. and Laing P M. "Aged DOC is a Net Consumer of NO2: Analyses of Vehicle, Engine-dynamometer and Reactor Data". Technical Report 2007-01-3984, SAE Technical Paper 2007-01-3984, 2007. (cited in p. 26)

[45] Sampara C S. *Global Reaction Kinetics for Oxidation and Storage in Diesel Oxidation Catalysts.* PhD Thesis, The University of Michigan, 2008. (cited in p. 27)

[46] Kim Y-D and Kim W-S. "Re-evaluation and Modeling of a Commercial Diesel Oxidation Catalyst". *Industrial & Engineering Chemistry Research*, Vol. 48 n^o 14, pp. 6579–6590, 2009. (cited in pp. 27 and 138)

[47] Khosravi M, Abedi A, Hayes RE, Epling WS and Votsmeier M. "Kinetic modelling of Pt and Pt: Pd diesel oxidation catalysts". *Applied Catalysis B: Environmental*, Vol. 154, pp. 16–26, 2014. (cited in pp. 27 and 138)

[48] Tanaka Y, Hihara T, Nagata M, Azuma N and Ueno A. "Modeling of diesel oxidation catalyst". *Industrial & engineering chemistry research*, Vol. 44 n^o 22, pp. 8205–8212, 2005. (cited in pp. 27 and 138)

[49] Rafigh M. *Exhaust aftertreatment modeling for efficient calibration in diesel passenger car applications*. PhD Thesis, 20177. (cited in p. 27)

[50] Lepreux O, Creff Y and Petit N. "Model-based temperature control of a diesel oxidation catalyst". *Journal of Process Control*, Vol. 22 n^o 1, pp. 41 – 50, 2012. (cited in p. 27)

[51] Zheng M and Banerjee S. "Diesel oxidation catalyst and particulate filter modeling in active Flow configurations". *Applied Thermal Engineering*, Vol. 29 n^o 14-15, pp. 3021 – 3035, 2009. (cited in p. 27)

[52] Kim Y-W, Van Nieuwstadt M, Stewart G and Pekar Ja. "Model predictive control of DOC temperature during DPF regeneration". In *SAE Technical Paper 2014-01-1165*. SAE International, 2014. (cited in pp. 27, 29, and 138)

[53] Surenahalli H.S., Parker G.G., Johnson J.H. and Devarakonda M.N. "A Kalman Filter estimator for a Diesel Oxidation Catalyst during active regeneration of a CPF". In *American Control Conference (ACC), 2012*, pp. 4969–4974, 2012. (cited in p. 27)

[54] Surenahalli H Shankar, Parker G and Johnson J H. "Extended Kalman Filter to Estimate NO, NO2, Hydrocarbon and Temperatures in a DOC during Active Regeneration and Under Steady State Conditions". In *SAE Technical Paper 2015-01-1059*. SAE International, 2015. (cited in p. 27)

[55] Frobert A, Creff Y, Lepreux O, Schmidt L and Raux S. "Generating Thermal Conditions to Regenerate a DPF: Impact of the Reductant on the Performances of Diesel Oxidation Catalysts". In *SAE Technical Paper 2009-01-1085*. SAE International, 04 2009. (cited in pp. 27 and 29)

[56] Kolaczkowski S., Ye S., Yap Y., Robinson K. and Lukyanov D. "Transient experiments on a full-scale DOC Methodology and techniques to support modelling". *Catalysis Today*, Vol. 188 n^o 1, pp. 53 – 61, 2012. Modeling of Exhaust-Gas After-Treatment. (cited in p. 27)

[57] Mallamo F, Longhi S, Millo F and Rolando L. "Modeling of diesel oxidation catalysts for calibration and control purpose". *International Journal of Engine Research*, Vol. 15 n^o 8, pp. 965–979, 2014. (cited in pp. 27 and 143)

[58] Chen P and Wang J. "Control-oriented model for integrated diesel engine and aftertreatment systems thermal management". *Control Engineering Practice*, Vol. 22, pp. 81–93, 2014. (cited in pp. 27, 110, 127, and 138)

[59] Johnson T V. "Diesel Emission Control in Review". In *SAE technical paper 2007-01-0233*. SAE International, 2007. (cited in pp. 6 and 28)

[60] Khair MK. "A Review of Diesel Particulate Filter Technologies". In *Future Transportation Technology Conference & Exposition 2003-01-2303*. SAE International, jun 2003. (cited in pp. 28 and 38)

[61] Bai S, Tang J, Wang G and Li G. "Soot loading estimation model and passive regeneration characteristics of DPF system for heavy-duty engine". *Applied Thermal Engineering*, Vol. 100, pp. 1292–1298, 2016. (cited in p. 29)

[62] Johnson TV. "Diesel Emission Control in Review". In *SAE 2001 World Congress 2001-01-0184*. SAE International, mar 2001. (cited in pp. 6 and 29)

[63] Stadlbauer S, Waschl H, Schilling A and del Re L. "DOC Temperature Control for Low Temperature Operating Ranges with Post and Main Injection Actuation". In *SAE Technical Paper 2013-01-1580*. SAE International, 2013. (cited in pp. 29 and 87)

[64] Nagar N, He X, Iyengar V, Acharya N, Kalinowski A, Kotrba A, Gardner T and Yetkin A. "Real Time Implementation of DOC-DPF Models on a Production-Intent ECU for Controls and Diagnostics of a PM Emission Control System". *SAE Int. J. Commer. Veh. 2009-01-2904*, Vol. 2, pp. 222–233, 10 2009. (cited in p. 29)

[65] Hoepfner A and Roduner C A. "PM Sensor Based On-Board Diagnosis of Particulate Filter Efficiency". In *SAE Technical Paper 10.4271/*. SAE International, 2013. (cited in pp. 8, 29, and 39)

[66] Husted H, Roth G, Nelson S, Hocken L, Fulks G and Racine D. "Sensing of Particulate Matter for On-Board Diagnosis of Particulate Filters". *SAE International Journal of Engines 2012-01-0372*, Vol. 5 n^o 2, pp. 235–247, apr 2012. (cited in pp. 29 and 39)

[67] Ochs T, Schittenhelm H, Genssle A and Kamp B. "Particulate Matter Sensor for On Board Diagnostics (OBD) of Diesel Particulate Filters (DPF)". *SAE International Journal of Fuels and Lubricants 2010-01-0307*, Vol. 3 n^o 1, pp. 61–69, apr 2010. (cited in pp. 8 and 29)

[68] B J Cooper, W Evans and B Harrison. "Catalysis and Automotive Pollution Control". 1987. (cited in p. 29)

[69] B, J Cooper and J, E Thoss. "Role of NO in Diesel Particulate Emission Control". *Society of Automotive Engineers*, 1989. (cited in p. 29)

[70] Yang L, Franco V, Campestrini A, German J and Mock P. "NOx control technologies for Euro 6 diesel passenger cars". *Int. Council Clean Transportation, white paper*, pp. 1–22, 2015. (cited in pp. 29 and 30)

[71] Michael J R. "ATP-LD; Cummins Next Generation Tier 2 Bin 2 Diesel Engine". Technical report, Cummins, 2014. (cited in p. 30)

[72] Xu F., Toyoda M., Yasui Y., Matsunaga H., Kato A. and Shen T. "Optimal control design for lean NOx trap regeneration in diesel engines". In *2017 56th Annual Conference of the Society of Instrument and Control Engineers of Japan (SICE)*, pp. 349–352, 2017. (cited in p. 30)

[73] Hsieh M. F. and Wang J. "Nonlinear model predictive control of lean NOx trap regenerations". In *Proceedings of the 48h IEEE Conference on Decision and Control (CDC) held jointly with 2009 28th Chinese Control Conference*, pp. 5182–5187, 2009. (cited in p. 30)

[74] Munguia N. *Lean NOx Trap Regeneration Control Strategy on a 1.9 L Turbocharged Diesel*. PhD Thesis, 2009. (cited in p. 30)

[75] M Weibel, N Waldbuesser, R Wunsch, D Chatterjee, B Bandl-Konrad and B Krutzsch. "A Novel Approach to Catalysis for NO x Reduction in Diesel Exhaust Gas". *Topics in Catalysis*, 2009. (cited in p. 30)

[76] Han M. and Lee B. "Control oriented model of a lean NOx trap for the catalyst regeneration in a 2.2 L direct injection diesel engine". *International Journal of Automotive Technology*, Vol. 16 n^o 3, pp. 371–378, 2015. (cited in p. 30)

[77] Marie-Luce D, Di-penta D, Bliman P-A and Sorine M. "Control-Oriented Modeling of a LNT-SCR Diesel After-Treatment Architecture". *SAE International Journal of Engines 2011-01-1307*, Vol. 4 n^o 1, pp. 1764–1775, apr 2011. (cited in p. 30)

[78] Pisu P., Canova M. and Soliman A. "Model-Based Fault Diagnosis of a NOx Aftertreatment System". *IFAC Proceedings Volumes*, Vol. 41 n^o 2, pp. 7072 – 7078, 2008. 17th IFAC World Congress. (cited in p. 30)

[79] Yang H and Chimner C. "Integration of Reformer Model Based Estimation, Control, and Diagnostics for Diesel LNT Based Aftertreatment Systems". *SAE International Journal of Engines 2010-01-0569*, Vol. 3 n^o 1, pp. 282–295, apr 2010. (cited in p. 30)

[80] Canova M, Midlam-Mohler S, Pisu P and Soliman A. "Model-based fault detection and isolation for a diesel lean NOx trap aftertreatment system". *Control Engineering Practice*, Vol. 18 n^o 11, pp. 1307 – 1317, 2010. Special Issue on Automotive Control Applications, 2008 IFAC World Congress. (cited in p. 30)

[81] Fritz N, Mathes W, Zuerbig J and Mueller R. "On-road demonstration of NOx emission control for diesel trucks with SINOx urea SCR system". Technical report, SAE Technical Paper 44716659, 1999. (cited in p. 30)

[82] Koebel M, Elsener M and Kleemann M. "Urea-SCR: a promising technique to reduce NOx emissions from automotive diesel engines". *Catalysis today*, Vol. 59 n^o 3-4, pp. 335–345, 2000. (cited in p. 30)

[83] Song Q and Zhu G. "Model-based Closed-loop Control of Urea SCR Exhaust Aftertreatment System for Diesel Engine". In *SAE 2002 World Congress & Exhibition 2002-01-0287*. SAE International, mar 2002. (cited in pp. 30 and 99)

[84] Shost M, Noetzel J, Wu M-C, Sugiarto T, Bordewyk T, Fulks G and Fisher G B. "Monitoring, Feedback and Control of Urea SCR Dosing Systems for NOx Reduction: Utilizing an Embedded Model and Ammonia Sensing". In *SAE Technical Paper Series 2008-01-1325*. SAE International, 2008. (cited in p. 30)

[85] Cloudt R, Saenen J, Eijnden E van den and Rojer C. "Virtual Exhaust Line for Model-based Diesel Aftertreatment Development". In *SAE 2010 World Congress & Exhibition 2010-01-0888*. SAE International, apr 2010. (cited in pp. 31, 38, and 188)

[86] Nova I and Tronconi E. *Urea-SCR technology for deNOx after treatment of Diesel exhausts*. Springer, 2014. (cited in pp. 32 and 151)

[87] Guan B, Zhan R, Lin H and Huang Z. "Review of state of the art technologies of selective catalytic reduction of NOx from diesel engine exhaust". *Applied Thermal Engineering*, Vol. 66 n^o 1, pp. 395–414, 2014. (cited in pp. 32 and 99)

[88] Colombo M, Nova I and Tronconi E. "A comparative study of the NH3-SCR reactions over a Cu-zeolite and a Fe-zeolite catalyst". *Catalysis Today*, Vol. 151 n^o 3, pp. 223 – 230, 2010. (cited in p. 32)

[89] Twigg M.V. "Advanced integrated exhaust aftertreatment systems and the mechanisms of {NOx} emissions control". In IMechE, editor, *Internal Combustion Engines: Performance, Fuel Economy and Emissions*, pp. 219 – 229. Woodhead Publishing, 2013. (cited in pp. 32 and 40)

[90] Delphi. "Worldwide emission standards". Technical report, Delphi, 2017. (cited in pp. 8 and 32)

[91] M V Twigg. "Urea-SCR Technology for deNOx After Treatment of Diesel Exhausts". Technical report, Johnson Matthey Technol, 2015. (cited in p. 32)

[92] Ostertag M. "Urea Reservoir Systems for Off-Highway and Heavy Duty Market". *CTI*, 2008. (cited in p. 32)

[93] Ning J and Yan F. "Detection of Injected Urea Quantity and Correction for SCR Urea Dosing Control". In *SAE 2015 World Congress & Exhibition 2015-01-1038*. SAE International, apr 2015. (cited in pp. 32 and 33)

[94] Birkhold F, Meingast U, Wassermann P and Deutschmann O. "Modeling and simulation of the injection of urea-water-solution for automotive SCR DeNOx-systems". *Applied Catalysis B: Environmental*, Vol. 70 n^o 1, pp. 119 – 127, 2007. (cited in p. 32)

[95] Zhan R, Li W, Eakle S T. and Weber P. "Development of a Novel Device to Improve Urea Evaporation, Mixing and Distribution to Enhance SCR Performance". In *SAE 2010 World Congress & Exhibition 2010-01-1185*. SAE International, apr 2010. (cited in p. 32)

[96] Chatterjee D, Koci P, Schmeisser V, Marek M, Weibel M and Krutzsch B. "Modelling of a combined NOx storage and NH3-SCR catalytic system for Diesel exhaust gas aftertreatment". *Catalysis Today*, Vol. 151 n^o 3, pp. 395 – 409, 2010. Diesel emissions control catalysis. (cited in pp. 32 and 99)

[97] Chi John N. and DaCosta Herbert F. M. "Modeling and Control of a Urea-SCR Aftertreatment System". In *SAE 2005 World Congress & Exhibition 2005-01-0966*. SAE International, apr 2005. (cited in p. 32)

[98] Yuan X, Liu H and Gao Y. "Diesel engine SCR control: current development and future challenges". *Emission Control Science and Technology*, Vol. 1 n^o 2, pp. 121–133, 2015. (cited in pp. 32 and 100)

[99] Skaf Z, Aliyev T, Shead L and Steffen T. "The State of the Art in Selective Catalytic Reduction Control". In *SAE 2014 World Congress & Exhibition 2014-01-1533*. SAE International, 2014. (cited in pp. 32 and 100)

[100] Chi J N. "Control Challenges for Optimal NOx Conversion Efficiency from SCR Aftertreatment Systems". In *SAE World Congress & Exhibition 2009-01-0905*. SAE International, apr 2009. (cited in p. 32)

[101] Devarakonda M, Parker G, Johnson J H., Strots V and Santhanam S. "Model-Based Estimation and Control System Development in a Urea-SCR Aftertreatment System". *SAE International Journal of Fuels and Lubricants 2008-01-1324*, Vol. 1, pp. 646–661, apr 2008. (cited in pp. 32, 33, 191, and 192)

[102] van Helden R, Verbeek R, Willems F and van der Welle R. "Optimization of Urea SCR deNOx Systems for HD Diesel Engines". In *SAE Technical Paper Series 2004-01-0154*. SAE International, mar 2004. (cited in pp. 32 and 38)

[103] McKinley Thomas L. and Alleyne Andrew G. "Model Predictive Control: A Unified Approach for Urea-Based SCR Systems". *SAE International Journal of Fuels and Lubricants 2010-01-1184*, Vol. 3 n^o 1, pp. 673–689, apr 2010. (cited in p. 32)

[104] Schar C M, Onder Christopher H and Geering Hans P. "Control of an SCR catalytic converter system for a mobile heavy-duty application". *IEEE Transactions on Control Systems Technology*, Vol. 14 n^o 4, pp. 641–653, 2006. (cited in p. 32)

[105] Meisami-Azad M, Mohammadpour J, Grigoriadis K M and Harold M P. "An adaptive control strategy for urea-SCR aftertreatment system". In *American Control Conference (ACC), 2010*, pp. 3027–3032. IEEE, 2010. (cited in p. 32)

[106] Devarakonda M., Parker G., Johnson J. H. and Strots V. "Model-based control system design in a urea-SCR aftertreatment system based on NH3 sensor feedback". *International Journal of Automotive Technology*, Vol. 10 n^o 6, pp. 653, Dec 2009. (cited in p. 33)

[107] Hsieh M F and Wang J. "An extended Kalman filter for NO x sensor ammonia cross-sensitivity elimination in selective catalytic reduction applications". In *American Control Conference (ACC), 2010*, pp. 3033–3038. IEEE, 2010. (cited in p. 33)

[108] Herman A, Wu M-C, Cabush D and Shost M. "Model Based Control of SCR Dosing and OBD Strategies with Feedback from NH3 Sensors". *SAE International Journal of Fuels and Lubricants 2009-01-0911*, Vol. 2 n^o 1, pp. 375–385, apr 2009. (cited in pp. 8 and 33)

[109] Willems F, Cloudt R, van den Eijnden E, van Genderen M, Verbeek R, de Jager B, Boomsma W and van den Heuvel I. "Is Closed-Loop SCR Control Required to Meet Future Emission Targets?". In *SAE Technical Paper Series 2007-01-1574*. SAE International, apr 2007. (cited in pp. 8, 33, 34, 37, and 99)

[110] Ma Y and Wang J. "Control of aged automotive selective catalytic reduction systems for consistent performances". *Journal of the Franklin Institute*, Vol. 354 n^o 18, pp. 8094 – 8116, 2017. (cited in p. 33)

[111] Shost M, Noetzel J, Wu M-C, Sugiarto T, Bordewyk T, Fulks G and Fisher G B. "Monitoring, Feedback and Control of Urea SCR Dosing Systems for NOx Reduction: Utilizing an Embedded Model and Ammonia Sensing". In *SAE World Congress & Exhibition 2008-01-1325*. SAE International, apr 2008. (cited in pp. 33 and 100)

[112] Marie-Luce D., Bliman P.-A., Di-Penta D. and Sorine M. "Reduced-Order Models for a LNT-SCR Diesel After-treatment Architecture with NO/NO2 Differentiation". *IFAC Proceedings Volumes*, Vol. 45 n^o 16, pp. 745 – 750, 2012. (cited in p. 33)

[113] Bartley G J., Chadwell C J., Kostek T M. and Zhan R. "SCR Deactivation Kinetics for Model-Based Control and Accelerated Aging Applications". In *SAE Technical Paper 2012-01-1077*. SAE International, 04 2012. (cited in pp. 33, 102, and 151)

[114] Cavataio G, Girard J, Patterson Joseph E, Montreuil C, Cheng Y and Lambert C K. "Laboratory Testing of Urea-SCR Formulations to Meet Tier 2 Bin 5 Emissions". In *SAE Technical Paper Series 2007-01-1575*. SAE International, 2007. (cited in p. 33)

[115] Maunula T., Kallinen K., Savimaeki A. and Wolff T. "Durability Evaluations and Rapid Ageing Methods in Commercial Emission Catalyst Development for Diesel, Natural Gas and Gasoline Applications". *Topics in Catalysis*, Vol. 59 n^o 10-12, pp. 1049–1053, 2016. (cited in p. 33)

[116] Maunula T, Kinnunen T and Iivonen M. "Design and Durability of Vanadium-SCR Catalyst Systems in Mobile Off-Road Applications". In *SAE 2011 World Congress & Exhibition 2011-01-1316*. SAE International, 2011. (cited in p. 33)

[117] Jen H-W, Girard J W., Cavataio G and Jagner M J. "Detection, Origin and Effect of Ultra-Low Platinum Contamination on Diesel-SCR Catalysts". *SAE Int. J. Fuels Lubr. 2008-01-2488*, pp. 1553–1559, 2008. (cited in p. 33)

[118] Upadhyay D and Van Nieuwstadt M. "Model based analysis and control design of a urea-SCR deNOx aftertreatment system". *Journal of dynamic systems, measurement, and control*, Vol. 128 n^o 3, pp. 737–741, 2006. (cited in pp. 33, 186, 191, and 192)

[119] Upadhyay D and Van Nieuwstadt M. "Modeling of urea SCR catalyst with automotive applications". 2002. (cited in pp. 33 and 156)

[120] Hsieh M F and Wang J. "An extended Kalman filter for ammonia coverage ratio and capacity estimations in the application of Diesel engine SCR control and onboard diagnosis". In *American Control Conference (ACC), 2010*, pp. 5874–5879. IEEE, 2010. (cited in pp. 33, 186, 191, and 192)

[121] Pezzini A., Canova M., Onori S., Rizzoni G. and Soliman A. "A Methodology for Fault Diagnosis of Diesel NOx Aftertreatment Systems". *IFAC Proceedings Volumes*, Vol. 42 n^o 8, pp. 911 – 916, 2009. (cited in p. 33)

[122] Matsumoto A, Furui K, Ogiso M and Kidokoro T. "Model-Based OBD Logic Utilizing Adsorption and Desorption Model of NH3 in SCR Catalyst". In *SAE Technical Paper 2016-01-0960*. SAE International, 04 2016. (cited in pp. 8, 33, and 151)

[123] Chen R and Wang X. "Model-Based Fault Diagnosis of Selective Catalytic Reduction Systems for Diesel Engines". *SAE Int. J. Passeng. Cars - Electron. Electr. Syst. 2014-01-0280*, Vol. 7, pp. 449–453, 04 2014. (cited in pp. 33 and 151)

[124] Yong-Wha K and Van Nieuwstadt M. "Threshold Monitoring of Urea SCR Systems". In *SAE 2006 Commercial Vehicle Engineering Congress & Exhibition 2006-01-3548*. SAE International, oct 2006. (cited in pp. 33 and 37)

[125] Wang Y-Y, Sun Y, Chang C-F and Hu Y. "Model-Based Fault Detection and Fault-Tolerant Control of SCR Urea Injection Systems". *IEEE Transactions on Vehicular Technology*, Vol. 65 n^o 6, pp. 4645–4654, 2016. (cited in p. 33)

[126] M Klaus and T Helmut. *Handbook of diesel engines*. Springer-Verlag Berlin Heidelberg 2010, 2010. (cited in p. 34)

[127] Riegel J, Neumann H and Wiedenmann H-M. "Exhaust gas sensors for automotive emission control". *Solid State Ionics*, Vol. 152, pp. 783–800, 2002. (cited in pp. 8, 9, 34, and 138)

[128] Mrosek M, Sequenz H and Isermann R. "Identification of emission measurement dynamics for diesel engines". *IFAC proceedings volumes (IFAC-PapersOnline)*, Vol. 18, pp. 11839–11844, 2011. (cited in pp. 34 and 79)

[129] Blanco-Rodriguez I.D. *Modelling and Observation of Exhaust Gas Concentrations for Diesel Engine Control*. PhD Thesis, Universitat Politecnica de Valencia, 2014. (cited in p. 34)

[130] Alberer D. *Fast Oxygen Based Transient Diesel Engine Control*. PhD Thesis, Johannes Kepler Universitaet Linz, 2012. (cited in p. 34)

[131] El-Awar N, Geer D, Krellner T and Straub P. "Automotive temperature sensing". *Keystone Thermometrics Corporation Application Notes*, 1999. (cited in p. 35)

[132] Dueker H, Friese KH and Haecker WD. "Ceramic aspects of the bosch lambda-sensor". Technical report, SAE Technical Paper 750223, 1975. (cited in p. 36)

[133] Regitz S and Collings N. "Study of cycle-by-cycle air-to-fuel ratio determined from the exhaust gas composition and a novel fast response device based on a wide band lambda sensor". Technical report, SAE Technical Paper 2008-01-2439, 2008. (cited in p. 36)

[134] Chiang C-J, Stefanopoulou A G and Jankovic M. "Nonlinear observer-based control of load transitions in homogeneous charge compression ignition engines". *IEEE Transactions on Control Systems Technology*, Vol. 15 n^o 3, pp. 438–448, 2007. (cited in pp. 3 and 36)

[135] Moos R. "A brief overview on automotive exhaust gas sensors based on electroceramics". *International Journal of Applied Ceramic Technology*, Vol. 2 n^o 5, pp. 401–413, 2005. (cited in pp. 9 and 36)

[136] Moos R and Schoenauer D. "Recent Developments in the Field of Automotive Exhaust Gas Ammonia Sensing". *Sensor letters*, Vol. 6 n^o 6, pp. 821–825, 2008. (cited in p. 37)

[137] Yu Wang D, Yao S, Cabush D and Racine D. "Ammonia Sensor For SCR NOx Reduction". Technical report, DELPHI, 2007. (cited in pp. 38 and 99)

[138] Schoenauer D, Nieder T, Wiesner K, Fleischer M and Moos R. "Investigation of the electrode effects in mixed potential type ammonia exhaust gas sensors". *Solid State Ionics*, Vol. 192 n^o 1, pp. 38 – 41, 2011. (cited in p. 38)

[139] Wang D Y, Yao S, Shost M, Yoo J-H, Cabush D, Racine D, Cloudt R and Willems F. "Ammonia Sensor for Closed-Loop SCR Control". *SAE International Journal of Passenger Cars - Electronic and Electrical Systems 2008-01-0919*, Vol. 1, pp. 323–333, apr 2008. (cited in pp. 9, 38, 99, and 138)

[140] Kong Y, Kozakiewicz T, Johnson R, Huffmeyer C, Huckaby J, Abel J, Baurley J and Duffield K. "Active DPF Regeneration for 2007 Diesel Engines". In *2005 SAE Commercial Vehicle Engineering Conference 2005-01-3509*. SAE International, nov 2005. (cited in p. 38)

[141] Wu Ming-Cheng and Micheli Adolph L. "Calorimetric hydrocarbon sensor for automotive exhaust applications". *Sensors and Actuators B: Chemical*, Vol. 100 n^o 3, pp. 291–297, 2004. (cited in p. 39)

[142] Sahner K, Fleischer M, Magori E, Meixner H, Deerberg J and Moos R. "HC-sensor for exhaust gases based on semiconducting doped SrTiO3 for On-Board Diagnosis". *Sensors and Actuators B: Chemical*, Vol. 114 n^o 2, pp. 861 – 868, 2006. (cited in pp. 8 and 39)

[143] Wiegaertner S, Hagen G, Kita J, Reitmeier W, Hien M, Grass P and Moos R. "Thermoelectric hydrocarbon sensor in thick-film technology for on-board-diagnostics of a diesel oxidation catalyst". *Sensors and Actuators B: Chemical*, Vol. 214, pp. 234–240, 2015. (cited in p. 39)

[144] Hagen G, Burger K, Wiegaertner S, Schoe Kamin D and Moos R. "A mixed potential based sensor that measures directly catalyst conversion a novel approach for catalyst on-board diagnostics". *Sensors and Actuators B: Chemical*, Vol. 217, pp. 158–164, 2015. (cited in pp. 8 and 39)

[145] Walker AP. "Controlling particulate emissions from diesel vehicles". *Topics in Catalysis*, Vol. 28, pp. 165–170, 2004. (cited in p. 39)

[146] Steppan J, Henderson B, Johnson K, Yusuf Khan M., Diller T, Hall M, Lourdhusamy A, Allmendinger K and Matthews R D. "Comparison of an On-Board, Real-Time Electronic PM Sensor with Laboratory Instruments Using a 2009 Heavy-Duty Diesel Vehicle". In *SAE 2011 World Congress & Exhibition 2011-01-0627*. SAE International, apr 2011. (cited in p. 39)

[147] Kamimoto T. "A review of soot sensors considered for on-board diagnostics application". *International Journal of Engine Research*, 2016. (cited in pp. 8 and 39)

[148] Blanco-Rodriguez D., Vagnoni G. and Holderbaum B. "EU6 C-Segment Diesel vehicles, a challenging segment to meet RDE and WLTP requirements". *IFAC-PapersOnLine*, Vol. 49 n^o 11, pp. 649 – 656, 2016. 8th IFAC Symposium on Advances in Automotive Control AAC 2016. (cited in pp. 10 and 39)

[149] Twigg M V. "Progress and future challenges in controlling automotive exhaust gas emissions". *Applied Catalysis B: Environmental*, Vol. 70 n^o 1, pp. 2 – 15, 2007. (cited in p. 39)

[150] Twigg M V. "Cleaning the Air We Breathe - Controlling Diesel Particulate Emissions from Passenger Cars". *Emission Control Technologies*, 2009. (cited in p. 40)

[151] Henry C, Gupta A, Currier N and Ruth M. "Advanced Technology Light Duty Diesel Aftertreatment System". Technical report, Cummins, 2012. (cited in p. 40)

[152] Malanga M T, Allen, M P Das, N S Kotnis, A Mikulic, I Vosejpka and P C Majkowski. "Future Trends for DPF....SCR on-Filter (SCRF)". Technical report, DEER Conference, 2012. (cited in p. 40)

[153] Tourlonias P and Koltsakis G. "Model-based comparative study of Euro 6 diesel aftertreatment concepts, focusing on fuel consumption". *International Journal of Engine Research*, Vol. 12 n^o 3, pp. 238–251, 2011. (cited in pp. 40 and 139)

[154] Schnitzler J. "Particulate Matter and NOx Exhaust Aftertreatment Systems". *FEV Motorentechnik GmbH*, 2006. (cited in p. 40)

[155] Theis J R., Dearth M and McCabe R. "LNT+SCR Catalyst Systems Optimized for NOx Conversion on Diesel Applications". In *SAE 2011 World Congress & Exhibition 2011-01-0305*. SAE International, apr 2011. (cited in p. 40)

[156] Chen P. *Modeling, Estimation and Control of Integrated Diesel Engine and Aftertreatment Systems*. PhD Thesis, The Ohio State University, 2014. (cited in p. 40)

[157] Alkemade U G. and Schumann B. "Engines and exhaust after treatment systems for future automotive applications". *Solid State Ionics*, Vol. 177 n^o 26-32, pp. 2291 – 2296, 2006. (cited in pp. 6 and 41)

[158] Guardiola C, Martín J, Pla B and Bares P. "Cycle by cycle NOx model for diesel engine control". *Applied Thermal Engineering*, Vol. 110, pp. 1011–1020, 2017. (cited in p. 42)

[159] Arsie I, Marra D, Pianese C and Sorrentino M. "Real-Time Estimation of Engine NOx Emissions via Recurrent Neural Networks". *IFAC Proceedings Volumes*, Vol. 43 n^o 7, pp. 228 – 233, 2010. 6th IFAC Symposium on Advances in Automotive Control. (cited in p. 42)

Chapter 3

System setup and measurement systems

Contents

3.1 Introduction

This chapter presents the setups used to perform the experimental tests and measurements, as well as a description of the kind of tests done. There are three main setups, namely A, B and C, in which a Diesel engine is used as a gas generator and a set of measurements is focused on the ATS. The setup A has a Diesel engine with a DOC, coupled to a test bench; the setup

Table 3.1. *Setup A engine main characteristics.*

Stroke (S) x Bore (D)	88x85 mm
Displacement	1997 cc
Compression ratio	16:1
Number of cylinders	inline 4
Valves by cylinder	4
Maximum torque	340 Nm @ 2000 rpm
Emissions standard	Euro 5

B has a Diesel engine to generate the gases, while the ATS is simulated in a detailed ATS modelling suite; and the Setup C has two variants, including test bench experiments in C.1 and vehicle tests in C.2. On the other hand, the experimental tests performed are classified as steady-state, dynamic and dedicated tests.

3.2 Experimental setups

The different experimental setups are described in this section. While setup A is dedicated to DOC experiments, setups B and C are dedicated to SCR experiments. For this purpose, in setups A and C.1, the CI engine is controlled through a bypassed ECU and a rapid prototyping system (RPS) that allows the execution of HIL tests, while in setups B and C.2, the engine is used with the original manufacturer calibration.

3.2.1 Setup A

The experimental core used in this study is a 2 liter CIDI engine placed in a test bench, which follows the Euro 5 emission standards, and it has a DOC as ATS. A table containing its relevant characteristics is presented in Table 3.1, while Figure 3.1 shows the system layout. The engine has an intercooled EGR and a VGT, while a throttle valve is present to bypass the air through the EGR cooler in case higher temperatures are required, i.e. in situations such as warm-up or DPF regeneration.

The water cooling system of the engine varies from the original, present in the vehicle: the air-to-liquid cooling system is replaced by a liquid-to-liquid, while the air cooling system after the compressor is replaced from an air-to-air

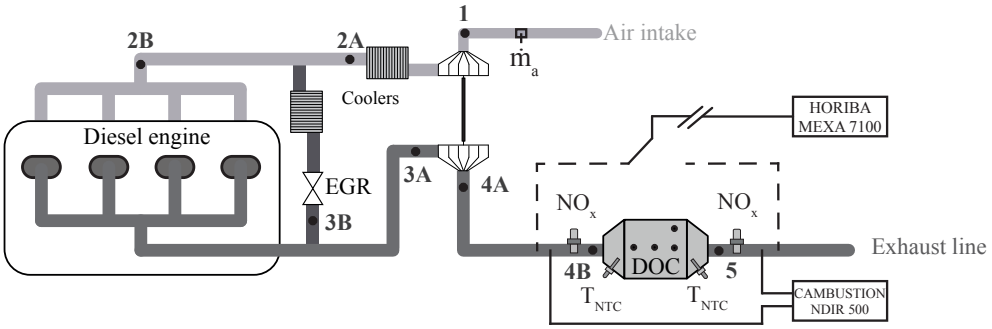

Figure 3.1. *Scheme of the engine, ATS and measurements of setup A. Dots stand for relevant measurements locations along the engine air path, which are specifically described in Table 3.3.*

system to an air-to-liquid system. The temperature of the coolant flow at the intercooler is kept constant by means of cooling system regulated with a PID. The EGR coolers were not replaced and the original air-to-liquid system was conserved. The performed changes are normal for test bench installed engines, and their effect on the engine performance is negligible for the purpose of the work presented.

Engine control

The engine control is performed by an open Delphi ECU under the manufacturer calibration. The ECU has an ETK port to stream data and bypass key signals from an external ETAS apparel. While the control of the fuel injection is done through look-up tables depending on the engine speed and pedal position, the control of the air path is more complex, having the EGR valve and the VGT position as the two main actors. The fuel strategy that the ECU is able to perform consists of two pilot, a main and two post-injections. Pilot injections, scheduled to reduce engine noise and vibrations represent, generally represent betwen 1 and 5% of the total injected amount and the post-injections are disabled during normal operating conditions, but they are fundamental for injecting raw HC into the exhaust line. SOI is set according to calibrated values, for which the crankshaft position sensor allows schedulling all necessary injection events at the specified angles. For the specific case of the post-injections, a constant angle of -155 BTDC is used.

Due to the coupling between EGR and VGT, closed-loop control is performed over one of the two actuators, so it is not done simultaneously. In fact, two control modes exist, which depend on the engine operating point. At low load and low speed conditions, in which the EGR valve has a crucial effect over NO_x emissions, the EGR valve is regulated in closed-loop control over the air mass flow, in order to achieve the desired quantity through a PID controller. In this case, the VGT positions control is determined by open-loop pre-calibrated look-up tables, producing an intake manifold pressure that is not controlled. When the VGT is controlled with closed-loop control over the intake pressure, the EGR valve is closed, which happens at high loads and high engine speeds. In this case, the VGT position control is also done with calibrated PIDs. In both cases, an actual measurement of the actual actuator position feeds the closed-loop control in each case. Finally, note that all calibrations are subjected to corrections due to warm-up phases, temperature, ambient conditions, etc.

3.2.1.1 DOCs with different failure modes

The ATS of this experimental setup contains a DOC as the only AT block in the exhaust line. However, this DOC is replaced when necessary with other DOCs with different ageing levels. In this sense, and for the sake of clarification, only one DOC is placed in the exhaust line at the same time. The set of DOCs used is described in Table 3.2, while the external appearance, as well as the measurements for one catalyst are sketched in Figure 3.1. The available parts have different failure modes, whose particularities are experimentally assessed in Chapter 4. The structure of the catalyst is composed of a ceramic monolith, surrounded by an isolation layer, which is placed between the monolith and the external canning. In order to limit the heat losses, another external layer is added over the canning and around the monolith area.

All catalysts had the same specifications in brand new conditions, apart from the non-impregnated, which followed a different construction procedure, in which the impregnation layer was not inserted. Then, different ageing procedures were applied to the catalysts. In this sense, while the nominal, the aged and the non-impregnated catalysts are different parts, the new catalyst is transformed firstly into DOC_{70} and then into DOC_{40}. Therefore, the necessary tests were done to the new catalyst before starting the DOC_{70} and DOC_{40} mechanization processes. Note that only the nominal and aged parts have the research thermocouples placed along the catalyst length, as shown in

Table 3.2. *DOCs used in experimental setup A.*

	Impregnation	L_m [cm]	Oven hours	Use hours
New	Pt-Pd	10	-	-
Nominal	Pt-Pd	10	-	800
Aged	Pt-Pd	10	25	-
DOC_{70}	Pt-Pd	7	-	-
DOC_{40}	Pt-Pd	4	-	-
Non-impregnated	-	10	-	-

Figure 3.1, while the new DOC is not instrumented with these thermocouples in order to ease the mechanization process.

The nominal catalyst is a catalyst with hundreds of hours of use, without presence of high temperature phases, i.e. without exceeding 600°C. On the other hand, an artificial ageing procedure was applied to the aged catalyst through exposure to high temperatures, i.e. temperature over 800°C during 25h hours in an oven. On the other hand, the DOC_{70} and DOC_{40} DOCs followed a mechanization procedure, removing the back part of the catalyst, in order to characterize its effective length. In this case, due to the homogeneous properties of the monolith, the effective length is considered instead as an effective area A_{eff}. Thereby, the effect of effective area A_{eff} decrease can be contrasted with the efficiency decrease.

The mechanization procedure to obtain the DOC_{70} and DOC_{40} consisted in opening the external canning and removing a slice of 30% length of the catalyst monolith. In the first phase, after removing the first 30% slice, the DOC_{70} was obtained. Then, after doing all necessary tests, the process was done again for the DOC_{40}, removing another 30% slice of the monolith. The portion of the monolith that was removed was at the back part, in order to maintain the distance from the cylinders to the DOC inlet and do not affect the temperature of the exhaust gases entering the DOC. Figure 3.2 represents this structure. Then, the DOC canning was welded again in each of the cases, so that the external dimensions of the brand new DOC are kept.

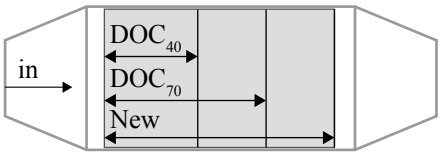

Figure 3.2. *Scheme of the new, DOC_{70} and DOC_{40} catalyst lengths.*

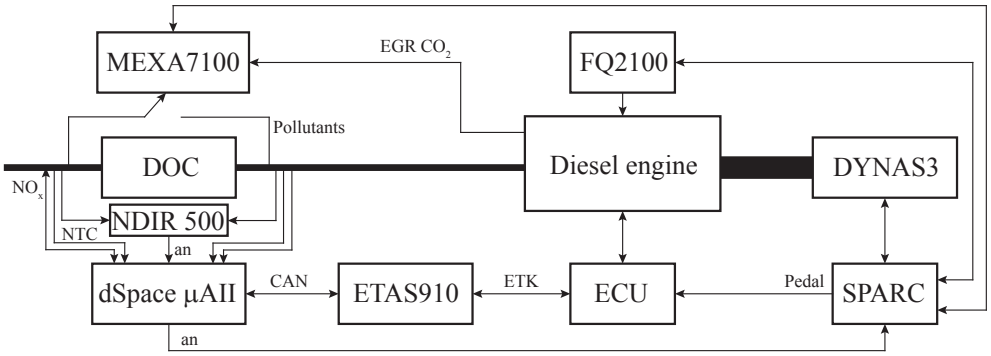

Figure 3.3. *Scheme of the HIL system, where an stands for analogic signal.*

3.2.1.2 Engine bench control system layout

The engine is coupled to an asynchronous Horiba DYNAS 33 dynos, which is able to perform steady-state, transient and dynamic tests, and it is controlled with a Horiba SPARC, which is controlled at the same time with the PC interface Horiba STARS. While the steady-state and transient tests are done with pre-defined engine operating points, the dyno is able to follow a speed trajectory by means of a vehicle model for the dynamic tests, named as road load simulation (RLS).

Hardware-in-the-loop tests The system used to perform HIL tests in the engine is next described. Figure 3.3 shows the connections among the employed hardware, mainly composed of the ECU, an ETAS 910 and a RPS dSpace Microautobox II, through which relevant sigals can be generated in the dSpace system and bypassed with the open ECU. The test bench apparatus such as the fuel balance FQ2100 and the gas analyzer (GA) Horiba MEXA

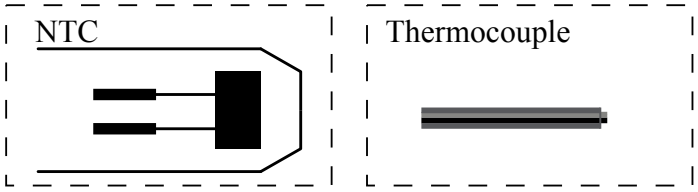

Figure 3.4. *Scheme of the temperature sensors layout.*

7100 series are connected to the STARS interface. Then, as in Figure 3.3, the NTC sensors and the Cambustion NDIR 500 gas analyzer are connected to the RPS dSpace by analogic signal, while the NO_x sensors are connected to the RPS dSpace by CAN protocol.

The injection strategy is adapted in order to inject raw fuel in the exhaust line through late post-injections. For this puspose, the the post-injections signals are generated from the RPS dSpace and sent to the ECU. On the other hand, the EGR valve position and the SOI are also bypassed, mainly to generate different levels of NO_x concentrations.

Regarding the data recording, the use of different systems to record data implies that three different files are obtained for each experiment in this setup, i.e. from dSpace, STARS and ETAS. In order to be able to phase afterwards the different files, the RPS dSpace triggers a square signal, which allows phasing then in post-processing.

3.2.1.3 Measurements acquisition and characterization

An exhaustive set of measurements is employed around the DOC, apart from several measurements also placed in the engine, as can be seen in Figure 3.1. The available measurements are ordered in Table 3.3 for the own engine measurements and the additional measurements present at the test bench. Temperatures and concentrations are the main focus, so they are explained in detail next, but air path pressures are also acquired and the intake mass flow is measured by the hot film flow meter of the engine and by a sensi-flow in the test bench.

Temperatures are measured by thin thermocouples in the test bench, whose structure is compared against the NTC sensors in Figure 3.4. Due to the

Table 3.3. *Scheme of relevant signals measured in Setup A. While columns stand for measurements: temperature, pressure, position, mass flow, rotational speed, λ and species concentrations; rows denote measurements locations at the engine according to the nomenclature in Figure 3.1. Engine own instrumentation is shown with black dots and bench instrumentation in gray dots.*

	T	P	Pos	$\dot{m}$	n	λ	Species
1	●●	●●		●●			
2A	●	●					
2B	●●	●●					
3A	●	●					
3B	●	●					
4A	●	●					
4B	●●	●				●●	●
DOC	●						
5	●●	●				●	●
CR	●	●		●			
EB	●●	●			●●		
EGR			●				
VGT			●				
Pedal			●				

lower weight of these sensors, its measurement is faster than the NTC, as it was shown in Figure 2.5, however, sometimes they can break and need to be replaced. Another fact of importance is their location in the exhaust line. Due to convection, conduction and radiation heat transmission, the measured signal can vary depending on the exact location of the sensor. For this reason, the thermocouples are set close to the NTC sensors, and their measuring location is centered in the axial section, although even so differences may appear, as shown in Figure 3.5. In this sense, the location of the NTC sensors is in accordance to their on-board place, in order to have the same lectures than once the ATS is installed in the vehicle.

The NTC sensor used is a Denso unit, able to measure in a range of temperatures from -30°C to 1000°C with standard responsiveness, whose error is ±7°C at mid temperatures and ±10°C at low and very high temperatures, according to the sensor manufacturer. However, no information is availble from manufacturers of NTC and thermocouples about their response time.

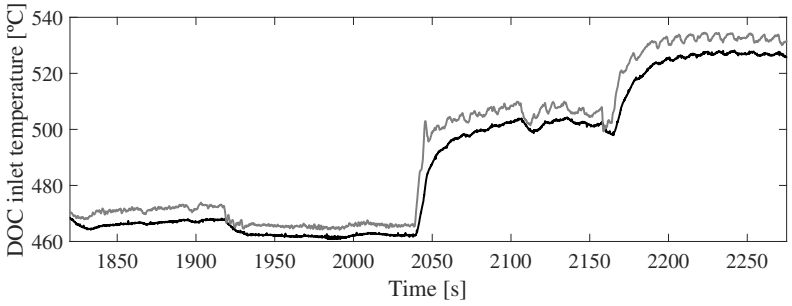

Figure 3.5. *Temperature measurements at the DOC inlet, in order to compare the effect of the location in the exhaust line between the thermocouple and the NTC sensor. Despite evident differences in dynamics, it is not the focus in this case. The black line stands for the NTC measurement, and the grey line stands for the thermocouple measurement.*

Concentrations

For the concentrations measurements in the test bench, the Horiba MEXA 7100 DEGR GA is used to measure HC, CO, NO_x, NO, CO_2 and O_2 [1], at one point of the exhaust line. For this reason, several tests are repeated in order to have the gas concentrations measurements up- and downstream the DOC. This apparatus employs several techniques, being the heated vacuum-type flame ionization detector (HFID) used for the HC, the non-dispersive infrarred (NDIR) for the NO_x and the heated flame ionization detector (HFID) for the CO, while an EGR probe allows measuring the CO_2 to calculate the actual EGR fraction. Note that the HC are measured as methane based HC, so the gas analyzer is able to provide non-methane HC (NMHC) and total HC (THC).

The Horiba GA measurement has a delay in its measurement due to the length between the samples probe and the measuring system. In this sense, the measurement process can also add an extra delay. This problem is corrected with a pure delay of 6 seconds, whose result can be appreciated by means of NO_x steps in Figure 3.6. In order to have fast measurements and avoid delays and bias problems due to dynamics, a faster gas analyzer may be used in specific tests. For this purpose, the Cambustion NDIR 500, with a response time of about 7 ms, is used.

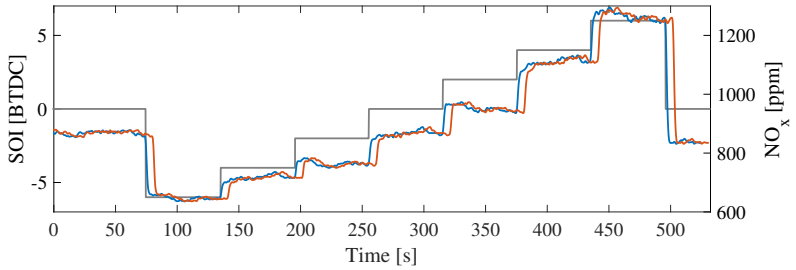

Figure 3.6. *Delay of the Horiba GA measurement in comparison with SOI steps (in grey), where the original measurement is orange and the corrected signal is in blue.*

NO_x sensors A set of steady-state NO_x measurements of the up- and downstream NO_x sensors is presented in Figure 3.7 in comparison with the Horiba GA measurement. Two different lines are fitted to each sensor, being therefore a different resulting equation for each, represented next:

$$NO_{x,sen}^{us,corr} = 0.9936 \cdot NO_{x,gasanalyzer}^{us} \tag{3.1}$$

$$NO_{x,sen}^{ds,corr} = 1.032 \cdot NO_{x,gasanalyzer}^{ds} \tag{3.2}$$

where $NO_{x,gasanalyzer}$ corresponds to the Horiba gas analyzer measurement and $NO_{x,sen}^{us,corr}$ and $NO_{x,sen}^{ds,corr}$ correspond to the upstream and downstream NO_x sensors measurements, respectively.

On ther other hand, as can be appreciated in Figure 3.8, the λ measurements of the NO_x sensors also present an offset between them in steady state conditions, fact that is represented in Figure 3.8, in which the points come from the engine operating points in Figure 3.11. In this case, the offset is constantly positive, while the dispersion is higher at low λ^{-1} values than at high values, reaching values of up to 0.023. In fact, at high λ^{-1} values, the tendency is to reduce the offset, due to the higher accuracy of λ measurements at richer conditions [2].

As it happens with temperature measurements, concentration sensors may be not fast enough to measure exhaust gas changes in highly transient conditions. However, this supposes a problem, since the contribution of the transient emission peaks during the standardized test cycles becomes is an important fraction of the cumulative total emissions [3]. In this sense, the problem of the dynamic response of concentration sensors has been addressed during last

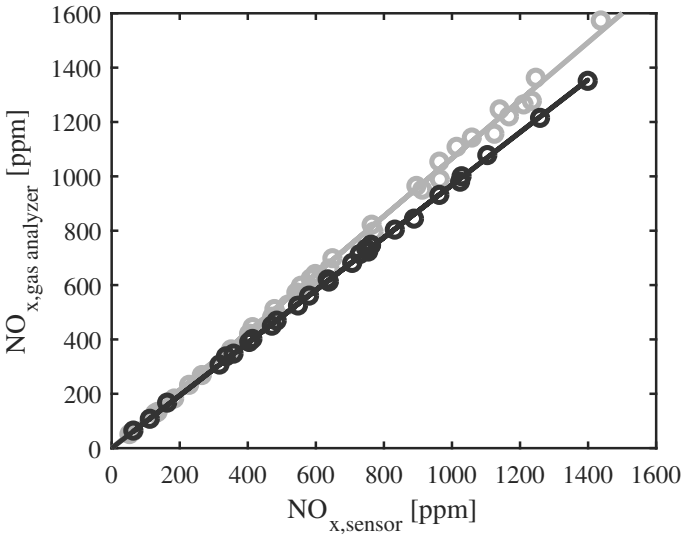

Figure 3.7. *NO_x sensors calibration, where circles are experimental values and lines are correction functions. — Upstream sensor — Downstream sensor. .*

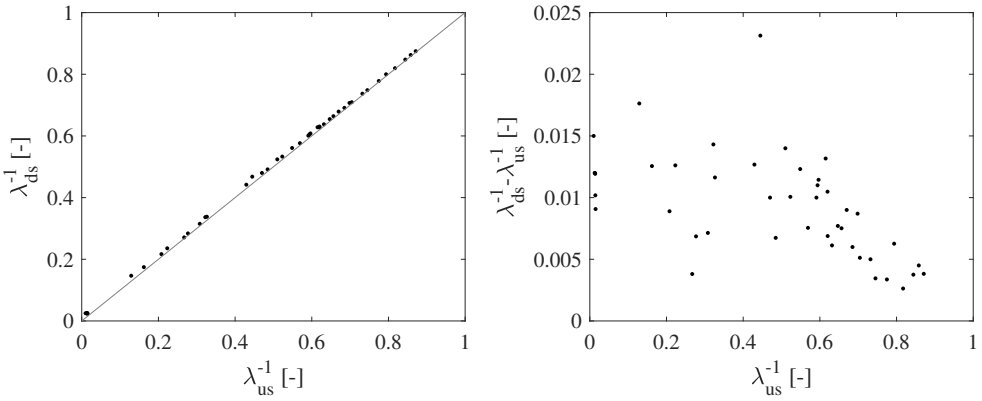

Figure 3.8. *Offset of up- and downstream λ sensors, with an average difference of 0.01.*

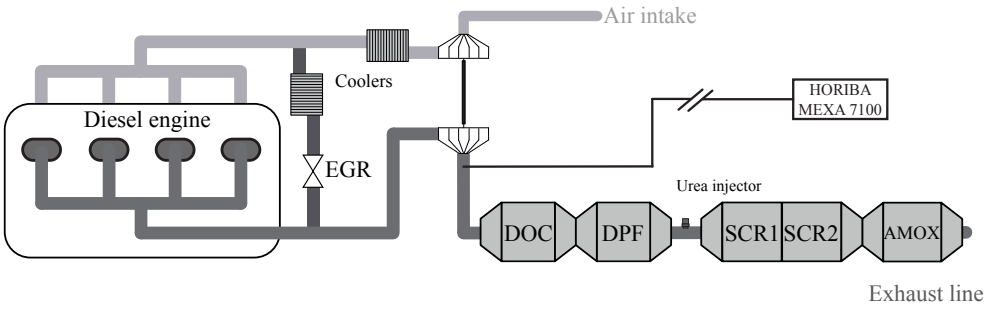

Figure 3.9. *Scheme of the physical engine and the simulated ATS of setup B.*

years in the automotive industry with the combination of sensors measurements and models estimations in order to rebuild the signal [4]. Authors like [5] and [6] have researched Diesel engine exhaust O_2 and NO_x concentrations with special focus in transient conditions through the use of UEGO and NO_x sensors. These authors have determined a wide methodology of data fusion from sensors and models by using filtering techniques in order to have fast estimations of exhaust gas concentrations.

3.2.2 Setup B

The core of Setup B is a Euro VI heavy duty engine. In this setup, the engine is used as a gas generator, in order to have raw exhaust gas measurements temperature, O_2 NO_x, NO, NO_2, CO_2, THC and CO. Then, a detailed modelling suite [7–9] is applied in order to have the schematic after-treatment shown in Figure 3.9, in which all modelled signals are available along the exhaust line.

Urea dosing control Despite the fact that for the purpose of this dissertation the urea dosing strategy is not the focus, since the focus is instead given to the downstream measurements. However, it is useful to know how the urea is injected in order to understand the operation of the SCR. In this sense, the urea dosing strategy of this setup is done following a closed-loop control considering NO_x and NH_3 measurements, in which the target is to reduce NO_x emissions to the desired level and keep an acceptable NH_3 slip that minimized the AdBlue consumption [8].

In this, the Ammonia to NO_x ratio (ANR), as the NH_3 molecules introduced per NO_x molecule, transformed into the nominal stoichiometric ratio (NSR) is mapped in steady-state to keep the NH_3 slip below 10 ppm, with dependence on space velocity (SV) and temperature T_{SCR}. However, the NSR map is also strongly dependent on the NO_2/ NO_x ratio, the absolute NO_x level and the catalyst dimensions. With the NH_3 slip limitation, the urea dosing is set according to the tailpipe NO_x target and the measured NO_x engine raw emissions, through a stoichiometric conversion and the estimated ammonia coverage ratio, for which a real-time model is necessary. Even so, a remaining transient compensation factor needs still to be included, which depends on the temperature of the SCR in combination with its derivative, in order to prevent excessive NH_3 slip peaks. In order to refine the dosing strategy, a NH_3 oxidation compensation factor, based on a SV and T_{SCR} map, is included, which prevent the oxidation of NH_3 at high temperatures.

For the closed-loop control, the NH_3 and NO_x measurements are considered to be available, and the cross-sensitivity of the NO_x sensor is compensated with the NH_3 measurement. With the information from the sensors, the NH_3 storage map is adapted according to if the measured slip is higher or lower than expected. In order to increase the closed-loop control efficiency, since NH_3 slip is necessary, the NH_3 sensor is placed in the middle of the SCR catalyst.

3.2.3 Setup C.1

The reason of separating setup C into Setup C.1 and Setup C.2 is that both setups share a common engine. While in the setup C.1 the Diesel engine is coupled to a test bench, in the setup C.2 the Diesel engine is part of a vehicle. The Diesel engine used in both cases is a CIDI 1.5 litres engine and incorporates a state-of-the art ATS. The fuel injection is done through look-up tables depending on the engine speed and pedal position, and the air path is controlled following a similar strategy for the EGR and VGT. However, the injection strategy differs from engine A since this engine is able to perform two pilot injections, two main and two post-injections, while the purpose of each injection remains the same.

As in the Setup A, the ECU has an ETK port to read and bypass the relevant signals. In fact, the engine control is mostly similar to that of the

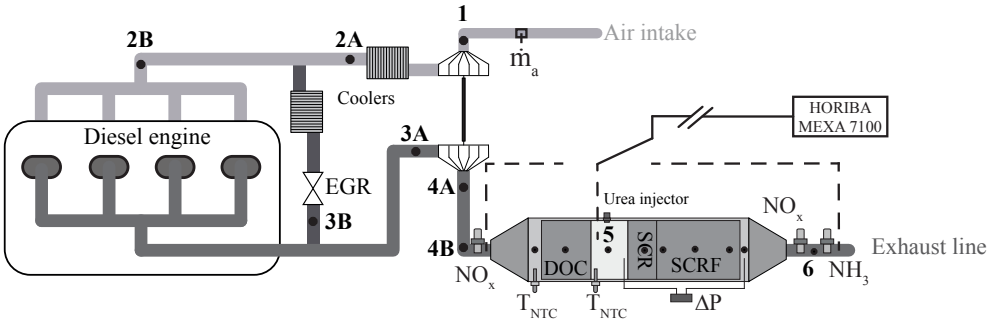

Figure 3.10. *Scheme of the engine, ATS and measurements of setup C.2. Dots stand for temperature measurements along the engine air path, which are specifically described in Table 3.4.*

engine A. The rapid prototyping technique used for the engine A is similarly used at the test bench in Setup C.2. In this, the RPS dSpace is connected to the ETAS 910, which is at the same time connected to the engine ECU, in order to perform ECU bypass. However, in this case, the sensors connection is different, since two up- and downstream DOC NTC sensors, two up- and downstream the ATS NO_x sensors and the up- and downstream SCR-SCRF differential pressure sensor are connected to the ECU, while an NH_3 sensor is connected to the RPS dSpace, as shown in 3.10. The urea injection system, composed of a tank with a compressor that pressurizes the line until the injector, and a solenoid that enables the urea flow through the injector are controlled by the ECU.

The main difference for the work presented relies on the fact that a new ATS is used in Setup C.1, while an aged ATS is used in Setup C.2. Besides, different calibrations are used in both cases by means of the same Bosch ECU, being the engine raw emissions of setup C.1 higher in order to stress the efficiency of the new SCR.

The ATS is composed of a compacted DOC*and*PNA, urea injector, SCR and SCRF system, in which two NTC sensors, two NO_x sensors, a pressure differential sensor and an NH_3 sensor are present. The engine has an intercooled EGR system and a VGT, with a throttle to bypass the air through the EGR cooler in case higher temperatures are required, as in the case of the Setup A engine. A table containing its relevant characteristics is presented in

Table 3.4. *Scheme of relevant signals measured in Setups C.1 and C.2. While columns stand for measurements: temperature, pressure, position, mass flow, rotational speed, λ and species concentrations; rows denote measurements locations at the engine according to the nomenclature in Figure 3.10. Engine own instrumentation is shown with black dots and bench instrumentation in gray dots.*

	T	P	Pos	$\dot{m}$	n	λ	NO_x	Species
1	●●	●●		●●				
2A	●	●						
2B	●●	●●						
3A	●	●						
3B	●	●						
4A	●							
4B	●●	●				●●	●●	●
DOC	●							
5	●●	●						●
SCR	●							
SCRF	●							
6	●●					●		●
CR	●	●		●				
EB	●●	●			●●			
EGR			●					
VGT			●					
Pedal			●					

Table 3.5, while Figure 3.10 shows the engine layout.

3.2.4 Setup C.2

The use of an engine bench to couple the engine of Setups C.1 and C.2 in Setup C.2 allows the use of a Horiba Mexa gas analyzer. In this case, the gas analyzer is the same than that described previously for Setup A. Besides, the rest of auxiliaries of the test bench like the engine dyno are also shared with Setup A, so the reader is referred to the previous section for further information.

Table 3.5. *Engine C.1 and C.2 main characteristics.*

Stroke (S) x Bore (D)	84.8 x 75 mm
Displacement	1498 cc
Compression ratio	16:1
Number of cylinders	inline 4
Valves by cylinder	4
Maximum torque	300 Nm @ 1750 rpm
Emissions standard	Euro 6

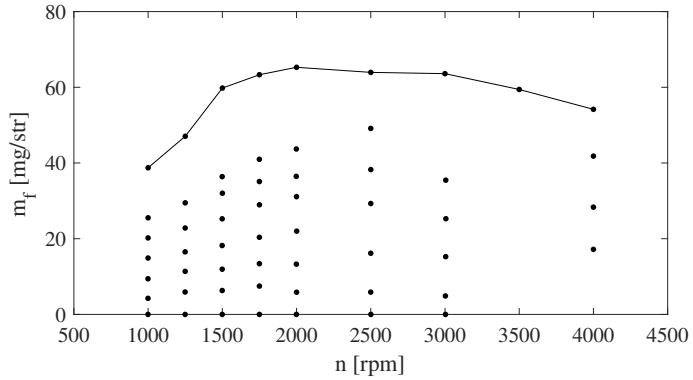

Figure 3.11. *Selected points of the steady-state engine characterization of setup A. While dots stand for operating points, the line stands for the full load curve. The poins density is higher for the operation area of the regulation tests.*

3.3 Engine tests

In this dissertation, several tests are presented, which are divided into steady-state tests, dynamic tests and dedicated tests. In the engine testing campaign, the relevant tests are repeated for catalysts with different ageing levels, in order to assess the catalysts ageing. With these tests, it is possible to determine the engine and the ATS operation, the ATS ageing and the development, calibration and validation of models and diagnostics functions. When necessary, the tests are repeated twice to measure up- and downstream with the Horiba GA.

3.3.1 Steady-state tests

A set of steady-state tests is done to characterize the engine and the ATS in constant conditions, which allows mapping their operation. In addition, a

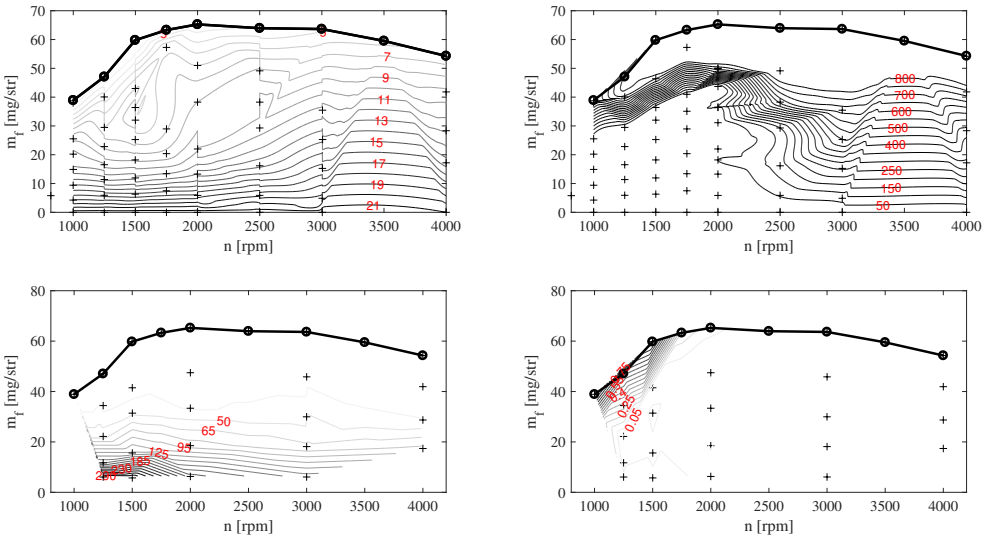

Figure 3.12. *CIDI emissions profile for O_2 [%], top left, NO_x [ppm], top right, THC [ppm], bottom left, and CO [%], bottom right. While the crosses stand for the measured operating points of the map, the black line connects the full load engine operating points.*

constant measurement allows to track offsets between system measurements. For these tests, a discrete and wide range of engine speed and pedal positions is used, which is shown in Figure 3.11 for setup A.

As a result of the engine steady-state tests, the emissions of a CIDI engine are shown in Figure 3.12, where the oxygen concentration decreases as the load increases, being scarce at low speed and high loads, the NO_x emissions are contained in the regulations area due to high EGR rates, the HC emissions are major at low load and low speed due to low temperatures and the CO emissions are high at high loads and low speeds due to incomplete combustion because of lack of oxygen. In the case of CO emissions, transient operation conditions have a major importance in its formation, since during strong accelerations, the fuel path is able to provide extra fuel, but the air path needs more time, during which interval peaks of CO appear due to lower oxygen concentrations than desired.

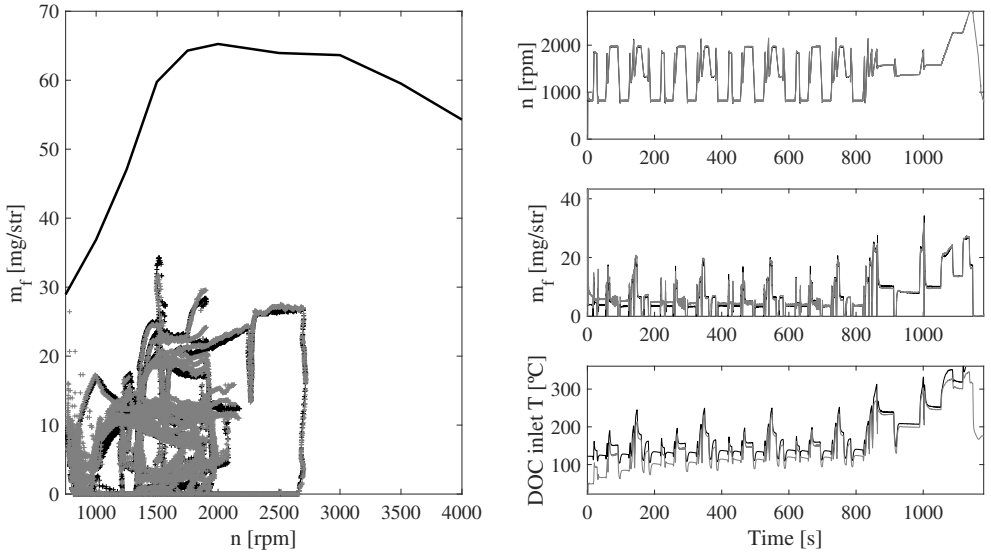

Figure 3.13. *NEDC performed by engine A at ambient, gray, and warm, black, starting conditions. Thick blac line stands for engine full load.*

3.3.2 Dynamic tests

The inclusion of dynamic tests is fundamental to calibrate and validate models and diagnostics functions of the ATS, as well as to characterize its operation. For this purpose, tests alternating engine operating points, along with regulation tests like the NEDC and the WLTC are performed. However, note that the purpose of the regulation tests performed is to have a database of dynamic cycles, while it is not neither the validation with an exact correspondence with the regulation procedures nor the validation of the systems used.

NEDC The NEDC is presented in Figure 3.13 with the engine A at both ambient and warm starting conditions. The test contains a first urban phase with four repetetions of a block in the range of time from 0 to 800 s, in which four temperature peaks can be appreciated. Then, a noticeable power demand in the extra urban part increases the temperature [10]. In the plot, it can be appreciated how the engine demand covers low load and low engine speed conditions, which are not sufficient to warm-up the engine at cold starting and equate the last extra-urban part of the test at warm starting.

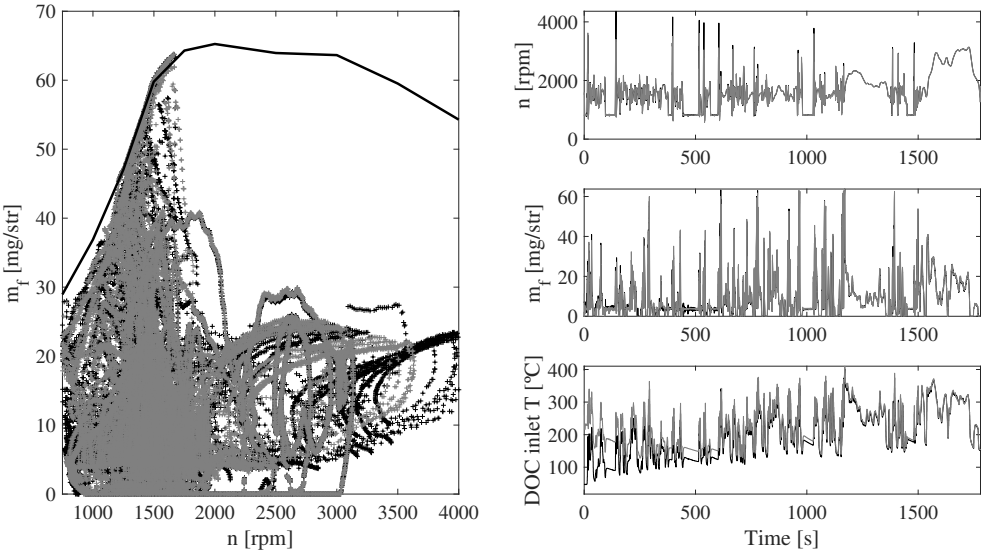

Figure 3.14. *WLTC performed by engine A at ambient, black, and warm,gray, starting conditions. Thick blac line stands for engine full load.*

WLTC The WLTC performed by the engine A is presented in Figure 3.14 at both ambient and warm starting conditions. This test is more demanding in terms of engine load and dynamics than the NEDC. In it, the four driving patterns present in the test are sketched, i.e. low, medium, high and extra high phases. Each phase has different dynamics, while the phases are sorted by increasing power demand. In this test, the differences between the cold starting and warm starting tests are minimized from the medium phase, in which measured temperatures are similar for both ambient and warm starting conditions.

Dynamic tests Dynamic tests, including a wide range of engine operating points are done in order to generate temperature steps. As it can be appreciated in Figure 3.15, the engine operating points include full load points alternated with other lower load points, which results in the temperature steps ranging from 200 to 600°C. As a representation of the 4 tests that alternate the same operation points, two tests are presented in Figure 3.15.

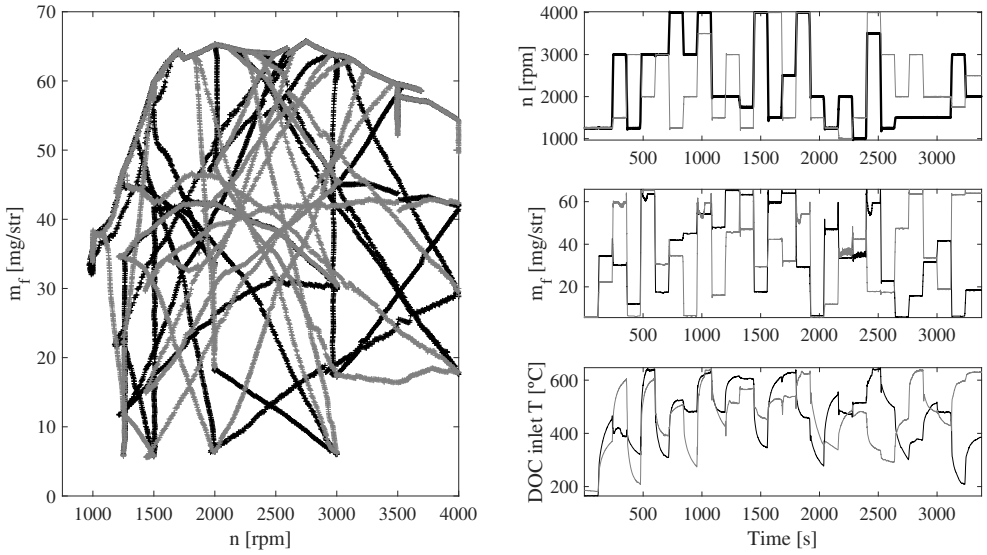

Figure 3.15. *Dynamic tests performed by engine A stressing the steps of temperature at the DOC inlet..*

WHTC The WHTC, as the WLTC version for heavy-duty engines, is done with the engine B. As in Figure 3.14 for the WLTC, the four phases are included in Figure 3.16 for the WHTC.

RDE A database with RDE tests like the one presented in Figure 3.17 is used to characterize the SCR operation and to calibrate and validate a control-oriented SCR model. These tests are performed by the engine of setup C.2, having a target of exhaust temperatures between 200 and 500°C, and inluding start&stop phases as well as several urea injection cases.

3.3.3 Dedicated tests

A set of dedicated tests to analyze and characterize the behaviour of parts with different ageing levels will be presented throughout the dissertation. These tests will include special conditions managed by the RPS in which the main functionalities of the catalysts are stressed. Several cases can be found in Chapter 4, in which the experimental characterization requires dedicated tests to stress catalysts characteristics.

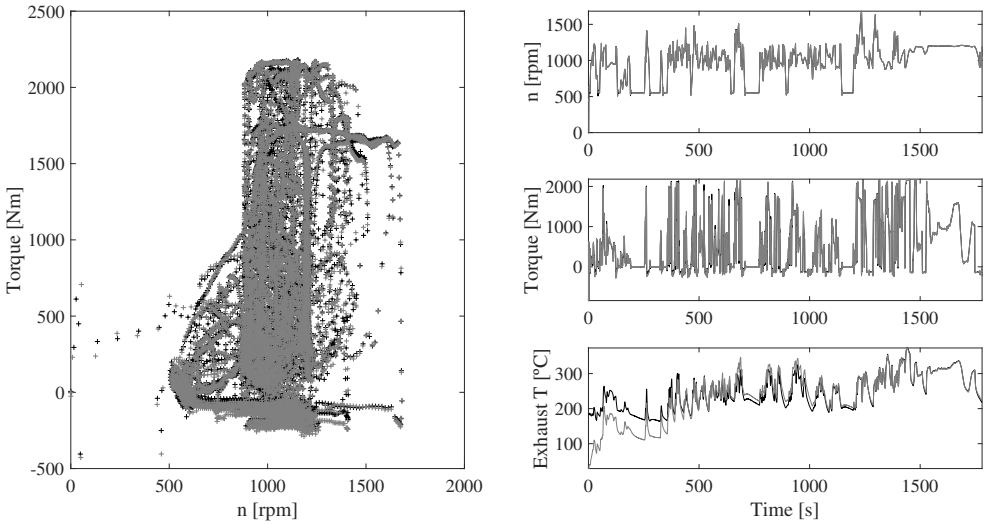

Figure 3.16. *WHTC performed by engine B at ambient, gray, and warm, black, starting conditions.*

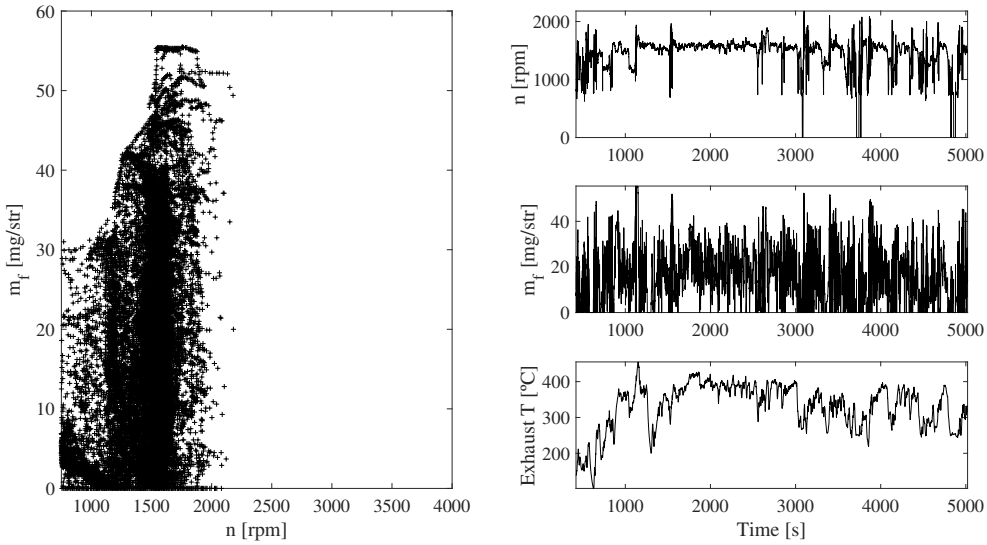

Figure 3.17. *RDE test performed with vehicle of setup C.1.*

3.4 Conclusions

Different configurations of after-treatment systems have been presented in order to collect the necessary data, in which the setup A is dedicated to DOC activities, while setups B and C are dedicated to SCR activities. In the case of setups A and C.1, an exhaustive measurement acquisition system is incorporated to analyze the behaviour of the after-treatment systems. The ATS measurements setup includes NO_x sensors, NTC sensors, Horiba MEXA 7100 DEGR gas analyzer, fast measurements Cambustion NDIR 500, thin thermocouples and NH_3 sensors. On the other hand, the engine setup B is used to generate gases that are then used to feed a detailed modelling AT suite. Finally, the setup C.2 is used to have a wide set of cases with RDE and the on-board sensors, with focus on SCR and including NO_x and NH_3 sensors.

References

[1] HORIBA. "Horiba MEXA-7100DEGR Instruction Manual". Technical report, Horiba, 2011. (cited in p. 63)

[2] Nieuwstadt M Van, Upadhyay D and Yuan F. "Diagnostics for Diesel Oxidation Catalysts". In *SAE Technical Paper 2005-01-3602*. SAE International, 2005. (cited in pp. 26, 64, and 164)

[3] Alberer D and del Re L. "Optimization of the transient Diesel engine operation". In *SAE Technical Paper 2009-24-0113*. Consiglio Nazionale delle Ricerche, 2009. (cited in pp. 64, 78, and 108)

[4] Del Re L, Allgöwer F, Glielmo L, Guardiola C and Kolmanovsky I. *Automotive model predictive control: models, methods and applications*, volume 402. Springer, 2010. (cited in pp. 66 and 108)

[5] Alberer D. *Fast Oxygen Based Transient Diesel Engine Control*. Advances in mechatronics. Trauner, 2012. (cited in pp. 66 and 108)

[6] Guardiola C, Climent H, Pla B and Blanco-Rodriguez D. "ECU-oriented models for NOx prediction. Part 2: adaptive estimation by using an NOx sensor". *Proceedings of the Institution of Mechanical Engineers, Part D: Journal of Automobile Engineering*, Vol. 229 n^o 10, pp. 1345–1360, 2015. (cited in pp. 66 and 108)

[7] Willems F, Mentink P, Kupper F and Van den Eijnden E. "Integrated emission management for cost optimal EGR-SCR balancing in diesels". *IFAC Proceedings Volumes*, Vol. 46 n^o 21, pp. 711–716, 2013. (cited in pp. 24 and 66)

[8] Willems F. and Cloudt R. "Experimental Demonstration of a New Model-Based SCR Control Strategy for Cleaner Heavy-Duty Diesel Engines". *IEEE Transactions on Control Systems Technology*, Vol. 19 n^o 5, pp. 1305–1313, 2011. (cited in pp. 66, 138, 151, and 152)

[9] Eijnden E v d, Cloudt R, Willems F and Heijden P v d. "Automated Model Fit Tool for SCR Control and OBD Development". In *SAE Technical Paper Series 2009-01-1285*. SAE International, apr 2009. (cited in pp. 8, 66, and 152)

[10] Zervas E. "Development of an indicator for the emission control of diesel passenger cars". *Applied Thermal Engineering*, Vol. 28 n^o 11, pp. 1437–1442, 2008. (cited in p. 72)

Chapter 4

Experimental characterization of sensors measurements and diesel catalysts with different ageing levels

Contents

4.1 Introduction

This chapter is devoted to characterize the DOC and the SCR operation in new and aged conditions, as well as to characterize some relevant measurements. A series of experiments will be used to characterize first the nominal operation of the catalysts, and analyze then aged catalysts in comparison to the new part.

The experimental differences due to catalysts ageing will be the key and the target for next chapters, in which models and diagnosis functions will be oriented to detect this experimental ageing, considering the particularities of the measurements.

4.2 Measurements characteristics

The DOC inlet temperature measurement, the measurement of the DOC oxidation phases and the delay between up- and downstream measurements are analyzed along the chapter. In the case of DOC inlet temperature measurement, the NTC sensor measurement provokes a loss of the signal bandwidth, whose experimental effect is analyzed next comparing the dynamics present in an exhaust line.

4.2.1 DOC inlet temperature measurement

The DOC inlet measured temperature is a consequence of the fuel injection, the combustion process, the heat transmission along the exhaust line and the own sensor measurement. The ECU fuel mass estimation is fast and non-delayed, since it is able to perform cycle-to-cycle variations [1]. Consequently, the dynamic response of ECU injection signals is faster than the exhaust temperature dynamics.

On the other hand, the air path of turbocharged engines has slower dynamics than the fuel injection system [2] due to mechanical, thermo- and fluid dynamic reasons. In this sense, as stated by [3], EGR dynamics are in between those of the fuel and the air path, so they may not be considered to add delay to the air path. Even so, the air path dynamics are much faster than the heat transfer phenomena driving the exhaust gas temperature. Therefore, λ^{-1} presents the fastest time response to an injection step, as shown in Figures 4.1

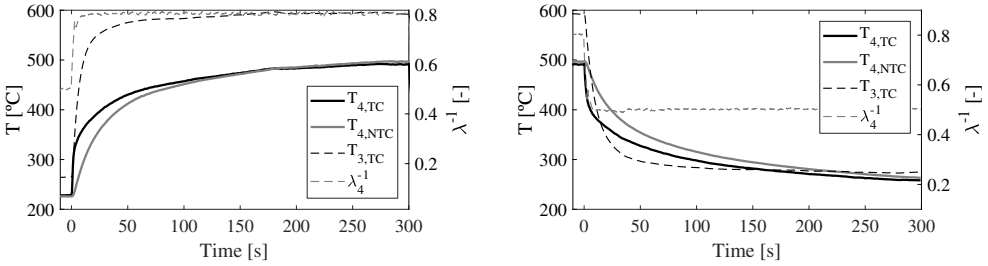

Figure 4.1. *Engine dynamics.*

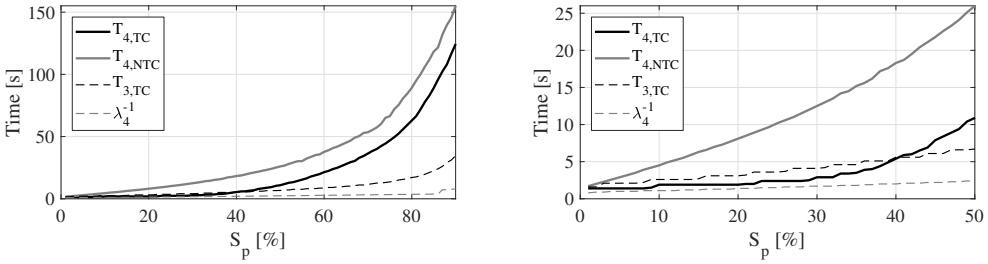

Figure 4.2. *Left: Time of the reached percentage of the signals at the tip in of Figure 4.1. Right: Zoom applied to the left plot.*

and 4.2.

Figure 4.1 shows how engine cylinder-raw temperature $T_{3,TC}$ still increases after the initial transient phase of λ^{-1}, present during the first seconds after the load step. The initial steep phase is due to in-cylinder changes, whilst the last phase with low slope is due to heat transmission effects of engine block and exhaust pipes. That is, cylinder gases temperature changes as fast as combustion settings change, but the surrounding metal follows slower heat transmission dynamics [4].

The DOC inlet temperature dynamics are affected by those described before plus an added degree of freedom, which is the heat transmission between the gases generated in the combustion process and the engine block, valves and exhaust manifold. Its time response is slower than λ^{-1}, as can be seen in Figure 4.1.

Fast themocouple measurement T_{TC}. The thermocouple measurement T_{TC}, whose signal can be appreciated in Figure 4.1, is supposed to be the

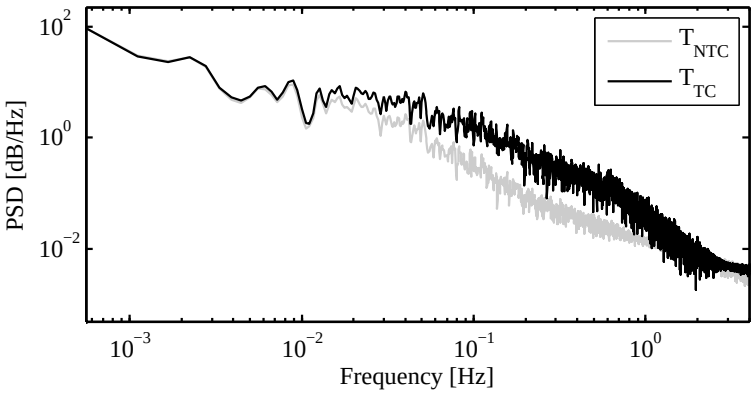

Figure 4.3. *T_{TC} and T_{NTC} presented in the frequency domain.*

fastest possible measurement of the gas temperature. As depicted during the first 40% at the right side of Figure 4.2, due to its lower thermal inertia, the fast thermocouple T_{TC} observes the effect of the load step faster than $T_{3,TC}$. Afterwards, heat transmission effects accumulated by the exhaust manifold, the turbine and the exhaust line may be appreciated at Figure 4.1 as a low steep increase and at Figure 4.2 from 60% at the steepest stage. As T_{TC} measurement is the best approximation to the real exhaust gas temperature, its signal will be considered hereinafter as the actual gas temperature.

NTC sensor measurement T_{NTC}. The NTC sensor has the slowest dynamics response, as can be appreciated in Figures 4.1 and 4.2. The signal from the NTC sensor follows thermocouple measurements T_{TC} when it comes to stationary engine operating conditions. Their time response is different due to its different masses, volumes, construction materials, locations and designs, which lead to different heat transmission due to conduction with the probe, convection with air, radiation with surrounding metals [5]. Despite these differences, temperature measurements have been traditionally modelled as first order systems, so that NTC sensor signal measurement will be considered as a first-order response of the TC measurement.

Figure 4.3 presents the measured T_{TC} and T_{NTC} in the frequency domain in order to show the effect of the sensor inertia on the temperature signals. For that purpose, a dynamic WLTC, which continuous transients cause continuous differences in sensors measurements, is used to generate the Power Spectral Density (PSD) of the signals. Frequency response of T_{TC} and T_{NTC}

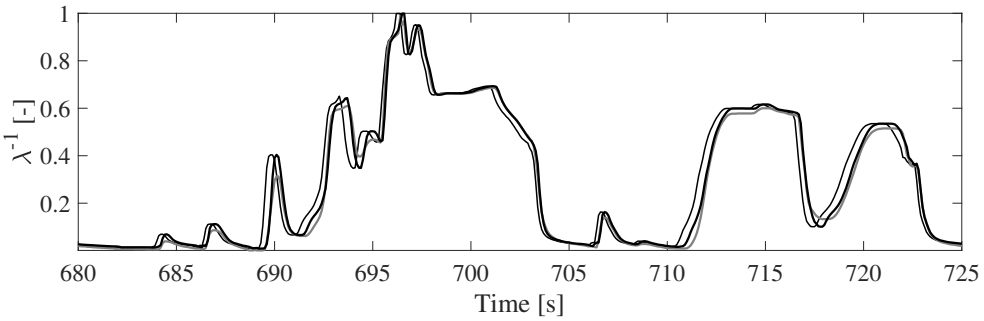

Figure 4.4. *Delay compensation between up- and downstream λ measurements during a phase of the WLTC. Thin black: measured upstream. Thick grey: measured downstream. Thick black: delayed upstream.*

behave very similar at low frequencies, from 1 mHz to 10 mHz. However, at the intermediate bandwidth there are noticeable differences, since the fast thermocouple presents more frequency content between 10 mHz and 2 Hz. At the highest frequencies shown in the plot, over 2 Hz, the two signals behave similarly, which indicates that higher frequencies are not relevant.

4.2.2 Delay between up-and downstream measurements

For some applications, the delay due to the travel time of the species between up and downstream needs to be compensated. With this, the differences between sensors measurements are reduced to sensors offsets and catalyst operation. For this purpose, the following model delay, based on the exhaust mass flow passing through, is used:

$$a = (\tau_{max} - \tau_{min})^z / (\dot{m}_{exh,max} - \dot{m}_{exh,min})^z \tag{4.1}$$

$$c = a * (\dot{m}_{exh,max} - \dot{m}_{exh,min})^z \tag{4.2}$$

$$\tau = \tau_{min} + (c - a * (min\{\dot{m}_{exh,filt}, \dot{m}_{exh,max}\} - \dot{m}_{exh,min})^z)^(1/z) \tag{4.3}$$

where τ is the applied delay, which needs to be filtered to avoid back steps in time, and τ_{max}, τ_{min}, z, $\dot{m}_{exh,max}$ and $\dot{m}_{exh,min}$ are calibrable parameters. Figure 4.4 shows a phase of the WLTC in which the delay is compensated.

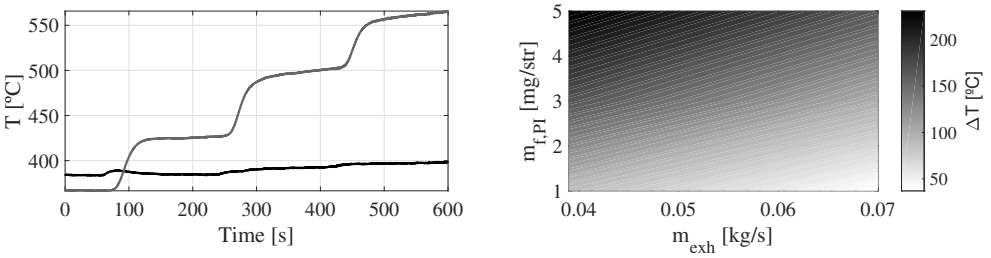

Figure 4.5. *Left plot: continuous post-injections of 1, 3 and 5 mg/str under steady state conditions. Black: inlet temperature. Grey: Outlet temperature. Right plot: experimental effect of air mass flow and continuous PI fuel on ΔT [°C].*

4.3 Experimental DOC behaviour and ageing

The experimental behaviour of DOCs is assessed in this section, in which parts with different failure modes are tested.

4.3.1 Oxidation capacity

The oxidation capacity of DOCs is triggered by injecting raw fuel in the exhaust line through late PI [6]. These PI are activated as a train of pulses or continuously. In the experiment shown in Figure 4.5, continuous steps of 1, 3 and 5 mg/str have been applied during engine steady state conditions, whose results can be used to analyse the effect of exhaust mass flow and post injected fuel on ΔT, where ΔT represents the temperature step in steady-state conditions between the original DOC downstream temperature and the measured temperature after the PI stabilization. In this sense, ΔT increases with increasing post-injected fuel, $\dot{m}_{f,PI}$, and with decreasing exhaust mass flow, $\dot{m}_{exh}$.

4.3.2 DOC oxidation measurement with λ sensors

Dynamics of the λ measurements The measurement of oxidation activity is done next with the fast Cambustion GA, the Horiba GA and the λ measurements from the NO_x sensors for gas concentrations, and with thermocouples for temperature measurements. These measurements are plotted in Figure 4.6 for two PI pulses of 3 mg/str during 5s at different $\dot{m}_{exh}$ during steady-state conditions and at a temperature of around 440°C. While the left

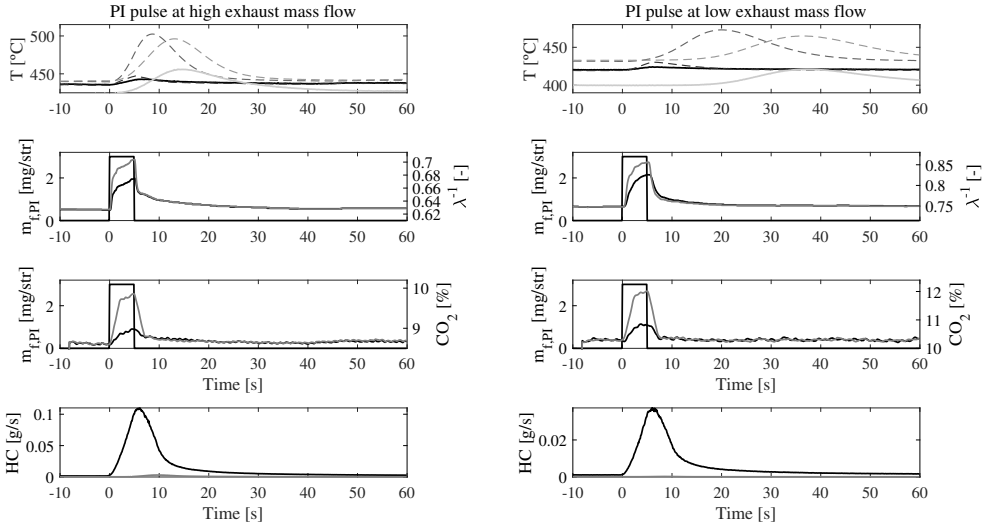

Figure 4.6. *Analysis of λ measurements dynamics capacities for two post-injection pulses at different exhaust mass flows, occurring oxidation at both events. In all plots, black to light grey stand for upstream to downstream signals. The squared signal of medium and bottom plots stands for the post-injection pulse. Offset between upstream and downstream λ measurements is compensated.*

hand plot has a flow of 0.08 kg/s, the right hand plot has a flow of 0.02 kg/s. In this Figure, different dynamics from the DOC and the own measurements can be appreciated. On the one hand, the PI pulse has a fast impact on the λ and CO_2 measurements, whose signal presents a peak at the end of the PI pulse. After the peak, the signal decreases to the original value, which points that the oxidation takes place during the PI pulse. However, the time that the λ signals need to go the original value is higher for the pulse at low $\dot{m}_{exh}$ than for the one at high $\dot{m}_{exh}$. On the other hand, despite the fact that the Horiba GA THC measurement shows the peak of THC generated by the PI pulse, its slow dynamics are not completely representative of the occuring phenomena.

When observing temperature plots, different dynamics on the PI oxidation and its effect on temperature can be appreciated between both pulses at low and high $\dot{m}_{exh}$, in which the temperature dynamics are significantly slower for this former. However, an important relation between the delay and the $\dot{m}_{exh}$ can be appreciated between low and high $\dot{m}_{exh}$ cases. In this sense, the test with lower $\dot{m}_{exh}$, which in this case is the right plot, shows a notable delay with respect to the other test. In addition, it can be seen in both figures how

the axial temperature at the core of the DOC is being passed from one section to the following, just like a wave of energy transmitted by the flow. It can be also seen how the temperature decreases inside the DOC due to DOC thermal inertia and heat transmission effects with the surroundings, since the DOC is not an isolated system. The peak of the outlet sensor is noticeably lower than that inside the DOC due to mainly two reasons. On the one hand, it is due to heat transmission effects, since it is placed after the last slice of the DOC. On the other hand, it is due to the rather slowness of the NTC sensor in comparison with a fast thermocouple.

Effect of DOC oxidation on species Figure 4.7 represents a different point of view of the DOC, in which a train of post-injection pulses starting at an upstream temperature of 290°C and finishing at 180°C, where the λ measurements of the NO_x sensors can be contrasted with the HC, CO and O_2 measurements of the Horiba gas analyzer. During the decrease of temperature, it can be appreciated how the O_2 consumed during the pulses decreases from a valley of 15.4% to a valley of 16.2% due to the loss of oxidation capacity of the catalyst. However, several aspects need to be assessed first in order to understand the λ measurements.

As it can be appreciated in Figure 4.7, both the HC and CO measurements are significantly reduced at the DOC downstream during all the test. However, the $O_{2,ds}$ valley at every post-injection pulse increases as the the capacity of the DOC decreases, which implies that the oxidation is being reduced by a lower DOC temperature. In this sense, the decrease in oxygen consumed while the downstream HC and CO emissions are maintained, is explained by the HC accumulation capacity of the DOC, i.e. the HC species that are not oxidized are accumulated in the catalyst. Moreover, the CO oxidation effect in terms of O_2 is sensitively less significant than that of the HC oxidation.

The increasing slip of HC, signifcant from 100s seconds, denotes the filling process, through which the catalyst is less able to retain HC and therefore it expulses them. By contrast, although the CO species are also oxidized during the most part of thest, a first peak appears at the downstream measurement at the end of the test, which is due to the fact that the DOC is reaching its CO LOT, lower than that of the HC, as it is also stated in [7].

Taking into account the behaviour of the species, it can be stated that the decrease of the λ_{ds}^{-1} signal in comparison with the λ_{us}^{-1} along the test is due to the decrease in HC oxidation capacity of the catalyst. However, two aspects that are assessed in next section must be noted; on one hand, the λ_{us}^{-1}

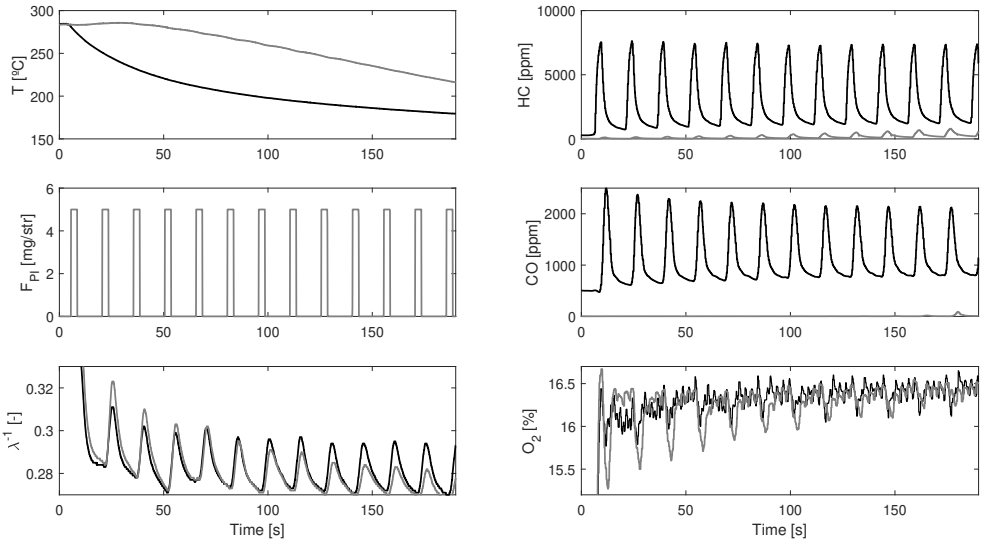

Figure 4.7. *Example of a train of post-injection pulses starting with HC oxidation and finishing without HC oxidation, during a phase of decreasing temperature. Offset between upstream and downstream λ and O_2 measurements is compensated. Upstream: black. Downstream: grey.*

presents peaks despite $O_{2,\text{us}}$ oxygen is not significantly affected. In this sense, while the $O_{2,\text{us}}$ measurement from the gas analyzer is a measurement of the raw $O_{2,\text{us}}$ concentration, the λ measurement is, theoretically, a measurement of the oxygen excess, taking into account the oxygen necessary to oxidize HC and CO species. On the other hand, the peaks of the λ_{ds}^{-1} are still significant at the end of the test, in which HC oxidation is not significant.

Measurements of λ during pulses oxidation Finally, the λ measurements of the NO_x sensors during the fuel post-injections are analyzed here. For this purpose, the λ measurements of Figure 4.7 are further detailed with measurements of the Horiba gas analyzer in Figure 4.8. Note that the offsets and delays of the measurements have been compensated beforehand in order to compare the pulses increments with respect to its steady value.

In the top plot, the three upstream measurements of λ from the sensors, λ_{sen}, λ from the gas analyzer, λ_{GA}, and oxygen from the gas analyzer converted to λ signal, $\lambda_{O_2,GA}$, are different. As detailed in previous section, the upstream measurements of λ are affected by the HC species during the post-injection pulses. In this sense, the λ_{sen} and λ_{GA} measure the oxygen excess, while the

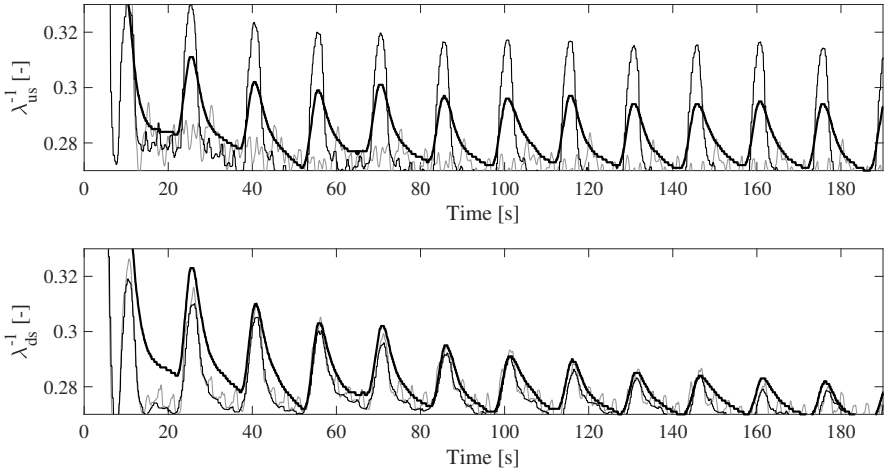

Figure 4.8. *λ measurements during the train of post-injection pulses of Figure 4.7. Offsets and delays are manually compensated. Thick black: λ measurements of NO_x sensors, λ_{sen}. Thin black: λ measurements of Horiba gas analyzer, λ_{GA}. Thin grey: Oxygen measured by Horiba gas analyzer converted to λ signal, $\lambda_{O_2,GA}$.*

$\lambda_{O_2,GA}$ represents the oxygen concentration, whose signal is converted into λ, i.e. the oxygen represented by λ_{GA} is the oxygen represented by $\lambda_{O_2,GA}$ minus the oxygen that the HC and CO species would consume if they were oxidized. However, the measurements of λ_{sen} do not match the λ_{GA}, despite these two measurements should have, theoretically, a similar signal.

The effect of HC in the λ_{sen} measurement, as an oxygen excess measurement apparatus, is not accurate, and it measures more oxygen excess than it should. In fact, this experimental bias of oxygen excess, $\Delta\lambda$, is the basis of the diagnostics strategy of Chapter 7, i.e. the oxidation of HC species provokes higher peaks in the downstream λ_{sen} signal than in the upstream λ_{sen} measurement, which allows the detection of oxidation phases in the DOC.

For this reason, the three downstream measurements of λ_{sen}, λ_{GA} and $\lambda_{O_2,GA}$ present similar values. In this sense, the λ signal is not affected by the HC species, since these are oxidized or accumulated in the catalyst. However, the λ_{ds}^{-1} peaks are still present at the end of the test, which are mainly due to undesired in-cylinder combustion of the fuel PI and due to CO oxidation.

In conclusion, if the λ_{sen} signal were proportional to the real λ value, it would be not possible to detect oxidation phases. However, the real λ_{sen} measurements are somewhere in between the real λ and the λ value that represents the actual oxygen concentration. In this sense, the difference with

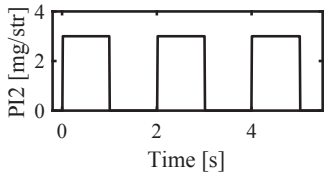

Figure 4.9. *Pulses train of late fuel post-injections.*

respect to the actual λ is sufficient and not critical, since a proper thresholds-based strategy allows the detection of oxidation phases, which is shown in Chapter 7.

4.3.3 Light-off temperature

The LOT divides the non-oxidation and oxidation temperature ranges, and it is a characteristic that affects HC, CO and NO species concentrations [7–9]. Some authors like [10] and [11] define the LOT as the temperature at which 50% of the incoming species are oxidized, since LOT does not really act as a binary threshold. The LOT values for HC, CO and NO species are estimated in test shown in Figure 4.10, in which the medium plots allow observing the effect of LOT in HC, CO and NO species concentrations.

The LOT test starts with both DOC up- and downstream temperatures below 130°C, which is a value under the LOT. Then, load steps of 2 minutes are applied to slowly increase the temperature, about 20°C each approximately. In order to ensure an enough exothermic event, in which the downstream temperature clearly increases over the upstream, a train of PI pulses of 3 mg/str, like the shown in Figure 4.9, is continuously applied at the start of the load steps, so the DOC is continuously being filled with HC.

An accumulation process of HC can be observed, as downstream HC, HC_{ds}, increases as a symptom of catalyst fill, whose capacity to store incoming HC decreases. Then, from the time when the LOT is reached, a noticeable temperature increase takes place, and the oxidation process empties the HC accumulated in the catalyst. Thus, a downstream HC decrease is observed. In this sense, the LOT can be observed through an exothermic increase of temperature and with a decrease of HC_{ds}. This behaviour can be observed for both new and aged DOCs, being the LOT of each one at a different temperature. In the case of the aged DOC, the HC accumulation even reaches the saturation

Table 4.1. *Light-off temperature test results.*

Catalyst	New	Nom	Aged	DOC_{70}	DOC_{40}	No-imp
LOT_{HC}	190	190	250	190	190	-
LOT_{CO}	150	150	205	150	150	-
LOT_{NO}	150	150	205	150	150	-

point, since HC_{ds} are similar to the upstream HC, HC_{us}. In this test, the peak of HC reveal the LOT step, however, during transient conditions, if HC oxidation was not high enough to observe differences in temperature, the LOT could not be evident, due to the inherent difficulty of differentiating between accumulation and oxidation processes, when observing HC_{us} and HC_{ds} concentrations.

In case of NO and CO, the LOT estimation is simpler, since the decrease of downstream DOC_{ds} species concentrations marks the temperature at which the light-off is reached. CO_{ds} is maintained constant, being CO_{us} equal to CO_{ds} until its LOT is achieved. This effect shows the lack of CO accumulation capabilities of the DOC. In case of NO, an analog effect happens. The light-off temperature can be appreciated through a decrease in concentration, although oxidation is not complete in this case. As it can be also observed, LOT for CO and NO is, in both new and aged cases, lower than for HC.

Table 4.1 shows the results of the LOT tests for the set of tested DOCs. As the cut procedure does not affect the activation energy, the cut DOCs have the same LOT, while the LOT of the thermally aged DOC has increased up to 250°C. Note that oxidation starts inside the DOC at a temperature that may differ from the inlet gas temperature, since the outlet temperature is lower due to thermal losses. However, as the DOC monolith temperature is not measured on-board, the light-off temperature is characterised by the upstream temperature sensor.

4.3.4 HC and NO accumulation

The HC accumulation [12] is characterized next by means of a specific test, whose objective is to measure how much HC a DOC is able to store, and characterize how the HC slip increases as the DOC is filled. For this purpose, PI are used to inject raw HC into the DOC until it is saturated, i.e. the

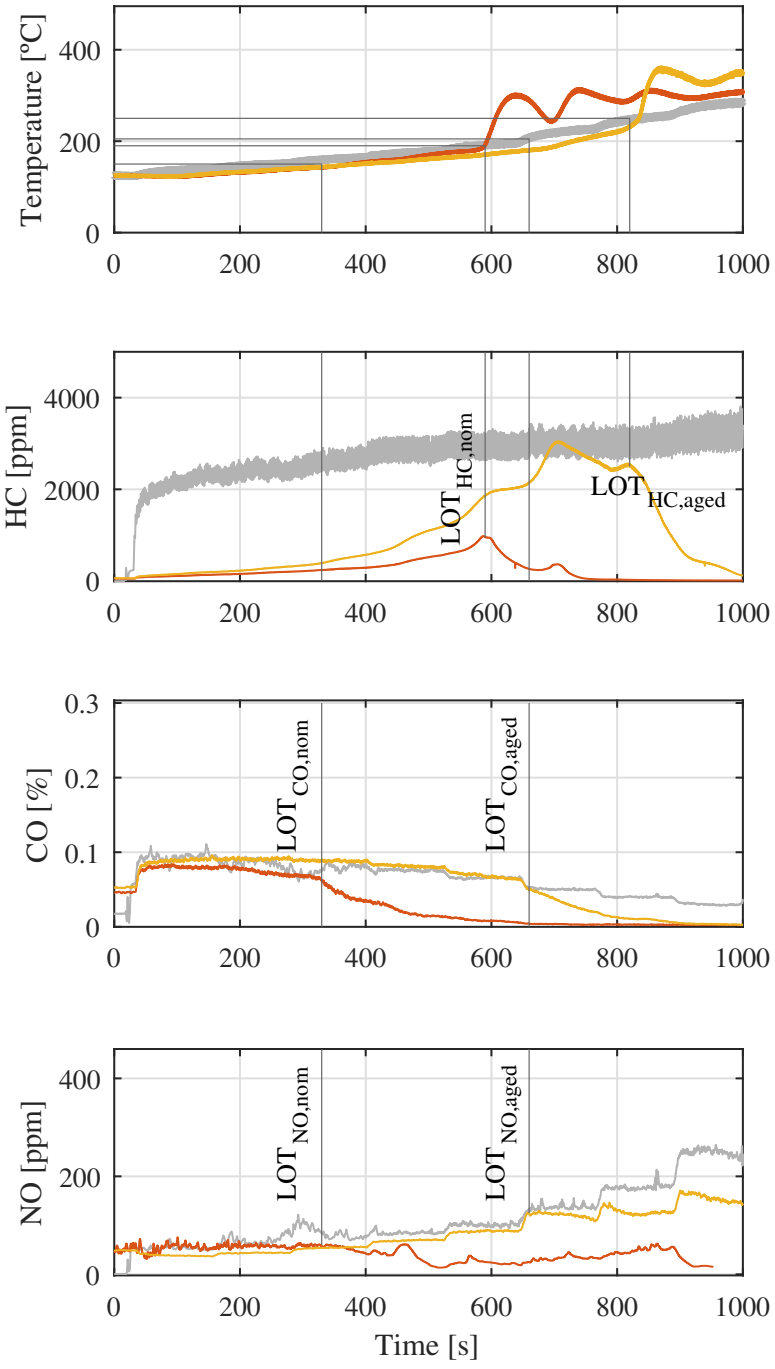

Figure 4.10. *Results of the light-off temperature test for the new and aged DOCs. — Upstream measurements. — New DOC downstream measurements. — Aged DOC downstream measurements.*

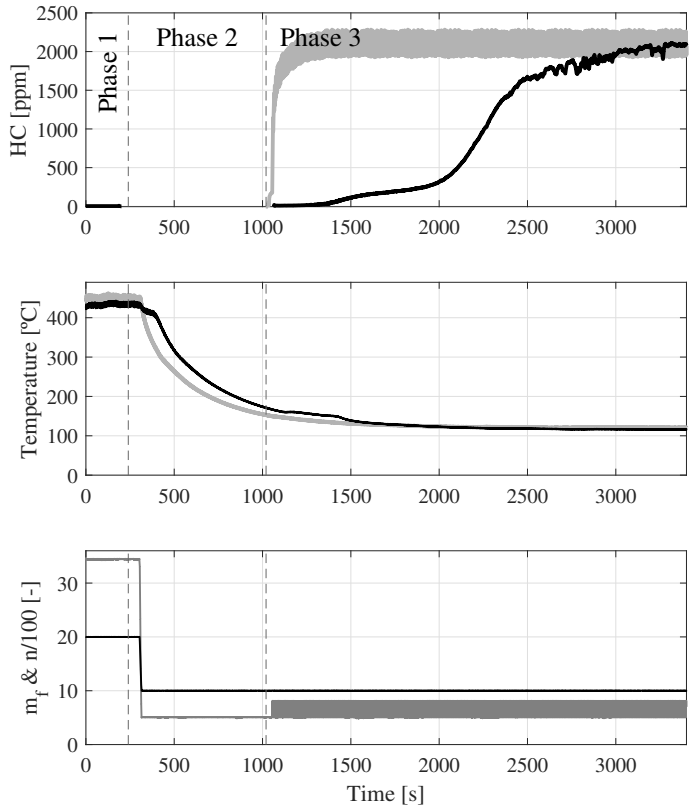

Figure 4.11. *Results of the HC accumulation test for the nominal DOC. Top and medium plots:* —— *Upstream measurements* —— *Nominal DOC downstream measurements. Bottom plot:* —— *Total fuel injected in mg/str* —— *Engine speed n/100 in rpm.*

measured HC_{ds} are stabilized and equal to the measured HC_{us}. This test is composed of three phases, as identified in Figure 4.11:

1. Emptying phase: the engine runs at a point in which the temperature is sufficiently high to ensure the removal of any possibly stored HC. For this purpose, the engine speed and the load are higher during phase 1, as shown at the bottom plot of Figure 4.11.

2. Temperature stabilization phase: from the starting point of this phase, the engine runs at steady-state conditions until the end of the test. This second phase is a transition phase, in which the DOC temperature is continuously decreasing until the downstream measurement reaches the LOT value, in which moment PI start.

3. Accumulation phase: it is the PI phase, during which PI pulses of 3 mg/str like the presented in Figure 4.9 are being continuously applied until the downstream HC measurement reaches the steady HC upstream measurement, as happens at the end of the test.

The results of the accumulation test applied to each DOC are shown in Figure 4.12, in terms of the observed slip against the accumulated HC during phase 3. In this sense, the slip increases as the DOC is filled, due to the reduction of its accumulation capacity. It can be also appreciated how as the DOC ages, its slip increases, i.e. the slope of the deteriorated catalysts is higher than the slope of the healthier catalysts. Moreover, the ability to filter the PI pulses decreases as the DOC is deteriorated.

The different ageing of the DOCs has impact on the slip increase, since the brand new DOC is able to accumulate HC with only a slight increase on slip, while the nominal and aged DOCs have more slip, following both a similar trend: they have an initial strong increase, followed by a smoothed slope. The DOC_{70} follows a similar trend than the new catalyst, but it gradually starts increasing its slip before. Then, the DOC_{40} is the less capable of storing HC, so its slip increases faster than for the others.

With regards to the NO_x accumulation, Figure 4.13 shows this effect in a dynamic cold phase. During the initial 45 seconds, the new DOC accumulates NO_x species, since the $NO_{x,ds}$ signal is sensitively lower than the $NO_{x,us}$ signal. Then, a release phase can be observed between 80 and 90 seconds. When analyzing the same effect in the aged DOC, this accumulation / release effect is not present, since both $NO_{x,us}$ and $NO_{x,ds}$ signals are similar during the first 45 seconds, and no release phase can be observed. Therefore, the ageing of DOC shows an effect on the NO_x accumulation capacity of DOCs.

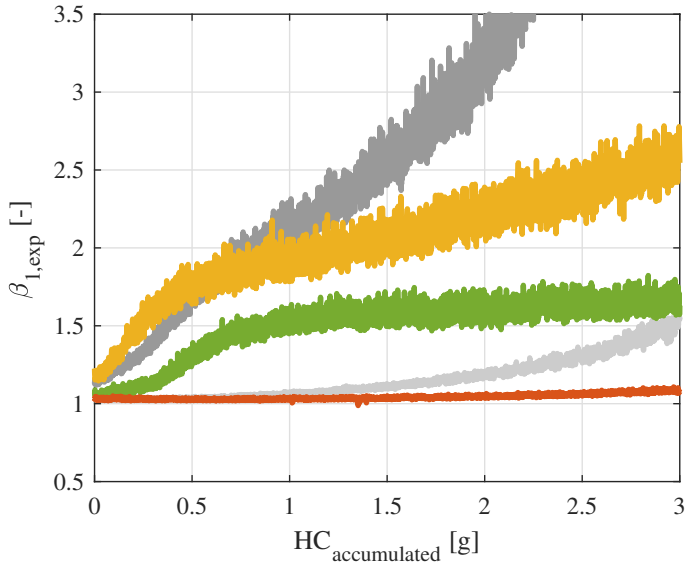

Figure 4.12. *Experimental results of the HC accumulation test.* — *New DOC* — *Nominal DOC* — *Aged DOC* — DOC_{70} — DOC_{40}.

4.3.5 Species slip

Figure 4.14 shows a test used to describe the experimental effect of ageing on HC and CO slip, for nominal and aged parts. This test follows the engine operating points described in Figure 3.12, being therefore a wide variety of temperatures and exhaust mass flows. In it, light-off temperature effects can be appreciated from 500 s approximately for both new and aged DOCs, when the slip is reduced for both HC and CO, since despite having different LOT, the temperature step is big enough to overcome the LOT of both catalysts almost at the same time. In case of HC, the slip for the aged catalyst is higher than for the nominal until the LOT is reached, from which point both slips are similar. In this line, CO slip has a similar behaviour, being the initial part at cold conditions with slip for the aged part, and being the warm part with high efficiency for both catalysts.

The NO to NO_2 conversion is analyzed through Figure 4.15, which includes a warm phase of the WLTC with $NO_{x,us}$, $NO_{x,ds}$, and NO_{ds} measurements for new and aged catalysts. Negligible differences may be appreciated between $NO_{x,us}$ and $NO_{x,ds}$, apart from the slight accumulation effects. Instead, the NO_{ds} signals present noticeable differences for the new and the aged DOC. In this sense, the NO to NO_2 conversion efficiency is decreased in the aged DOC,

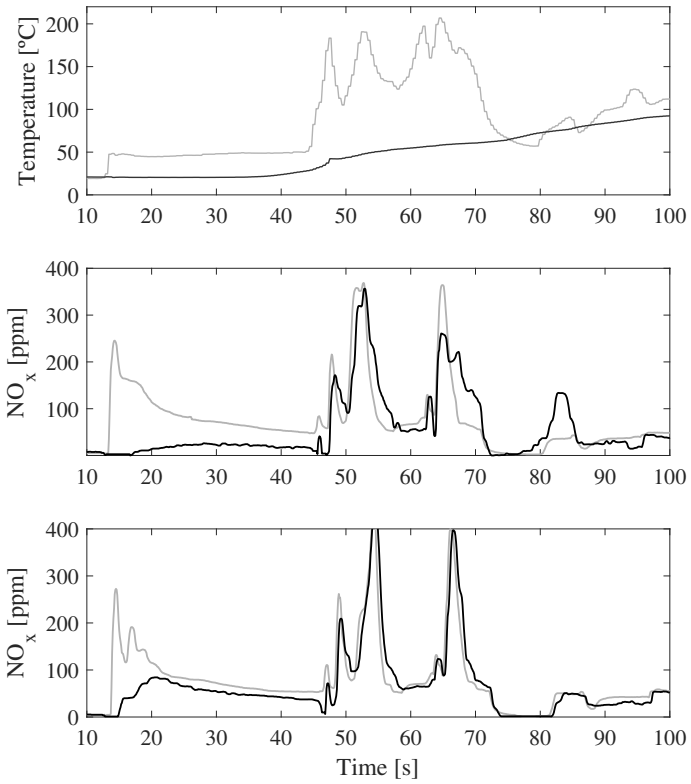

Figure 4.13. *Measured effect of ageing on the NO_x accumulation process at the cold starting phase of the WLTC. Top plot: —— Upstream temperature —— Downstream temperature. Medium (new) and bottom (aged) plots: —— $NO_{x,us}$ —— $NO_{x,ds}$.*

as the lower averaged conversion shows, being around 0.5 for aged and 0.8 for the new.

4.3.6 DOCs operation in regulation tests

The operation of new and aged DOCs during the NEDC and WLTC regulation tests is assessed in this section for the CI engine A.

NEDC The DOC operation in the NEDC is analyzed by means of temperature and λ measurements in Figure 4.16. Note that the temperature signal is acquired with a fast thermocouple, in order to guarantee a detailed lecture of the temperature dynamics. For this figure, the upstream λ^{-1} signal is delayed using the method previously described in this chapter in order to compensate

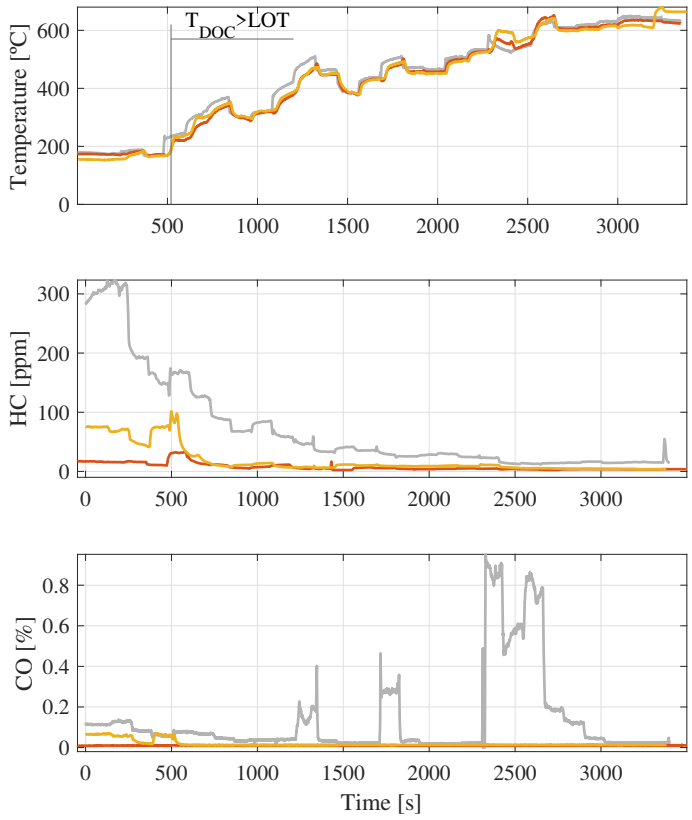

Figure 4.14. *Reference test with HC and CO to develop the model. — Upstream measurements — New DOC downstream measurements. — Aged DOC downstream measurements.*

the dynamics between the up- and downstream measurements, resulting in the blue line of the central plots.

The NEDC is used as a dynamic cycle to observe oxidation phases with λ measurements. Since this test is not as dynamic as the WLTC, it has phases under and over the LOT, as the WLTC also has, but the oxidation phases can still be well appreciated. For the generation of oxidation phases, the DOC is filled with raw HC species during phases in which the engine is running below the LOT. Then, the oxidation phases are estimated using a thresholds method that exposes when the λ_{ds}^{-1} overcomes λ_{us}^{-1} with a sufficient margin, in sufficiently steady conditions and during sufficient time. As a result, the red lines show when these conditions are true, and therefore, when oxidation is occuring.

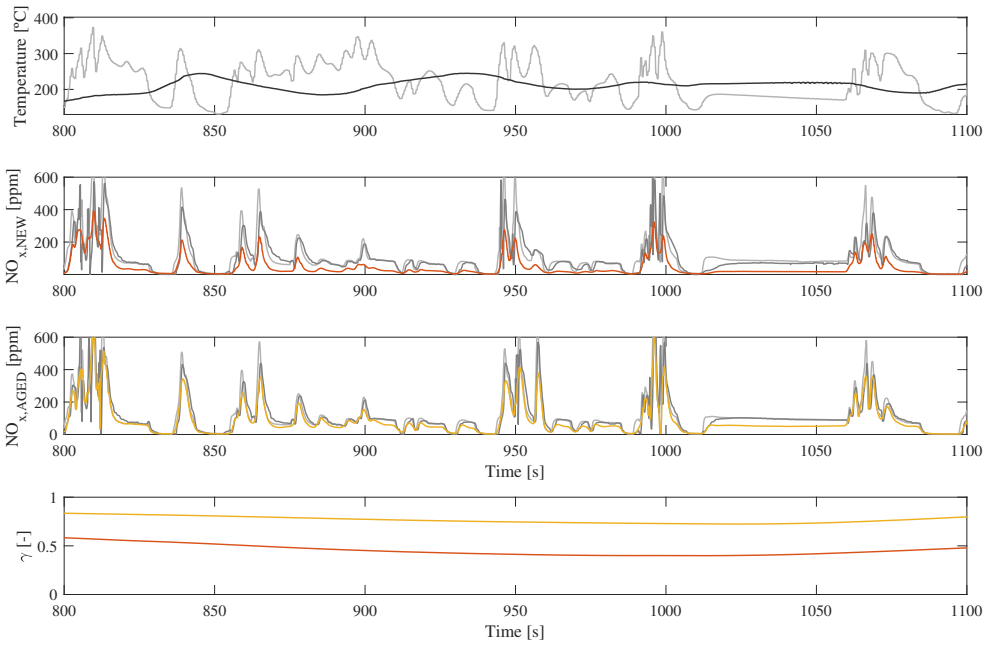

Figure 4.15. *Measured NO_x signals during a warm phase of the WLTC. Top plot: Upstream temperature — Downstream temperature. Medium plots: $NO_{x,us}$ $NO_{x,ds}$ $NO_{ds,new}$ $NO_{ds,aged}$. Bottom plot: Averaged NO_{new} conversion Averaged NO_{aged} conversion.*

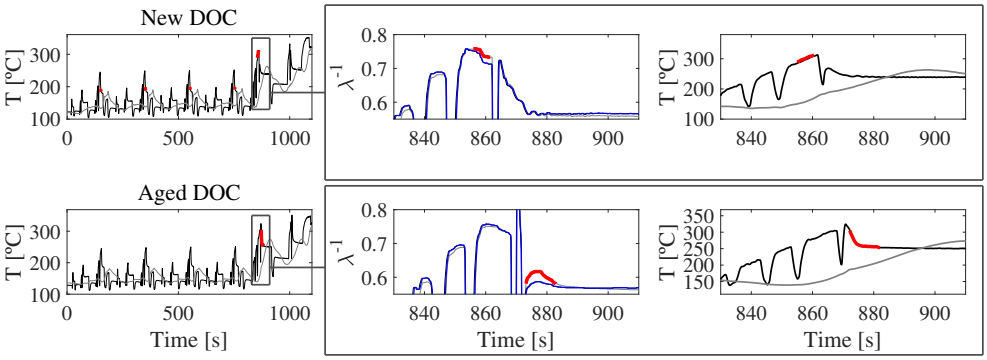

Figure 4.16. *Detection of oxidation phases in dynamic conditions with λ measurements at an NEDC cycle for a new DOC, top plots, and an aged DOC, bottom plots. Central and right plots are a zoom of the oxidation event at the extra-urban step. Left and right plots: upstream temperature is black, downstream temperature is grey, temperature during oxidation is red. Central plot: upstream delayed λ is blue, downstream λ is grey and oxidation phase is red.*

As it can be observed, while the new DOC suffers 5 oxidation phases, the aged DOC only suffers 1 oxidation phase. In this sense, the first 4 oxidation phases of the new DOC take place at the 4 peaks originated during the urban conditions, at an approximate temperature of 200°C, while the common oxidation phases at the start of the extra-urban phase take place at a higher temperature for both DOCs. This fact is due to the different LOT that these DOCs present. On the other hand, the extra-urban oxidation phase of the new DOC takes place before than that of the aged DOC, due to the fact that the LOT of the new DOC is achieved earlier. However, when comparing the temperatures during oxidation, the measurements show that the temperature of the new DOC is higher than the oxidation of the aged DOC, which seems contradictory. The cause of this resides in the different dynamics of λ and temperature, i.e. while the λ measurement is representative of the oxidation instants, the temperature measurement is sensitively delayed due to heat transmission. Therefore, the oxidation effect on temperature is delayed and mixed with other dynamics, which make impossible the oxidation detection with temperature measurements.

WLTC The experimental effect of ageing in the WLTC test is analyzed at cold and warm starting conditions, focusing on the effect of temperature. In

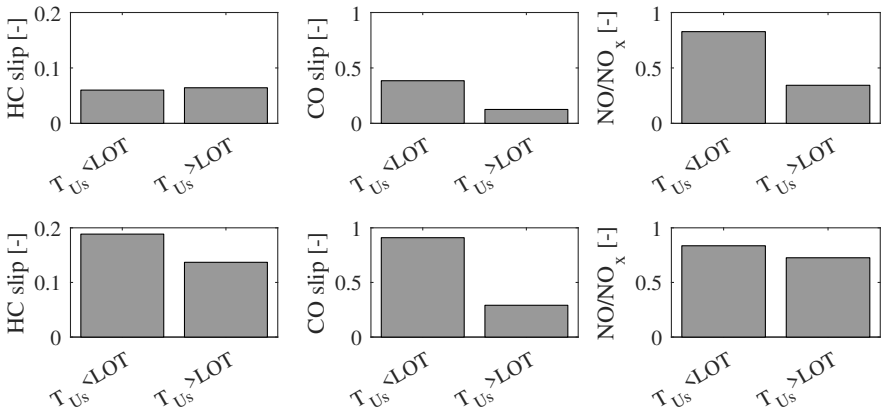

Figure 4.17. *Importance of LOT on emissions, described through emissions slip over engine-raw emissions, when DOC upstream temperature is under and over LOT in a WLTC starting at ambient temperature. Engine raw emissions are considered for each case taking into account the DOC upstream temperature. Top plots: New DOC. Bottom plots: Aged DOC.*

this sense, Figure 4.17 shows the HC and CO slip, and the NO/NO_2 conversion, correlating the phases with the DOC_{us} temperature, i.e. the slip of HC and CO is considered as the integration of the downstream species when the DOC_{us} temperature is under and over the LOT, over the integration of the total upstream species. The LOT of the new DOC is defined at 200°C and the LOT of the aged DOC is defined at 250°C. An analogous procedure is done for the NO/NO_x conversion. In this WLTC test, the difference in average HC and CO slip while T_{us} is under and over LOT is more pronounced for the aged DOC than when the DOC is in new conditions. Moreover, the T_{us} is under LOT during 48% of time for the new DOC, while the T_{us} is under LOT during 74% of time for the aged DOC. For the case of the HC slip in the new DOC, both under and over LOT cases are similar due to the effect of accumulation.

For the analysis of the HC and CO DOC_{ds} emissions in the WLTC, the set of equations (4.4) to (4.7) is used, whose results are shown in Tables 4.2 and 4.3 for HC and CO, respectively. Equation (4.4) represents the fraction of engine-raw emissions during a test phase over the total engine-raw emissions. Equation (4.5) represents the fraction of DOC out emissions during a test phase over the total emissions emitted. Equation (4.6) represents the same than equation (4.5), but for the aged DOC. Finally, Equation (4.7) represents the fraction of the DOC new emissions over the aged DOC.

$$\phi_{raw} = \frac{\int_{phase} \dot{m}^{us}_{raw}}{\int_{total} \dot{m}^{us}_{raw}} \tag{4.4}$$

$$\phi_{new} = \frac{\int_{phase} \dot{m}^{ds}_{new}}{\int_{total} \dot{m}^{ds}_{new}} \tag{4.5}$$

$$\phi_{aged} = \frac{\int_{phase} \dot{m}^{ds}_{aged}}{\int_{total} \dot{m}^{ds}_{aged}} \tag{4.6}$$

$$\phi = \frac{\int_{phase} \dot{m}^{ds}_{new}}{\int_{phase} \dot{m}^{ds}_{aged}} \tag{4.7}$$

where $\dot{m}^{us}_{raw}$ stands for the upstream DOC mass flow of HC or CO, $\dot{m}^{ds}_{new}$ is the downstream mass flow of HC or CO of the new DOC, $\dot{m}^{ds}_{aged}$ is the downstream HC or CO mass flow of the aged DOC and ϕ are the coefficients used to characterize the four phases of the WLTC.

From a 45.7% of total HC engine-raw emissions during the low phase, a 55.4-56.5% of the total tailpipe emissions is emitted during this phase for both new and aged catalysts, i.e. half of the total emissions are emitted during the warming up phase for both catalyst. Percentual emissions during the second phase are higher for the aged DOC, since its higher LOT is still affected by the warming up phase. Then, in the third and fourth phases, emissions for both DOCs are similar, being ϕ around 90%, since both catalysts are operating at warm conditions.

The CO emissions suffer a similar behaviour, being a 51.1% and a 74.9% of emisisons for the new and aged catalysts, respectively, during the first phase, due to their different LOT. Since the LOT of CO is lower than for HC, the ϕ at the low and medium phases evidence the fact that the LOT of the new DOC is mostly overcome, but the LOT of the aged is still not overcome. Both HC and CO emissions for both the new and the aged DOCs are similar in the third and fourth phases, in which the catalyst is already warm. Despite the low value of ϕ is 22.9% for CO in the fourth phase, which denotes big difference, both catalysts are around 2%, which is an almost negligible value. This analysis remarks the influence of the cold start in emissions. The $\mathrm{DOC_{ds}}$ emissions transition from the new to the aged DOC is simulated in Chapter 7 using the model presented in Chapter 6.

Table 4.2. *Emissions effect of WLTC phases for HC species.*

HC	Low	Medium	High	Extra high
ϕ_{raw}	45.7%	22.5%	16.7%	14.8%
ϕ_{new}	55.4%	13.8%	13.5%	16.3%
ϕ_{aged}	56.5%	21.9%	9.7%	11.5%
ϕ	63.5%	40.9%	91%	92.1%

Table 4.3. *Emissions effect of WLTC phases for CO species.*

CO	Low	Medium	High	Extra high
ϕ_{raw}	34.9%	20.5%	23.8%	20.3%
ϕ_{new}	51.1%	20.1%	23.4%	1.5%
ϕ_{aged}	74.9%	14.4%	8.3%	2.1%
ϕ	21.7%	44.4%	90%	22.9%

4.4 Selective catalytic reduction systems

In the case of SCR, a direct measurement of the relevant concentrations affecting its performanse can be done by means of an NO_x sensor and an NH_3 sensor [13–17]. Therefore, the focus is given to the slip of these species, rather than other indirect techniques like in the case of DOC. Even so, in order to understand how slip appears, its operation principles are first analyzed next.

Once the urea has been injected, and after its hydrolysis and thermolysis decomposition processes, it is adsorbed into the catalyst washcoat [18]. Thus, a buffer of accumulated NH_3 is generated, being the accumulation capacity mainly dependent on temperature [19, 20]. Then, the catalyst is ready to reduce the incoming NO_x species [21, 22].

4.4.1 NO_x and NH_3 slip dynamics

The NH_3 accumulation and the NO_x reduction lead to different slip formation principles. On the one hand, the NH_3 slip is originated by the lack of the catalyst surface to retain the accumulated NH_3, while the NO_x slip is originated by the limited capacity of the catalyst to reduce the total amount of

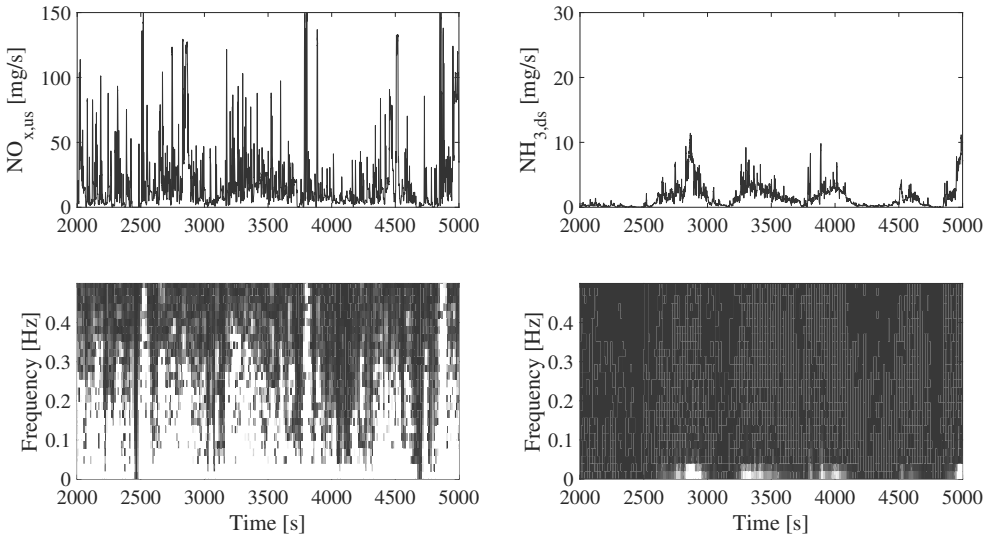

Figure 4.18. *Spectrogram result from the application to the upstream NO_x signal, left plots, and to the downstream NH_3 signal, right plots, during an NH_3 slip dominant phase.*

incoming NO_x species at a certain instant. This process results in the appearance of different dynamics in the slip of NO_x and NH_3, since the SCR acts as a filter for the NH_3 slip and as a non-filtering reductor for NO_x. In this sense, while NO_x dynamics are dominated by the engine operation conditions, the NH_3 dynamics are mainly dominated by temperature. Thus, peaks of temperature during dynamic driving conditions can lead to undesired emptying phases of ammonia on the catalyst surface, which will result in undesired NH_3 slip [23–25].

Figures 4.18 and 4.19 show the dynamics of the slip in the frequency domain for an NH_3 slip case and an NO_x slip case, respectively. In both cases, the slip of the other species is negligible, e.g. in the case of NH_3 slip, the NO_x slip is negligible. Therefore, the NH_3 sensor is used for the NH_3 slip, and the NO_x sensor is used for the NO_x slip, in which it is specially relevant to remark that there is no NH_3 slip in the NO_x slip case, due to its cross-effect in the sensor measurement [26]. For the realization of these figures, the Fast Fourier Transform (FFT) method is applied to the $NO_{x,us}$ signal in both cases, and to the NH_3 signal and the $NO_{x,ds}$ signal, respectively. Due to the induction of a significant dynamic excitation in the $NO_{x,us}$ signal, its frequency response in

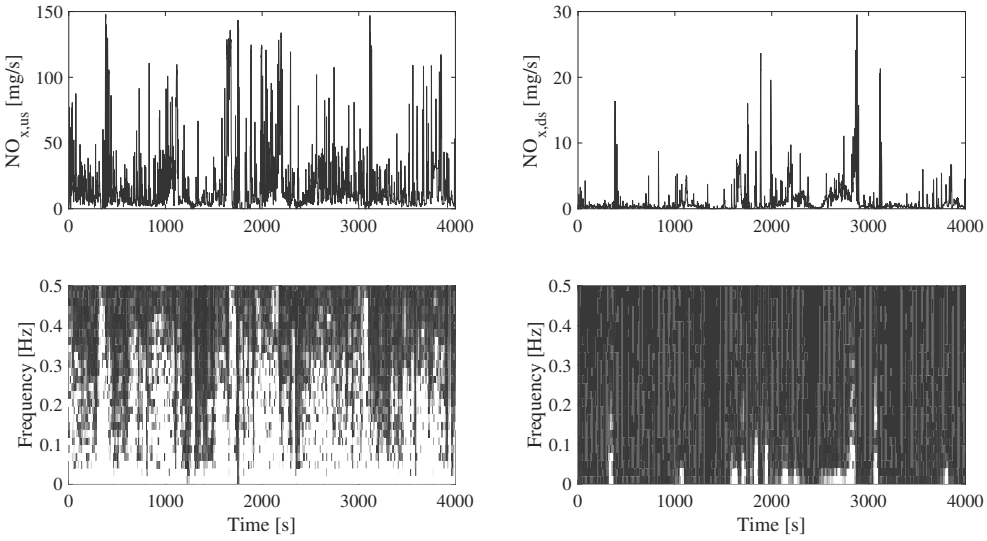

Figure 4.19. *Spectrogram result from the application to the upstream NO_x signal, left plots, and to the downstream NO_x signal, right plots, during an NO_x slip dominant phase.*

terms of PSD has high values in the range from 0 to 0.5 Hz in both Figures. Note that this is a qualitative analysis, and for this reason the scale of the PSD is not shown.

On the other hand, the bandwidth of the NH_3 slip and NO_x slip signals is different. As can be seen in Figure 4.18, the NH_3 frequency response is under 0.05 Hz, while in Figure 4.19, the NO_x frequency response reaches higher values. It can be also appreciated the ppm peaks of NO_x are corresponded with peaks in PSD.

The NH_3 slip is dominated by the SCR temperature. As it can be well appreciated in Figure 4.21, three peaks of NH_3 slip occur following the temperature tendency. This phenomena is related to the accumulation capacity of the SCR, since it decreases at increasing temperature. In this sense, at a certain level of accumulated NH_3, if the temperature increases and the catalyst has not been emptied beforehand, a urea slip is unavoidably generated.

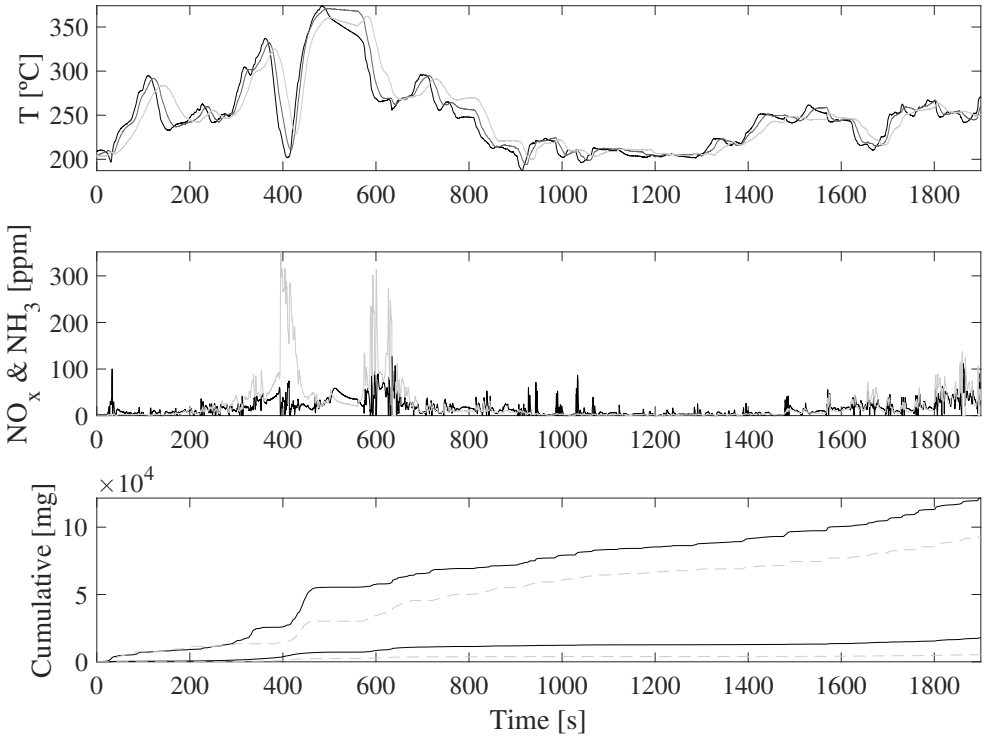

Figure 4.20. *NO_x and NH_3 slips of the new SCR. Top plot: black to grey corresponds to us to ds measurements. Medium and bottom plots: black stands for NO_x and grey NH_3, while continuous stands for us and dashed stands for ds.*

4.4.2 Ageing effect on NO_x and NH_3 slip

The ageing effect on emissions is qualitatively analyzed here. In comparison with the effect of ageing in a DOC, in which the main effects take place at cold conditions, the slip of NO_x and NH_3 in the case of an SCR are affected during all operation conditions, mainly due to the NH_3 storage capacity, Ω, decrease [27]. In this sense, the decrease of Ω decreases the NO_x reduction efficiency and increases the NH_3 slip.

In order to validate the behaviour described with experimental data, Figures 4.20 and 4.21 represent two dynamic tests with a new and an aged SCR, respectively. In both cases, a significant slip of NH_3 is present, while there is also some NO_x slip. The injected urea, the $NO_{x,us}$, the $NO_{x,ds}$ and the NH_3 are represented through cumulative values at the bottom plot. With this, the amount of injected urea and $NO_{x,us}$ that the SCR is processing can be

Table 4.4. *SCR efficiency and slip of tests in Figures 4.18 and 4.19.*

	NO_x efficiency	NH_3 Slip
New	93%	10%
Aged	93%	50%

observed. In addition, the slip of both species can be also compared in time domain and in cumulative values. However, for the cumulative values, notice that 1g of NH_3 is not equivalent to 1g of NO_x, so that the difference between species is not equivalent to a non stoichiometric case.

In order to compare efficiencies and slip between both catalysts, the range of temperatures is similar, despite being slightly higher for the new SCR. For the comparison, Table 4.4 has representative values of the catalyst behaviour, i.e. NO_x reduction efficiency and NH_3 slip. However, before comparing results in Table 4.4, some considerations need to be taken, i.e. a higher amount of both urea and NO_x is injected into the new SCR, and although temperatures are similar, the slightly higher temperature of the new SCR leads to a higher NH_3 slip. Even so, with unfavourable conditions in the new SCR operation, for a similar value of 93% efficiency, the NH_3 slip increases from a 10% in the new SCR to a 50% in the aged SCR.

4.5 Conclusions

The main effects of ageing on DOC and SCR emissions are described in this chapter. While the DOC ageing is assessed with direct and indirect measurements as the LOT, since its effect on HC and CO cannot be measured by on-board sensors, the SCR ageing is explicitly analyzed with NO_x and NH_3 measurements, which can be measured with current on-board technology.

The DOC ageing effects are mainly noticed in cold conditions for the HC accumulation and oxidation, the CO oxidation and the NO to NO_2 conversion. On the other hand, the ageing effect on the SCR is also present during its warm operation, due to the effect that the Ω decrease has on NO_x reduction efficiency and NH_3 slip.

References

[1] Payri F, Luján JM, Guardiola C and Rizzoni G. "Injection diagnosis through common-rail pressure measurement". *Proceedings of the Institution of Mechanical Engineers,*

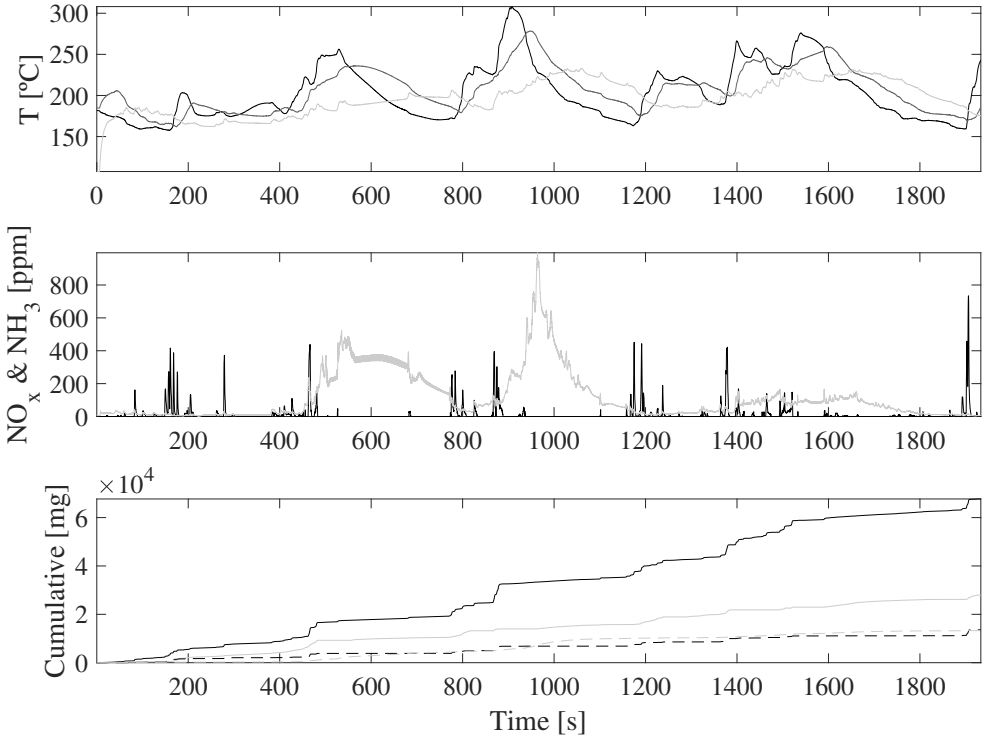

Figure 4.21. *NO_x and NH_3 slips of the aged SCR. Top plot: black to grey corresponds to us to ds measurements. Medium and bottom plots: black stands for NO_x and grey NH_3, while continuous stands for us and dashed stands for ds.*

Part D: Journal of Automobile Engineering, Vol. 220 n^o 3, pp. 347–357, 2006. (cited in pp. 78 and 109)

[2] Galindo J, Luján JM, Climent H and Guardiola C. "Turbocharging system design of a sequentially turbocharged diesel engine by means of a wave action model". Technical report, SAE Technical Paper 2007-01-1564, 2007. (cited in p. 78)

[3] Alberer D and del Re L. "Optimization of the transient Diesel engine operation". In *SAE Technical Paper 2009-24-0113*. Consiglio Nazionale delle Ricerche, 2009. (cited in pp. 64, 78, and 108)

[4] Mrosek M, Sequenz H and Isermann R. "Identification of emission measurement dynamics for diesel engines". *IFAC proceedings volumes (IFAC-PapersOnline)*, Vol. 18, pp. 11839–11844, 2011. (cited in pp. 34 and 79)

[5] Kar K, Roberts S, Stone R, Oldfield M and French B. "Instantaneous exhaust temperature measurements using thermocouple compensation techniques". *SAE SP 2004-01-1418*, pp. 169–190, 2004. (cited in pp. 80 and 108)

[6] Yamamoto K, Takada K, Kusaka J, Kanno Y and Nagata M. "Influence of Diesel Post Injection Timing on HC Emissions and Catalytic Oxidation Performance". In *SAE Technical Paper 2006-01-3442*. SAE International, 2006. (cited in pp. 82 and 169)

[7] Ye S, Yap Y H., Kolaczkowski S T., Robinson K and Lukyanov D. "Catalyst light-off experiments on a diesel oxidation catalyst connected to a diesel engine-methodology and techniques". *Chemical Engineering Research and Design*, Vol. 90 n^o 6, pp. 834 – 845, 2012. (cited in pp. 25, 84, 87, and 146)

[8] Bartley G J. "Identifying Limiters to Low Temperature Catalyst Activity". In *SAE Technical Paper 2015-01-1025*. SAE International, 2015. (cited in pp. 25, 87, and 139)

[9] Stadlbauer S, Waschl H, Schilling A and del Re L. "DOC Temperature Control for Low Temperature Operating Ranges with Post and Main Injection Actuation". In *SAE Technical Paper 2013-01-1580*. SAE International, 2013. (cited in pp. 29 and 87)

[10] Sutjiono R, Tayal P, Zhou K and Meckl P. "Real-Time On-Board Indirect Light-Off Temperature Estimation as a Detection Technique of Diesel Oxidation Catalyst Effectiveness Level". In *SAE Technical Paper 2013-01-1517*. SAE International, 04 2013. (cited in pp. 26, 87, 138, and 175)

[11] Li J, Szailer T, Watts A, Currier N and Yezerets A. "Investigation of the Impact of Real-World Aging on Diesel Oxidation Catalysts". *SAE Int. J. Engines 2012-01-1094*, Vol. 5, pp. 985–994, 04 2012. (cited in pp. 8, 26, and 87)

[12] Sampara C S., Bissett E J. and Assanis D. "Hydrocarbon storage modeling for diesel oxidation catalysts". *Chemical Engineering Science*, Vol. 63, pp. 5179–5192, 2008. (cited in pp. 26, 88, and 140)

[13] Bonfils A, Creff Y, Lepreux O and Petit N. "Closed-loop control of a SCR system using a NOx sensor cross-sensitive to NH3". *Journal of Process Control*, Vol. 24 n^o 2, pp. 368 – 378, 2014. (cited in p. 99)

[14] Yu Wang D, Yao S, Cabush D and Racine D. "Ammonia Sensor For SCR NOx Reduction". Technical report, DELPHI, 2007. (cited in pp. 38 and 99)

[15] Wang D Y, Yao S, Shost M, Yoo J-H, Cabush D, Racine D, Cloudt R and Willems F. "Ammonia Sensor for Closed-Loop SCR Control". *SAE International Journal of Passenger Cars - Electronic and Electrical Systems 2008-01-0919*, Vol. 1, pp. 323–333, apr 2008. (cited in pp. 9, 38, 99, and 138)

[16] Willems F, Cloudt R, van den Eijnden E, van Genderen M, Verbeek R, de Jager B, Boomsma W and van den Heuvel I. "Is Closed-Loop SCR Control Required to Meet Future Emission Targets?". In *SAE Technical Paper Series 2007-01-1574*. SAE International, apr 2007. (cited in pp. 8, 33, 34, 37, and 99)

[17] Song Q and Zhu G. "Model-based Closed-loop Control of Urea SCR Exhaust Aftertreatment System for Diesel Engine". In *SAE 2002 World Congress & Exhibition 2002-01-0287*. SAE International, mar 2002. (cited in pp. 30 and 99)

[18] Colombo M, Nova I and Tronconi E. "Detailed kinetic modeling of the NH3-NO/NO2 SCR reactions over a commercial Cu-zeolite catalyst for Diesel exhausts after treatment". *Catalysis Today*, Vol. 197 n^o 1, pp. 243 – 255, 2012. (cited in p. 99)

[19] Figura J, Pekar J, Krejza P, Mracek D, von Wissel D and Zhang T. "NO2/NOx Ratio and NH3 Storage Estimation of Automotive SCR Multi-Brick Systems". In *SAE Technical Paper 2017-01-0972*. SAE International, 2017. (cited in p. 99)

[20] Chatterjee D, Koci P, Schmeisser V, Marek M, Weibel M and Krutzsch B. "Modelling of a combined NOx storage and NH3-SCR catalytic system for Diesel exhaust gas aftertreatment". *Catalysis Today*, Vol. 151 n^o 3, pp. 395 – 409, 2010. Diesel emissions control catalysis. (cited in pp. 32 and 99)

[21] Feng T and Lue L. "The characteristics of ammonia storage and the development of model-based control for diesel engine urea-SCR system". *Journal of Industrial and Engineering Chemistry*, Vol. 28, pp. 97 – 109, 2015. (cited in p. 99)

[22] Guan B, Zhan R, Lin H and Huang Z. "Review of state of the art technologies of selective catalytic reduction of NOx from diesel engine exhaust". *Applied Thermal Engineering*, Vol. 66 n^o 1, pp. 395–414, 2014. (cited in pp. 32 and 99)

[23] Yuan X, Liu H and Gao Y. "Diesel engine SCR control: current development and future challenges". *Emission Control Science and Technology*, Vol. 1 n^o 2, pp. 121–133, 2015. (cited in pp. 32 and 100)

[24] Skaf Z, Aliyev T, Shead L and Steffen T. "The State of the Art in Selective Catalytic Reduction Control". In *SAE 2014 World Congress & Exhibition 2014-01-1533*. SAE International, 2014. (cited in pp. 32 and 100)

[25] Shost M, Noetzel J, Wu M-C, Sugiarto T, Bordewyk T, Fulks G and Fisher G B. "Monitoring, Feedback and Control of Urea SCR Dosing Systems for NOx Reduction: Utilizing an Embedded Model and Ammonia Sensing". In *SAE World Congress & Exhibition 2008-01-1325*. SAE International, apr 2008. (cited in pp. 33 and 100)

[26] Frobert A, Raux S, Creff Y and Jeudy E. "About Cross-Sensitivities of NOx Sensors in SCR Operation". In *SAE 2013 World Congress & Exhibition 2013-01-1512*. SAE International, apr 2013. (cited in pp. 100 and 211)

[27] Bartley G J., Chadwell C J., Kostek T M. and Zhan R. "SCR Deactivation Kinetics for Model-Based Control and Accelerated Aging Applications". In *SAE Technical Paper 2012-01-1077*. SAE International, 04 2012. (cited in pp. 33, 102, and 151)

Chapter 5

Thermal modelling and temperature observation

Contents

5.1 Introduction

Temperature plays a key role in the efficiency and behaviour of aftertreatment systems. For this reason, this chapter is devoted to present algorithms for heat transfer and temperature modelling.

In this sense, an observer of the DOC upstream temperature, a 1D heat transfer model, a 0D lumped heat transfer model, and a model to estimate

the temperature peak due to a post-injection pulse are presented. Different modelling approaches are assessed in order to reproduce the downstream sensor measurements with the thermal models, while a sensor model is required for this purpose. In this sense, a 3D approach requires the use of detailed processes and the volume discretization of the domain, which is out of the scope due to the high cost required in terms of computational resources.

5.2 Fast DOC upstream temperature estimation

The dynamics problem of the DOC upstream NTC sensor was presented in Chapter 4. Then, the work presented in this chapter improves the dynamic response of the DOC upstream temperature measurement by means of a data fusion (DF) technique. In this sense, DF methodologies have been developed during last years [1] to improve the dynamic response of exhaust gas concentrations measurements [2], since the contribution of the transient emission peaks during the standardized test cycles results in an important fraction of the cumulative total emissions [3]. Authors like *Alberer* [4] and *Guardiola et al.* [5–7] have developed a wide DF methodology for O_2 and NO_x species concentrations, improving the UEGO and NO_x sensors measurements on transient conditions. In these cases, the use of KF based observers allows the fast estimation of gas concentrations

In the case presented, the data fusion technique is applied to the DOC upstream temperature measurement by means of a KF-based observer, for what the reliable but slow measurement of the sensor is combined with a fast but non-necessary precise model, based on real-time ECU variables. Particularly, the fast model is based on a look-up table that depends on the injected fuel quantity and engine speed, and the heat transfer dynamics present along the exhaust line. Then, for the observer, the DOC upstream NTC sensor, the hot film flow-meter and the engine speed sensor are the required on-board sensors, while a couple of fast thermocouples, up- and downstream the turbine, are used to develop and validate the method. In this sense, the analysis performed in Chapter 4 showed the dynamics of these measurements.

The problem of the dynamic measurements of temperature sensors was firstly adressed by authors like *Kenneth et al.* [8] and *Kee et al.* [9]. However, the reconstruction technique was based on applying an energy balance to the heat transfer around two thermocouples at the same place, whose on-board

applicability is limited due to the requirement of two temperature sensors.

While the observer presented is focused on the DOC because it is the first after-treatment block placed in the exhaust line, the presented methodology could be also applied to other exhaust line configurations with different after-treatment platforms. In fact, the fast temperature estimation provides a better measurement of the thermal energy entering in the system at the location of the NTC sensor.

5.2.1 DOC upstream temperature modelling

This part of the section contains the description of the different models used in the fast DOC inlet temperature estimation. First, the engine exhaust temperature, i.e. the turbine upstream temperature, is modelled with an engine look-up table, whose signal is named T_{mod}. Then, the rest of the models mainly describe the dynamics of the system. While $T_{us,fast}$ represents the modelled T_{TC}, T_{us} represents the modelled T_{NTC}.

Procedures based on inducing step-like transitions can be used to identify and calibrate the modelled dynamic response of temperature sensors [10, 11]. However, due to heat transfer effects on the exhaust line, those step-like transitions applied in experimental tests are smoothed when exhaust mass flow arrives to the DOC inlet, where the TC and NTC sensors are located.

5.2.1.1 Fast DOC upstream temperature model, T_{mod}

The DOC upstream temperature is modelled as a Mean Value Engine Model (MVEM) based on a map calibrated off-line, which depends on engine speed n and fuel m_f in mg/str. On the one hand, ECU fuel mass estimation is fast and non-delayed, so it is able to perform cycle-to-cycle variations [12]. Consequently, ECU injection signals have enough dynamic response to be used as input to the fast temperature model. On the other hand, due to the measurement procedure itself, engine speed sensor dynamics allow to perform cylinder-to-cylinder combustion diagnostics [13,14], thus its dynamics response can be as well used as an input to the fast model.

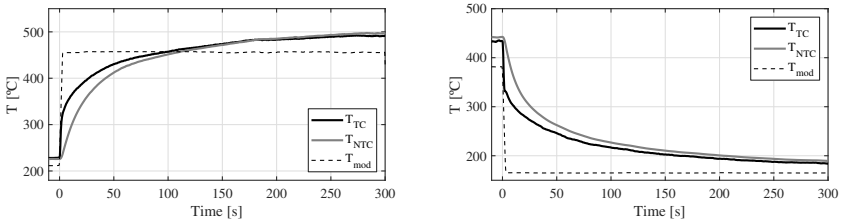

Figure 5.1. *Mean value temperature model applied to a load step.*

$$T_{mod,k} = \Theta(n_k, m_{f,k}) \tag{5.1}$$

Engine mapping has been traditionally used in internal combustion engine modelling [15]. However, the engine map look-up table must be calculated off-line because learning algorithms for temperature are difficult to implement in real time. This option was preferred instead of an air path model, which is fast enough as stated in Chapter 4 although it would be more complex and possibly less robust. Other authors like *Chen* and *Wang* [16] or *Eriksson* [17] also proposed control-oriented models based on look-up tables. In this sense, *Chen* and *Wang* [16] use a turbine efficiency look-up table whilst *Eriksson* [17] directly uses a temperature look-up table. The aim of the proposed model is to represent the steady temperature in order to have an a priori estimation of the temperature step, even if uncertainties may appear, for instance, due to different ambient conditions.

In this work, the employed look-up table has a density for n of one point every 400 rpm between 700 and 4500 rpm; and one point every 4mg/str for m_f. In this sense, higher density can improve the accuracy, although excessive density could lead to require excessive computational resources and in the limit, it could be redundant.

As depicted in Figure 5.1, the temperature increment provided by the model is representative of the temperature step. However, the steady state temperature does not perfectly match the final value. To solve this issue, the bias is modelled and so that the observer handles the difference between measured and modelled values when it comes to steady state.

5.2.1.2 T_{TC} from T_{mod}

Unfortunately, step-like transitions cannot be performed on-board for the characterization of the sensors due to exhaust line heat transfer up to the

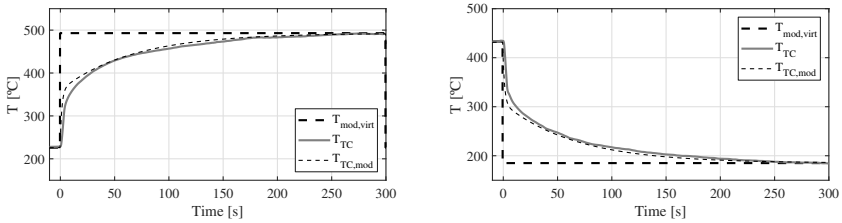

Figure 5.2. *Identification result of the second order system applied to T_{mod} to obtain $T_{TC,mod}$.*

sensors location. Previous dynamics study in Chapter 4 suggested two different dynamics in the exhaust line after a load step, one faster and one slower. This effect is modelled as a second order system, in order to obtain the signal of T_{TC} from T_{mod}. One pole (eq. 5.2) is meant to represent fast dynamics due to in-cylinder changes, whilst the other pole (eq. 5.3) is meant to represent slow dynamics due to heat transfer effects in the exhaust line. Model equations are:

$$T_1 = \frac{(1-b)d}{1-bz^{-1}} T_{mod} z^{-\tau/T_s} \tag{5.2}$$

$$T_2 = \frac{(1-c)(1-d)}{1-cz^{-1}} T_{mod} z^{-\tau/T_s} \tag{5.3}$$

$$T_{TC,mod} = T_1 + T_2 \tag{5.4}$$

where z is the z-transform variable, b is the filtering quantity of the fast pole, c is the filtering quantity of the slow pole, d is a factor to weight both fast and slow poles, τ is the model-to-sensor pure delay and T_s is the sampling period. Note that these equations are transformed into discrete form in order to be used in the KF algorithm.

A dynamic characterization of the sensor is mandatory to identify eq. (5.4). As seen in the previous Figure 5.1, model accuracy may not be perfect, so a synthetic signal of the ideal T_{mod} value is generated to calibrate the second order system. Therefore, the second order discrete filter is applied to a virtual signal of T_{mod}, named $T_{mod,virt}$, as represented in Figure 5.2. Note that this synthetic signal can only be generated off-line, since it is calculated from the steady-state value of T_{TC}.

Even if the measurements with the sensor are calibrated, it remains an inherent error because time invariant models for sensors are not completely

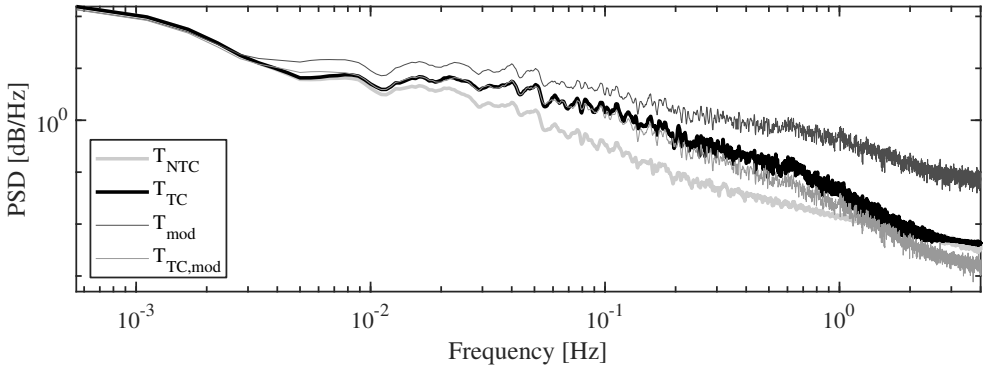

Figure 5.3. *Validation of the T_{mod} to T_{TC} model in the frequency domain.*

realistic. Although modelling shows good results, model parameters may depend on operating conditions, manufacturing discrepancies and others, which may lead to uncontrolled behaviours.

Results of the system identification can be seen in Figure 5.2. Identified values for the coefficients are: b=0.94, c=0.998 and d=0.5. These coefficients are kept constant for all engine operating conditions and are calculated off-line. The delay, τ, between T_{mod} and the sensors' measurements is not higher than 1 second, as it can be seen in Figures 4.2 and 5.1. Therefore, its value can be considered negligible in comparison with the dynamics, of dozens of seconds, of the system.

Even if dynamics could be appreciated in time domain, the bias would make difficult to validate the modelled temperature by comparing it with the actual measured temperature. Therefore, performance of the model is discussed in the frequency domain in Figure 5.3. A WLTC test is used for this validation because of its highly different conditions of exhaust mass flows and temperatures. In this sense, the range of frequencies shown embraces low frequencies in which the thermocouple and the NTC sensor responses are similar for being slow enough conditions, i.e. below 2 10^{-3}Hz, up to high frequencies, which may be associated to measurement noise, i.e. above 2Hz. Plots are slightly filtered in order to reduce possible confusion due to the number of different variables represented and their original high noise level.

It can be appreciated how the second order filter reduces the frequency content of T_{mod}, which can be considered the input signal, since it depends on engine speed and fuel consumption, until its signal matches T_{TC}. $T_{TC,mod}$ temperature presents slightly less frequency content than T_{TC} at high frequencies, although it is still higher than T_{NTC}. At the highest frequencies present

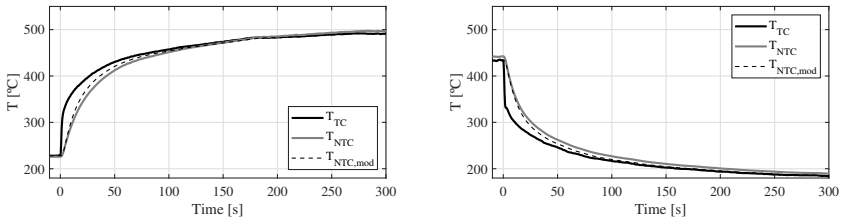

Figure 5.4. *Identification result of the first order system applied to T_{TC} to obtain $T_{NTC,mod}$.*

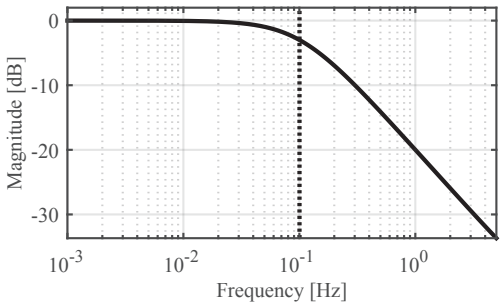

Figure 5.5. *Magnitude Bode of the first order system applied to T_{TC} to obtain $T_{NTC,mod}$.*

in the plot, the frequency content of $T_{TC,mod}$ is even lower than that of T_{NTC}, although in this range, frequency content of T_{NTC} is almost equal to T_{TC}.

Model output $T_{TC,mod}$ can be related to the actual value of T_{TC} considering a bias, θ:

$$T_{TC} = T_{TC,mod} + \theta \tag{5.5}$$

5.2.1.3 T_{NTC} from T_{TC}

Although other model structures could be used, a discrete linear first order model is chosen to represent the temperature measurement of the NTC sensor with respect to the thermocouple. The modelling equation results in:

$$T_{NTC,mod} = T_{NTC} + \nu = \frac{1-a}{1-az^{-1}} T_{TC} + \nu \tag{5.6}$$

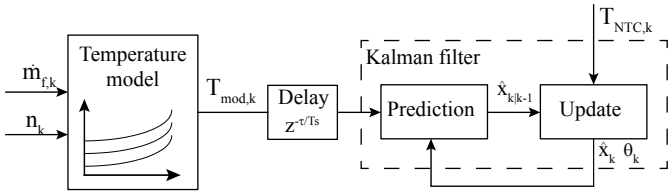

Figure 5.6. *Scheme of the proposed estimation procedure.*

where a is the filtering quantity and the main parameter, since no delay between sensors' measurements is considered due to its closed location. A noise ν is added to the delayed and filtered value T_{TC} in order to represent the measurement noise and other uncontrolled effects. Results of the system identification can be seen in Figure 5.4.

The Bode plot of the identified system, if a=0.986, is shown in Figure 5.5, which is calculated by transforming the transfer function in the z domain to the s domain through the Tustin method [18, 19]. The cut-off frequency, established when bode gain is -3 dB, is 0.14 Hz. Although the obtained value of the coefficient a is used throughout the section, some effect of operating conditions on the optimal filtering quantity a is expected.

5.2.2 Fast temperature estimation

A Kalman filter is used in order to fuse data from the sensor measurement and the model. Kalman filter behaves as a low pass filter for the temperature model and as a high pass filter for the sensor measurement [7]. Through the combination of the sensor measurement and the model information, the Kalman filter is used to track the value of the bias θ between T_{TC} and $T_{TC,mod}$, thus providing an estimate of T_{TC}, $\hat{T}_{TC}$.

Figure 5.6 shows a scheme of the proposed temperature estimation structure. All calculations and equations are set-up in discrete form with a constant sampling frequency f_s of 10 Hz. Main inputs are injected fuel mass m_f, engine speed n and NTC sensor measurement T_{NTC}.

5.2.2.1 Observer design

The proper combination of equations (5.1)-(5.6) allows to write the system in the following linear discrete-time state-space representation:

$$\mathbf{x_k} = \mathbf{A}\mathbf{x_{k-1}} + \mathbf{B}u_k + \mathbf{W_k} \tag{5.7}$$

$$y_k = \mathbf{C}\mathbf{x_k} + \nu_k \tag{5.8}$$

where $\mathbf{x_k}$, the states vector of the system; y_k, the NTC temperature measurement; and u_k, the model input, are defined as:

$$\mathbf{x_k} = \begin{bmatrix}\theta & T_1 & T_2 & T_{TC,mod} & T_{NTC,mod}\end{bmatrix}^T_{\mathbf{k}} \tag{5.9}$$

$$y_k = T_{NTC,k} \tag{5.10}$$

$$u_k = T_{mod,k-\tau/T_s} \tag{5.11}$$

The description of the system matrices (5.7) is:

$$\mathbf{A} = \begin{bmatrix} 1 & 0 & 0 & 0 & 0 \\ 0 & b & 0 & 0 & 0 \\ 0 & 0 & c & 0 & 0 \\ 1 & 1 & 1 & 0 & 0 \\ 0 & 0 & 0 & 1-a & a \end{bmatrix} \tag{5.12}$$

$$\mathbf{B} = \begin{bmatrix} 0 & (1-b)d & (1-c)(1-d) & 0 & 0 \end{bmatrix}^T \tag{5.13}$$

$$\mathbf{C} = \begin{bmatrix} 0 & 0 & 0 & 0 & 1 \end{bmatrix} \tag{5.14}$$

$$\mathbf{W_k} = \begin{bmatrix} w_k & 0 & 0 & 0 & 0 \end{bmatrix}^T \tag{5.15}$$

The selected distribution of noises considers that a white noise is related to the sensor measurement (ν_k) and other white noise is related to the model (w_k). *Kalman* [20] addressed the optimal solution of the estimation problem, i.e. estimating the state x of the system from the evolution of y and u. In a first step, the state is estimated considering the system inputs and their expected dynamic characteristics:

$$\hat{\mathbf{x}}_{\mathbf{k|k\text{-}1}} = \mathbf{A}\hat{\mathbf{x}}_{\mathbf{k\text{-}1}} + \mathbf{B}u_k \tag{5.16}$$

and in a second step the *a priori* estimate of the state $\hat{\mathbf{x}}_{\mathbf{k|k\text{-}1}}$ is updated using the error calculation ϵ_k and the Kalman filter gain $\mathbf{K_k}$:

$$\epsilon_k = y_k - \mathbf{C}\hat{\mathbf{x}}_{\mathbf{k|k\text{-}1}} \tag{5.17}$$

$$\hat{\mathbf{x}}_{\mathbf{k}} = \hat{\mathbf{x}}_{\mathbf{k|k\text{-}1}} + \mathbf{K_k}\epsilon_k \tag{5.18}$$

where the Kalman gain $\mathbf{K_k}$ could be generally obtained on-line with the covariance matrices of the noises distribution by solving the Riccati equation. However, the considered system is Linear Time Invariant (LTI) and fully observable system, then the Kalman gain is constant [21]. Then, it can be calculated off-line with the variances of the noises σ_w^2 and σ_u^2 by an iterative process:

$$\mathbf{K}_\infty\left(\sigma_w^2/\sigma_v^2\right) = \lim_{k\to+\infty} \mathbf{K_k} \tag{5.19}$$

The use of a constant gain $\mathbf{K}_\infty$ avoids $\mathbf{K_k}$ calculation in each iteration using the Riccati equation, so it is more efficient in terms of ECU computational resources. Eventually, temperature estimation is the fourth state of the state-space vector:

$$\hat{T} = \hat{T}_{TC,mod} \tag{5.20}$$

5.2.2.2 Algorithm tuning

Algorithm tuning consists in the calibration of the system coefficients a, b, c, d and τ, which have been previously obtained for each system independently, as well as the calibration of the observer.

Observer tuning consists in the calibration of sensor v_k and model w_k noises, which are considered as Gaussian distributions with zero mean and variances given by σ_w^2 and σ_v^2. Uncertainties in sensor characterization and bias cancelling performance make difficult the selection of an optimal noises combination. According to [22], the time needed to cancel the bias depends on the variances fraction σ_w^2/σ_v^2.

An analysis of a, b, c, d, τ and σ_w^2/σ_v^2 reveals that a and σ_w^2/σ_v^2 have major impact on the calibration. Therefore, a parametric study of how these two variables affect estimation dynamics is shown in Figure 5.7 for 3 different values of each coefficient. Table 5.1 contains those values with their corresponding errors: the root mean squared error (RMSE), the squared error, R^2, or determination coefficient, and the integral error (IE). The second value corresponds to the final calibration, whilst the first value is lower and the third is higher. The rest of coefficients b, c and d are those used for the fast temperature estimation.

In both plots of Figure 5.7, the estimated temperature is shown as the intermediate line of the parametric study. The calibrated value for a, found

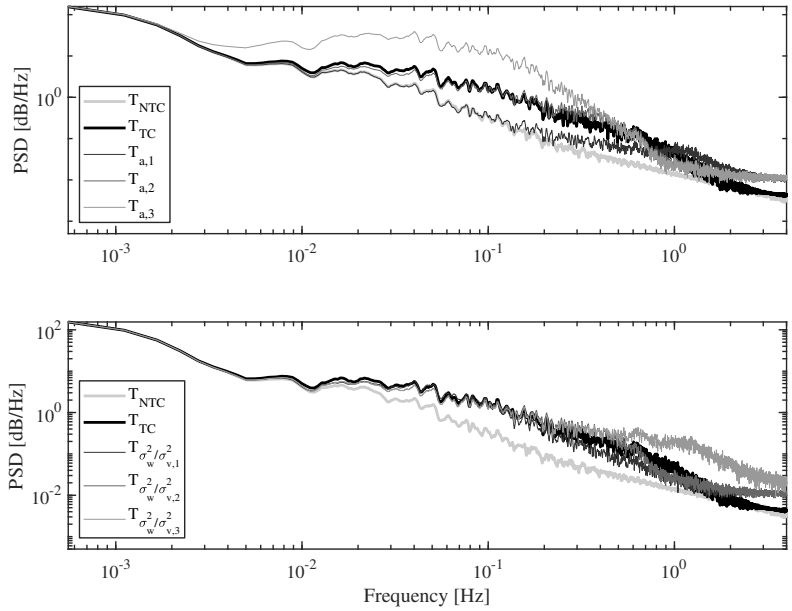

Figure 5.7. *Sensitivity analysis of a (Top plot) and σ_w^2/σ_v^2 (Bottom plot) in the frequency domain.*

Table 5.1. *Values of the parametric study.*

Coefficient	Value	RMSE	R^2	IE
a_1	0.9	217.7	0.14	-39,199
a_2	0.986	11.7	0.998	6,760
a_3	0.999	29.2	0.985	11,392
$\sigma_w^2/\sigma_{v,1}^2$	0.01	13.1	0.997	9,054
$\sigma_w^2/\sigma_{v,2}^2$	50	11.7	0.998	6,760
$\sigma_w^2/\sigma_{v,3}^2$	5000	13.6	0.997	6,579

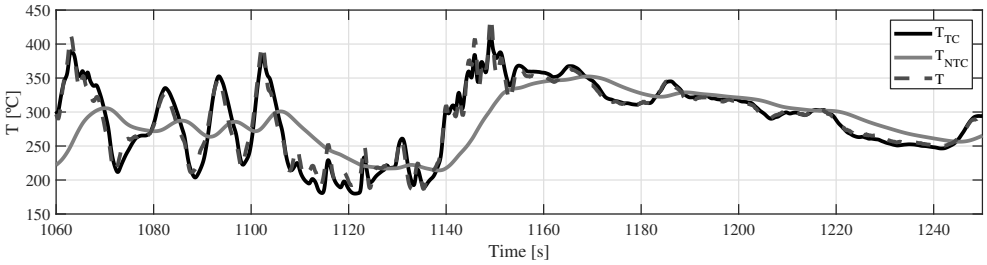

Figure 5.8. *Result of estimated temperature in a time window of a WLTC.*

with the step test, results in a good characterization of the sensor dynamics, whilst σ_w^2/σ_v^2 has been calibrated using the PSD. Top plot shows how by varying a, the estimation has more (a decreases) or less (a increases) frequency content. Bottom plot shows how by varying σ_w^2/σ_v^2, frequency content at high frequencies is increased (σ_w^2/σ_v^2 increases) or decreased (σ_w^2/σ_v^2 decreases). σ_w^2/σ_v^2 also marks from which frequency the variation has impact on the PSD. The errors study shows the best results for the calibrated values.

The parametric study of a and σ_w^2/σ_v^2 in Figure 5.7 points out how the observer could increase its frequency content if necessary by decreasing a and increasing σ_w^2/σ_v^2. In this sense, the second order system applied to T_{mod} could apply a less severe filter by modifying its coefficients. That is, adapting the presented algorithm to other pair of sensors can be done by re-tuning the coefficients. Then, in case the thermocouple used were not able to reproduce the actual temperature due to thermal inertia and it were necessary, response speed of the estimation could be increased by coefficients tuning.

5.2.3 Algorithm validation

An experimental validation of the algorithm is carried out in next paragraphs. Validation tests use the fast thermocouple measurement as a reference to compare with the estimated temperature.

Results of the calibration for the WLTC, in time domain during a temporal window, can be seen in Figure 5.8. Despite minor differences in severe peaks and valleys, estimation matches quite well the temperature measured by the thermocouple. The analysis made in the frequency domain for this test may explain the high performance achieved for the temperature estimation in this test.

A test that stresses the dynamics of the system, with high steps of exhaust mass flow and temperature, is shown in Figure 5.9. A difference in steady-

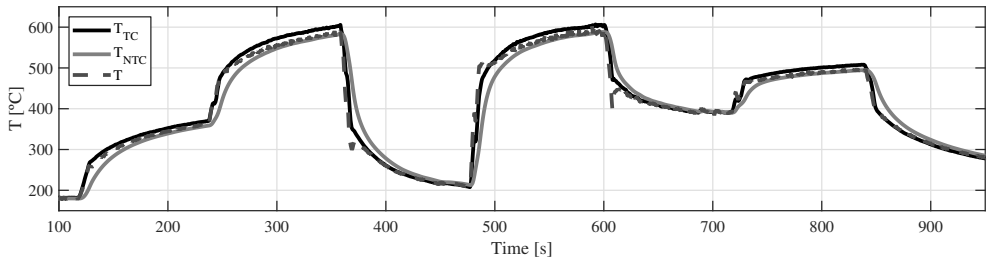

Figure 5.9. *Result of estimated temperature in a time window of a test with high steps in engine operating conditions.*

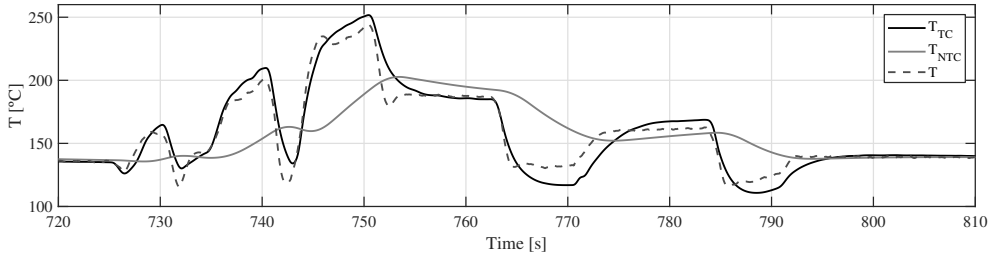

Figure 5.10. *Result of estimated temperature in a time window of a NEDC.*

state temperature can be noticed between NTC and TC measurements, due to its slight different location in the exhaust line: NTC sensor is slightly closer to the DOC ceramics, which may interfere in sensor measurements. In some cases, and due to non-modelled phenomena with a first order sensor model, there is an overshoot of estimated temperature at the steps. Even so, it can be appreciated that during a transient, the estimated temperature $\hat{T}$ performs faster than the NTC measurement, matching the thermocouple signal T_{TC}.

Algorithm performance is eventually proved in a NEDC for a time window of the cycle. Results of the NEDC (Figure 5.10) show that even if the model has some difference with the measured TC temperature due to the effect of operating conditions, it is able to reproduce fast transients. Differences are mainly appreciated during valleys of temperature, where uncertainties in modelling may cause under-estimations of measured T_{TC} temperature. During non-transient phases, estimated value is the T_{NTC} signal.

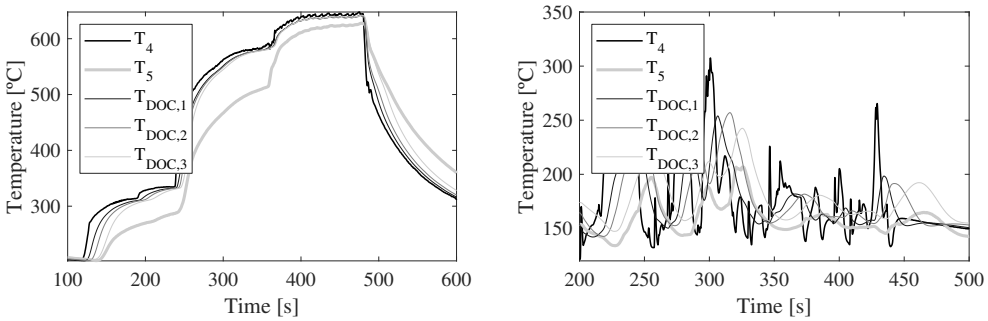

Figure 5.11. *Transient phases to show the non-linear evolution of temperature at high temperature steps, left plot, and the more linear evolution during high dynamic phases, right plot. From black to light grey represents the temperature evolution from upstream to downstream measurements of the DOC, being $textT_{DOC,1}$, $textT_{DOC,2}$ and $textT_{DOC,3}$ thermocouple measurements in the catalyst axial direction.*

5.3 Control-oriented 1D model

This section presents a 1D temperature model for a catalyst, which is complemented with a sensor model, in order to reproduce the downstream sensor measurement of the DOC. Therefore, the model is able to estimate the DOC downstream temperature and its axial temperatures distribution. Note that for this section, the measurements are shown for the non-impregnated DOC, in order to characterize the heat transfer and avoid exothermic phases due to species oxidation.

Results of the model are compared for different upstream measurements as model inputs, i.e. the NTC sensor measurement, a fast thermocouple measurement and the fast estimation by means of the observer described before. In this sense, these results will be compared in next section with the performance of a lumped 0D model.

The necessity of implementing a sensor model is reflected in Figure 5.11, where upstream, downstream and DOC intermediate temperature measurements are shown for two transients phases. In the left plot, a step of temperature from 200°C to 600°C shows that while the upstream and intermediate temperatures are close, the downstream temperature presents a sensitive bias, so there is not a linear correlation of the temperature evolution between the upstream and downstream measurements. On the other hand, the right plot, which contains a phase of the WLTC, presents a more linear correlation of the

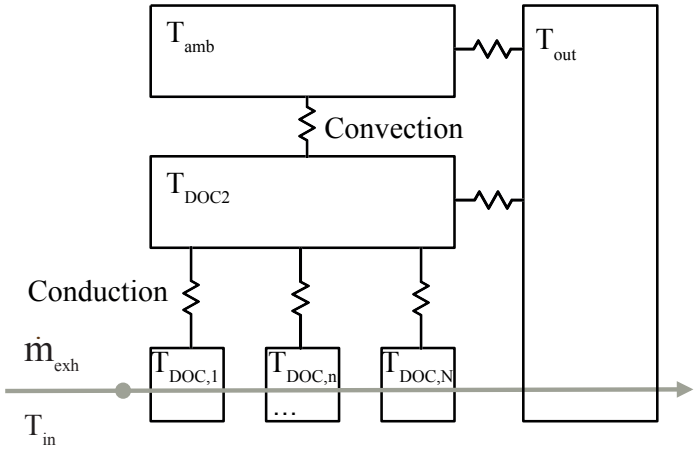

Figure 5.12. *Structure of the 1D temperature model.*

temperatures evolution between up-and downstream measurements. Therefore, the need for the sensor model is better appreciated during high temperature steps, while it is not evident in highly dynamic phases like the WLTC.

The 1D model structure is presented in Figure 5.12, which is composed of N axial slices that have heat conduction with a DOC layer named T_{DOC_2}. Then, this layer has heat convection with the ambient, while the sensor model is affected by both $T_{DOC,2}$ and ambient temperatures. The equations of the model are the following:

$$\frac{dT_{DOC,n}}{dt} = c_1 \, \dot{m}_{exh}(T_{gas} - T_{DOC,n}) + c_2(T_{DOC_2} - T_{DOC,n}) \tag{5.21}$$

where $T_{DOC,n}$ represents the monolith temperature of the n axial section, c_1 represents the heat convection coefficient between the gas and the $\mathrm{T_{DOC}}$, and c_2 represents the conduction coefficient between $\mathrm{T_{DOC}}$ and $\mathrm{T_{DOC_2}}$, whose equations are shown next:

$$c_1 = c_{p,gas}/(m_{DOC} \; c_{p,DOC}) \tag{5.22}$$

$$c_2 = k_{DOC-DOC_2} \; A_{DOC-DOC_2}/(m_{DOC} \; c_{p,DOC}) \tag{5.23}$$

where $c_{p,gas}$ and $c_{p,DOC}$ represent the specific heat of the gas and the DOC bulk, respectively, m_{DOC} represents the DOC mass, while $k_{DOC,n-DOC_2}$ and

$A_{DOC,n-DOC_2}$ represent the conduction coefficient and the area between $\mathrm{T_{DOC}}$ and $\mathrm{T_{DOC_2}}$.

$$\frac{dT_{DOC_2}}{dt} = c_3 \sum_{n=1}^{N} (T_{DOC,n} - T_{DOC,2}) + c_4 \ (T_{amb} - T_{DOC,2}) \tag{5.24}$$

c_3 and c_4 are the conduction and convection constants, between $\mathrm{T_{DOC}}$ and $\mathrm{T_{DOC_2}}$, and $\mathrm{T_{DOC}}$ and T_{amb}, respectively, while T_{amb} represents the ambient temperature. The equations of c_3 and c_4 are described next:

$$c_3 = k_{(DOC-DOC_2)} \ A_{DOC-DOC_2}/(m_{DOC,2} \ c_{p,DOC,2}) \tag{5.25}$$

$$c_4 = h_{DOC_2-amb} \ A_{DOC_2-amb}/(m_{DOC,2} \ c_{p,DOC,2}) \tag{5.26}$$

where $c_{p,DOC,2}$ and $m_{DOC,2}$ represent the specific heat and the mass of $\mathrm{T_{DOC_2}}$. The sensor model equation that represents the measured temperature T_{out} is next represented in the discrete time domain, due to the filtering techniques used.

$$\begin{aligned} &T_{out,k} = T_{out,k-1} \ \beta_k + (1 - \beta_k) \ T_{DOC_{N,k}} + \\ &dt \ h_{sen} \ A_{sen}/(m_{sen} \ c_{p,sen}) \ ((\gamma \ T_{DOC2_{k-1}} + (1 - \gamma) \ T_{amb}) - T_{out,k-1}) \end{aligned} \tag{5.27}$$

where k is the temporal step in the discrete form, γ is a filter between $\mathrm{T_{DOC_2}}$ and the ambient temperature, which is a tunable parameter, while β is a filter for the effect of $T_{DOC,N}$ and the previous sensor temperature, modelled as a nonlinear function that depends on $\dot{m}_{exh}$ through equation (5.28).

$$\beta = \beta_{min} + \left[(\beta_{max} - \beta_{min})^z - (\beta_{max} - \beta_{min})^z \frac{(\dot{m}_{exh} - \dot{m}_{exh,min})^z}{(\dot{m}_{exh,max} - \dot{m}_{exh,min})^z} \right]^{(1/z)} \tag{5.28}$$

where β_{max}, β_{min}, $\dot{m}_{exh,min}$, $\dot{m}_{exh,max}$ and z are tunable parameters. This equation results in a curve that varies from $\beta(\dot{m}_{exh} = \dot{m}_{exh,min}) = \beta_{max}$ to $\beta(\dot{m}_{exh} = \dot{m}_{exh,max}) = \beta_{min}$. Then, depending on the value of z, expression (5.28) becomes concave or convex, which is represented in Figure 5.13 for different values of the exponent z.

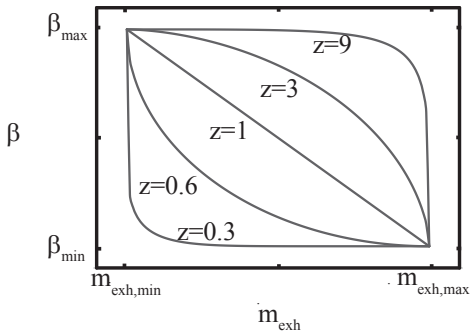

Figure 5.13. *Graphical representation of equation (5.28) for 5 different values of parameter z.*

Summarizing the sensor model presented in eq. (5.27), it contains a low pass filter, as well as the energy balance between the sensor and an averaged factor between the DOC external layer and the ambient temperature. In this sense, the γ parameter represents the incidence of the DOC external layer and the ambient temperature on the sensor temperature.

5.3.1 Model performance with different upstream temperatures as model inputs

Next paragraphs are oriented to assess the effect of different temperature inputs on the model, comparing results for the DOC upstream thermocouple measurement, the NTC sensor measurement and the fast estimation, previously presented, using data fusion of the NTC measurement and a fast model. For this purpose, the model is calibrated by means of a minimization routine for the defined error, using experimental data of the non-impregnated DOC.

The test selected to validate the model contains a WLTC and a combination of the engine operating points presented in Figure 3.15, so that it contains high dynamic driving conditions and high temperature steps, representative of a wide range of operating conditions. Figures 5.14, 5.15 and 5.16 represent the model application with the thermocouple, the NTC sensor, and the fast estimation as inputs, respectively.

The selected error for the minimization routine is the absolut maximum error. Otherwise, if the integral error were used, high temperature steps would lead to high errors peaks, which do not effectively affect the integral. However, these error peaks represent a bad characterization of the dynamics of the

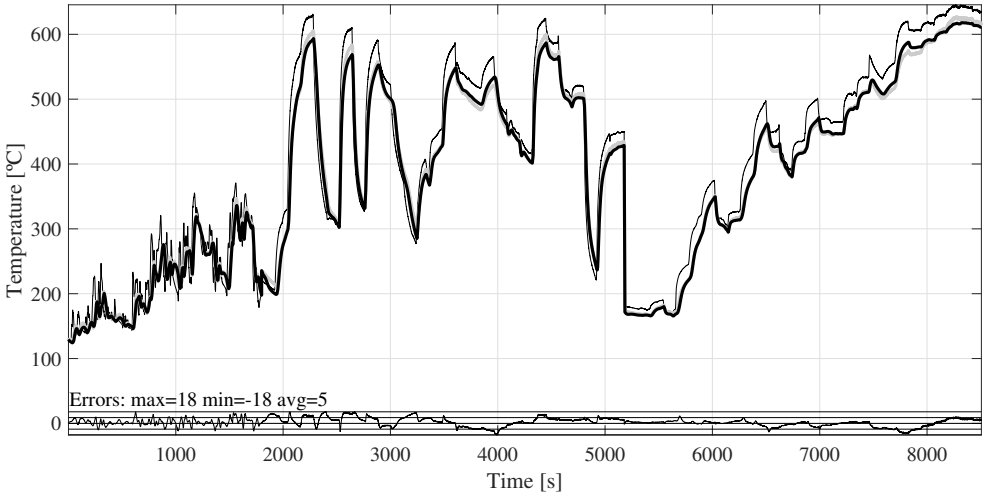

Figure 5.14. *Model evaluation test with thermocouple measurement as input. Thin black stands for model input, thick grey stands for downstream measurement and thick black stands for model estimation. The bottom part contains the instantaneous model error, with horizontal lines that represent* ϵ_{max}*, 3/4* ϵ_{max}*, 1/2* ϵ_{max} *and 1/4* ϵ_{max}*.*

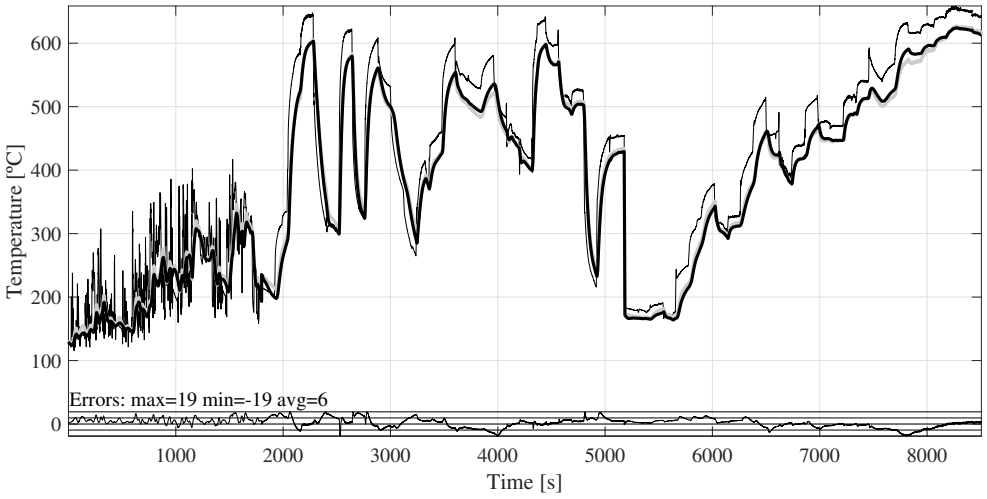

Figure 5.15. *Model evaluation test with NTC sensor measurement as input. Thin black stands for model input, thick grey stands for downstream measurement and thick black stands for model estimation. The bottom part contains the instantaneous model error, with horizontal lines that represent* ϵ_{max}*, 3/4* ϵ_{max}*, 1/2* ϵ_{max} *and 1/4* ϵ_{max}*.*

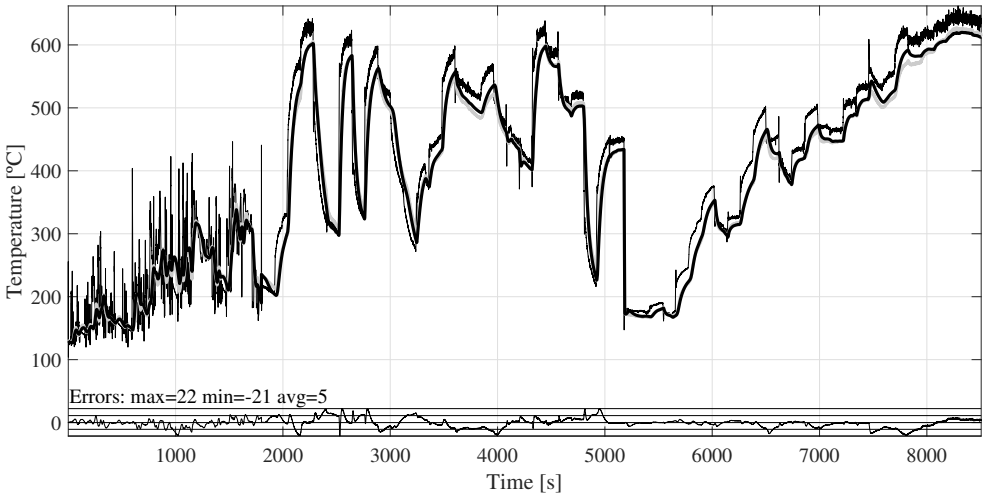

Figure 5.16. *Model evaluation test with fast temperature estimation measurement as input. Thin black stands for model input, thick grey stands for downstream measurement and thick black stands for model estimation. The bottom part contains the instantaneous model error, with horizontal lines that represent* ϵ_{max}*, 3/4* ϵ_{max}*, 1/2* ϵ_{max} *and 1/4* ϵ_{max}*.*

Table 5.2. *Model errors for the different upstream temperaure inputs.*

Input	ϵ_{max}	ϵ_{min}	$\int \lvert\epsilon\rvert$
T_{TC}	18	-18	318
T_{NTC}	19	-19	368
T_{Kalman}	22	-21	492

model. For this reason, the absolut maximum error is used, since the DOC dynamics are better characterized by the model.

Table 5.2 contains the errors of the maximum, minimum and integral errors of the different model inputs. In this sense, the accuracy is similar for T_{TC} and T_{NTC} measurements, which indicates that the outlet measurement can be modelled with a NTC sensor. However, the axial temperature, not considered in the error, is better represented with the thermocouple measurement. On the other hand, the error using the fast temperature estimation as input is higher than both T_{TC} and T_{NTC}, which can be explained by the extra error that the estimation induces. In any case, the accuracy of the model for estimating the

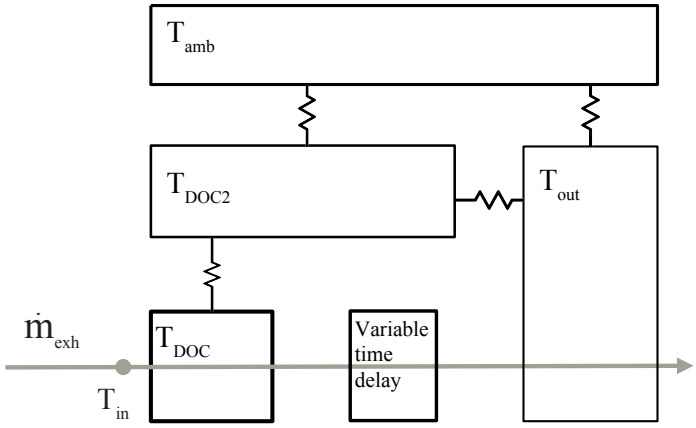

Figure 5.17. *Structure of the 0D temperature model.*

downstream temperature is similar for the three inputs, which is contained in a range of around $\pm 20°$C.

5.4 Control-oriented 0D lumped model

The control-oriented 0D model is presented in this section, whose objective is to capture the DOC outlet temperature. To that aim, the model requires the upstream temperature and the exhaust mass flow as inputs. In the previous section, the NTC sensor measurement is proven to be sufficient to estimate the downstream temperautre, so it is the used input.

The DOC model presented is based on two lumped thermal energy reservoirs, as in the previously presented 1D model for T_{DOC} and T_{DOC_2}, which represent the DOC core and its housing, respectively. Its scheme is shown in Figure 5.17. In this model, the exhaust gas $\dot{m}_{exh}$ entering into the DOC leaves it at the DOC inner part temperature. In this sense, the equations governing the DOC temperature estimation are presented next:

$$m_{DOC}\ c_{v,DOC}\ \frac{dT_{DOC}}{dt} = \dot{m}_{exh}\ c_p, gas\ (T_4 - T_{DOC}) + kA\ (T_{DOC_2} - T_{DOC}) \quad (5.29)$$

where m_{DOC} is the mass of the inner part of the DOC, $c_{v,DOC}$ is the heat capacity, kA represents the heat transfer coefficient between the outer part of

the DOC and DOC bulk. The external covering to the DOC bulk is considered next, which allows a better representation of the temperature dynamics:

$$m_{DOC_2}\ c_{v,DOC_2}\ \frac{dT_{DOC_2}}{dt} = - kA'\ (T_{DOC_2} - T_{DOC}) - hA'\ (T_{DOC_2} - T_{amb}) \quad (5.30)$$

where kA' represents the heat transfer coefficient between the DOC bulk and its outer part and hA' represents the convection coefficient with the ambient temperature. Note that radiation is neglected and that convective coefficients are considered constant for the sake of simplicity.

In order to represent the DOC dynamics with the lumped model, the DOC temperature is modelled by means of a variable delay, τ, which depends on the exhaust mass flow:

$$T^{\tau}_{DOC}\,(t) = T_{DOC}\,(t - \tau) \quad (5.31)$$

where τ is a nonlinear function that depends on the exhaust mass flow:

$$\tau = \tau\,(\dot{m}_{exh}) \quad (5.32)$$

The $\tau\,(\dot{m}_{exh})$ is an analogous function of the β function presented in equation (5.28), i.e. a parameter z defines the concave or convex shape of the curve between their minimum and maximums, being τ_{max}, τ_{min}, $\dot{m}_{exh,min}$, $\dot{m}_{exh,max}$ and z tunable parameters. Then, $\tau(\dot{m}_{exh} = \dot{m}_{exh,min}) = \tau_{max}$ and $\tau(\dot{m}_{exh} = \dot{m}_{exh,max}) = \tau_{min}$. In this sense, considering such variable delay approach allows simulating the effects of the heat transfer along the monolith while keeping a very simple model.

Finally, the downstream DOC temperature estimation, T_{out}, is considered to be equal to the DOC bulk temperature in the next time step. Such simplified DOC models show good performance for control tasks [16]. However, as in the previously shown 1D model, the sensor dynamics are analogically modelled with the following expression:

$$T_{out,k} = \beta\ T_{out,k-1} + (1 - \beta)\ T^{\tau}_{DOC,k-1} - \alpha\ (T_{out,k-1} - (\gamma T_{DOC_2,k-1} + (1 - \gamma)\ T_{amb})) \quad (5.33)$$

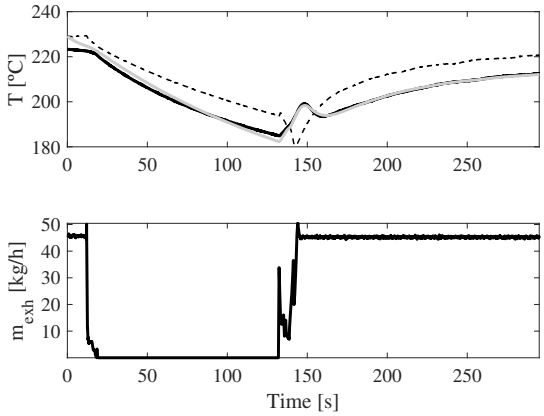

Figure 5.18. *Start and stop test with model estimation. Top plot: dotted black stands for T_4, thick grey stands for $T_{out,exp}$ and thick black stands for $T_{out,mod}$.*

where this equation contains the same low pass filter and energy balance structure of the 1D model in equation (5.27). In this sense, β and γ have an equivalent meaning, while α represents the heat transfer coefficient between the sensor and its surroundings.

The β definition enables the reproduction of the sensor output during start&stop operation: the sensor temperature decreases when the engine is stopped and the exhaust flow is zero due to thermal losses with the ambient; however the DOC monolith temperature losses are slower. Then, when the engine is started again, the sensor temperature rapidly increases as a consequence of the heat released from the monolith to the exhaust gas flow. Figure 5.18 illustrates such behaviour during a start&stop event, where the model estimation is able to capture the described process.

Model parameters identification As done with the previous 1D model calibration, the use of a passive DOC allows decoupling the thermal model from the chemical model, allowing an independent identification of the heat transfer, thermal capacity and dynamics related coefficients. Due to the non-physical approach of some parts of the model, its calibration and validation is intense, showing a set of training and validation tests, which are presented next, and the start&stop phase of Figure 5.18.

The α parameter is identified with the start&stop tests, since $\beta(\dot{m}_{exh} = 0) = 1$. However, the rest of parameters are identified with the set of training tests presented in Figure 5.19, in which the error is contained within a $\pm 22°$C interval, similar to the 1D model performance. This set of training tests

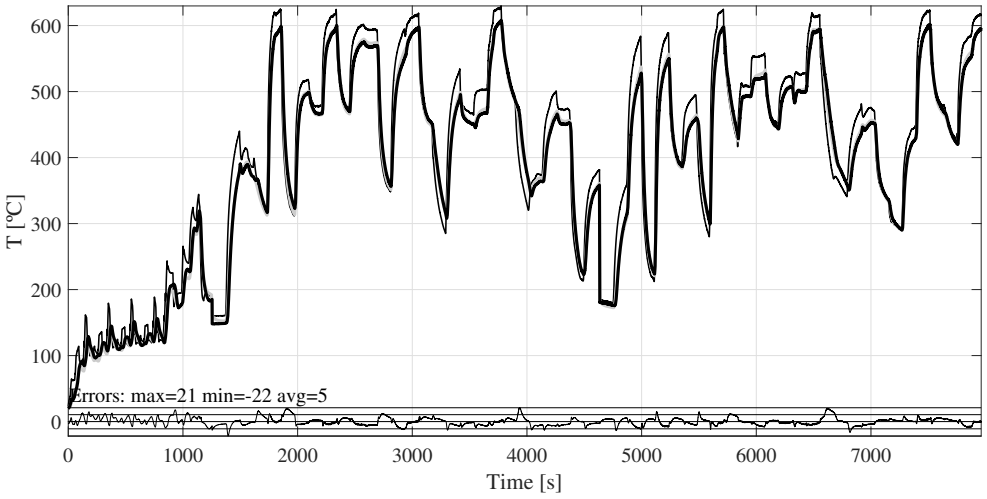

Figure 5.19. *Results of the thermal model fit to the passive DOC for the training dataset. Top plot: NEDC (cold starting) homologation cycle. Bottom plot: dynamic tests. Black: T_{in} Grey: $T_{out,exp}$ Dashed grey: $T_{out,mod}$.*

include an NEDC starting at ambient conditions, representative of a common driving cycle at mid exhaust temperatures, and a test with abrupt steps, stressing the dynamics of the system, covering a wide range of temperatures.

Then, Figure 5.20 shows the results of the validation tests, which are the same than those presented for the 1D model validation. Remind that these tests contain high dynamic phases and high temperature steps. As a result, its errors are contained in a $\pm 22°$C interval, similar to the 1D model performance. Therefore, the accuracy of this model is proven to be similar to a more demanding 1D model in terms of computation requirements.

The residuum generated by comparing the measured outlet temperature of an impregnated DOC with the model outlet temperature can be used for diagnostics purposes. This highlights the necessity of replicating the sensor signal rather than the actual gas temperature, while the diagnosis concept is detailed in Chapter 7.

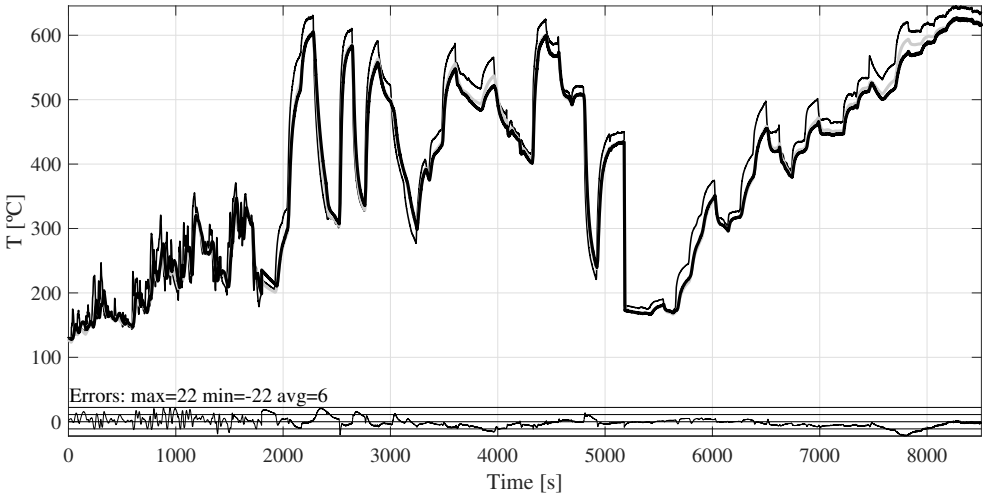

Figure 5.20. *Results of the thermal model fit to the passive DOC for the validation dataset. Top plot: NEDC (warm starting) and WLTP homologation cycles. Bottom plot: Dynamic tests. Black:* T_{in} *Grey:* $T_{out,exp}$ *Dashed grey:* $T_{out,mod}$*.*

5.5 Temperature model of oxidized post-injection pulses

This section of the chapter presents a method to estimate the pulse of temperature due to DOC oxidation of a post-injection event. Specifically, the purpose of the model is to estimate the increment between the steady-state measurement and the pulse increment, named ΔT.

A set of specific experimental tests is necessary in order to evaluate the behaviour of the pulse under different injection profiles and exhaust mass flows. Tests consist of a train of 5 pulses at 6 different exhaust mass flows, as shown in Figure 5.21, and 3 different post-injection rates: 4, 6 and 8 mg/str. In total, 90 samples of pulses of different characteristics are performed. An example of the DOC up- and downstream temperatures, for a given test, is shown in Figure 5.22. The small temperature peak at the inlet is due to small burning of the post-injection inside the combustion chamber during the last stages of the exhaust stroke.

In equation (5.34), the normalization of the temperature pulse under steady state conditions is described. The energy released by the oxidation of the pulse

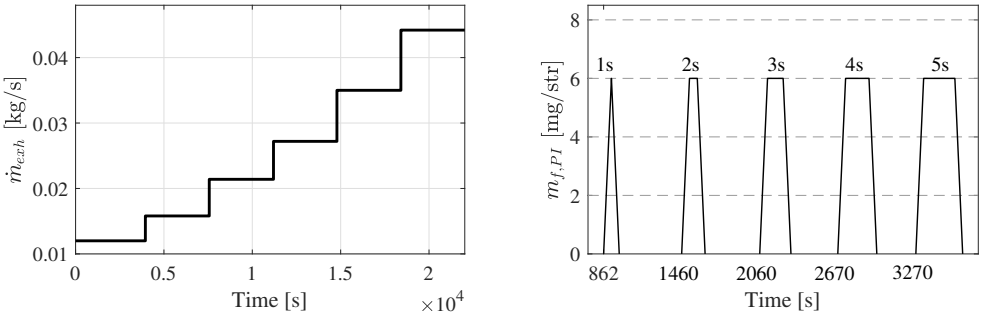

Figure 5.21. *Left plot: Exhaust mass flow of the post-injection pulses test. Right plot: Shape of the 6 mg/str post-injection train for every exhaust mass flow step.*

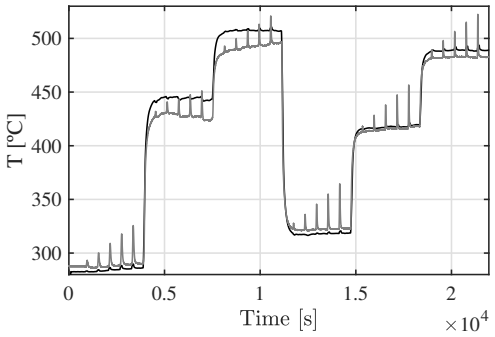

Figure 5.22. *Inlet (black) and outlet(grey) temperatures at the post-injection pulses test of 6 mg/str.*

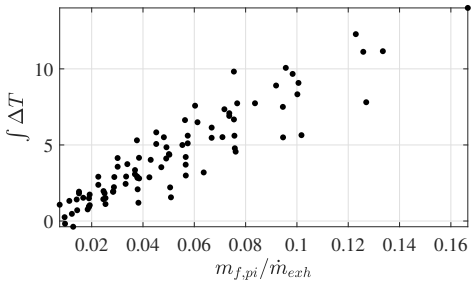

Figure 5.23. *Linear correlation between the integral of the temperature pulse and the fraction of post-injection mass over exhaust mass flow.*

in the DOC is the energy used to increase the temperature of the air during the pulse:

$$\int \dot{m}_{PI} H_f dt = \int \dot{m}_{exh} c_p \frac{\Delta T}{dt} dt \tag{5.34}$$

where $\dot{m}_{PI}$ is the mass flow of post injected fuel, H_f is the lower heating value of the fuel, c_p is the specific heat capacity of the air, ΔT is the temperature increment due to oxidation and $\dot{m}_{exh}$ is the exhaust mass flow. $\dot{m}_{exh}$ is calculated through the addition of the exhaust mass flow and the fuel mass flow.

After integrating the mass of post injected fuel and, whilst keeping constant the exhaust mass flow and keeping the integral of the temperature pulse:

$$m_{f,PI} H_f = \dot{m}_{exh} c_p \int \Delta T \tag{5.35}$$

A linear correlation is eventually obtained:

$$\int \Delta T = \frac{m_{f,pi}}{\dot{m}_{exh}} \frac{H_f}{c_p} \tag{5.36}$$

where H_f/c_p is constant and therefore $m_{f,pi}/\dot{m}_{exh}$ and $\int \Delta T$ are correlated with a polynomial function of grade 1 with origin in 0 and slope H_f/c_p, as shown in Figure 5.23. Despite dispersion can be appreciated, which may be due to inaccuracies in the ECU calculations of post-injected fuel and heat transfer effects, a linear increasing tendency is appreciated as $m_{f,pi}/\dot{m}_{exh}$ increases.

One pulse of temperature is taken as a reference vector ΔT_m, *i.e.* a model (Fig. 5.24), whilst the rest of the pulses at different conditions, ΔT_{pulse}, can be estimated through a convolution process (eq. 5.37). The convolution equation

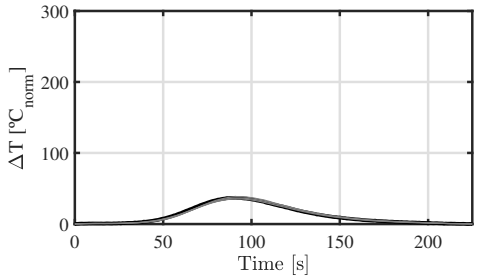

Figure 5.24. *Black: Reference vector model at 0.016g/s, 0.3s injection and 6 mg/str. Grey: normalized temperatures increment at 0.016 g/s and 0.3s injection for 4, 8 and 10 mg/str.*

(5.37) combines the temperature pulse vector model with the post-injection profile p, which is defined by injection duration and rate.

$$\Delta T_{pulse} = p * \Delta T_m = \sum_{i=1}^{n} p[i]\Delta T_m[n - i + 1] \tag{5.37}$$

where n is the length of the post-injection vector p.

The duration of the temperature pulse (eq. 5.38), as well as the peak temperature (eq. 5.39), have to be resized by a correction factor Γ, which depends on the exhaust mass flow. This factor, fitted for the previously mentioned tests, describes a linear correlation, as shown in Figure 5.25. Since the correction factor keeps constant the area of the normalized temperature pulse, energy is conserved.

$$t_{pulse,corr} = \frac{t_{pulse}}{\Gamma} \tag{5.38}$$

$$\Delta T_{pulse,corr} = \Delta T_{pulse}\Gamma \tag{5.39}$$

where t_{pulse} is the pulse duration and ΔT_{pulse} is the normalized temperature increment of the pulse.

It can be observed in Figure 5.26 the results of the application of the temperature normalization to pulse tests with 4, 6 and 8 mg/str at 0.044 g/s. Although the model is not completely able to reproduce temperature dynamics, ΔT_{max} is well captured. As shown in Figure 5.27, the model can be used to calibrate a strategy based on PI pulses with a map of ΔT_{max} depending on exhaust mass flow.

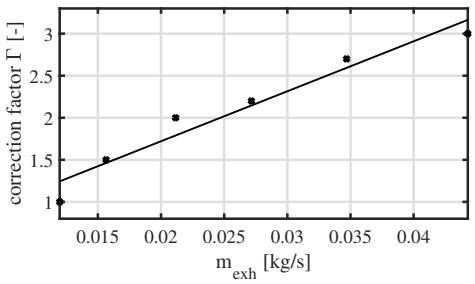

Figure 5.25. *Correction factor for the pulse duration and the normalized temperature pulse.*

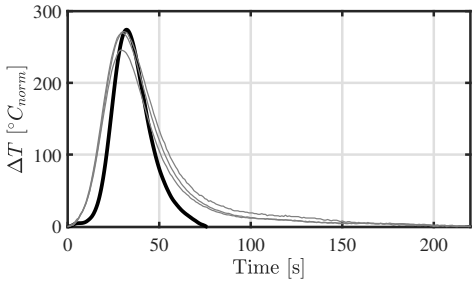

Figure 5.26. *Black: Modelled temperature increment at 0.044 g/s and 0.6s injection. Grey: experimental normalized temperature at 0.044 g/s and 0.6s injection.*

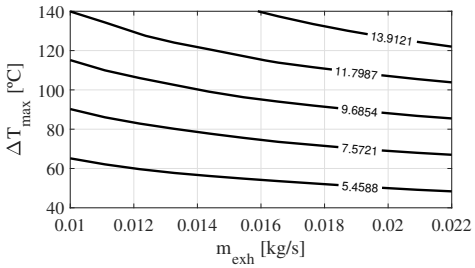

Figure 5.27. *Modelled post-injection duration (seconds) to generate a pulse with ΔT_{max} depending on exhaust mass flow. Injection rate is 8 mg/str.*

5.6 Conclusions

This chapter has presented a fast temperature estimation of the DOC upstream NTC sensor measurement, a 1D thermal model, a 0D control-oriented thermal model and a model to estimate temperature peaks during post-injection pulses.

The fast temperature estimation uses a Kalman observer, using data from a model and the NTC sensor measurement to reproduce the fast thermocouple measurement, which allows to have a better representation of the energy entering into the DOC, which may enable the detection of oxidation phases. However, the errors study done with the 1D model states the non-necessity of a fast temperature estimation to have a more accurate estimation of the downstream measurement. Finally, the 0D model presented shows a good accuracy to estimate the downstream DOC temperature with a lower computational burden than a 1D model.

Then, the 1D model is used for applications that require an axial distribution of temperatures. However, if an axial distribution is not required, a lighter model in terms of computational burden like the 0D model presented becomes useful to estimate the downstream temperature of the catalyst. In the case presented, the estimation of the DOC downstream temperature of a non-impregnated catalyst is the basis for DOC diagnosis.

References

[1] Simon D. "Kalman filtering, embedded systems programming". *Embedded. com*, 2001. (cited in p. 108)

[2] Del Re L, Allgöwer F, Glielmo L, Guardiola C and Kolmanovsky I. *Automotive model predictive control: models, methods and applications*, volume 402. Springer, 2010. (cited in pp. 66 and 108)

[3] Alberer D and del Re L. "Optimization of the transient Diesel engine operation". In *SAE Technical Paper 2009-24-0113*. Consiglio Nazionale delle Ricerche, 2009. (cited in pp. 64, 78, and 108)

[4] Alberer D. *Fast Oxygen Based Transient Diesel Engine Control*. Advances in mechatronics. Trauner, 2012. (cited in pp. 66 and 108)

[5] Guardiola C, Pla B, Blanco-Rodriguez D and Calendini P Olivier. "ECU-oriented models for NOx prediction. Part 1: a mean value engine model for NOx prediction". *Proceedings of the Institution of Mechanical Engineers, Part D: Journal of Automobile Engineering*, Vol. 229 n^o 8, pp. 992–1015, 2015. (cited in p. 108)

[6] Guardiola C, Climent H, Pla B and Blanco-Rodriguez D. "ECU-oriented models for NOx prediction. Part 2: adaptive estimation by using an NOx sensor". *Proceedings of the Institution of Mechanical Engineers, Part D: Journal of Automobile Engineering*, Vol. 229 n^o 10, pp. 1345–1360, 2015. (cited in pp. 66 and 108)

[7] Guardiola C, Pla B, Blanco-Rodriguez D, Mazer A and Hayat O. "A bias correction method for fast fuel-to-air ratio estimation in diesel engines". *Proceedings of the Institution of Mechanical Engineers, Part D: Journal of Automobile Engineering*, Vol. 227 n^o 8, pp. 1099–1111, 2013. (cited in pp. 108 and 114)

[8] Kar K, Roberts S, Stone R, Oldfield M and French B. "Instantaneous exhaust temperature measurements using thermocouple compensation techniques". *SAE SP 2004-01-1418*, pp. 169–190, 2004. (cited in pp. 80 and 108)

[9] Kee R J., Hung P, Fleck B, Irwin G, Kenny R, Gaynor J and McLoone S. "Fast Response Exhaust Gas Temperature Measurement in IC Engines". In *SAE Technical Paper 2006-01-1319*. SAE International, 2006. (cited in p. 108)

[10] Ogata K. *Modern control engineering*. Prentice Hall PTR, 2009. (cited in p. 109)

[11] Galindo J, Serrano JR, Guardiola C, Blanco-Rodriguez D and Cuadrado IG. "An on-engine method for dynamic characterisation of NOx concentration sensors". *Experimental Thermal and Fluid Science*, Vol. 35 n^o 3, pp. 470–476, 2011. (cited in p. 109)

[12] Payri F, Luján JM, Guardiola C and Rizzoni G. "Injection diagnosis through common-rail pressure measurement". *Proceedings of the Institution of Mechanical Engineers, Part D: Journal of Automobile Engineering*, Vol. 220 n^o 3, pp. 347–357, 2006. (cited in pp. 78 and 109)

[13] Connolly FT and Rizzoni G. "Real time estimation of engine torque for the detection of engine misfires". *Journal of dynamic systems, measurement, and control*, Vol. 116 n^o 4, pp. 675–686, 1994. (cited in p. 109)

[14] Lee D and Rizzoni G. "Detection of partial misfire in IC engines using a measurement of crankshaft angular velocity". Technical report, SAE Technical Paper 951070, 1995. (cited in p. 109)

[15] Guzzella L and Onder C. *Introduction to modeling and control of internal combustion engine systems*. Springer Science & Business Media, 2009. (cited in p. 110)

[16] Chen P and Wang J. "Control-oriented model for integrated diesel engine and aftertreatment systems thermal management". *Control Engineering Practice*, Vol. 22, pp. 81–93, 2014. (cited in pp. 27, 110, 127, and 138)

[17] Eriksson L. "Mean Value Models for Exhaust System Temperatures". In *SAE Technical Paper 2002-01-0374*. SAE International, 2002. (cited in p. 110)

[18] Proakis G and Manolakis G. *Digital signal processing: principles, algorithms, and applications*. 1996. (cited in p. 114)

[19] Haugen F. *Discrete-time signals and systems*. Tech, 2005. (cited in p. 114)

[20] Kalman RE. "A new approach to linear filtering and prediction problems". *Journal of basic Engineering*, Vol. 82 n^o 1, pp. 35–45, 1960. (cited in p. 115)

[21] Kalman RE and Bucy RS. "New results in linear filtering and prediction theory". *Journal of basic engineering*, Vol. 83 n^o 1, pp. 95–108, 1961. (cited in p. 116)

[22] Payri F, Guardiola C, Blanco-Rodriguez D, Mazer A and Cornette A. "Methodology for Design and Calibration of a Drift Compensation Method for Fuel-To-Air Ratio Estimation". In *SAE Technical Paper 2012-01-0717*. SAE International, 2012. (cited in p. 116)

Chapter 6

Control-oriented modelling of diesel catalysts including ageing

Contents

6.1 Introduction

This chapter contains the model-based estimation of the catalysts efficiency and of the pollutants slip for both DOC and SCR. DOC and SCR are catalysts exist since more than 20 years, so that a good fist of references to them in the field is available, including flow bench experiments, engine bench tests, CFD models, 1D phenomenological models and control-oriented models. In this sense, a novel lumped control-oriented model including ageing is presented for DOC, while two reactions-based models, following 1D and 0D approaches, based on literature, are presented for SCR.

In the case of DOC, the species affecting its efficiency are not directly measured on-board [1, 2], as explained in Chapter 2, so that the model is devoted to explore the catalyst diagnosis possibilities and to estimate the emissions increase due to the ageing process. On the other hand, the models presented for SCR are developed to be used on-board, since their inputs can be measured by the on-board sensors or accurately estimated [3–6]. As in the case of the DOC model, the SCR model contains an ageing factor that allows estimating the emissions increase with the ageing process.

6.2 Diesel oxidation catalyst

The DOC model that includes ageing effects on THC and CO emissions is presented next. 1D models for DOC contain detailed equations for physical and chemical processes [7–9], so that the calibration of this model approach is subjected to a time-consuming testing campaign. Moreover, its accuracy may not be suitable for practical needs. For this reason, lumped models are valuable to reproduce functional processes of the catalyst. Authors like [1] [10,11] have presented models for DOC including oxidation, but the novelty of this model is the inclusion of ageing.

The functions of the presented control-oriented model are based on experimental tests that show in terms of slip the ageing effect on light-off temperature and HC accumulation capabilities. These tests are available in Chapter 4.

The HC and CO inputs to the model are obtained from gas analyzer measurements, although some empirical models are available in literature. For instance, a method used to estimate the engine raw HC and CO emissions is to model them as a function of the fuel injection rate [12], while a method used by [13] to estimate the DOC upstream HC from fuel post-injections is to map them as a function of the injection angle, the post-injected fuel quantity and the exhaust gas mass.

In this work, no differentiation among THC species is taken into account, despite the fact that THC are composed of a large variety of hydrocarbons chains [9]. [14] and [8] considered two main groups: easy-to-oxidize, represented by C_3H_6, and difficult-to-oxidize compounds, in which chains with higher number of carbons are included, being $C_{10}H_{22}$ the most representative. [15] assumed THC as C_3H_6 for modelling purposes.

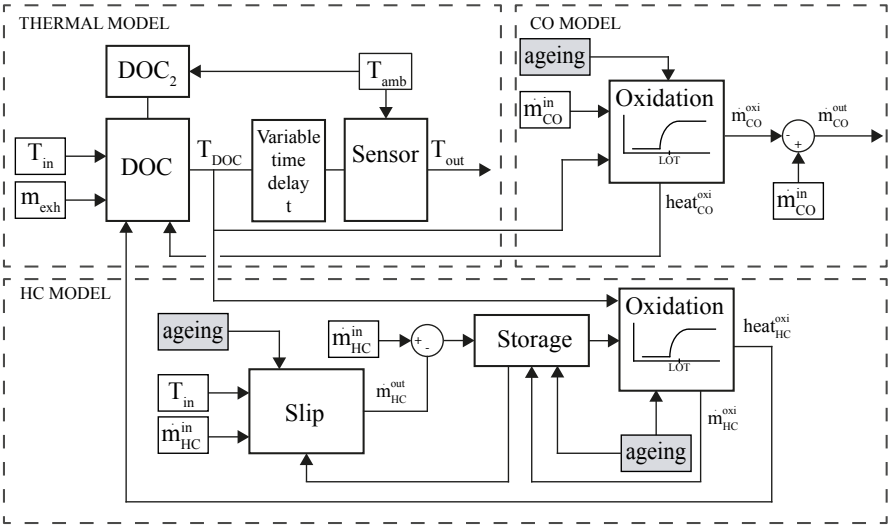

Figure 6.1. *DOC model layout.*

6.2.1 Modelling approach

The presented control-oriented model is composed of three main parts, which are the thermal model, previously described in Chapter 4, the THC model and the CO model, as shown in Figure 6.1. Its aim is to estimate THC and CO slip emissions during normal engine operating conditions, rather than during excitation events like high post-injections used in DPF regeneration. For this purpose, the HC and CO LOT [16, 17] and the HC accumulation [18] play a key role in the model. In this line, the main model equations are described next:

$$m_{HC}^{acc} = \int (\dot{m}_{HC}^{in} - \dot{m}_{HC}^{out} - \dot{m}_{HC}^{oxi})dt \tag{6.1}$$

$$\dot{m}_{HC}^{out} = \beta_{HC} \cdot \dot{m}_{HC}^{in} \tag{6.2}$$

$$\dot{m}_{CO}^{out} = \beta_{CO} \cdot \dot{m}_{CO}^{in} \tag{6.3}$$

where m_{HC}^{acc} is the accumulation HC state, $\dot{m}_{HC}^{oxi}$ is the oxidation rate of HC species, $\dot{m}_{HC}^{in}$ is the mass flow of entering HC, the slip function β_{HC} is outlined in equation (6.5), $\dot{m}_{HC}^{out}$ is the mass flow of HC released, $\dot{m}_{CO}^{in}$ is the mass flow of entering CO, β_{CO} is outlined in equation (6.6), $\dot{m}_{CO}^{out}$ is the mass flow

of released CO. The capacity of the DOC for accumulating HC [19] is also modelled and the slips β_{HC} and β_{CO} are considered to be the ratio of species escaping from the DOC over those entering in it. Equations (6.4) and (6.6) show which are the model inputs:

$$\dot{m}_{HC}^{oxi} = f(T_{DOC}, \xi) \tag{6.4}$$

$$\beta_{HC} = f(T_{us}, \dot{m}_{HC}^{us}, m_{HC}^{acc}, LOT_{HC}, \xi) \tag{6.5}$$

$$\beta_{CO} = f(T_{us}, \dot{m}_{CO}^{us}, LOT_{CO}, \xi) \tag{6.6}$$

where T_{us} is the upstream DOC temperature, m_{HC}^{acc} is the accumulated HC, $\dot{m}_{HC}^{us}$ and $\dot{m}_{CO}^{us}$ are the upstream mass flows of HC and CO, respectively, LOT is the light-off temperature of HC and CO and ξ is the ageing parameter. The experimental tests of Chapter 4 are used to characterize how the DOC operates and how it is affected by ageing. In this line, the modelled functions are selected taking into account an ageing perspective, so that the ageing factor ξ allows varying from new to aged behaviours.

The combination of simple equations allows having a model that combines species slip, oxidation, HC accumulation and light-off temperature, since a compromise between calibration complexity, functions flexibility and process physical description is necessary.

6.2.2 Control-oriented model

The hypothesis of the model presented in this chapter are experimentally described in Chapter 4. Specifically, the HC emissions are higher for the aged DOC when the DOC is below the LOT, while once the DOC is warmed up, its HC emissions are similar for new and aged parts. In this line, the CO slip follows a similar behaviour, being the emissions higher when the DOC is under the CO LOT. However, in case of HC species, the DOC accumulation capacity plays an important role that needs to be modelled in the HC model part. Coefficients of the model are shown in Table 6.1, separated into HC oxidation, HC accumulation and slip, and CO oxidation.

Table 6.1. *Model coefficients.*

HC oxidation	
LOT_{HC}	HC light-off temperature
$\Delta\mathrm{LOT}_{HC}$	HC temperature activation interval
n_{HC}	HC shape coefficient for temperature activation interval
$\chi_{HC,min}$ $\chi_{HC,max}$	Minimum and maximum HC oxidation rates
$\left(\frac{d\chi_{HC}}{dt}\right)_{min}$ $\left(\frac{d\chi_{HC}}{dt}\right)_{max}$	Minimum and maximum activation and deactivation rates for HC oxidation
HC accumulation and slip	
a_1 to a_4	slip_0 function coefficients
s, a and m_{HC}^{ref}	slip_1 function coefficients, which are affected by A_eff
A_{eff}	Effective area
CO oxidation	
LOT_{CO}	CO light-off temperature
$\Delta\mathrm{LOT}_{CO}$	CO temperature activation interval
n_{CO}	CO shape coefficient for temperature activation interval
$\chi_{CO,min}$ $\chi_{CO,max}$	Minimum and maximum CO oxidation rates
$\left(\frac{d\chi_{CO}}{dt}\right)_{min}$ $\left(\frac{d\chi_{CO}}{dt}\right)_{max}$	Minimum and maximum activation and deactivation rates for HC oxidation

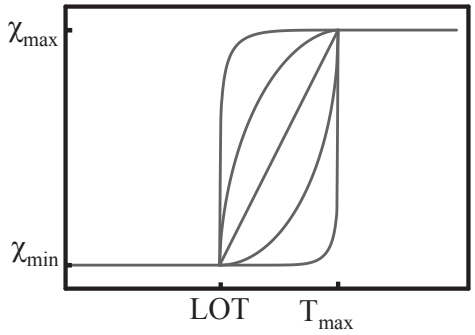

Figure 6.2. *Modelled DOC oxidation rate curve of HC and CO.*

6.2.2.1 HC and CO oxidation model

Traditional chemical modelling for oxidation reactions like (6.7) and (6.8) follows an Arrhenius reaction rate approach [20]. However, the reaction rate in this paper is modelled through equation (6.9), which is a more flexible function, and allows setting the interval range from no oxidation to oxidation, the increasing shape and the maximum reaction rate, whose shape is shown in Figure 6.2.

$$CH_4 + 2O_2 \rightarrow CO_2 + 2H_2O \tag{6.7}$$

$$2CO + O_2 \rightarrow 2CO_2 \tag{6.8}$$

$$\chi = \chi_{max} + \left(\chi_{max}^n + \frac{(\chi_{max} - \chi_{min})^n \cdot (T_{DOC} - LOT)^n}{\Delta LOT^n} \right)^{n^{-1}} \tag{6.9}$$

where χ is the oxidation rate of HC or CO. Increasing and decreasing oxidation rates are limited to avoid too fast DOC emptying processes:

$$\left(\frac{d\chi}{dt}\right)_{min} < \frac{d\chi}{dt} < \left(\frac{d\chi}{dt}\right)_{max} \tag{6.10}$$

Then, the oxidation reactions are limited by the available oxygen, the available HC or CO, and a maximum oxidation rate.

6.2.2.2 HC slip model

T_{us}, $\dot{m}_{HC}^{us}$ and m_{HC}^{acc} are the factors influencing this model function, since it is experimentally observed that the slip in cold conditions is lower than in warm conditions, while $\dot{m}_{HC}^{us}$ is related to the residence time of the THC in the DOC and follows the idea of the higher the mass flow the higher the slip. Regarding the amount of THC stored in the DOC, the higher the amount of THC stored, the lower the ability of the DOC to capture more THC and therefore the higher the slip. In the limit, when the DOC is completely saturated of THCs, its ability to retain more THC is 0, and then a slip of 100% appears, as shown in Figure 4.11.

Slip is modelled through the function β_{HC}, being β_0 a function that depends on $\dot{m}_{HC}^{us}$ and T_{in}, and β_1 a function that depends on m_{HC}^{acc}. β_0 represents the basic slip of the DOC, while β_1 includes to this basic slip the increase due to accumulation.

$$\beta_{HC} = \beta_0(T_{us}, \dot{m}_{HC}^{us}) \cdot \beta_1(\dot{m}_{HC}^{acc}) \tag{6.11}$$

where β_0 is a quadratic polynomial:

$$\beta_0 = a_1 \cdot \dot{m}_{HC}^{us} + a_2 \cdot T_{us} + a_3 \cdot T_{us}^2 + a_4 \cdot \dot{m}_{HC}^{us} \cdot T_{us} \tag{6.12}$$

where a_i are calibrable coefficients. Figure 6.3 shows the experimental versus modelled relation between $\dot{m}_{HC}^{us}$ and T_{us}, where dots represent experimental measurements and contour lines represent modelled slip. These results are obtained by computing steady state points measured with the nominal DOC and fitting the parameters in equation (6.12) to the experimental data. Due to the complexity of the HC reaction in the DOC, non-linear fitting procedures and mapping are used in modelling [21].

The effect of m_{HC}^{acc} on the slip is modelled through the function β_1, shown in Figure 6.4. Results of the accumulation process versus slip of Figure 4.12 show that when the DOC does not have HCs stored, m_{HC}^{acc}=0, its slip increases linearly as it is progressively filled with HCs. Then, some reduction in the slope between m_{HC}^{acc} and slip is observed as m_{HC}^{acc} increases. Finally, as the amount of HC stored reaches the maximum capacity of the DOC a sudden increase happens. According to the previous description, the β_1 factor is defined as a piecewise function containing a linear and an exponential term modelling the effect of m_{HC}^{acc} on the slip:

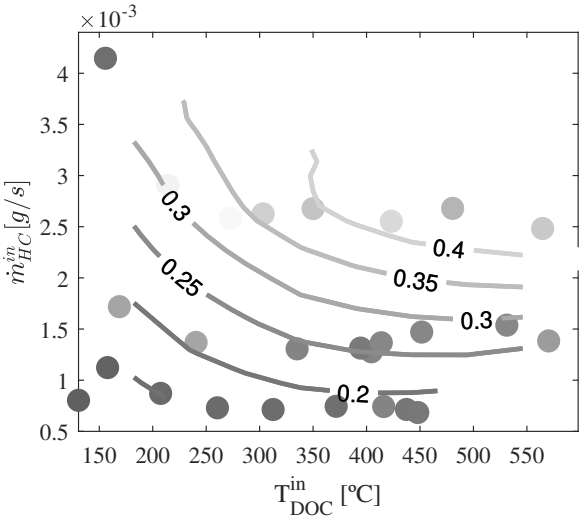

Figure 6.3. *Results of the non-linear fitting of the slip function $slip_0$, where z values correspond to slip values. Dots stand for experimental measurements, while lines stand for modelled values.*

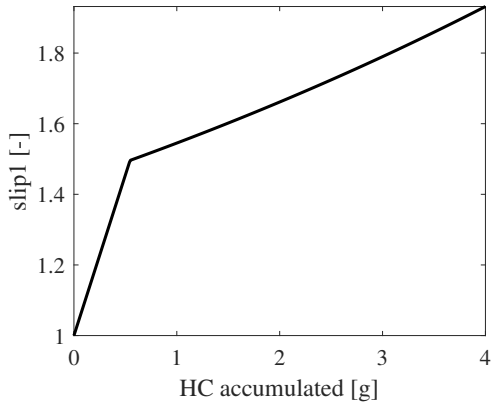

Figure 6.4. *Graphical representation of the β_1 function.*

$$\beta_1 = max(\beta_{1,slope}, \beta_{1,exp}) \tag{6.13}$$

where $\beta_{1,slope}$ and $\beta_{1,exp}$ are the functions that describe the slip due to HC accumulation, shown experimentally in Figure 4.12. This behaviour is modelled through equations (6.14) and (6.15), represented in Figure 6.4 and described next:

$$\beta_{1,slope} = 1 + s \cdot m_{HC}^{acc} \tag{6.14}$$

where s is the slope of function $\beta_{1,slope}$, while the constant is set to 1 to leave the THC slip as β_0 when there is no HC accumulation.

$$\beta_{1,exp} = a + e^{\frac{m_{HC}^{acc}}{m_{HC}^{ref}}} \tag{6.15}$$

where a and m_{HC}^{ref} are calibrable parameters. The m_{HC}^{ref} parameter is related with the HC storage capability of the DOC, which is related with its ageing state.

6.2.2.3 CO slip model

The CO model is simpler than the HC model, since CO is not accumulated in the catalyst. In this case, the CO oxidation curve points which is the slip, since if CO are not being oxidized, then they are being released.

6.2.2.4 Model calibration and application

Since the model is oriented to simulate tests like the NEDC or the WLTC, rather than engine extreme conditions of load and speed or high post-injections, the model is applied to these kind of tests. Therefore, while LOT and slip tests are performed separately, the identification of the active model parameters is globally done using a WLTC. Then, the application of the model to a WLTC with the parameters from the resulting calibration is shown in Figure 6.7. In case of high post-injections, like during DPF regeneration conditions, a more detailed heat transmission and heat release model would be required.

Separating the passive model from the chemical model results in essential to decouple heat transmission and dynamics from HC and CO heat delivery effects. Otherwise, coefficients could overlap the effects of a physical process

which correspond to others whereby the model fitting would result in a more complex task.

The current model calibration consists of two main steps: passive model calibration and active model calibration. Passive model calibration is done using the non-impregnated DOC through a least squares error minimization routine combined with manual tuning to provide the optimization function with good initial values.

While the passive model calibration is detailed in Chapter 4, the active model calibration is explained next. The HC and CO slip functions are calibrated following a similar procedure than that of the thermal model, in which manual tuning and parametric studies are used. On the other hand, the LOT values are obtained from the experiments of Figure 4.10 in section 4.3.3, whose results are shown in Table 4.1.

When fitting slip coefficients, engine exhaust flows from the WLTC cycle are higher than for the HC accumulation tests and therefore DOCs are filled faster. Then, the parameters of these functions are selected as a compromise solution for the engine operating ranges of the NEDC and WLTC tests.

As the engine load and catalyst temperature increases, some of the stored THCs may be released without being oxidized, resulting in a decrease in conversion. However, this effect is not normally observed in light-off small-scale [22] events. Therefore, this model is not appropriated for large post-injections, but it is to be used in conventional use cases. Note that slip and LOT are treated as independent processes, so that the effective area is not used to characterize the LOT.

The model is applied to a WLTC test in Figure 6.7, in which results for temperature and cumulative efficiencies $\eta_{cumulative}$ of HC and CO are shown. The HC excitation is high enough as a result of engine-raw emissions, since the engine operates in zones near high HC emissions. It can be seen that the passive model of [1] captures the heat transference and dynamics, whilst the HC and CO models are able to represent the DOC-outlet emissions. The following set of equations is used to evaluate the model performance:

$$eff_{exp} = 1 - \frac{\int \dot{m}^{out,exp}}{\int \dot{m}^{in}} \tag{6.16}$$

$$eff_{mod} = 1 - \frac{\int \dot{m}^{out,mod}}{\int \dot{m}^{in}} \tag{6.17}$$

$$\epsilon = \left| \frac{\int \dot{m}^{out,exp} - \int \dot{m}^{out,mod}}{\int \dot{m}^{in}} \right| \tag{6.18}$$

where eff_{exp} is the experimental efficiency, eff_{mod} is the modelled effiency, ϵ is the efficiency error and $\dot{m}$ is the mass flow of either HC or CO, whose results are shown in Table 6.2.

With the application of the model, the new DOC has an error of 1.4% for HC and 3.5% for CO, while the nominal DOC has an error of 0.2% for HC and 6.7% for CO. In both cases, the error obtained is acceptable, being slightly lower for HC than for CO. Unfortunately, the accumulated HC cannot be validated, since it is a non-measurable state.

6.2.2.5 Ageing modelling

Experimental data from the cut DOCs is used to define a parameter that characterizes the ageing level of a DOC. This approach allows defining an ageing parameter in terms of effective area A_{eff}, despite the mixed effect of residence time and loss of monolith efficiency. Then, according to their HC emissions in a WLTC, the effective area of the nominal and aged DOCs is set with respect to the new, the DOC_{70}, the DOC_{40} and the non-impregnated DOC, as shown in Figure 6.5. In this figure, 0% is referenced to the non-impregnated DOC, in which DOC-outlet HC emissions are equal to the engine-raw, while 100% corresponds to the new DOC. In this line, when the nominal DOC has an equivalent effective area of 85%, this value is reduced to 56% for the aged DOC. The effect of ageing in the oxidation function is modelled by means of the LOT for both HC and CO, using the values presented in Table 4.1.

Since results show that new and aged DOCs present similar slip at warm conditions, the main differences are appreciated during cold phases, i.e.: during HC accumulation, so that the ageing effect on HC slip is taken into account with the accumulated HC. Therefore, the HC slip ageing function is introduced to equation (6.11), and the expression for the slip becomes:

$$\beta_{HC} = \beta_0(T_{us}, \dot{m}^{us}_{HC}) \cdot \beta_1(m^{acc}_{HC}, A_{eff}) \tag{6.19}$$

where β_1 function (eq. 6.13) is upgraded with ageing. For this purpose, the WLTC test is fitted in terms of temperature, HC slip and CO slip for each catalyst and the resulting coefficients are then combined with the effective area:

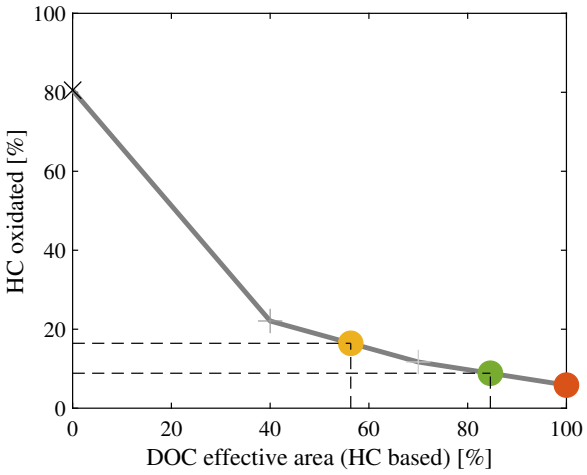

Figure 6.5. *Experimental results for the effective area determination, where x is the non-impregnated DOC, + is the DOC_{40}, • is the aged DOC, + is the DOC_{70}, • is the nominal DOC and • is the new DOC.*

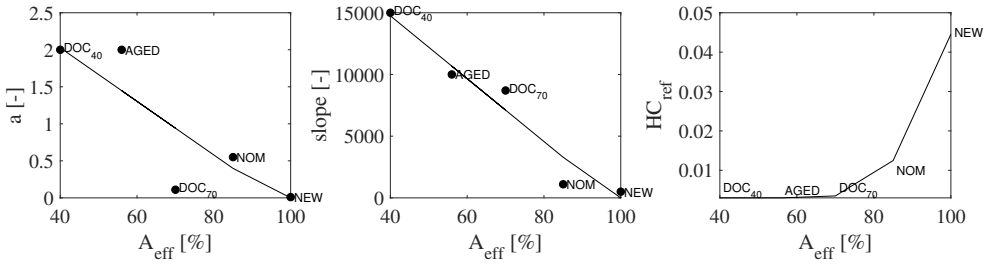

Figure 6.6. *Results of the effective area for the HC slip ageing modelling.*

$$s = A_{eff} \cdot c_1 + c_2 \tag{6.20}$$

$$a = A_{eff} \cdot c_3 + c_4 \tag{6.21}$$

$$HC_{ref} = (A_{eff} \cdot c_5)^{-1} \tag{6.22}$$

where coefficients of the linear functions a and s (c_1 to c_4) are fitted with a minimum least squares error routine to a first order polynomial, while the coefficient c_5 is obtained by means of a parametric study, choosing the value of the coefficient that minimises the difference between the HC_{ref} value obtained from the fitting of the experimental results to the model and the result of applying equation (6.22). Note that parameters of cut DOCs were manually tuned focusing on low flow intervals, since differences in behaviour were observed at medium to high flows due to different residence times. Figure 6.6 shows the fitting of the model coefficients identified experimentally for the different DOCs and the correlations (6.20)-(6.22).

The maximum storage capacity also decreases as the DOC ages, although DOCs are able to store much more HC than those accumulated during WLTC conditions due to engine-raw emissions. Figure 6.8 shows the result of the model including ageing in the WLTC, whose performance is shown in Table 6.2. It can be observed how the DOC efficiency for HC fits well in average for the three catalysts, while the CO error increases up to 8 %.

An ageing parameter ξ is used as the global ageing factor that relates A_{eff} and LOT, being 0 for the new DOC and 1 for the aged DOC, which are the reference catalysts. Despite a more complex function including the nominal catalyst could be used, a linear function from the new to the aged catalyst is used in order to have experimental measures to compare. In this line, two reference catalysts lead to a first order relation between ξ and both LOT and A_{eff}, whre ξ=0 corresponds to the new DOC and ξ=1 corresponds to the artificially aged DOC. The following equations represent this relation:

$$LOT_{HC} = 14.93\ \xi + 47.31 \tag{6.23}$$

$$LOT_{CO} = 58.82\ \xi + 127.65 \tag{6.24}$$

$$A_{eff} = -43.48\ \xi - 98.7 \tag{6.25}$$

Table 6.2. *Efficiency of DOCs and model errors.*

	eff_{exp} [%]	eff_{mod} [%]	ϵ [%]
New: HC	93.8	92.4	1.4
New: CO	83.5	80	3.5
Nominal: HC	91.1	92.3	0.2
Nominal: CO	76.6	93.3	6.7
Aged: HC	83.6	83.6	0
Aged: CO	61.9	53.9	8

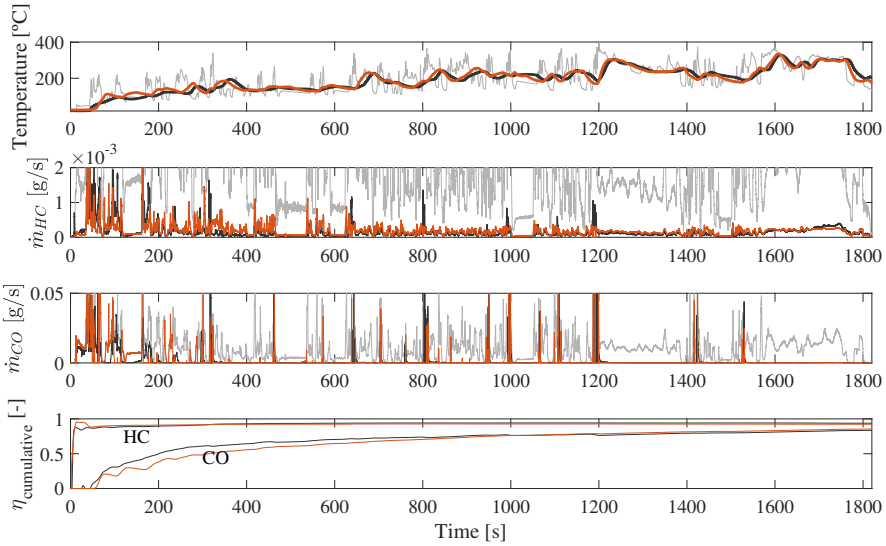

Figure 6.7. *New DOC model results in a WLTC. Upper plots:* —— *Upstream measurements* —— *Downstream measurements* —— *Downstream model. Bottom plot:* —— *Cumulative efficiency from measurements* —— *Cumulative efficiency from model.*

While the validation of ξ=0 and ξ=1 is presented in this chapter in comparison with experimental data, a study simulating intermediate states is done in next chapter.

6.3 Selective catalytic reduction system

Two models are presented in this section, each one based on a different approach. On the one hand, a 1D SCR model, and on the other hand, a 0D SCR model. While the 0D model is better for control-oriented purposes due

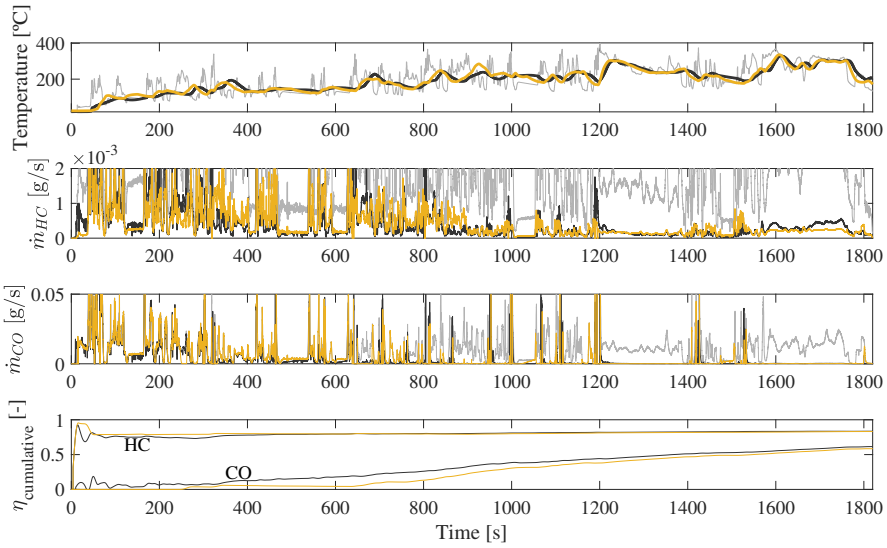

Figure 6.8. *Aged DOC model results in a WLTC. Upper plots:* —— *Upstream measurements* —— *Downstream measurements* —— *Downstream model. Bottom plot:* —— *Cumulative efficiency from measurements* —— *Cumulative efficiency from model.*

its lower computational burden, the 1D model can still be used if properly optimized [4]. Both approaches include an ageing factor, as the previously presented DOC model has. In this sense, the ageing factor of the SCR models is a physical parameter that represents the ammonia storage capacity of the catalyst [23–26].

An important difference of SCR modelling with DOC modelling is that the measurements of NO_x and NH_3, the main actors in SCR kinetics, are well defined chemical species. In this sense, NO_x composition is simpler than the high diversity of HC existing in a Diesel exhaust line, and gas analyzer devices can separate NO and NO_2. Another difference with DOC modelling is that the NO_x reduction reactions are not as exothermic as the oxidation reductions taking place in a DOC, so that the energy release is not as relevant as for DOC modelling. Complexity of SCR modelling is rooted instead on the different dynamics found in the SCR, since NO_x dynamics are dominated by the engine operating conditions but ammonia dynamics are dominated by the ammonia storage factor, the exhaust mass flow and the temperature.

The SCR model used next in the ageing observer has to be linearized, which excludes the possibility of using a 1D model for its real time execution. On the other hand, the algorithm presented in next chapter runs another model

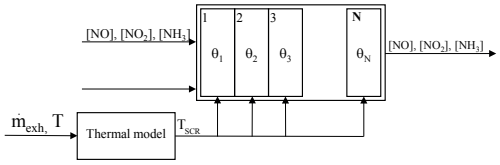

Figure 6.9. *1D SCR model scheme.*

in parallel, so that this second model can be benefited from a more detailed model, which is the 1D approach. Then, validation of both 0D and 1D models are presented for the SCR system for new and aged states.

One of the assumptions taken into account for both models is to consider that all the AdBlue injected is directly converted into NH_3. Therefore, neglecting the influence of this process on the SCR performance and bypassing the H_4N_2CO and HNCO species reactions [27].

6.3.1 1D SCR model

The 1D SCR model is based on the available literature [4, 28, 29], whose scheme is shown in Figure 6.9. Specifically, the model is applied in dynamic tests for a new and an aged catalysts. For this purpose, the ageing is modelled through a tunable parameter Ω_A whose value relies in the interval $\Omega_A \in [0, 1]$, being 1 for a new part and 0 for a completely aged.

The model reactions taking place in the catalyst are presented in Chapter 2, from eq. (2.8) to (2.15). From this set of equations, that includes AdBlue thermolysis and hydrolisis, adsorption and desorption, NO and NO_2 oxidation, N_2O formation and NH_3 oxidation, only adsorption, desorption, NO and NO_2 oxidation are used for simplification. In this sense, NH_3 oxidation and N_2O take place at temperatures higher than 400°C, so that the tests data presented do not include this range of temperatures.

The equations that model the reaction rates and the species balances are presented next, where eq. (6.26), eq. (6.27) and (6.28) present the species balance for the NH_3, NO and NO_2 species, respectively. Due to the 1D approach of this model, the process is discretized in the time and axial domains. In this sense, no local accumulation of species is considered.

$$\frac{\delta C_{NH_3}}{\delta t} = -v \ \frac{\delta C_{NH_3}}{\delta x} - \Omega \ \Omega_A \ (r_a - r_d) \tag{6.26}$$

$$\frac{\delta C_{NO}}{\delta t} = -v \ \frac{\delta C_{NO}}{\delta x} - \Omega \ \Omega_A \ (r_{std} + r_{fst}) \tag{6.27}$$

$$\frac{\delta C_{NO_2}}{\delta t} = -v \ \frac{\delta C_{NO_2}}{\delta x} - \Omega \ \Omega_A \ (r_{fst} + r_{slw}) \tag{6.28}$$

where v is the exhaust gas speed, Ω is the NH_3 accumulation capacity and Ω_A is the ageing factor. The reaction rates r_a, r_d, r_{std}, r_{fst} and r_{slw} are calculated with the following Arrhenius equations:

$$r_a = k_a \ e^{\left[\frac{-E_a}{R} \ \left(\frac{1}{T_{SCR}} - \frac{1}{T_{ref}}\right)\right]} \ C_{NH_3} \ (1 - \theta_{NH_3}) \tag{6.29}$$

$$r_d = k_d \ e^{\left[\frac{-E_d \ (1-\alpha \ \theta_{NH_3})}{R} \ \left(\frac{1}{T_{SCR}} - \frac{1}{T_{ref}}\right)\right]} \ \theta_{NH_3} \tag{6.30}$$

Note that the r_d reaction includes the Temkin mechanism, whose assumptions are in line with easy ammonia adsorption over SCR catalysts and with surface heterogeneity, in agreement with the physico-chemical characterization of the catalysts in [30–32].

$$r_{std} = k_{std} \ e^{\left[\frac{-E_{std}}{R} \ \left(\frac{1}{R_{SCR}} - \frac{1}{T_{ref}}\right)\right]} \ C_{NO} \ \theta^*_{NH_3} \ \left(1 - e^{\left(\frac{-\theta_{NH_3}}{\theta^*_{NH_3}}\right)}\right) \tag{6.31}$$

where the parameter $\theta^*_{NH_3}$ is included, since the rate of the standard SCR reaction does not depend on the ammonia surface coverage ratio above a characteristic value of the NH_3 coverage [28].

$$r_{fst} = k_{fst} \ e^{\left[\frac{-E_{fst}}{R} \ \left(\frac{1}{R_{SCR}} - \frac{1}{T_{ref}}\right)\right]} \ C_{NO} \ C_{NO_2} \ \theta_{NH_3} \tag{6.32}$$

$$r_{slw} = k_{slw} \ e^{\left[\frac{-E_{slw}}{R} \ \left(\frac{1}{R_{SCR}} - \frac{1}{T_{ref}}\right)\right]} \ C_{NO_2} \ \theta_{NH_3} \tag{6.33}$$

where k_a, E_a, k_d, E_d, k_{std}, E_{std}, k_{fst}, E_{fst}, k_{slw}, E_{slw} and $\theta^*_{NH_3}$ are tunable parameters. On the other hand, the exhaust gas speed v is calculated next:

$$v = \dot{m}_{exh} / \delta_{gas} / \zeta_{SCR} / V_{SCR} \tag{6.34}$$

where $\dot{m}_{exh}$ is the exhaust mass flow, δ_{gas} is the gas density, ζ_{SCR} is the factor that represents the open portion of the SCR volume, i.e. it represents the porous media, and V_{SCR} is the SCR volume. Finally, the ammonia storage ratio, $\theta_{\mathrm{NH_3}}$, is calculated with the following equation:

$$\frac{\delta\theta_{NH_3}}{\delta t} = r_a - r_d - r_{std} - 2r_{fst} - \frac{4}{3}r_{slw} \tag{6.35}$$

Note that this balance is only time-dependent and therefore it is not axial dependent, i.e., the value of the NH_3 accumulated in a given axial section only depends on its previous state.

The difference of time and axial integration approaches for species concentrations and $\theta_{\mathrm{NH_3}}$ is related to the actual dynamics of the system. While NO_x species are not accumulated and its dynamics are translated to the downstream signal, the NH_3 storage acts as a low pass filter and disengages the upstream NH_3 from its downstream signal.

6.3.1.1 1D SCR model application

The 1D model is applied to a new and an aged parts in two dynamic tests, in Figure 6.10 and 6.11, respectively. For this purpose, the calibration is done such that both catalysts share the same parameters but only the ageing factor Ω_{A} varies from one another. The objective of the model calibration is to have two tests in a similar range of temperatures in order to have two cases in which only the Ω_{A} is varied.

While the test of the new catalyst is an RDE from engine setup C.1, the test of the aged catalyst is an WLTC repeated three times, in order to have more time of continuous processes occurring into the SCR, which is done in the engine setup C.2. In this sense, it is necessary to track the evolution of the $\theta_{\mathrm{NH_3}}$ in order to use a model, i.e. if $\theta_{\mathrm{NH_3}}$ is excessively biased over time, the model may lead to errors. In fact, the initial conditions of $\theta_{\mathrm{NH_3}}$ for both tests are set to 0.2, since high NO_x efficiency and NH_3 slip at the beginning of the test require it. On the other hand, as it can be observed in the $\theta_{\mathrm{NH_3}}$ plot of Figures 6.10 and 6.10, the initial sections have more variability with respect to the final ones, since the final ones contain the addition of the NH_3 filter from all the previous sections.

A problematic whose origin takes place in the measurement systems can be observed during high NH_3 slip phases. Although the measured downstream NO_x signal is compensated removing 0.63 of the measured downstream NH_3

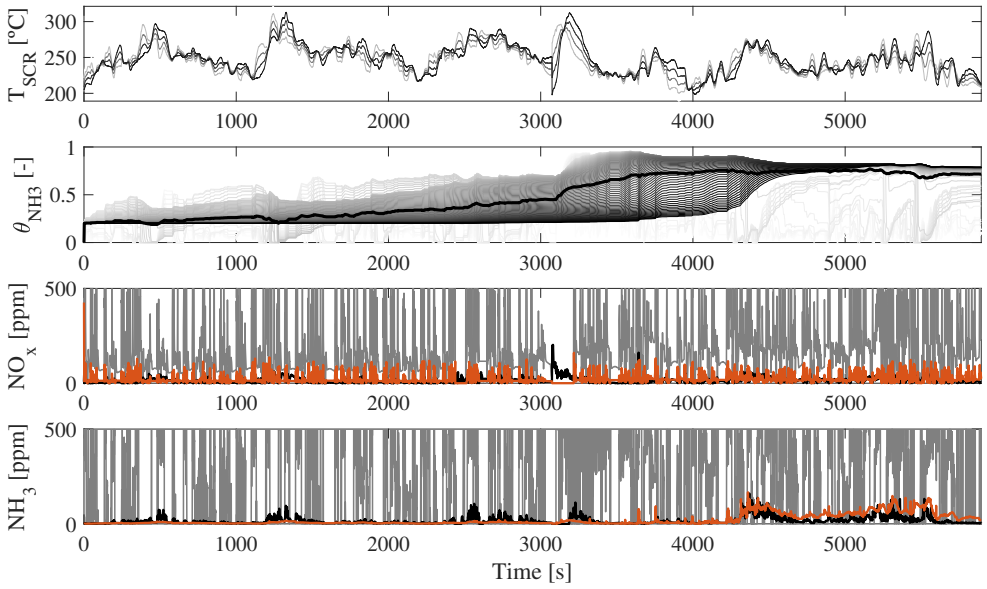

Figure 6.10. *1D SCR model application to a new part during transient operation. Top plots: dark to gray lines represent upstream to downstream signals. Thick line in θ_{NH_3} represents the average of all axial sections. Bottom plots: gray stands for upstream, black stands for downstream and orange stands for downstream modelled signal.*

Table 6.3. *Efficiency of SCRs and 1D model errors.*

	eff_{exp} [%]	eff_{mod} [%]	ϵ [%]
New: NO_x	92.2	89.5	2.7
New: NH_3	93.7	91.2	6.4
Aged: NO_x	68.9	62	6.9
Aged: NH_3	69.4	66.9	2.5

signal, the shape of the NH_3 signal can still be appreciated in the NO_x measurements. For this reason, the calibration of the model becomes difficult to assess quantitatively, since an inherent error due to the NO_x sensor cross-sensitivity to NH_3 is soiling the measurement. Even so, a good correlation for both new and aged parts can be appreciated in the time domain for both NO_x and NH_3 species.

The SCR performances for both new and aged parts, in comparison with the model estimation can be appreciated in Table 6.3. In this, the maximum

performance error is 6.9% for NO_x species in the aged SCR and 6.4% for NH_3 species in the new SCR. As a result of the calibration, and establishing Ω_A =1 for the new part, the aged part has a Ω_A of 0.3. A simulation analysis of the emissions increase in the WLTC for this $\Delta\Omega_A$ is done in next chapter.

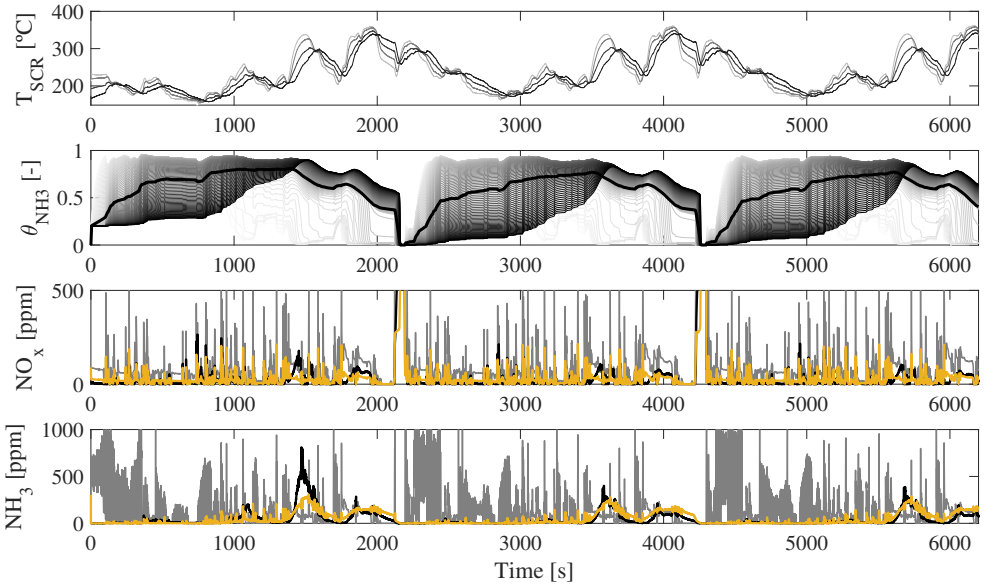

Figure 6.11. *1D SCR model application to an aged part during transient operation. Top plots: dark to gray lines represent upstream to downstream signals. Thick line in θ_{NH_3} represents the average of all axial sections. Bottom plots: gray stands for upstream, black stands for downstream and yellow stands for downstream modelled signal.*

6.3.2 0D SCR model

The 0D SCR model presented here is based on the work presented in [33], whose structure is shown in Figure 6.12. It follows the continuous stirred tank reactor (CSTR) approach, in which the NO, NO_2 and NH_3 species concentrations are considered as states of the lumped. In this sense, while the reaction rates are equivalent to those presented previously, the species concentration states are presented in the following equations:

$$\frac{\delta NH_3}{\delta t} = -\Omega\ \Omega_A\ (r_a - r_d) + SV\ (C_{NH_3,us} - C_{NH_3}) \tag{6.36}$$

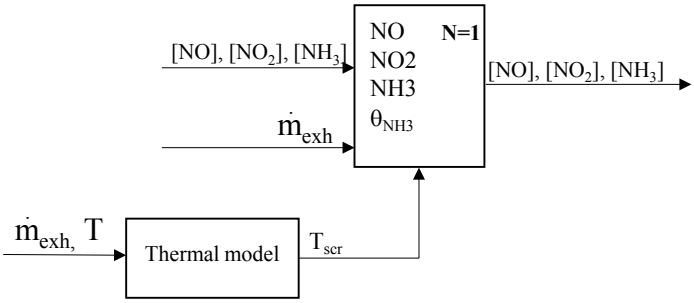

Figure 6.12. *0D SCR model scheme.*

$$\frac{\delta NO}{\delta t} = -\Omega\ \Omega_A\ (r_{std} + r_{fst}) + SV\ (C_{NO,us} - C_{NO}) \tag{6.37}$$

$$\frac{\delta NO_2}{\delta t} = -\Omega\ \Omega_A\ (r_{fst} + r_{slw}) + SV\ (C_{NO_2,us} - C_{NO_2}) \tag{6.38}$$

where SV is the spatial velocity of the exhaust gas flow and r_a, r_d, r_{std}, r_{fst} and r_{slw} contain the same tunable parameters than those described for the 1D SCR model. The main difference between the 1D and the 0D models remains in equations (6.36) to (6.38). In order to have the effect of the residence time of the species inside the catalyst the term $SV(C_{us} - C)$ is added, whose approach is the CSTR. Then, the $\theta_{\mathrm{NH_3}}$ is also equivalent to the 1D SCR model, as:

$$\frac{\delta \theta_{NH_3}}{\delta t} = r_a - r_d - r_{std} - 2r_{fst} - 4/3 r_{slw} \tag{6.39}$$

The performance of the 0D model may not be as good as the 1D model, since the detailed model includes the axial discretization of temperatures. In this sense, the detail on equations, including thermolysis, hydrolysis, NH_3 oxidation and N_2O formation could be included for the model running in parallel to the ageing observer. However, the purpose of the 0D model is to be used in an observer, for which the simplification of the model becomes crucial for observability and real time purposes.

6.3.2.1 0D SCR model application

The 0D SCR model is applied to the same tests than the 1D SCR model, i.e., the new part is validated with a dynamic RDE from the engine setup C.1

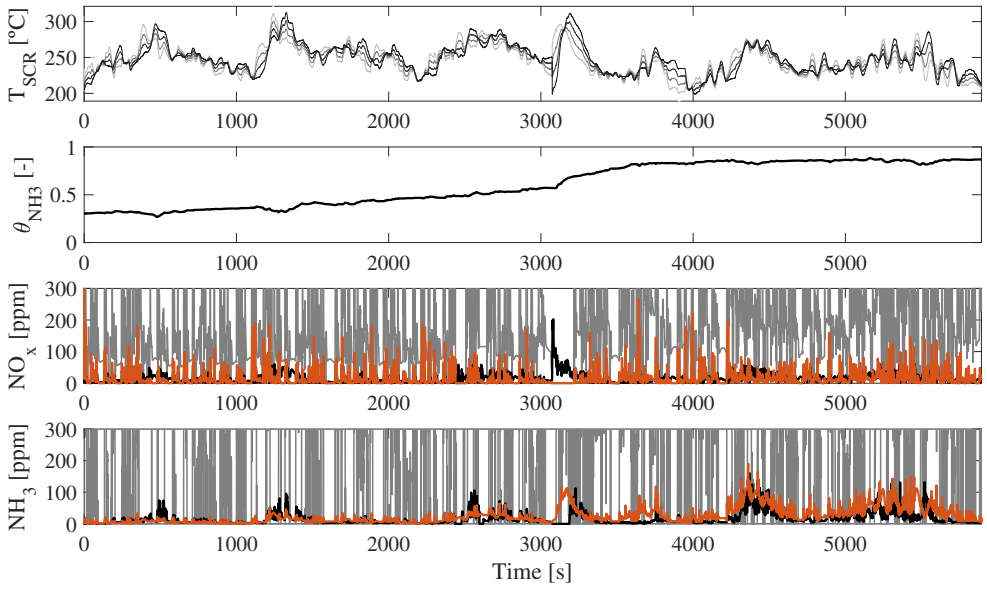

Figure 6.13. *0D SCR model application to a new part during transient operation. Top plot: dark to gray lines represent upstream to downstream signals. Bottom plots: gray stands for upstream, black stands for downstream and orange stands for downstream modelled signal.*

and the aged part is validated with 3 continuous WLTC tests from the engine setup C.2. Note that the urea injection strategy is also the same.

As the data presents the problematic of the NO_x sensor cross-sensitivity to NH_3, the calibration is also artisan as in the 1D model. This kind of calibration allows having a sufficient model accuracy, without the need for an extensive experimental plan to characterize the SCR under a wide range of NH_3 loads, bed temperatures, NO, NO_2 and NH_3 species concentrations, exhaust mass flows, and their corresponding dynamics.

The accuracy of the 0D control-oriented model is similar to that of the 1D model previously presented for the shown tests. When looking to the θ_{NH_3}, estimations are similar for both approaches. In fact, the same values of Ω_A are used for both model approaches and for both new and aged catalysts. However, a re-tuning of the reaction rates parameters is required, since even if the θ_{NH_3} is similar, the average estimation of the 0D does not have the same effect than the heterogeneous distribution of the NH_3 in the 1D approach.

Table 6.4. *Efficiency of SCRs and 0D model errors.*

	eff_{exp} [%]	eff_{mod} [%]	ϵ [%]
New: NO_x	92.2	93	0.8
New: NH_3	93.7	90.4	3.3
Aged: NO_x	68.9	65.5	3.4
Aged: NH_3	69.4	64.5	3.9

The Table 6.4 show a more contained error for the 0D model, although it is still similar to the 1D approach. In this sense, more effort is put into the 0D model, since it will be the one used for ageing estimations.

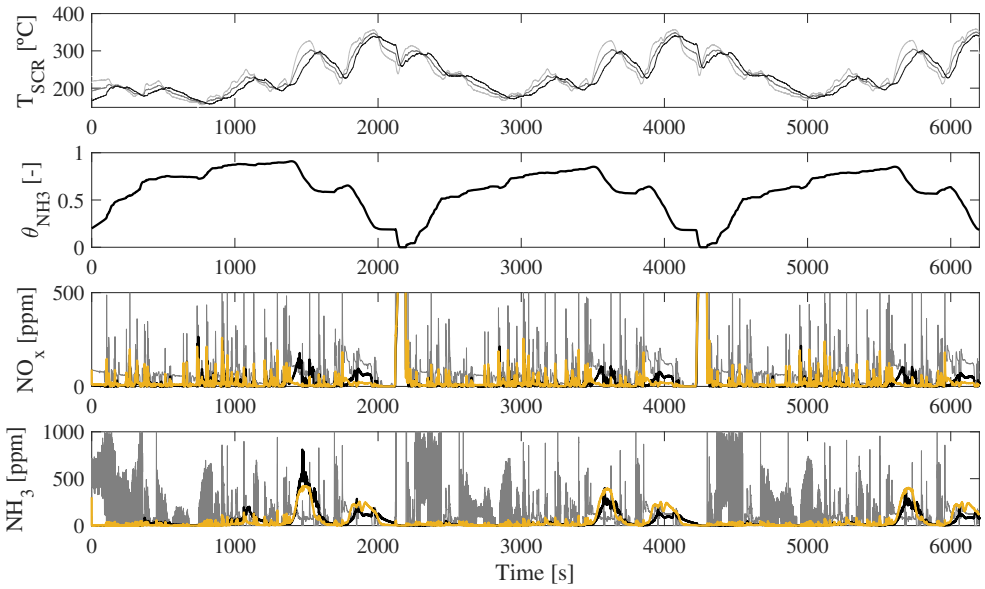

Figure 6.14. *0D SCR model application to an aged part during transient operation. Top plot: dark to gray lines represent upstream to downstream signals. Bottom plots: gray stands for upstream, black stands for downstream and yellow stands for downstream modelled signal.*

6.4 Conclusions

Control-oriented models for species estimation are shown for DOC and SCR catalysts. While the DOC model is based on experimental tests and it

follows a 0D lumped approach, the SCR models rely more on a physical approach. For all models, an ageing factor that can be considered as a parameter that allows varying from new to aged states is included and validation is done for new and aged parts in dynamic tests.

The presented DOC model shows an error lower than 3.5% in terms of efficiency, which is judged to be acceptable for control-oriented purposes. However, its HC and CO inputs are complex to estimate on-board since no measurements are available, so it is used for simulation rather than for their embedded application.

The 1D and 0D SCR models present up to 6% error in efficiency, so that both models show similar accuracy in the tests shown. On the other hand, the inputs of the SCR models presented are more accessible on-board, so its performance can be used in next sections for the algorithms development.

References

[1] Guardiola C., Pla B., Mora J. and Lefebvre D. "Control Oriented Model for Diesel Oxidation Catalyst Diagnosis". *IFAC-PapersOnLine*, Vol. 48 n^o 15, pp. 427 – 433, 2015. (cited in pp. 26, 27, 138, and 146)

[2] Sutjiono R, Tayal P, Zhou K and Meckl P. "Real-Time On-Board Indirect Light-Off Temperature Estimation as a Detection Technique of Diesel Oxidation Catalyst Effectiveness Level". In *SAE Technical Paper 2013-01-1517*. SAE International, 04 2013. (cited in pp. 26, 87, 138, and 175)

[3] Wang D Y, Yao S, Shost M, Yoo J-H, Cabush D, Racine D, Cloudt R and Willems F. "Ammonia Sensor for Closed-Loop SCR Control". *SAE International Journal of Passenger Cars - Electronic and Electrical Systems 2008-01-0919*, Vol. 1, pp. 323–333, apr 2008. (cited in pp. 9, 38, 99, and 138)

[4] Willems F. and Cloudt R. "Experimental Demonstration of a New Model-Based SCR Control Strategy for Cleaner Heavy-Duty Diesel Engines". *IEEE Transactions on Control Systems Technology*, Vol. 19 n^o 5, pp. 1305–1313, 2011. (cited in pp. 66, 138, 151, and 152)

[5] Hommen G, Kupper F and Seykens X. "Robust, Model-Based Urea Dosing Control for SCR Aftertreatment Systems using a Cross-Sensitive Tailpipe NOx Sensor". In *SAE Technical Paper Series 2017-01-0938*. SAE International, mar 2017. (cited in p. 138)

[6] Riegel J, Neumann H and Wiedenmann H-M. "Exhaust gas sensors for automotive emission control". *Solid State Ionics*, Vol. 152, pp. 783–800, 2002. (cited in pp. 8, 9, 34, and 138)

[7] Khosravi M, Abedi A, Hayes RE, Epling WS and Votsmeier M. "Kinetic modelling of Pt and Pt: Pd diesel oxidation catalysts". *Applied Catalysis B: Environmental*, Vol. 154, pp. 16–26, 2014. (cited in pp. 27 and 138)

[8] Sampara C S, Bissett E J and Chmielewski M. "Global kinetics for a commercial diesel oxidation catalyst with two exhaust hydrocarbons". *Industrial & Engineering Chemistry Research*, Vol. 47 n^o 2, pp. 311–322, 2008. (cited in pp. 25, 27, and 138)

[9] Sampara C S, Bissett E J, Chmielewski M and Assanis D. "Global kinetics for platinum diesel oxidation catalysts". *Industrial & Engineering Chemistry Research*, Vol. 46 n^o 24, pp. 7993–8003, 2007. (cited in pp. 25, 27, and 138)

[10] Chen P and Wang J. "Control-oriented model for integrated diesel engine and aftertreatment systems thermal management". *Control Engineering Practice*, Vol. 22, pp. 81–93, 2014. (cited in pp. 27, 110, 127, and 138)

[11] Kim Y-D and Kim W-S. "Re-evaluation and Modeling of a Commercial Diesel Oxidation Catalyst". *Industrial & Engineering Chemistry Research*, Vol. 48 n^o 14, pp. 6579–6590, 2009. (cited in pp. 27 and 138)

[12] Chen P and Wang J. "Control-oriented modeling of thermal behaviors for a Diesel oxidation catalyst". In *American Control Conference (ACC), 2012*, pp. 4987–4992, 2012. (cited in p. 138)

[13] Kim Y-W, Van Nieuwstadt M, Stewart G and Pekar Ja. "Model predictive control of DOC temperature during DPF regeneration". In *SAE Technical Paper 2014-01-1165*. SAE International, 2014. (cited in pp. 27, 29, and 138)

[14] Kryl D, Kocí P, Kubícek M, Marek M, Maunula T and Härkönen M. "Catalytic converters for automobile diesel engines with adsorption of hydrocarbons on zeolites". *Industrial & engineering chemistry research*, Vol. 44 n^o 25, pp. 9524–9534, 2005. (cited in pp. 26 and 138)

[15] Tanaka Y, Hihara T, Nagata M, Azuma N and Ueno A. "Modeling of diesel oxidation catalyst". *Industrial & engineering chemistry research*, Vol. 44 n^o 22, pp. 8205–8212, 2005. (cited in pp. 27 and 138)

[16] Bartley G J. "Identifying Limiters to Low Temperature Catalyst Activity". In *SAE Technical Paper 2015-01-1025*. SAE International, 2015. (cited in pp. 25, 87, and 139)

[17] Henry C, Currier N, Ottinger N, Yezerets A, Castagnola M, Chen H-Y and Hess H. "Decoupling the Interactions of Hydrocarbons and Oxides of Nitrogen Over Diesel Oxidation Catalysts". In *SAE 2011 World Congress & Exhibition 2011-01-1137*. SAE International, 2011. (cited in pp. 25 and 139)

[18] Tourlonias P and Koltsakis G. "Model-based comparative study of Euro 6 diesel aftertreatment concepts, focusing on fuel consumption". *International Journal of Engine Research*, Vol. 12 n^o 3, pp. 238–251, 2011. (cited in pp. 40 and 139)

[19] Sampara C S., Bissett E J. and Assanis D. "Hydrocarbon storage modeling for diesel oxidation catalysts". *Chemical Engineering Science*, Vol. 63, pp. 5179–5192, 2008. (cited in pp. 26, 88, and 140)

[20] Arvajova A, Koci P, Schmeisser V and Weibel M. "The impact of CO and C3H6 pulses on PtOx reduction and NO oxidation in a diesel oxidation catalyst". *Applied Catalysis B: Environmental*, Vol. 181, pp. 644 – 650, 2016. (cited in p. 142)

[21] Mallamo F, Longhi S, Millo F and Rolando L. "Modeling of diesel oxidation catalysts for calibration and control purpose". *International Journal of Engine Research*, Vol. 15 n^o 8, pp. 965–979, 2014. (cited in pp. 27 and 143)

[22] Ye S, Yap Y H., Kolaczkowski S T., Robinson K and Lukyanov D. "Catalyst light-off experiments on a diesel oxidation catalyst connected to a diesel engine-methodology and techniques". *Chemical Engineering Research and Design*, Vol. 90 n^o 6, pp. 834 – 845, 2012. (cited in pp. 25, 84, 87, and 146)

[23] Matsumoto A, Furui K, Ogiso M and Kidokoro T. "Model-Based OBD Logic Utilizing Adsorption and Desorption Model of NH3 in SCR Catalyst". In *SAE Technical Paper 2016-01-0960*. SAE International, 04 2016. (cited in pp. 8, 33, and 151)

[24] Nova I and Tronconi E. *Urea-SCR technology for deNOx after treatment of Diesel exhausts*. Springer, 2014. (cited in pp. 32 and 151)

[25] Chen R and Wang X. "Model-Based Fault Diagnosis of Selective Catalytic Reduction Systems for Diesel Engines". *SAE Int. J. Passeng. Cars - Electron. Electr. Syst. 2014-01-0280*, Vol. 7, pp. 449–453, 04 2014. (cited in pp. 33 and 151)

[26] Bartley G J., Chadwell C J., Kostek T M. and Zhan R. "SCR Deactivation Kinetics for Model-Based Control and Accelerated Aging Applications". In *SAE Technical Paper 2012-01-1077*. SAE International, 04 2012. (cited in pp. 33, 102, and 151)

[27] Figura J, Kihas D, Pekar J, Uchanski M, Khaled N and Srinivasan S. "Automotive Selective Catalytic Reduction System Model-Based Estimators for On-ECU Implementation: A Brief Overview". In *SAE 2016 World Congress and Exhibition 2016-01-0972*. SAE International, apr 2016. (cited in p. 152)

[28] Nova I, Lietti L and Tronconi E. "Transient response method applied to the kinetic analysis of the DeNO x-SCR reaction". *Chemical Engineering Science*, Vol. 56 n^o 4, pp. 1229–1237, 2001. (cited in pp. 152, 153, and 192)

[29] Eijnden E v d, Cloudt R, Willems F and Heijden P v d. "Automated Model Fit Tool for SCR Control and OBD Development". In *SAE Technical Paper Series 2009-01-1285*. SAE International, apr 2009. (cited in pp. 8, 66, and 152)

[30] Busca G, Lietti L, Ramis Go and Berti F. "Chemical and mechanistic aspects of the selective catalytic reduction of NOx by ammonia over oxide catalysts: A review". *Applied Catalysis B: Environmental*, Vol. 18 n^o 1, pp. 1 – 36, 1998. (cited in p. 153)

[31] Lietti L, Nova I, Ramis G, DallAcqua L, Busca G, Giamello E, Forzatti P and Bregani F. "Characterization and Reactivity of V2O5-MoO3 TiO2 De-NOx SCR Catalysts". *Journal of Catalysis*, Vol. 187 n^o 2, pp. 419 – 435, 1999. (cited in p. 153)

[32] Schneider H., Tschudin S., Schneider M., Wokaun A. and Baiker A. "In Situ Diffuse Reflectance FTIR Study of the Selective Catalytic Reduction of NO by NH3 over Vanadia-Titania Aerogels". *Journal of Catalysis*, Vol. 147 n^o 1, pp. 5 – 14, 1994. (cited in p. 153)

[33] Upadhyay D and Van Nieuwstadt M. "Modeling of urea SCR catalyst with automotive applications". 2002. (cited in pp. 33 and 156)

Chapter 7

Diesel after-treatment catalysts diagnostics

Contents

7.1 Introduction

The aim of this chapter is to develop methods to diagnose both the DOC and the SCR. The nature of the algorithms is born from the emissions regulations, the observation of the effects of ageing on emissions and the possibilities that models can offer. In this line, a simulation-based study is first done for

each catalyst to analyze the effect of ageing in comparison with OBD limits. Then, the algorithms are presented.

On the one hand, the DOC algorithms take into account the lack of on-board HC and CO measurements, since the catalyst ageing is controlled in the ECU through the available set of sensors. However, sensors accuracy and tight thresholds make diagnostics difficult for DOCs, as stated by [1], so that the ageing state of a DOC has to be monitored through indirect techniques. Taking this consideration into account, and following regulations, two algorithms are presented. First, an algorithm for detection of total removal, and next, an algorithm to estimate efficiency loss. In this sense, the efficiency loss is detected with an indirect technique, whose result can be related to an emissions increase through the model presented in Chapter 6.

On the other hand, the SCR algorithms are mainly fed with on-board measurements. Therefore, the 1D and 0D models shown in Chapter 6 are used in the algorithms. In this case, the deviations that the urea injector can present are also estimated in the algorithm, since that would affect the model inputs and therefore the observer estimation.

7.2 Diesel oxidation catalyst diagnostics

The diagnostics methods next presented require the use of a hot film flow anemometer, present in most vehicles, up- and downstream NTC temperature sensors, up- and downstream λ measurements (only for the DOC efficiency estimation) and the modification of the post-injection strategy of the engine ECU.

7.2.1 Ageing effect on species slip

The emissions increase is next analyzed by means of a simulation study using the model presented in Chapter 6, in which the combined effect of the LOT increase and the A_{eff} decrease is quantified. For this purpose, the ageing factor ξ is now treated as the variable that states the LOT_{HC}, LOT_{CO} and A_{eff}, varying its value from 0 to 1.17, i.e. from new to a more aged state than the experimental catalyst.

$$LOT_{HC} = 60\ \xi + 190 \tag{7.1}$$

$$LOT_{CO} = 60\ \xi + 130 \tag{7.2}$$

Table 7.1. *Each column of the table represents a simulated ageing state in Figures 7.1 and 7.2. ξ=0 corresponds to the new DOC and ξ=1 corresponds to the aged DOC.*

ξ	0	0.17	0.33	0.5	0.67	0.83	1	1.17
LOT_{HC}	190	200	210	220	230	240	250	260
LOT_{CO}	130	140	150	160	170	180	190	200
A_{eff}	100	92.6	85.3	78	70.6	63.3	56	48.7

$$A_{eff} = -44\,\xi + 100 \tag{7.3}$$

The intermediate ageing levels are described in Table 7.1, while simulation results are shown in Figure 7.1, where the transition in HC and CO emissions from the new catalyst to the aged catalyst can be appreciated. An increase in DOC downstream temperature can be observed at the instants in which LOT_{HC} is exceeded.

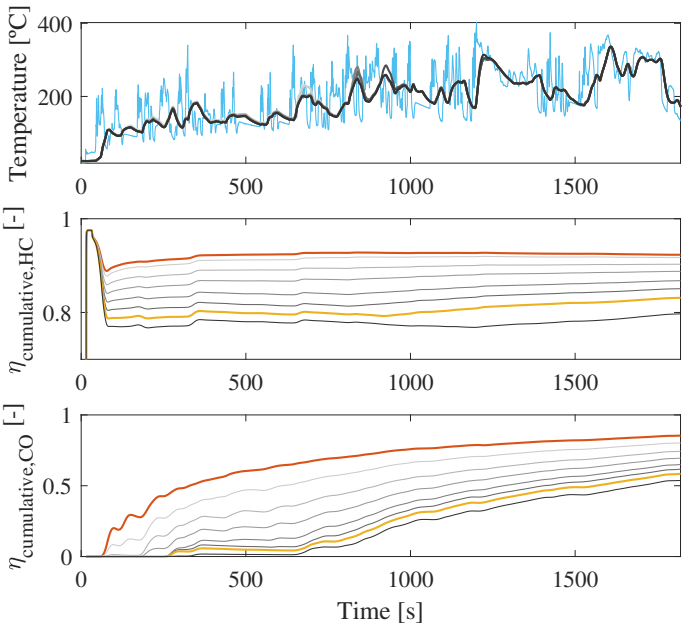

Figure 7.1. *Ageing parametric study at ambient starting conditions. Top plot: —— upstream temperature. Medium plot: cumulative HC emissions. Bottom plot: cumulative CO emissions. The gray degraded corresponds to the downstream signal: from —— ξ=0 to —— ξ=1.17.*

While the capacity of the new DOC to accumulate HC is higher, its LOT is also lower. On the other hand, since the aged DOC is less able to accumulate HC and its LOT temperatures is higher, these 2 effects are combined to increase its HC slip, so that its efficiency is lower than that of the new DOC.

In the case of the CO emissions, as they are affected by the LOT, only the slight change in temperaure due to different HC accumulated in the oxidation events when HC LOT is overcome changes its emissions apart from the LOT_{CO}.

Effect of actual DOC ageing at warm starting conditions The effect of ageing on DOCs is more accused at cold conditions, when the DOC temperature is under light-off. Once the DOC is warm, the ageing effects are almost negligible, so no differences can be appreciated from the second or third phase of the WLTC. In these phases, the engine demand and the engine warm conditions provide a DOC upstream temperature over light-off, even for aged DOCs. Then, as a DOC becomes aged, its increase in emissions will be higher at each cold starting. In this sense, when temperature valleys appear at warm conditions, the HC slip emissions will be potentially more affected as the DOC is more aged.

The effect of the low and medium phases of the WLTC is mixed with the cold starting conditions. Therefore, to decouple the effect of engine warming up from the first two phases power demand, Figure 7.2 shows a WLTC starting at warm conditions, being the initial DOC upstream temperature at 260°C approximately. Note that after 900 s, cold start and warm start WLTC tests temperatures are already similar, i.e. from 900s the DOC upstream temperature is not yet influenced by the starting temperature. It can be observed a decrease of temperature from the test start, whose valley is at 500s, due to the fact that the engine operating conditions of the first two phases is not high enough to operate above DOCs LOT. Therefore, in case this conduction mode lasted more time in RDE, the ageing effect would be increased.

7.2.1.1 Critical default size as derived from OBD requirements

In this section, the emissions increase due to ageing are compared with the regulation thresholds, for both HC and CO species. While Figure 7.3 represents the HC slip as a percentage of the inlet HC for the two deterioration considered modes, Figure 7.4 is the equivalent figure for CO. In both figures, experimental results for the new, the nominal and the aged DOCs are presented in comparison with simulation results. Apart from the simulations

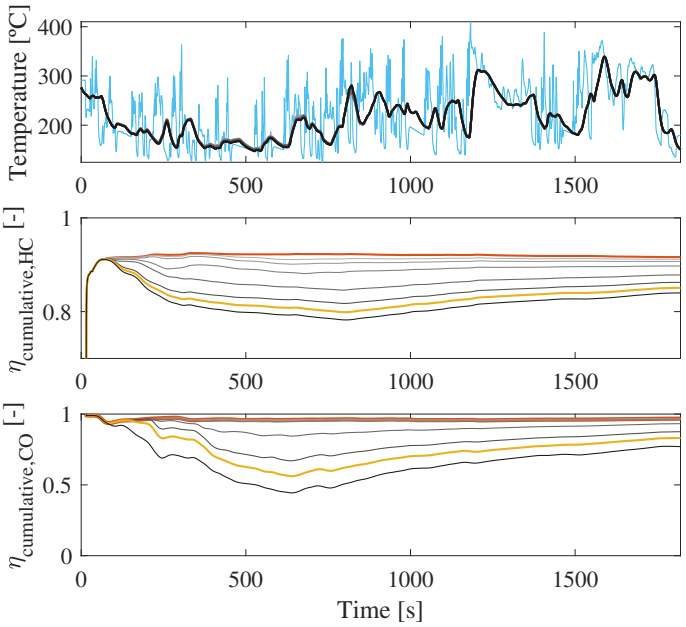

Figure 7.2. *Ageing parametric study at warm starting conditions. Top plot: —— upstream temperature. Medium plot: cumulative HC emissions. Bottom plot: cumulative CO emissions. The gray degraded corresponds to the downstream signal: from —— ξ=0 to —— ξ=1.17.*

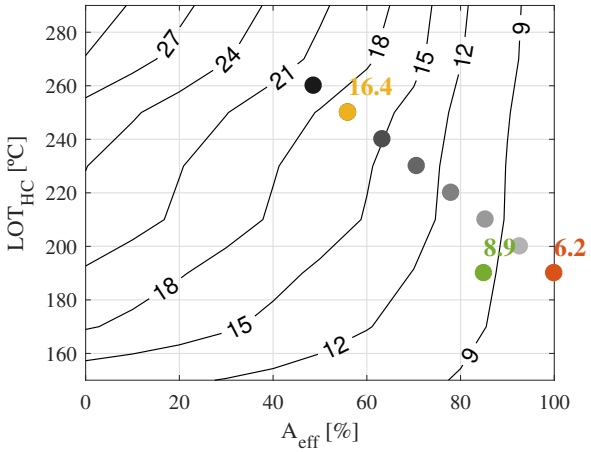

Figure 7.3. *HC slip at LOT and A_{eff} as a percentage of inlet HC. Colored dots stand for experimental measurements: • New DOC • Nominal DOC • Aged DOC. Gray dots stand for ageing states simulated in Figures 7.1 and 7.2.*

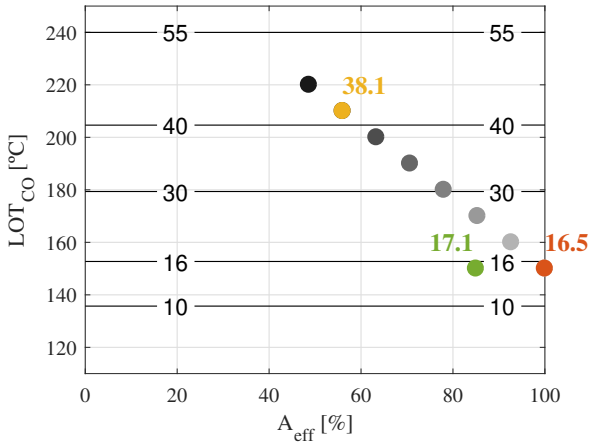

Figure 7.4. *CO slip at LOT and A_{eff} as a percentage of inlet CO. Colored dots stand for experimental measurements: • New DOC • Nominal DOC • Aged DOC. Gray dots stand for ageing states simulated in Figures 7.1 and 7.2.*

presented in previous figures, another set of simulations was done to map the performance as a function of LOT and A_{eff}.

As presented in Figures 7.3 and 7.4, the actual ageing parameter ξ is considered to be a linear function from the new to the aged catalyst. Then, using the model, a maximum ageing threshold could be established for OBD requirements from the experimental measurements of two catalysts. Figure 7.5 shows the experimental emissions measurements of the raw, the new and the aged catalysts in comparison with the european Euro 6 regulation for new and OBD vehicles. Even though the aged DOC is able to comply with new regulation, this is a particular case and the methodology could be applied to other engines with different DOCs or DOC-upstream conditions. In case of CO emissions, the aged catalyst would not comply with new Euro 6 regulations, although it would do for the OBD threshold. However, note that different RDE cycles could affect results.

Finally, ageing, LOT and A_{eff} are related and by estimating for example LOT, an emissions level could be associated.

7.2.2 Removal detection

The regulation for DOC requires an algorithm able to detect if the catalyst has been removed or if it has a complete failure. Then, an on-board real-time diagnostics strategy to discern whether a DOC is able to oxidize or not, based

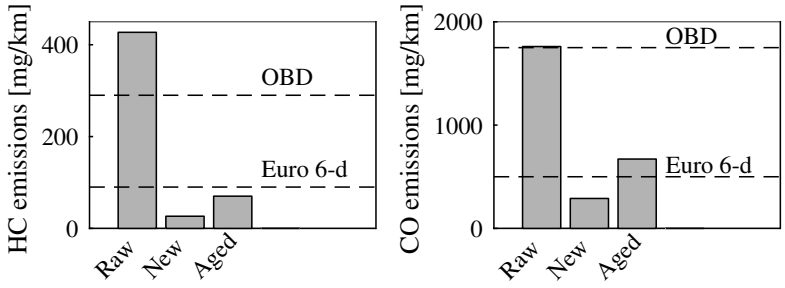

Figure 7.5. *Experimental measurements of engine-raw and tailpipe emissions for new and aged DOCs in comparison with Euro 6-d limits for new and OBD vehicles.*

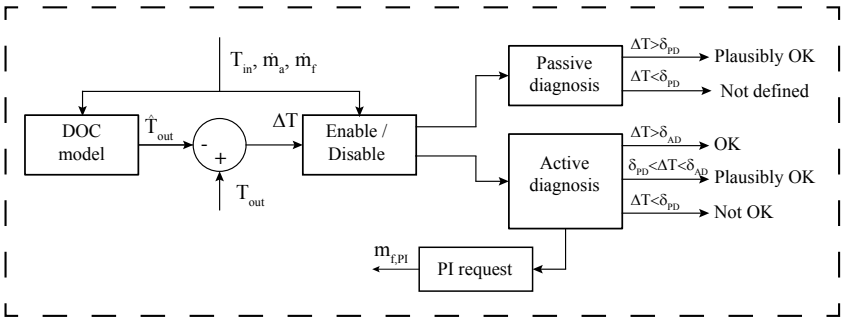

Figure 7.6. *Scheme of the diagnostics strategy.*

on the exothermic generated by the DOC when there is presence of oxidable species, is presented.

For this purpose, the residuum generated ΔT by comparing the measured outlet temperature of an impregnated DOC with the model outlet temperature of a non-impregnated DOC can be used for diagnostics purposes. Then, the DOC diagnosis strategy is able to detect activity when the measured temperature is higher than the estimated ($T_{out} > \hat{T}_{out}$).

The strategy is divided into passive diagnostics and active diagnostics. On the one hand, the passive diagnostics take place during normal driving conditions without external excitation, while on the other hand, post-injections are used in active diagnostics as an extra excitation to increase HC concentration at the inlet of the DOC [2, 3]. In this line, post-injections used during DPF active regeneration phases can also be used for DOC diagnostics purposes.

Figure 7.6 shows the general diagnostics strategy, whose elements will be described in subsequent paragraphs, and table 7.2 shows its main coefficients.

Table 7.2. *Coefficients of the diagnostics strategy.*

Coefficient	Description
T_{in}	Measured DOC inlet temperature
T_{out}	Measured DOC outlet temperature
$\hat{T}_{out}$	Estimated non-impregnated DOC outlet temperature
m_a	ECU estimated air mass flow
m_f	ECU estimated injection fuel
ϵ	Temperature model error
$m_{f,PI}$	ECU estimated post-injection fuel
ΔT	Residuum $T_{ds} - \hat{T}_{ds}$
δ_{PD}	Low diagnosis threshold
δ_{AD}	High diagnosis threshold

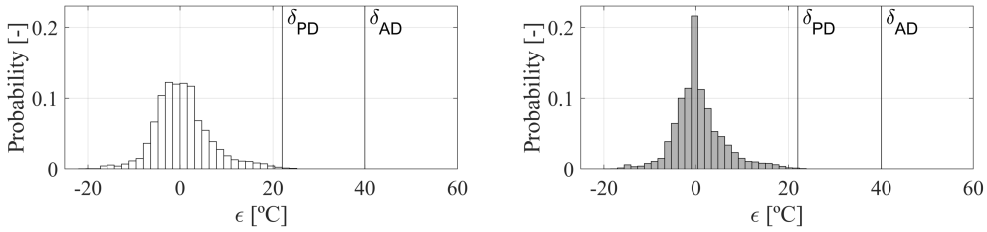

Figure 7.7. *Histogram of the raw residuum (left) and 5 seconds filtered residuum (right) generated by the model and the non-impregnated DOC in the complete set of tests.*

In order to set thresholds taking into account the errror of the passive model, a set of tests during more than 5 hours, including dynamic tests like 3.15 and homologation cycles like the NEDC or the WLTC at both warm and cold starting conditions, are used. The result of all those tests together is shown in Fig. 7.7 as an error histogram. On the one hand, white filled histogram, represents the probability of a given error during 0.1s, while on the other hand, gray filled histogram represents the filtered error, in which a clear peak at 0 can be observed. This is basically due to the fact that errors are increased during dynamic situations in short time lapses.

7.2.2.1 Diagnostics conditions

Limiting the strategy to situations out of model errors lead to a better performance. For this purpose, effective monitoring time is then ruled by

enabler conditions which depend on engine operating points, system dynamics and catalyst temperature. Then, the suitable conditions for DOC diagnostics are next outlined:

- The DOC is sufficiently hot, since the light-off temperature sets the minimum temperature from which the DOC is able to oxidize.
- There is sufficient exhaust mass flow. Completely absence of flow in the DOC does not allow diagnosis with oxidation due to obvious reasons.
- The DOC temperature is not excessive, in which case it is hard to detect DOC activity due to huge heat transfer effects.
- dT/dt is not excessive. NTC sensors are rather slow, which causes significant bias in the case of fast varying transients. Therefore, even if the model shows good performance during transients, severe dynamics are to be avoided.
- There is enough oxygen in the exhaust line after the in-cylinder combustion.

7.2.2.2 Low and high diagnosis thresholds

Low threshold The error generated by the comparison of the outlet temperature of a passive DOC and the modelled temperature are inside an interval of $\pm 22^{\circ}$C, as can be seen in Figure 7.7. Although the 3σ criteria suggests an error interval of $\pm 18^{\circ}$C, an error interval of $\pm 22^{\circ}$C ensures that the error will not surpass that range during 0.1s with a probability of $10^{-6}\%$. Therefore, passive detection will provide positive results regarding DOC state when ΔT is higher than a low threshold δ_{PD} of 22 °C.

High threshold Even if the model error does not overcome the low threshold, a higher threshold δ_{AD}, for active diagnosis, is set to completely ensure the proper state of the DOC. The probability of making a proper diagnostic of the DOC results in a trade-off between the size of the post-injection and the value of δ_{AD}, where the size of the post-injection is the combination of the post-injection duration and the injection rate.

Error type I: DOC Failure Miss-detection
If δ_{AD} is too low, a big model error could increase ΔT over δ_{AD} and a faulty DOC could be considered as faulty free.

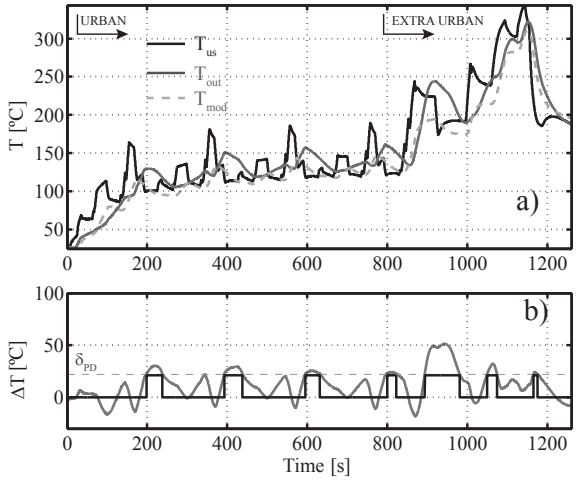

Figure 7.8. *Passive diagnostics with the nominal catalyst during a NEDC test. a) Temperatures. b) Gray: ΔT. Black: 0 when no oxidation and δ_{PD} when $\Delta T > \delta_{PD}$.*

Error type II: DOC Failure Over-detection

If the size of the post-injection is not big enough and ΔT does not overcome δ_{AD}, a faulty free DOC would be considered as faulty. It can be considered as a cost parameter, since it determines the size of the post-injection.

Thus, δ_{AD} should be high enough to avoid error type I but, accordingly, the size of the post-injection must ensure that ΔT will overcome the threshold to avoid error type II.

7.2.2.3 Passive diagnostics

Passive diagnosis consists in the evaluation of ΔT during normal driving operation conditions. When diagnosis is enabled and $\Delta T > \delta_{PD}$, there is a plausibly but non-demanded check that the DOC is oxidising. During cold starting and during some phases in which the exhaust line temperature is under the light-off temperature, a DOC is able to accumulate HC. Therefore, if enough amount of fuel is accumulated in the DOC, when it overcomes the light-off temperature under certain conditions, the accumulated HC will be oxidized and ΔT will increase.

Figure 7.8 shows the residuum ΔT generated during an NEDC homologation cycle. The DOC accumulates HC during the urban phase, except for the

short four temperature peaks of the urban part, so when the cycle comes to the extra-urban part and the exhaust temperature rises above the light-off temperature during enough time, the DOC efficiency increases enough to oxidize accumulated HC and ΔT clearly overcomes δ_{PD}. Despite oxidation phases can be appreciated when $\Delta T > \delta_{PD}$, negative phases mark the presence of the inherent error of the model. In fact, the combined effect of the error model and the temperature increment due to oxidation may not be separated when using the nominal DOC.

The passive diagnostics strategy has a relevant drawback, though. The HC and CO concentrations at the DOC upstream significantly vary with the considered engine, the operation temperature and many uncontrolled disturbances. Indeed, HC and CO engine-raw emissions are usually low for a diesel engine with conventional combustion when in warm operation and experience suggests that exothermic reaction generated by normal combustion operation does not overcome a ΔT of 50°C. On the other hand, if diagnosis conditions are enabled but $\Delta T < \delta_{PD}$, a decision cannot be taken regarding the DOC state in order to avoid error type II.

7.2.2.4 Active diagnostics

Active diagnosis consists in the evaluation of ΔT when specific post-injection events are performed. Note that only active diagnosis is able to decide whether the DOC is completely OK or if by contrast is not OK. The active diagnosis algorithm decides when a post-injection event is required depending on how many kilometres have passed since the last high-check. It can take advantage of the post-injections demanded by the DPF regeneration system or it can request their own. When fuel is post injected in the exhaust line, a temporary window is opened, during which active diagnosis is enabled, as long as the rest of diagnosis conditions are accomplished. If $\Delta T > \delta_{AD}$ during a certain time inside the window, the result of the diagnosis will be positive. If $\delta_{AD} > \Delta T > \delta_{PD}$, diagnosis can not assure completely the proper state of the DOC, so it results in a low check and the DOC is plausibly OK. Otherwise, if $\Delta T < \delta_{PD}$, the result of the diagnosis is negative, the DOC is not OK and the vehicle should go to the workshop after a certain number of failure checks (Fig. 7.6).

Post-injection pulses Post-injection pulses are an efficient way in terms of fuel consumption to increase ΔT over δ_{AD} during the minimum required time. For this purpose, the steady state model for pulses and the ΔT pulses models

presented in Chapter 5 can be used. However, since steady state conditions cannot be assured during real driving conditions, the pulses model can only be used as a reference to calibrate the post-injection strategy. Of course, the calibration should be in the side of security and estimated ΔT should be higher than δ_{AD}.

Note that the DOC diagnostics strategy can also take advantage of the DPF regeneration system. Then, active diagnosis post-injection requests can be combined with DPF regeneration events in order to save fuel.

Application to active diagnostics Figure 7.9 shows active diagnostics for the nominal catalyst during an NEDC cycle in which post-injections have been applied. During the urban phase, small oxidation intervals may be appreciated due to the oxidation of accumulated engine-raw HC emissions, while the inlet temperature overcomes the activation temperature. This phenomena can be also appreciated in Figure 7.8 during passive diagnosis, due to the fact that post-injections have not been applied yet. When the cycle comes to the extra-urban phase, the DOC temperature rises above the light-off and two post-injections are applied. Both post-injections have 8 mg/str rate. The first post-injection has 7 seconds duration and the second post-injection has 3 seconds duration. Although the fuel signal might have accuracy errors, the model does not predict temperature increments, so post-injection events are set to provide sufficient temperature increase.

The first post-injection shows how enough post-injected fuel during normal engine operation can rise ΔT until a maximum value of 100°C, which ensures a proper diagnostics. Thus, in this case, when active diagnostics is enabled, the applied post-injections increase sufficiently $\Delta T > \delta_{AD}$ and there is a high check that the DOC is working properly.

By contrast, results of active diagnostics are shown for the non-impregnated DOC, also during a NEDC in Figure 7.10, in which the same post-injections have been virtually applied. In this case, during the temporal window opened after the post-injections, the residuum ΔT does not overcome in any case neither δ_{PD} nor δ_{AD} so according to the diagnostics strategy shown in Figure 7.6, the result is negative and the DOC is not able to oxidize.

7.2.3 DOC efficiency estimation

As stated previously, the lack of HC nor CO on-board measurements lead to the need for estimating the DOC efficiency through indirect techniques.

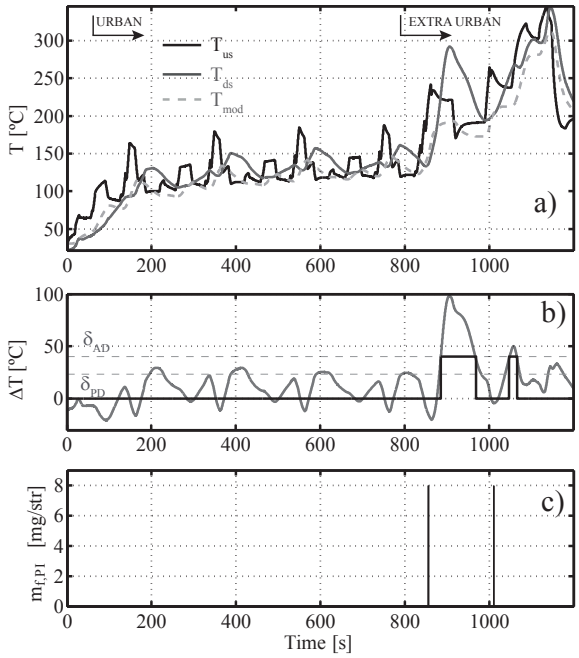

Figure 7.9. *Active diagnostics with the nominal catalyst during a NEDC test. a) Temperatures b) Gray: ΔT. Black: 0 when no oxidation and δ_{AD} when $\Delta T > \delta_{AD}$. c) Post-injection.*

Using the available set of on-board sensors, the estimation of the DOC light-off temperature seems more feasible than the estimation of an HC or CO emissions increase, so the light-off temperature could be used as an indicator of the DOC performance [4, 5]. In this sense, the DOC model presented in Chapter 6 allows associating a LOT increase to an ageing state and therefore to a given emissions increase, as previously simulated in this chapter. With this, the efficiency of the DOC can be indirectly estimated, which combined with a regulation-based threshold criteria, can be used to alert the driver with the MIL when the DOC efficiency is too low.

The presented strategy is based on the capacity of the NO_x sensors to detect oxidation events through λ measurements. Then, the strategy makes use of the upstream temperature sensor to associate oxidation events to representative temperatures and generate a database, which will be evaluated to establish the no-oxidation to oxidation ranges, as schematically outlined in Figure 7.11. Note that this strategy makes use of the state-of-the-art set of sensors present in a complete after-treatment system of a diesel exhaust line.

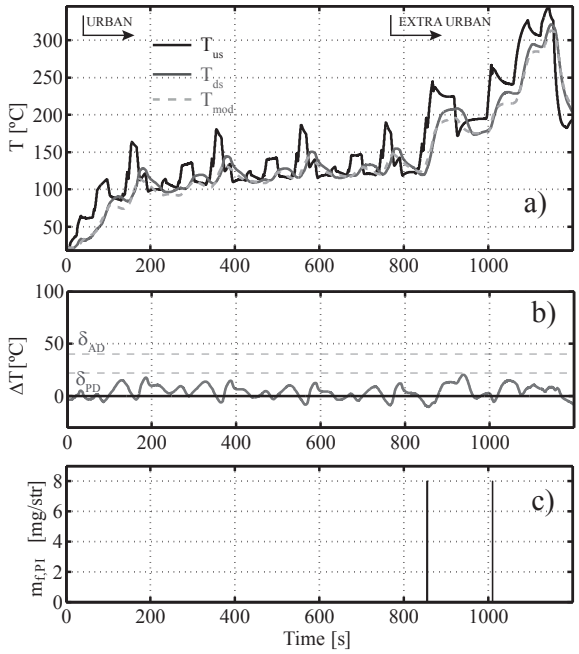

Figure 7.10. *Active diagnostics with the non-impregnated catalyst during a NEDC test. a) Temperatures b) Gray: ΔT. Black: 0 when no oxidation and δ_{AD} when $\Delta T > \delta_{AD}$. c) Post-injection.*

An analogic method could be used for lean NO_x trap (LNT) systems, which accumulate and reduce NO_x species, although this is out of the scope of this work.

In the algorithm, idle is used as a steady engine operating point at low temperature [6], which allows having more controlled conditions during the temperature transition through the LOT. Then, oxygen concentration measurements, which can be obtained from NO_x sensors or UEGO sensors, are measured with a pair of NO_x sensors in this work.

7.2.3.1 Detection concept feasibility

The LOT estimation strategy is based on the difference between up- and downstream oxygen concentrations during oxidation phases, and the association of a representative temperature to the oxidation event. Several aspects should be considered for this strategy, accounting for the sensors precision, dynamics and offsets, as well as the own DOC dynamics, its ageing state and

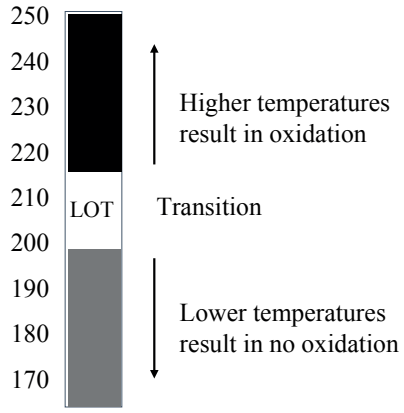

Figure 7.11. *LOT detection strategy scheme.*

engine operating conditions. In this sense, the λ measurements are proven to be fast and precise enough to capture the difference in oxygen concentration that an oxidation event produces in Chapter 4. Then, the temperature associated to oxidation can come from the temperature measurement or from a model estimation.

First, the potential to estimate the LOT without neither controlled engine operating situation nor excitation with post-injections is evaluated in Section 5.5, where a dynamic case was presented. Although in the previous chapter the objective was to show the oxidation events of a DOC during normal driving conditions in an NEDC, these oxidation events were captured with a couple of λ measurements from NO_x sensors. However, the method described for the oxidation detection is based on static calibrations, fit for the pair of sensors used. For this reason, this oxidation estimation is not adaptive to possible sensors offsets, which makes impossible the use of this strategy for on-board purposes.

In this line, once oxidation is observed, a representative temperature should be associated to oxidation, which outlines another problem in dynamic situations. Coming back to Figure 4.16, even if the nominal and aged catalysts have different LOT, the measured temperature during the oxidation event at the extra-urban step is similar for both DOCs. In fact, the temperature during oxidation detection is higher for the nominal DOC, approximately more than 300°C, than for the aged DOC, approximately less than 300°C. Therefore, the feasibility of associating a representative temperature to each DOC is low. Moreover, the HC and CO are rather low during normal driving conditions, which would make more difficult the presence of oxidation phases. In this

sense, post-injections could be applied during low temperature phases to increase the level of excitation and therefore increase the λ difference, although the temperature step problem would remain.

Summarizing, the LOT estimation in dynamic conditions has the following drawbacks, which cannot be overcome for on-board applications:

- The thresholds-based calibration is subjected to sensors offset. A different pair of sensors could need different threshold values.
- In case of an oxidation event is detected, a representative temperature could not be associated, since temperature is highly unsteady in dynamic conditions.
- The required temperature to fill the database cannot be provoked, since temperature is subjected to particular driving conditions.

In order to avoid these problems, the presented strategy makes use of idling and post-injections to generate decision events. Idle periods are characterized by low temperatures at steady state conditions, since the fuel injected is low. Note that idling is not the lowest achievable temperature because tip-off events and coasting conditions can have lower temperatures. Regarding the prior-to-idle engine operating conditions, the initial engine-raw temperature has to be above the LOT to observe oxidation events. A non controllable and limiting aspect is the idle phase duration, since it has to be enough to apply the post-injection pulses and allow the temperature to decrease. On the other hand, if the vehicle follows a start&stop strategy, idle could be forced if conditions are favourable and required for the strategy. For instance, a vehicle running that stops at a red light, or a vehicle that comes out from the highway and park during a moment, would be potential cases to apply the strategy. For this reason, the use of embedded GPS systems and smart city connections can help to decide the suitable moments, since they can predict if the engine will be enough time at idling.

In order to decide whether the DOC is able to oxidize or not at a certain temperature, post-injection pulses are applied. Then, post-injection pulses can be applied as long as the temperature is appropriate, since a database of post-injections at different temperatures has to be generated. If the temperature at which the engine is running prior to idle is above the light-off, the first post-injections will be oxidized. Next, if more post-injection pulses are applied as temperature decreases, the λ measurements will reach a threshold from which no oxidation will be detected.

Regarding the constraints of the regulation for DOC diagnosis, it considers an in-use performance ratio (IUPR) of 0.336. As stated in the Euro regulation [7], the denumerator must be increased by 1 at least after 800km, so that the strategy can collect cases during 2400km, when the LOT estimation would be triggered and the IUPR counter would reset. The regulation also considers an idle period of 30s as a correct order of magnitude [7], during which the strategy can at least perform one complete pulse to feed the database.

7.2.3.2 Strategy measurements characterization

With the previously described method fundamentals, sensors requirements and their limitations are evaluated in this section. Temperature signals in Figure 4.7 are obtained from thin thermocouples measurements, to highlight the dynamics problem of the temperature during driving conditions. In this line, on-board NTC sensors measurements are slower than gas temperature variations. However, despite the upstream measurement could be improved by means of the data fusion technique described in Chapter 5, the problem of associating a representative temperature would remain.

The λ measurements are a key part of the strategy, since they have to measure the decrease in oxygen concentration produced by DOC oxidation. In this sense, their capacity to detect oxidation conditions is discussed in Chapter 4 in terms of dynamic response. However, its accuracy, precision, ageing and capacity to measure oxygen concentration in presence of raw HC are considered next.

A problem raised in previous Section 7.2.3.1 was the offset of the λ measurements, which is characterized in Figure 3.8 and it is manually compensated in the already commented Figures 4.7 and 4.6. Figure 7.12 represents the difference between the up- and downstream measurements during a WLTC test for a pair of sensors. The WLTC test was selected due to its strong dynamic conditions, which provoke continuous differences between up- and downstream λ measurements, mixing the effects of sensors offset, engine dynamics and transport time of the species. The sensors were located initially and vice-versa to see the effect that offset can have on the strategy. As dynamics lead to a wide range of cases between up and downstream λ measurements, the histogram of Figure 7.12 have both negative and positive values, which can be compared to the effect of oxidation on λ. The order of magnitude that an oxidation event produces in λ is about 0.05. Then, as the dynamic detection strategy had non-adaptive thresholds as tunable parameters, these are not valid for any pair of sensors, so it can be concluded that sensors offset distortion disable the

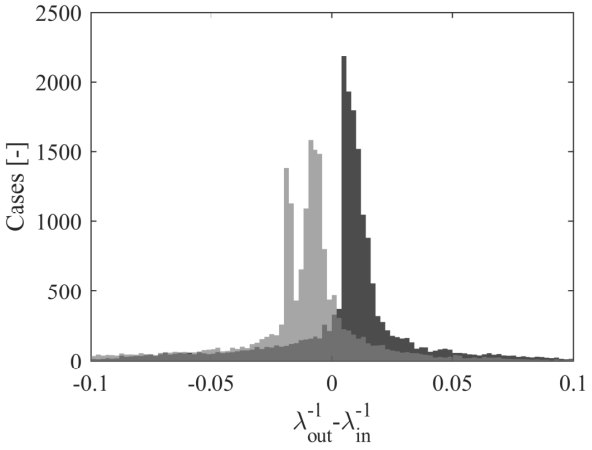

Figure 7.12. *Offset between λ_{us} and λ_{ds} measurements during a WLTC. Dark gray: Original sensors layout distribution. Light gray: Sensors located viceversa. The intermediate gray is the intersection of both histograms.*

dynamic strategy.

Finally, the λ measurements of the NO_x sensors during the fuel post-injections were previously analyzed in Section 4.3.2, whose conclusion is that λ measurements can be used to detect oxidation phases with a proper thresholds-based strategy.

7.2.3.3 On-board LOT estimation

The method to estimate the light-off temperature is detailed next. As stated before, idle-like conditions are used to avoid dynamics and to have a controlled decrease of temperature, while post-injections are applied. Figure 7.13 shows an example of the method application during an idle period of 300s, whose initial temperature is around 300 °C. Then, the temperature decreases to near 185°C. During this period, a train of post-injection pulses of 5 mg/str of fuel during 3 seconds each 15 seconds is being applied. The λ signal is tunnelled between minimums and maximums, so it is easier to appreciate how the differences between both tunnels decrease as temperature decreases.

When a post-injection pulse is applied, a temporal window is open until the peak of λ^{-1} is reached. Then, the initial λ^{-1}_{ini} and peak λ^{-1}_{peak} values obtained during this window for both up- and downstream signals are used to take a decision of the post-injection event according to equations (7.4) to (7.6). These

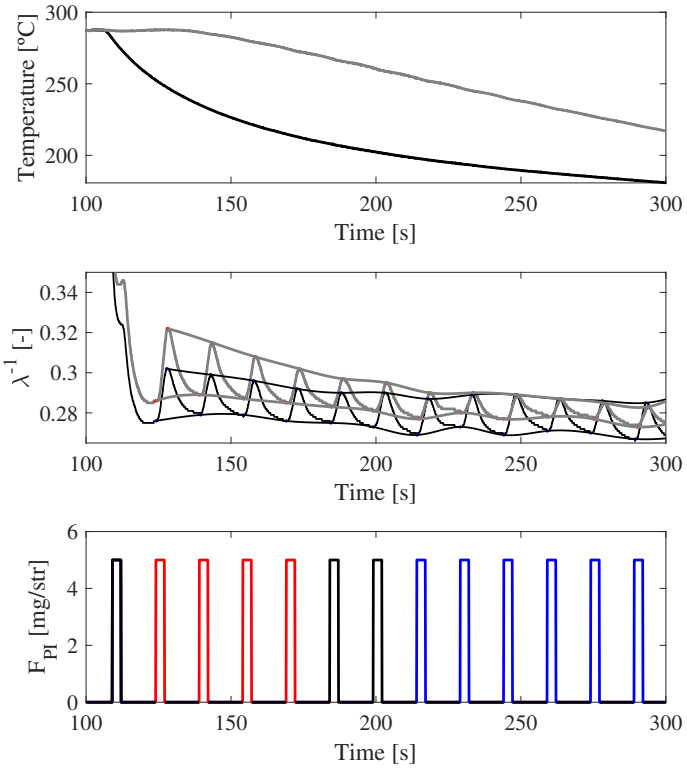

Figure 7.13. *Method application to a 300s idle period. Black and gray colors stand for upstream and downstream measurements in temperature (top) and λ (medium) plots. λ signals are tunnelled in medium plot. In the F_{PI} plots, black stands for non-defined, red stands for oxidation and blue stands for no oxidation.*

particular values are highlighted in Figure 7.14 for a post-injection pulse. If inequation (7.4) is true, no oxidation is observed. Inequation (7.5) stands for an undefined range, in which neither oxidation nor no oxidation can be ensured. Finally, in equation (7.6) is true when oxidation occurs. A threshold for no oxidation $\Delta\lambda_1$ and a threshold for oxidation $\Delta\lambda_2$ allow taking the decision of the pulse. Equations (7.4) to (7.6) are described next:

$$\lambda_{ds,peak}^{-1} - \lambda_{ds,ini}^{-1} - (\lambda_{us,peak}^{-1} - \lambda_{us,ini}^{-1}) < \Delta\lambda_1 \tag{7.4}$$

$$\Delta\lambda_1 < \lambda_{ds,peak}^{-1} - \lambda_{ds,ini}^{-1} - (\lambda_{us,peak}^{-1} - \lambda_{us,ini}^{-1}) < \Delta\lambda_2 \tag{7.5}$$

$$\lambda_{ds,peak}^{-1} - \lambda_{ds,ini}^{-1} - (\lambda_{us,peak}^{-1} - \lambda_{us,ini}^{-1}) > \Delta\lambda_2 \tag{7.6}$$

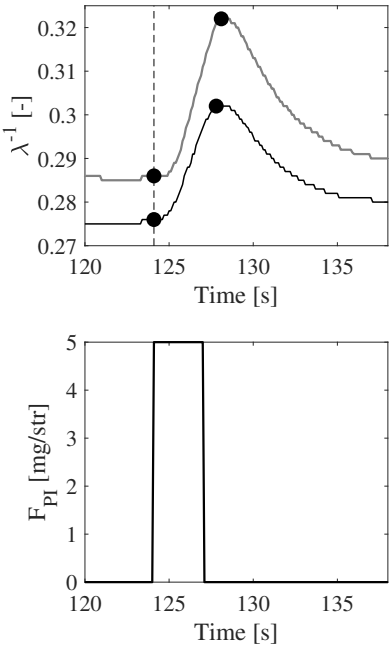

Figure 7.14. *Initial and maximum values used in the algorithm for both up- and downstream λ measurements during a post-injection pulse event with oxidation. Top plot: dots stand for initial and maximum values, black line stands for upstream λ, gray line stands for downstream λ and dashed line stands for post-injection start. Bottom plot: post-injection pulse.*

where λ_{peak}^{-1} is the peak value due to the post-injection pulse and λ_{ini}^{-1} is the initial value of the signal when the post-injection is applied. λ_{us}^{-1} stands for upstream λ^{-1}, while λ_{ds}^{-1} stands for downstream λ^{-1}.

Other techniques could be used to separate oxidation from no oxidation, like taking into consideration the frequency content of the pulse, as it is done for the pulses calibration. However, the simple method presented, based on initial values and peaks, shows enough accuracy. In Figure 7.13, the post-injections are coloured with the oxidation result, being the initial 4 pulses associated to oxidation, the 2 following pulses undetermined and the subsequent associated to no oxidation. The initial pulse is not identified, since it was done during the transition phase from the initial engine operating condition to idle-like condition, during which λ is still stabilizing.

A test to characterize the required level of post-injection was carried out with different post-injections pulses, from 1 to 10 mg/str, and different durations, from 0.5 to 3s, at idle-like conditions, characterized by no oxidation

Table 7.3. *Frequency based contrast indicator F_{ind} between λ_{ds} and λ_{us} peaks due to post-injection pulses.*

	F_{PI} [mg/str]								
t [s]	1	2	3	4	5	6	7	8	10
0.5	1.17	1.75	1.55	1.58	1.85	1.79	2.07	1.42	1.15
1	1.33	1.22	2.13	1.74	2.07	1.89	1.90	2.09	1.70
1.5	1.42	1.40	1.60	2.25	2.18	2.12	1.94	2.06	1.96
2	1.64	1.80	1.63	2.37	**2.50**	**2.52**	2.05	2.03	2.10
3	1.44	1.72	1.95	2.04	**2.54**	**2.45**	2.03	1.94	2.14

and lean mixture conditions. A spectrogram is applied to the test, in order to obtain the frequency content of each pulse with the power spectral density (PSD). For each pulse, the spectrogram is integrated between 1.7 and 2.3 Hz, and a 10 s window, resulting in PSD_{us} for the upstream signal and PSD_{ds} for the downstream signal. Then, the indicator F_{ind} shown in the equation (7.7) is used to fill the Table 7.3. This indicator is related to the contrast between up- and downstream λ measurements when a post-injection pulse is applied.

$$F_{ind} = PSD_{ds}/PSD_{us} \tag{7.7}$$

According to Table 7.3, post-injections of 5 and 6 mg/str during 2 and 3 seconds have the highest contrast, being 5 mg/str and 3 seconds the best for a small difference. Less post-injected fuel could be more early confused with signal noise, while more fuel post-injected would not add more differentiation between up- and downstream signals. Figure 7.15 shows an example of the spectrogram application for 5 pulses of 0.5, 1, 1.5, 2 and 3 seconds of duration and 5 mg/str. As it can be appreciated in the top plot, the original λ signals are noisy in this engine operating point, but λ peaks can still be appreciated. Looking at the spectrogram plots, the upstream signal peaks have more frequency content than the downstream peaks, since there is no oxidation.

The selected temperature to associate the result of the post-injection events is the upstream temperature measured by the NTC sensor. Despite the fact that the DOC bed temperature is not constant over the axial length of the catalyst, the low flow conditions of idle cause that the entering HC are treated by the catalyst in the first sections of the monolith. For this reason, from the two measurements available, i.e. upstream and downstream, the upstream one is more representative. A 1D thermal model could be used to have an intermediate estimation, although no results show better strategy performance

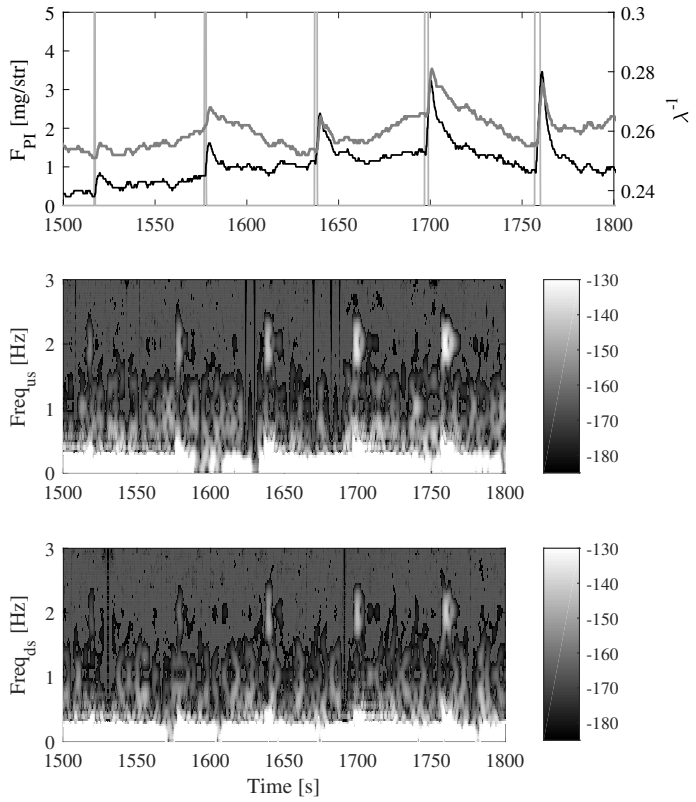

Figure 7.15. *Spectrogram of post-injection pulses at low engine speed and low load: 1000 rpm and 5 Nm of torque. Top plot: black stands for upstream, and gray stands for downstream. Spectrogram color is power spectrum density in dB/Hz.*

considering this estimated temperature. In this sense, the upstream NTC sensor measurement leads to a temperatures distribution like Figure 7.16, from which LOT thresholds can be extracted. By contrast, using the downstream measurement does not lead to a clear differentiation, due to the filtering process that the DOC causes on temperature.

A set of tests like the presented in Figure 7.13 was applied to generate a database. These tests are characterized by steps from high load to low load. During the high load part, the temperature raised and no post-injections were applied, and during the low load, a train of post-injections like the shown in Figure 7.13 was applied. In these tests, the high load part had a steady-state temperature significantly over the LOT, while the low load had a steady temperature below the LOT.

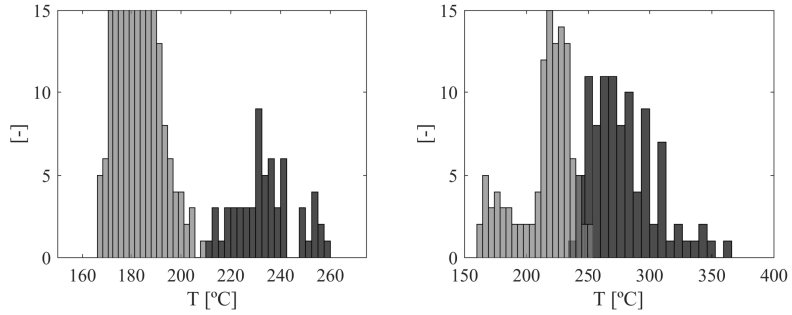

Figure 7.16. *Databases of LOT detection strategy for the nominal (left) and the aged (right) DOCs. Dark bars: oxidation. Light bars: no oxidation.*

Figure 7.16 shows the results from the post-injection tests for the nominal and aged DOCs. As it can be observed for the nominal DOC, oxidation events start at 210°C and no oxidation events end at the same temperature. However, for the aged DOC, an undefined area between 235 and 255°C, in which both cases coexist, can be appreciated. This phase depends on the t_1 and t_2 thresholds calibration. Increasing t_1 and t_2 thresholds separates the oxidation and no oxidation, but also increases the number of non-defined cases. Therefore, a trade-off between accuracy and number of defined cases is observed. Although the DOC used in the experiments is able to accumulate HC species, in case all the HC slipped from the catalyst, the downstream signal would be equal to the upstream, not interfering in the method results.

In the case presented, a database was generated once for the nominal DOC and once for the aged DOC. For real operating conditions, the database should be recreated at a certain time or mileage to compare results and observe the increase of LOT.

7.3 Selective catalytic reduction system diagnostics

The SCR diagnostics method presented next requires the upstream and downstream NO_x and NH_3 signals, the exhaust mass flow and the axial distribution of temperatures. In this line, the upstream NH_3 is considered as an input since no control is done over the urea dosing strategy, while the upstream NO_x concentration is measured with an NO_x sensor. On the other hand, the downstream emissions are measured with an NO_x and an NH_3 sensors, although other configurations could be used.

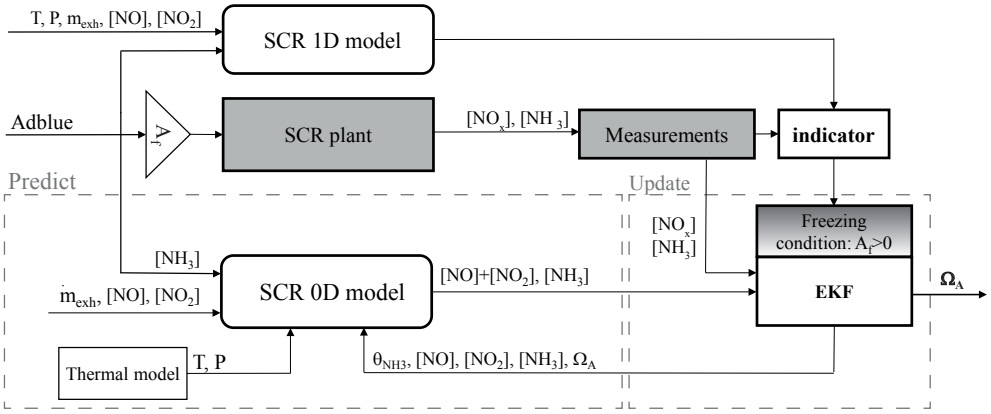

Figure 7.17. *Scheme of the OBD strategy.*

The objective of the presented strategy is to recognize the cause of a decrease in SCR performance, which can be due to SCR ageing, urea dilution or urea injector drift. Then, an adaptive control strategy would be benefited from this estimation and would allow extending its operating range prior to MIL appearance, as well as the fact that catalyst monitoring allows actual condition based maintenance.

First, the strategy composed of an observer for SCR ageing and an urea quality indicator is presented in simulation. Then, the observer for SCR ageing is validated experimentally with a new and an aged catalysts.

On the other hand, the SCR diagnostics technique is a direct indicator of the SCR efficiency, since it is done through the regulated emissions of NO_x and NH_3. For this reason, the ageing study for SCR is not as exhaustively performed for SCR as it is previously done for DOC.

7.3.1 SCR ageing state estimation: strategy approach

The presented strategy estimates the ageing state of an SCR, while the urea quality is surveilled in parallel. Figure 7.17 shows a schematic description. Despite other authors have presented strategies or observers to estimate the SCR ageing like [8] or [9], this observer includes the NO and NO_2 differentiation, being a 5 states observer completed with NH_3, ammonia surface coverage θ_{NH_3} and ammonia storage capacity Ω. For this purpose, convergence and emissions increase are next discussed. Finally, results of the urea

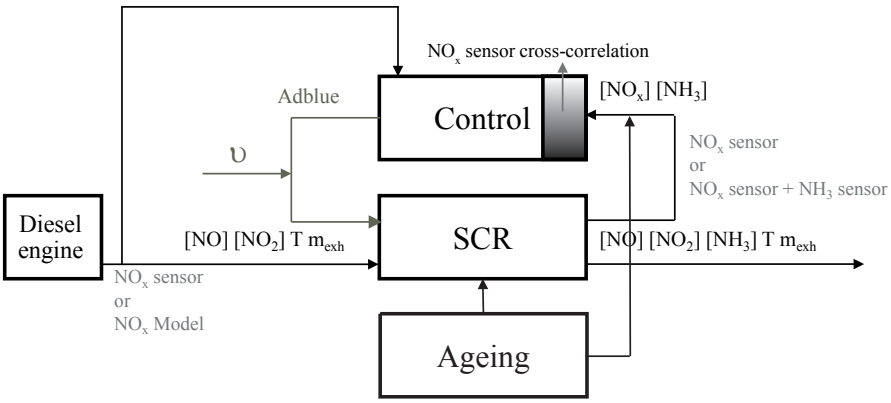

Figure 7.18. *Scheme of the SCR disturbances.*

quality indicator are presented with the analysis of a downstream NO_x and NH_3 sensors offset of 15%.

Figure 7.18 shows a scheme of the disturbances that can affect SCR behaviour. Catalyst ageing and the urea quality are the two disturbances that are considered in simulation. However, other disturbances are related to the measurements and/or models used. In this sense, the set of signals required for the strategy is specified next.

The separation of the NO_x upstream signal into NO and NO_2 is already used in state-of-the-art engines, which can be obtained by a model, although an upstream NO_x sensor would increase its accuracy. The SCR downstream signals of NO_x and NH_3 are considered to be available, since the downstream NO_x sensor is mandatory to perform SCR diagnostics, although its cross-sensitivity with NH_3 opens several possibilities. On the one hand, the NO_x sensor could be placed after the AMOX if a NH_3 sensor is used between the SCR and the AMOX. On the other hand, if the NH_3 signal is to be measured isolating the NH_3 signal from the NO_x sensor measurement, the NO_x sensor should be located between the SCR and the AMOX. In any case, if an AMOX catalyst is placed after the SCR, as NH_3 excitation is required for the ageing estimation and for the urea quality indicator, the NH_3 measurement preferably needs to be taken upstream of the AMOX catalyst.

The OBD strategy can use two models with different accuracies in parallel. I.e. a model for the observer of SCR ageing and a different model for the urea quality indicator. In both cases, the best model available that suits the approach should be used. In this line, as the strategy is firstly presented in simulation, an accurate model is used to represent the after-treatment behaviour,

as the plant system. Therefore, a physics-based model that provides highly detailed 1D-segmented, real-time state reconstruction of the after-treatment system [10], is used for both the AT representation and for the urea quality indicator. This kind of models are optimized to be light enough to run in Euro VI ECUs of production engines. In the strategy, the detailed model used for the urea quality indicator emulates a new part, while the same model is used in simulation to represent different ageing levels and apply the ageing observer.

On the other hand, the observer for SCR ageing is based on an extended Kalman filter that requires a lighter model. For this purpose, the 0D SCR model is used to estimate the states of the observer, since observability and model linearization are required to fit into a state-space. Although other algorithms can also be used to estimate slowly varying parameters as the recursive parameter estimation, the EKF is selected due to its simplicity and the low computational burden that requires.

While the simulation part is composed of the AT described in engine setup B, the experimental validation is composed of setups C.1 and C.2 for the new and aged catalysts. In this sense, the simulation is done with a heavy duty engine, and the experimental validation is done with a light duty engine, being the setup C.1 engine installed in a vehicle and the setup C.2 engine installed in an engine test bench.

As stated with the model calibrations for new and aged parts in Chapter 6, the main effect of SCR ageing is the decrease of NH_3 storage capacity, so that this is the observation target. Whilst SCR ageing is considered to be a slowly varying process, a urea fault can be generated by adding a portion of water in the urea tank. However, urea injector drifts can also be present over time, so that dynamics differentiation between these two processes is not the base on which the strategy is supported. Then, no extra excitation of neither NO_x nor NH_3 signals is required in the strategy, since, by contrast, both ageing and urea quality can be estimated during normal operating conditions. In other cases like DOC diagnostics, as shown previously in this chapter, excitation through late fuel post-injections may be required [11].

Finally, despite closed-loop feedback is one of the possible applications, the urea injection is considered as an input, and its dosing strategy is not modified by the ageing estimation.

7.3.2 Observer for SCR ageing

The algorithm of the observer for SCR ageing is presented next. The ageing parameter Ω_A is to be observed by means of an extended Kalman filter through the NO_x and NH_3 measurements at the SCR downstream.

The EKF approach makes use of the different dynamics that can be differentiated in an SCR system. On the one hand, NO_x dynamics are the fastest, since the engine operation conditions are very transient and NO_x emissions follow them. Then, NH_3 emissions dynamics are more similar to temperature dynamics. On the other hand, downstream SCR NO_x and NH_3 emissions dynamics are faster in orders of magnitude than the impact that ageing has on the SCR. A slowly gradual increment of both NO_x and NH_3 emissions is foreseen during the ageing process, which it is a priori undefined, since depends on the driving conditions on the long term.

The equations used follow the traditional algorithm of an EKF, which is used due to the non-linearities of the SCR model. The 0D model is then linearized to use it in state-space following the first order expansion Taylor series. On the other hand, the observation process follows the two steps of a Kalman filter. The 0D model is used to have an a priori prediction of the states, whilst the measurements are used in the update step to calculate the Kalman gain and correct the initial prediction of the 0D model.

7.3.2.1 Observer development

First, the hypothesis followed supposes that Ω_A variation is a very slowly varying process, so that its temporal variation is considered to be 0 in equation (7.8). However, as this value is considered as a state, the Kalman gain updates it in correlation with the measured emissions.

$$d\Omega_A/dt = 0 \tag{7.8}$$

In this line, the equations of the rest of states, i.e. NO, NO_2, NH_3 and θ_{NH_3} is presented in Chapter 6 in the 0D model approach. Then, the predict/update process of the EKF is presented next.

Predict step:

$$\hat{\mathbf{x}}_{k|k-1} = \begin{bmatrix} \Omega_A & NO & NO_2 & NH_3 & \theta_{NH_3} \end{bmatrix}^T = \mathbf{f}(\hat{\mathbf{x}}_{k-1|k-1}, \mathbf{u}_k) \tag{7.9}$$

where $\mathbf{x}$ is the states vector and function $\boldsymbol{f}$ makes reference to eq. (7.8) and the 0D model estimation from the updated states in the previous timestep and the inputs of the current time-step. Then, the predicted covariance, $\mathbf{P}$, is estimated:

$$\mathbf{P}_{k|k-1} = \mathbf{F}_k \mathbf{P}_{k-1|k-1} \mathbf{F}_k^T + \mathbf{Q}_k \tag{7.10}$$

where $\mathbf{F}$ is the state transition matrix, calculated with the Jacobian of the $\mathbf{f}$ function, and $\mathbf{Q}$ is the process noise matrix:

$$\mathbf{F}_k = \left. \frac{\delta \mathbf{f}}{\delta x} \right|_{\hat{x}_{k-1|k-1}, u_{k-1}} \tag{7.11}$$

$$\mathbf{Q} = \begin{bmatrix} \sigma^2_{\Omega_A} & \cdots & 0 \\ \vdots & \sigma^2_{C_i} & \vdots \\ 0 & \cdots & \sigma^2_{\theta_{\mathrm{NH_3}}} \end{bmatrix}_{5x5} \tag{7.12}$$

Update step: In this phase of the timestep, the states are updated, $\hat{\mathbf{x}}_{k|k}$, with the Kalman gain $\mathbf{K}_k$. For this purpose, the error between the measurements and the model estimations is calculated first:

$$\hat{\mathbf{y}}_k = \mathbf{z}_k - \mathbf{h}(\hat{\mathbf{x}}_{k|k-1}) \tag{7.13}$$

where $\hat{\mathbf{y}}$ represents the error between the measurements and the model. In this sense, $\mathbf{z}$ represents the measurements and the function $\mathbf{h}$ contains the addition of the NO and NO_2 modelled species concentrations in order to be compared with the measured NO_x concentration.

$$\mathbf{h}(\hat{\mathbf{x}}_{k|k-1}) = \begin{bmatrix} \mathrm{NO} + \mathrm{NO_2} & \mathrm{NH_3} \end{bmatrix}^T \tag{7.14}$$

$$\mathbf{z}_k = \begin{bmatrix} \mathrm{NO_x} \\ \mathrm{NH_3} \end{bmatrix} \tag{7.15}$$

Then, the innovation or residual covariance, $\mathbf{S}$, is calculated.

$$\mathbf{S}_k = \mathbf{H}_k \mathbf{P}_{k|k-1} \mathbf{H}_k^T + \mathbf{R}_k \tag{7.16}$$

where $\mathbf{H}$ is the observation matrix, calculated with the Jacobian of the $\mathbf{h}$ function, and $\mathbf{R}$ is the measurements noise matrix.

$$\mathbf{H}_k = \frac{\delta \mathbf{h}}{\delta x}\bigg|_{\hat{x}_{k-1|k-1}} \tag{7.17}$$

$$\mathbf{R} = \begin{bmatrix} \sigma_\nu^2 & 0 \\ 0 & \sigma_\nu^2 \end{bmatrix} \tag{7.18}$$

where σ_ν^2 is the variance of the measurements noise. Next, the Kalman gain is calculated and the states are updated:

$$\mathbf{K}_k = \mathbf{P}_{k|k-1} \mathbf{H}_k^T \mathbf{S}_k^{-1} \tag{7.19}$$

$$\hat{\mathbf{x}}_{k|k} = \hat{\mathbf{x}}_{k|k-1} + \mathbf{K}_k \hat{\mathbf{y}}_k \tag{7.20}$$

Finally, the covariance is updated to be used in the next time-step.

$$\mathbf{P}_{k,k} = (\mathbf{I} - \mathbf{K}_k \mathbf{H}_k) \mathbf{P}_{k|k-1} \tag{7.21}$$

The states are initialized with model estimations for $\theta_{\mathrm{NH_3}}$, NO, NO_2, NH_3, while Ω_A is set to 1.

7.3.2.2 System observability

The selection of the observer states depends on the algorithm purpose and the system observability. In this sense, *Upadhyay* and *Van Nieuwstadt* [9], *Devarakonda et al.* [12] and *Hsieh* and *Wang* [8] present relevant systems related to this topic, with different states and measurement approaches, while the system previously presented is more complete than those presented in these works.

In 2006, *Upadhyay* and *Van Nieuwstadt* [9] confirmed the observability of a system composed of NO_x, NH_3 and $\theta_{\mathrm{NH_3}}$ as states, in combination with an NO_x measurement. Then, *Devarakonda et al.* [12] checked in 2008 the observability of a four state observer, i.e. $\theta_{\mathrm{NH_3}}$, NO, NO_2 and NH_3, using a NO+NO_2 +NH_3 measurement. In this case, note that Ω_A is not included,

Table 7.4. *States, measurements and dimensions of model, F, measurement, H, and Kalman Gain, K, matrices of the observable systems [9], [12], [8] and the presented 5 state system.*

	[9]	[12]	[8]
States	NO_x,NH_3,θ_{NH_3}	NO,NO_2,NH_3,θ_{NH_3}	Ω,θ_{NH_3}
Measurements	NO_x	NO_x+NH_3	NO_x,NH_3
F	3x3	4x4	2x2
H	1x3	1x4	2x2
K	3x1	4x1	2x2
	5 states		
States	Ω_A,NO,NO_2,NH_3,θ_{NH_3}		
Measurements	NO_x, NH_3		
F	5x5		
H	2x5		
K	5x2		

as in [9]. Finally, *Hsieh* and *Wang* [8] showed in 2010 the observability of a system composed of θ_{NH_3} and Ω as states and NO_x and NH_3 as measurements. A summary of this information is compiled in Table 7.4.

The observability is next checked for the 5 state system composed of θ_{NH_3}, NO, NO_2, NH_3 and Ω_A as states, and NO_x and NH_3 signals as measurements. In addition, the Temkin mechanism [13] is also included, which improves the model performance.

First, the **F** and **H** matrices are shown:

$$\mathbf{F} = \begin{bmatrix} 0 & 0 & 0 & 0 & 0 \\ A_{21} & A_{22} & 0 & 0 & A_{25} \\ A_{31} & 0 & A_{33} & 0 & A_{35} \\ A_{41} & 0 & 0 & A_{44} & A_{45} \\ 0 & A_{52} & A_{53} & A_{54} & A_{55} \end{bmatrix} \tag{7.22}$$

where

$$A_{21} = -C_{NO}\ (\Omega\ r_{fst}\ \theta NH_3 + \Omega\ r_{std}\ \theta_{NH_3}) \tag{7.23}$$

$$A_{31} = -C_{NO_2}(\Omega\ r_{fst}\ \theta_{NH_3} + \Omega\ r_{slw}\ \theta_{NH_3}) \tag{7.24}$$

$$A_{41} = \Omega\ r_{des}\ \theta_{NH_3} + \Omega\ C_NH3\ r_{ads}\ (\theta_{NH_3} - 1) \tag{7.25}$$

$$A_{22} = -SV - \Omega\ \Omega_A\ r_{fst}\ \theta_{NH_3} - \Omega\ \Omega_A\ r_{std}\ \theta_{NH_3} \tag{7.26}$$

$$A_{52} = -\theta_{NH_3}(r_{std} + 2\ C_{NO_2}\ r_{fst}) \tag{7.27}$$

$$A_{33} = -SV - \Omega\ \Omega_A\ r_{fst}\ \theta_{NH_3} - \Omega\ \Omega_A\ r_{slw}\ \theta_{NH_3} \tag{7.28}$$

$$A_{53} = -\theta_{NH_3}(4/3\ r_{slw} + 2\ C_{NO}\ r_{fst}) \tag{7.29}$$

$$A_{44} = \Omega\ \Omega_A\ r_{ads}(\theta_{NH_3} - 1) - SV \tag{7.30}$$

$$A_{54} = r_{ads} - r_{ads}\ \theta_{NH_3} \tag{7.31}$$

$$A_{25} = -C_{NO}\ (\Omega\ \Omega_A\ r_{fst} + \Omega\ \Omega_A\ r_{std}) \tag{7.32}$$

$$A_{35} = -C_{NO_2}\ (\Omega\ \Omega_A\ r_{fst} + \Omega\ \Omega_A\ r_{slw}) \tag{7.33}$$

$$A_{45} = \Omega\ \Omega_A\ r_{des} + C_{NH_3}\ \Omega\ \Omega_A\ r_{ads} \tag{7.34}$$

$$A_{55} = -r_{des} - C_{NH_3}\ r_{ads} - 4/3\ C_{NO_2}\ r_{slw} - C_{NO}\ r_{std} - 2\ C_{NO}\ C_{NO_2}\ r_{fst} \tag{7.35}$$

$$\mathbf{H} = \begin{bmatrix} 0 & 1 & 1 & 0 & 0 \\ 0 & 0 & 0 & 1 & 0 \end{bmatrix} \tag{7.36}$$

where the concentrations are taken out from the reaction rates in order to consider the rest, i.e. the pre-exponential constant, the activation energy, the reference temperature, the SCR temperature, etc. constant.

If the rank of the observability matrix, in eq. (7.37), is equal to the number of states, the system is observable and therefore the EKF can be applied to observe the Ω_{A} state. Note that coefficients of the observability matrix are described in Appendix 7.A

$$\mathbf{O} = \begin{bmatrix} H \\ HF \\ HF^2 \\ HF^3 \\ HF^4 \end{bmatrix} \tag{7.37}$$

$$\mathbf{O} = \begin{bmatrix} 0 & 1 & 1 & 0 & 0 \\ 0 & 0 & 0 & 1 & 0 \\ A_{21} + A_{31} & A_{22} & A_{33} & 0 & A_{25} + A_{35} \\ A_{41} & 0 & 0 & A_{44} & A_{45} \\ C_{51} & C_{52} & C_{53} & C_{54} & C_{55} \\ D_{61} & D_{62} & D_{63} & D_{64} & D_{65} \\ E_{71} & E_{72} & E_{73} & E_{74} & E_{75} \\ F_{81} & F_{82} & F_{83} & F_{84} & F_{85} \\ G_{91} & G_{92} & G_{93} & E_{94} & G_{95} \\ H_{101} & H_{102} & H_{103} & E_{104} & H_{105} \end{bmatrix} \tag{7.38}$$

Finally, the rank of $\mathbf{O}$ is 5, so that the EKF can be applied. The use of several segments would increase the 0D model accuracy. However, the observability of the states would be lost and the model could not be used for an EKF application, as it is necessary for the case presented. In this sense, neither the 1D model can be applied.

7.3.2.3 Observer calibration

With the model calibrated, the EKF observer calibration consists in the identification of the noises. In this sense, the purpose of the noises values is to have a slow estimation of Ω_{A}, in which the EKF acts as a low pass filter to extract dynamics from its signal, while still keeping enough potential to vary Ω_{A} as the SCR ages. As a result, the Ω_{A} estimation is the average value that the model requires to meet the measured NO_x and NH_3 emissions avoiding the errors induced by dynamics. For this purpose, a parametric study to the experimental data of the aged SCR is done, whose results are shown analytically in Table 7.5 for the errors and in Figure 7.19. Three combinations are performed for $\mathbf{Q}$:

$$\sigma_{\Omega_{A,1-3}} = \sigma_{\theta_{\mathrm{NH}_{3,1\text{-}3}}} = \{0.5,\ 1,\ 2\}10^{-6} \tag{7.39}$$

$$\sigma_{C_{i,1-3}} = \{0.5,\ 1,\ 2\}10^{-9} \tag{7.40}$$

and five combinations are performed for $\mathbf{R}$:

$$\sigma_{\nu,1-5} = \{0.001,\ 0.005,\ 0.01,\ 0.05,\ 0.1\} \tag{7.41}$$

where σ_{Ω_A} and $\sigma_{\theta_{\mathrm{NH}_3}}$ make reference to equation (7.12), and σ_ν makes reference to equation (7.18).

The errors between observer estimations and measurements in Table 7.5 show that for increasing values of process noises $\mathbf{Q}_1$ to $\mathbf{Q}_3$, as well as measurements noises $\mathbf{R}_1$ to $\mathbf{R}_5$, the error increases. In this sense, higher errors are due to lower filtering of the observed Ω_{A}, since the observer takes more time to compensate the differences between estimations and measurements. This effect can be appreciated in Figure 7.19, where filtered Ω_{A} are correlated with higher errors, and more dynamic Ω_{A} are correlated with lower errors. Therefore, by tuning noises parameters, the observer can make Ω_{A} slowly varying, as the ageing process, to match model estimation to sensors measurements.

Table 7.5. *Absolut integral errors of NH_3 and NO_x emissions, applying the EKF observer with initial Ω_A =1, to the aged SCR in the test presented in Figure 7.19.*

$\int \lvert\epsilon_{NH_3}\rvert\ 10^5$	$\mathbf{R}_1$	$\mathbf{R}_2$	$\mathbf{R}_3$	$\mathbf{R}_4$	$\mathbf{R}_5$
$\mathbf{Q}_1$	8.51	12.66	13.83	16.55	17.55
$\mathbf{Q}_2$	9.37	13.32	14.45	16.64	17.58
$\mathbf{Q}_3$	10.28	13.82	14.95	16.69	17.59
$\int \lvert\epsilon_{NO_x}\rvert\ 10^5$	$\mathbf{R}_1$	$\mathbf{R}_2$	$\mathbf{R}_3$	$\mathbf{R}_4$	$\mathbf{R}_5$
$\mathbf{Q}_1$	8.9	9.13	9.33	9.58	9.63
$\mathbf{Q}_2$	8.93	9.24	9.38	9.59	9.63
$\mathbf{Q}_3$	8.96	9.36	9.43	9.59	9.63

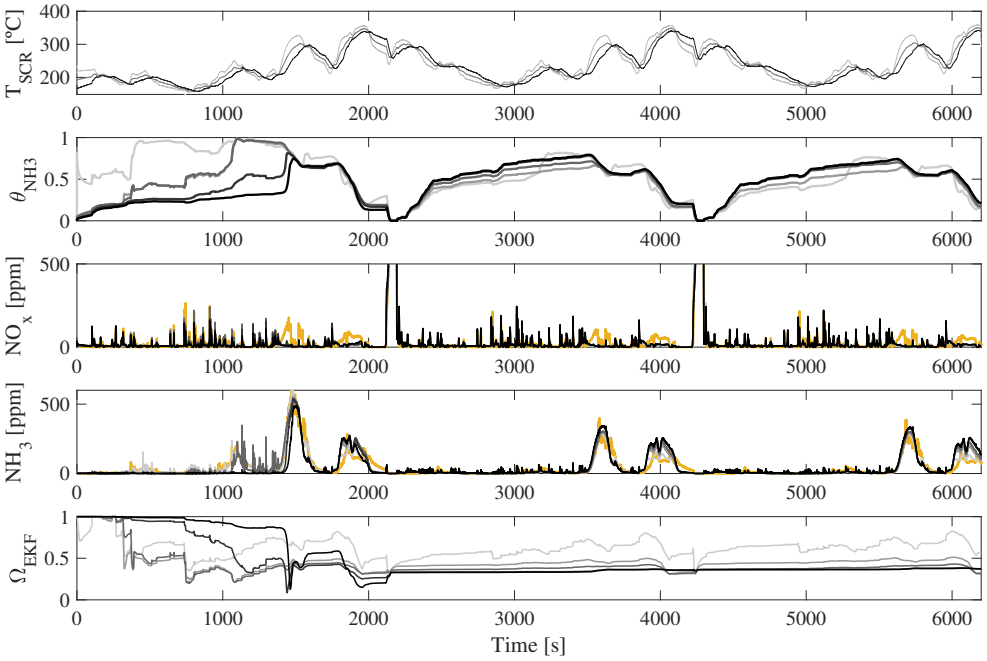

Figure 7.19. *Parametric study of noises calibration for $\sigma_{v,2}$ and $\sigma_{w,1}$ to $\sigma_{w,5}$. Top plots: dark to gray lines represent upstream to downstream signals. Rest of plots: dark to gray represents $\sigma_{w,1}$ to $\sigma_{w,5}$, while yellow stands for the measurements.*

As the ageing process cannot be quantitatively predicted, the noises calibration selected avoids excessive Ω_A dynamics while keeping the observer able to compensate the error, so $\mathbf{Q}_2$ and $\mathbf{R}_4$ is selected.

7.3.2.4 Simulation results

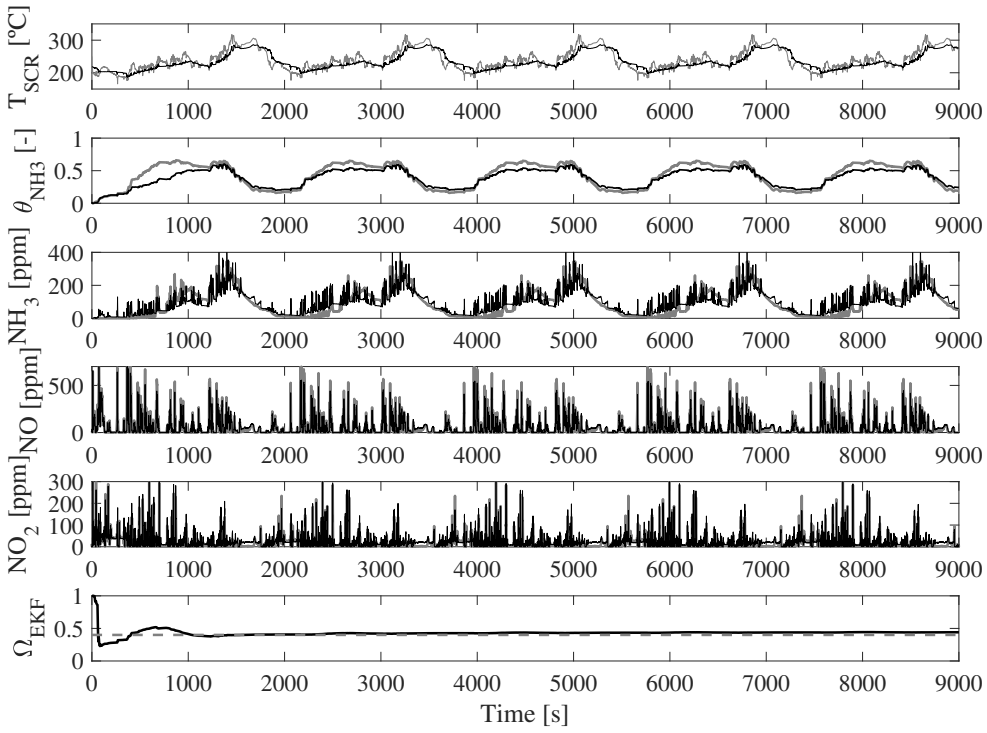

Figure 7.20. *Simulation results of the EKF observer for a given Ω_A=0.4. Top plot: upstream is gray and downstream is black. Medium plots: 1D SCR downstream is thick gray and EKF downstream estimation is thin black. Bottom plot: black is EKF estimation and dashed gray is the original Ω_A =0.4.*

The simulation results are presented from data compiled in Setup B. Then, the observer is applied to a dynamic WHTC at warm starting conditions and $\theta_{NH_3,0}$=0. The 1D model is used as the aged SCR plant and ageing is achieved by varying the Ω_A factor, whilst the observer has to match the Ω_A value established by the 1D model. As it can be appreciated in Figure 7.20 for 1D value of Ω_A=0.4, the EKF needs more than one WHTC to converge to the solution. In fact, it requires up to 14 cycles for Ω_A values higher than 0.6. Note that the EKF shows convergence for the 4 driving patterns present in a WHTC, i.e. low, medium, high and extra high.

A correct selection of noise matrices is crucial for the correct operation of the observer. In this sense, the process matrix Q is a diagonal matrix, which

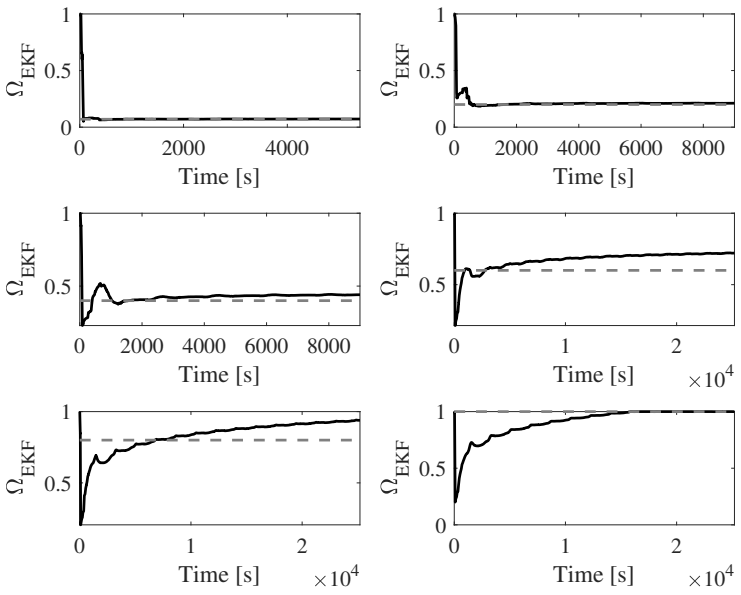

Figure 7.21. *Convergence results of the EKF observer for Ω_A=0.07, 0.2, 0.4, 0.6, 0.8 and 1.*

stands for the plant-to-model noise. Then, and due to the differences observed in SCR model between the plant model and the control-oriented model, the measurements matrix is also a diagonal matrix. The values of this matrix are selected for the EKF to be stable in the noisiest estimation, which takes place at Ω_A near 1. As it can be seen in Figure 7.21, Ω_{EKF} dynamics at Ω_A=0.07 are completely cancelled, whilst as Ω_A increases, more frequency content appears in the Ω_{EKF} estimation.

A convergence study is also shown in Figure 7.21. As it can be appreciated, the x axis does not have the same length for all the plots. Whilst low Ω_A values require a few WHTC cycles to converge, Ω_{EKF} needs up to WHTC 14 cycles in the Ω_A=0.8 to converge. The Kalman filter theory establishes that the observation provided reduces the least mean square error between the model and the measurement. As the control-oriented model is not able to accurately reproduce the real SCR behaviour, a slow noise cancellation is necessary to obtain robust results. In this sense, 14 WHTC does not represent an out-of-range of time for the Ω_A estimation, since ageing is considered to be a very slowly varying process. In fact, due to the slowness of the ageing process, other estimation methods like the parameter estimation present also potential to be applied.

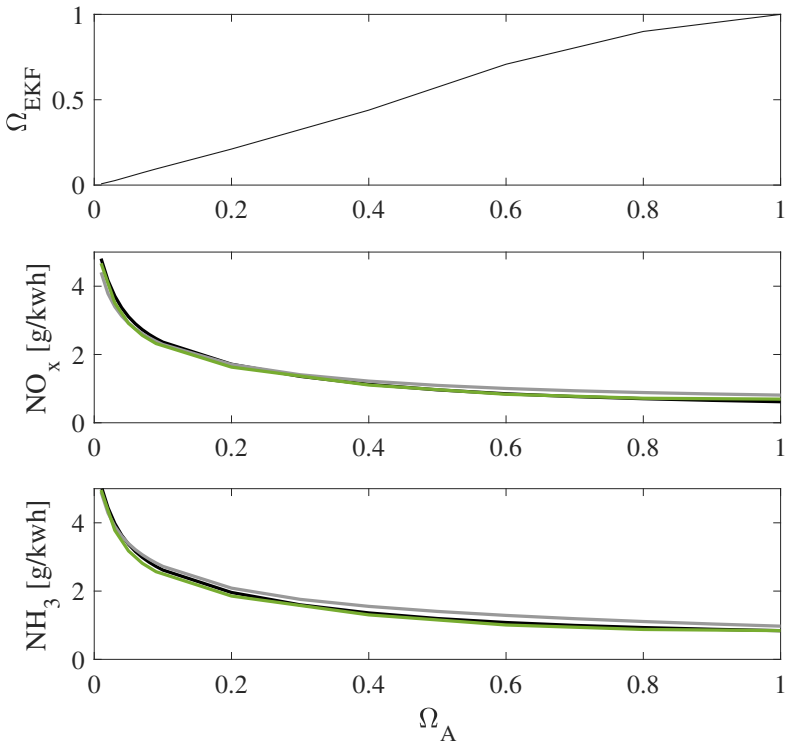

Figure 7.22. *Overall results of the Ω_A estimation. Medium and bottom plots: cumulated NO_x and NH_3 comparing 1D, original 0D and EKF 0D emissions for hot WHTC. Black: 1D. Gray: original 0D. Green: EKF 0D.*

Figure 7.22 shows how the NO_x and NH_3 emissions increase as the SCR ages from Ω_A=1 to Ω_A=0. The consideration of SCR ageing with this simplification factor allows tracking its state through an observer. As it can be seen, at the beginning of the SCR ageing, i.e. for Ω_A values between 1 and 0.5, emissions increase represents 7.5%. Then, for the variation between 0.5 and 0, emissions increase the remaining 92.5%.

Due to the fact that emissions are higher and also the slope of Figure 7.22 is higher at low Ω_A than at close to 1 values of Ω_A, the Ω_{EKF} needs also more time to cancel the noises and estimate the Ω_A at values close to 1.

7.3.2.5 Experimental validation

The experimental validation is done with the tests performed in Setup C.1 for the new SCR, and setup C.2 for the aged SCR. In this sense, the SCR

observer is applied to both catalysts during the tests shown in Chapter 6 for the validation of the model calibration. Figures 7.23 and 7.23 show the results for the new and the aged parts, respectively. As it can be appreciated the increase of slip in terms of NO_x and NH_3 species is captured by the EKF observer to apply the corresponding Ω_A to the model that matches the measured emissions.

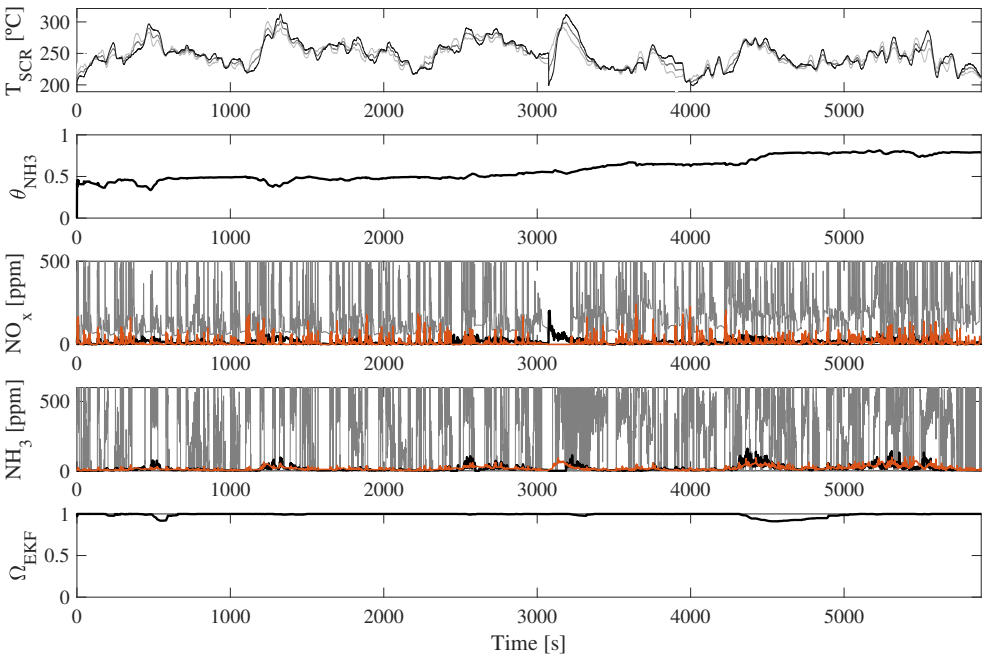

Figure 7.23. *Results of the observer for SCR ageing applied to data from the new SCR. Grey to black stands for upstream to downstream. Orange stands for observer estimation in emissions plots.*

The results show that the strategy works while the model represents the SCR behaviour. In this sense, the accuracy of the strategy strongly depends on the accuracy of the model. For this reason, for on-board purposes, either the model is calibrated in a wider range of temperatures, including NH_3 oxidation and N_2O formation, or the strategy is only applied when the actual operation conditions meet the suitable conditions for which the strategy is calibrated.

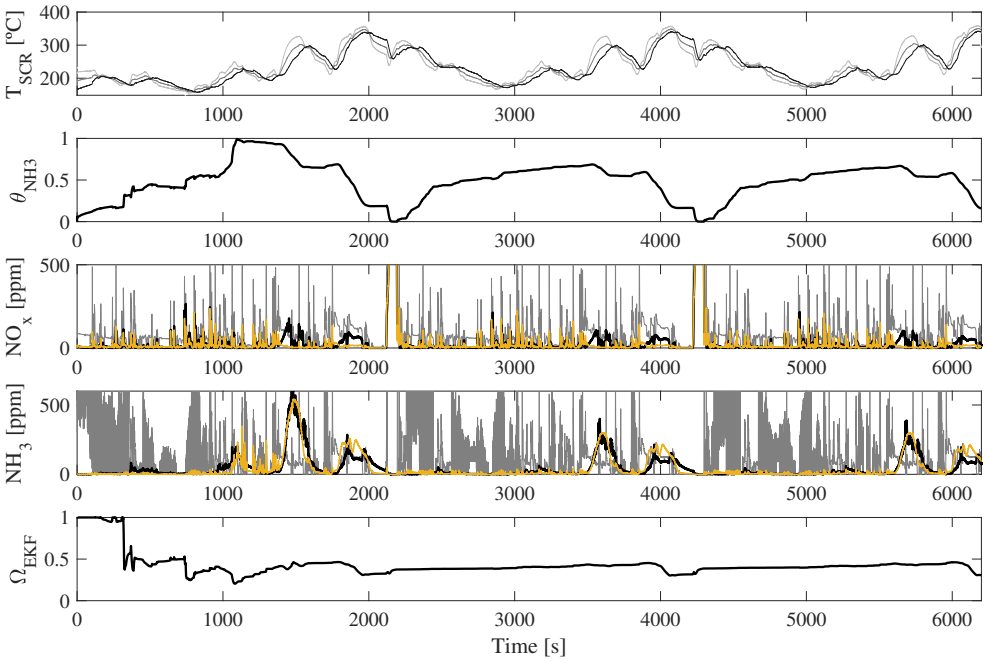

Figure 7.24. *Results of the observer for SCR ageing applied to data from the aged SCR. Grey to black stands for upstream to downstream. Yellow stands for observer estimation in emissions plots.*

7.3.3 Urea quality indicator

The urea quality indicator uses the NO_x and NH_3 downstream measurements to compare the model vs. measurements errors. The hypothesis behind this approach is based on the fact that if the urea solution is diluted or the injector presents a drift, NO_x emissions will increase but NH_3 emissions will decrease. By contrast, ageing effects on emissions result in an increase of both emissions concentrations. However, the strategy cannot differentiate between poor urea solution and injector drift. In this sense, the result is an indicator of the amount of urea injected.

The NH_3 emissions are normalized to NO_x equivalent emissions by using the molecular weight of NO_x instead of the molecular weight of NH_3. In this way, ageing increases NO_x and NH_3 in the same proportion, whilst poor urea injected results in opposite errors from the model estimation, as can be seen in Figure 7.25. On the other hand, as the model estimates the nominal emissions,

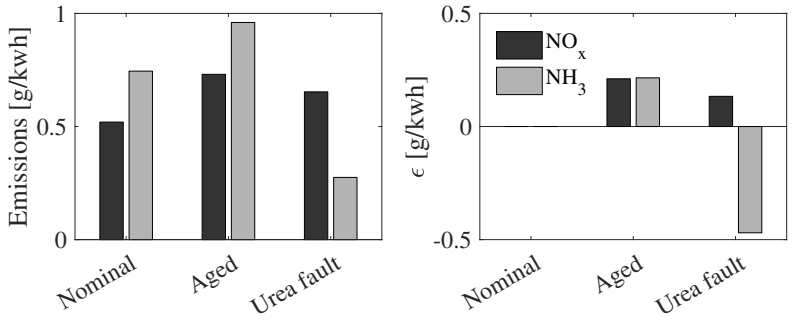

Figure 7.25. *Operating principles of the urea quality indicator with emissions comparison in a hot WHTC for a nominal, an aged and a urea fault case for the urea quality indicator. Nominal case: Ω_A=1, A_f=1. Aged case: Ω_A=0.7, A_f=1. Urea fault: Ω_A=1, A_f=0.9.*

its error is 0 for both NO_x and NH_3. Equations (7.42) to (7.44) are used for the urea indicator calculation:

$$\gamma = \epsilon_{NO_x} - \epsilon_{NH_3} \tag{7.42}$$

$$\epsilon_{NO_x} = \frac{\int_{t_1}^{t_2} NO_{x,measured} - \int_{t_1}^{t_2} NO_{x,modelled}}{W} \tag{7.43}$$

$$\epsilon_{NH_3} = \frac{\int_{t_1}^{t_2} NH_{3,measured} + (\theta_{NH_3,act,2} - \theta_{NH_3,act,1})}{W} - \frac{\int_{t_1}^{t_2} NH_{3,modelled} + (\theta_{NH_3,mod,2} - \theta_{NH_3,mod,1})}{W} \tag{7.44}$$

where γ is the urea quality indicator, the integration of the NO_x and NH_3 signals is in grams, t_1 and t_2 are the limits of the integral window, $\theta_{NH_3\ ,act}$ is the actual θ_{NH_3}, $\theta_{NH_3\ ,mod}$ is the modelled θ_{NH_3} and W is the engine work in kWh.

As the urea quality indicator requires the actual θ_{NH_3}, in case a dedicated estimator could not be applied, the indicator should use singular cases like a complete emptying process. These situations can take place either at high temperature events, which are not controlled by the control system unless a DPF regeneration takes place, or at SCR model θ_{NH_3} estimation recovery, for which the NH_3 solution is not injected until NO_x upstream is as NO_x downstream.

7.3.3.1 Simulation results

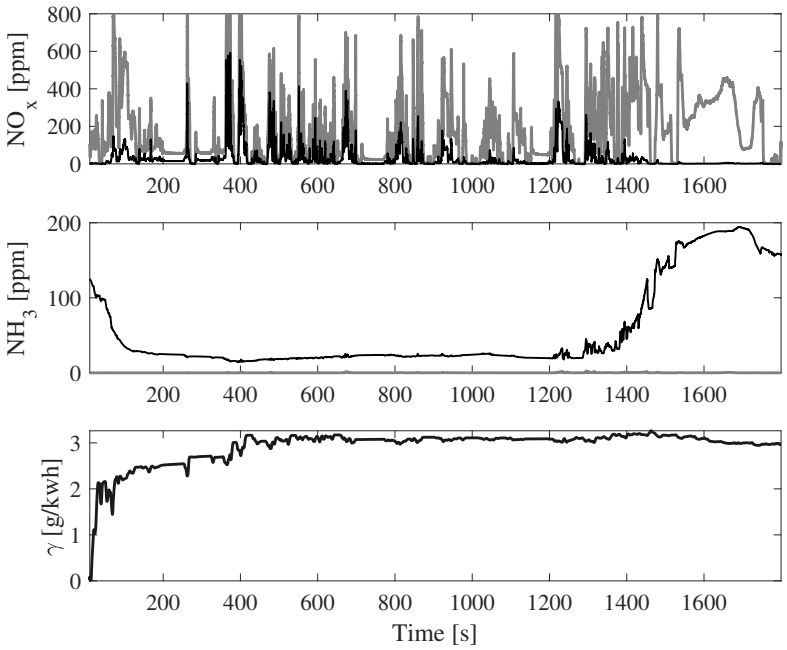

Figure 7.26. *Time-based convergence results of the urea quality indicator for hot WHTC. Black: Model. Gray: Measurement.*

The urea quality indicator is also applied to a WHTC. Figure 7.26 shows time-based results. It can be appreciated how poor urea provokes an increase for NO_x emissions, whilst NH_3 emissions disappear. Due to the fact that the time-scale of the urea concentration is unpredictable, an observer like the one used for the EKF cannot be applied. In the case of SCR ageing, it is ruled by a very slow varying process, but unexpected urea can happen due to several reasons, from injector drift until instantaneous water dissolution by the driver. For this last case, time-based results show that a big step in urea quality can be detected within a time horizon of 400 s in the WHTC.

Figure 7.27 shows results of the urea quality indicator for ageing variations with Ω_A and urea quality variations with the ammonia factor A_f. In order to validate the robustness of the indicator, the indicator is applied separately to the 4 driving patterns present in a WHTC. Despite the actual θ_{NH_3} may not be estimated, this methodology shows the robustness against different driving conditions.

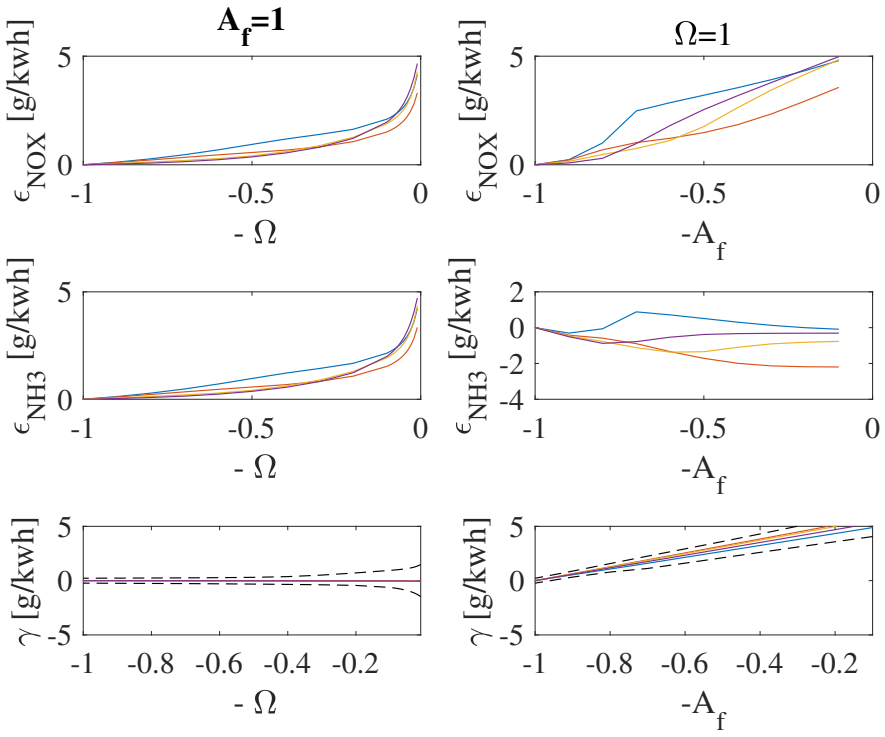

Figure 7.27. *Indicator results for ageing study in hot WHTC with A_f=1 and ammonia factor study with Ω_A=1. Dark to light representes low, medium, high and extra high driving patterns. Dashed black: downstream measurements errors dispersion.*

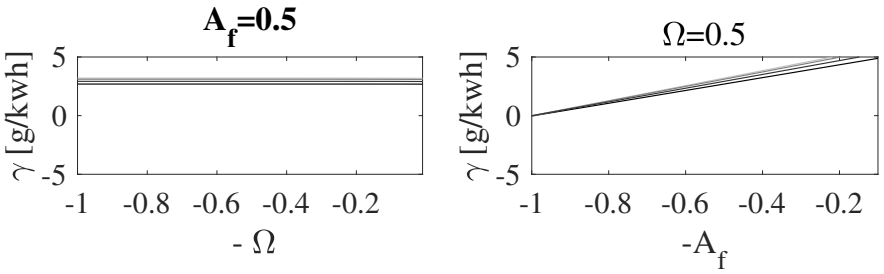

Figure 7.28. *Indicator results for ageing study for hot WHTC with A_f=0.5 and ammonia factor study with Ω_A=0.5. Dark to light represents low, medium, high and extra high driving patterns.*

The increase of NO_x emissions at both Ω_A and A_f is contrasted with the opposite trend of NH_3 at both situations. Whilst the indicator remains 0 for the ageing increase, it increases for a decrease in urea quality. As the indicator is not normalized, a calibration procedure should be used to establish the required thresholds to be detected. However, the scope of this paper is only to show the potential of this technique to detect urea dosing faults.

The black dashed lines represent the performance that this technique would have in case of downstream NO_x and NH_3 sensors offsets. The worst cases are represented, considering a 15% error for each sensor, and considering the driving pattern 1 for the lower line and the driving pattern 2 for the upper line, since these are the extreme lines in the worst direction.

In order to validate the performance of the indicator in case of combined ageing and poor quality of injected urea, the study shown in Figure 7.28 was done. In this, the ageing Ω_A from 1 to 0 is done at A_f=0.5, while the ammonia factor study with Af from 1 to 0 is done respectively for at Ω_A=0.5. With view for on-board application, the actual NH_3 storage required for urea quality indicator should be obtained by a model that includes ageing. For this reason, a proper separation of time-scales should be necessary in order to be able to run both strategies in parallel, based on the same sensor measurement.

7.4 Conclusions

This chapter contains ageing detection algorithms for both DOC and SCR. The strategies presented are based on the regulation requirements and the on-board sensors available. In this sense, a total failure or removal algorithm, and an indirect efficiency estimation by means of LOT detection are presented for

DOC, while an observer for SCR ageing in combination with a urea quality indicator are presented for the SCR system.

The diagnostics strategy for total failure or removal detection uses passive and active diagnostics strategies. For this purpose, the signal from the 0D passive DOC model is compared with the downstream temperature measurement of a DOC. In this sense, only through the use of post-injections during active diagnostics, the strategy is able to identify a DOC as a completely faulty. As a result, the simplicity of the model allows to use it in ECU environment.

The LOT detection strategy compares both upstream and downstream λ measurements from the NO_x sensors in order to associate a post-injection pulse with oxidation or no oxidation during idle conditions. In this sense, the λ measurements are contrasted in comparison with gas analyzer measurements in order to evaluate its potential. Then, the strategy generates a database from the pulses results at different temperatures that enables to detect temperature intervals of oxidation, undefined and no oxidation.

The OBD presented strategy for SCR combines an SCR ageing state observer and a urea quality indicator to detect in parallel urea injection faults. An observability study is done for the 5 states observer, which includes Ω_A as the ageing parameter, NO, NO_2, NH_3 and θ_{NH_3}, and a parametric study for the noises selection is also presented. For this case, simulation results from Ω_A =0 to Ω_A =1 are contrasted with experimental results for a new and an aged parts, whose 0D model calibrations are shown in Chapter 6. Then, the urea quality indicator is based on the different effect on NO_x and NH_3 species between SCR ageing and low urea injected. In this sense, the indicator is computationally light and can be used in real time, although the actual θ_{NH_3} needs to be known, which may limit its applicability. Finally, offsets in NO_x and NH_3 sensors are simulated to generate a dispersion range of results.

7.A Observability matrix

The observability matrix of the observer for SCR ageing is:

$$\mathbf{O} = \begin{bmatrix} 0 & 1 & 1 & 0 & 0 \\ 0 & 0 & 0 & 1 & 0 \\ A_{21}+A_{31} & A_{22} & A_{33} & 0 & A_{25}+A_{35} \\ A_{41} & 0 & 0 & A_{44} & A_{45} \\ C_{51} & C_{52} & C_{53} & C_{54} & C_{55} \\ D_{61} & D_{62} & D_{63} & D_{64} & D_{65} \\ E_{71} & E_{72} & E_{73} & E_{74} & E_{75} \\ F_{81} & F_{82} & F_{83} & F_{84} & F_{85} \\ G_{91} & G_{92} & G_{93} & E_{94} & G_{95} \\ H_{101} & H_{102} & H_{103} & E_{104} & H_{105} \end{bmatrix} \tag{7.45}$$

where the coefficients are as follows:

$C_{51} = A_{21}A_{22} + A_{31}A_{33}$
$C_{52} = A_{22}^2 + A_{52}(A_{25} + A_{35})$
$C_{53} = A_{33}^2 + A_{53}(A_{25} + A_{35})$
$C_{54} = A_{54}(A_{25} + A_{35})$
$C_{55} = A_{55}(A_{25} + A_{35}) + A_{22}A_{25} + A_{33}A_{35}$
$D_{61} = A_{41}A_{44}$
$D_{62} = A_{45}A_{52}$
$D_{63} = A_{45}A_{53}$
$D_{64} = A_{44}^2 + A_{45}A_{54}$
$D_{65} = A_{44}A_{45} + A_{45}A_{55}$
$E_{71} = A_{21}(A_{22}^2 + A_{52}(A_{25} + A_{35})) + A_{31}(A_{33}^2 + A_{53}(A_{25} + A_{35})) + A_{41}A_{54}(A_{25} + A_{35})$
$E_{72} = A_{22}(A_{22}^2 + A_{52}(A_{25} + A_{35})) + A_{52}(A_{55}(A_{25} + A_{35}) + A_{22}A_{25} + A_{33}A_{35})$
$E_{73} = A_{33}(A_{33}^2 + A_{53}(A_{25} + A_{35})) + A_{53} * (A_{55}(A_{25} + A_{35}) + A_{22}A_{25} + A_{33}A_{35})$
$E_{74} = A_{54}(A_{55}(A_{25} + A_{35}) + A_{22}A_{25} + A_{33} * A_{35}) + A_{44} * A_{54}(A_{25} + A_{35})$
$E_{75} = A_{25}(A_{22}^2 + A_{52}(A_{25} + A_{35})) + A_{35}(A_{33}^2 + A_{53}(A_{25} + A_{35})) + A_{55}(A_{55}(A_{25} + A_{35}) + A_{22}A_{25} + A_{33}A_{35}) + A_{45}A_{54}(A_{25} + A_{35})$
$F_{81} = A_{41}(A_{44}^2 + A_{45}A_{54}) + A_{21}A_{45}A_{52} + A_{31}A_{45}A_{53}$
$F_{82} = A_{52}(A_{44}A_{45} + A_{45}A_{55}) + A_{22}A_{45}A_{52}$
$F_{83} = A_{53}(A_{44}A_{45} + A_{45}A_{55}) + A_{33}A_{45}A_{53}$
$F_{84} = A_{44}(A_{44}^2 + A_{45}A_{54}) + A_{54}(A_{44}A_{45} + A_{45}A_{55})$
$F_{85} = A_{45}(A_{44}^2 + A_{45}A_{54}) + A_{55}(A_{44}A_{45} + A_{45}A_{55}) + A_{25}A_{45}A_{52} + A_{35}A_{45}A_{53}$
$G_{91} = A_{41}(A_{54}(A_{55}(A_{25} + A_{35}) + A_{22}A_{25} + A_{33}A_{35}) + A_{44}A_{54}(A_{25} + A_{35})) + A_{21}(A_{22}(A_{22}^2 + A_{52}(A_{25} + A_{35})) + A_{52}(A_{55}(A_{25} + A_{35}) + A_{22}A_{25} + A_{33}A_{35})) + A_{31}(A_{33}(A_{33}^2 + A_{53}(A_{25} + A_{35})) + A_{53}(A_{55}(A_{25} + A_{35}) + A_{22}A_{25} + A_{33}A_{35}))$
$G_{92} = A_{52}(A_{25}(A_{22}^2 + A_{52}(A_{25} + A_{35})) + A_{35}(A_{33}^2 + A_{53}(A_{25} + A_{35})) + A_{55}(A_{55}(A_{25} + A_{35}) + A_{22}A_{25} + A_{33}A_{35}) + A_{45}A_{54}(A_{25} + A_{35})) + A_{22}(A_{22}(A_{22}^2 + A_{52}(A_{25} + A_{35})) + A_{52}(A_{55}(A_{25} + A_{35}) + A_{22}A_{25} + A_{33}A_{35}))$

$G_{93} = A_{53}(A_{25}(A_{22}^2+A_{52}(A_{25}+A_{35}))+A_{35}(A_{33}^2+A_{53}(A_{25}+A_{35}))+A_{55}(A_{55}(A_{25}+A_{35}) + A_{22}A_{25} + A_{33}A_{35}) + A_{45}A_{54}(A_{25} + A_{35})) + A_{33}(A_{33}(A_{33}^2 + A_{53}(A_{25} + A_{35})) + A_{53}(A_{55}(A_{25} + A_{35}) + A_{22}A_{25} + A_{33}A_{35}))$
$G_{94} = A_{44}(A_{54}(A_{55}(A_{25} + A_{35}) + A_{22}A_{25} + A_{33}A_{35}) + A_{44}A_{54}(A_{25} + A_{35})) + A_{54}(A_{25}(A_{22}^2 + A_{52}(A_{25} + A_{35})) + A_{35}(A_{33}^2 + A_{53}(A_{25} + A_{35})) + A_{55}(A_{55}(A_{25} + A_{35}) + A_{22}A_{25} + A_{33}A_{35}) + A_{45}A_{54}(A_{25} + A_{35}))$
$G_{95} = A_{45}(A_{54}(A_{55}(A_{25} + A_{35}) + A_{22}A_{25} + A_{33}A_{35}) + A_{44}A_{54}(A_{25} + A_{35})) + A_{55}(A_{25}(A_{22}^2 + A_{52}(A_{25} + A_{35})) + A_{35}(A_{33}^2 + A_{53}(A_{25} + A_{35})) + A_{55}(A_{55}(A_{25} + A_{35}) + A_{22}A_{25} + A_{33}A_{35}) + A_{45}A_{54}(A_{25} + A_{35})) + A_{25}(A_{22}(A_{22}^2 + A_{52}(A_{25} + A_{35})) + A_{52}(A_{55}(A_{25} + A_{35}) + A_{22}A_{25} + A_{33}A_{35})) + A_{35}(A_{33}(A_{33}^2 + A_{53}(A_{25} + A_{35})) + A_{53}(A_{55}(A_{25} + A_{35}) + A_{22}A_{25} + A_{33}A_{35}))$
$H_{101} = A_{41}(A_{44}(A_{44}^2 + A_{45}A_{54}) + A_{54}(A_{44}A_{45} + A_{45}A_{55})) + A_{21}(A_{52}(A_{44}A_{45} + A_{45}A_{55}) + A_{22}A_{45}A_{52}) + A_{31}(A_{53}(A_{44}A_{45} + A_{45}A_{55}) + A_{33}A_{45}A_{53})$
$H_{102} = A_{52}(A_{45}(A_{44}^2+A_{45}A_{54})+A_{55}(A_{44}A_{45}+A_{45}A_{55})+A_{25}A_{45}A_{52}+A_{35}A_{45}A_{53})+A_{22}(A_{52}(A_{44}A_{45} + A_{45}A_{55}) + A_{22}A_{45}A_{52})$
$H_{103} = A_{53}(A_{45}(A_{44}^2+A_{45}A_{54})+A_{55}(A_{44}A_{45}+A_{45}A_{55})+A_{25}A_{45}A_{52}+A_{35}A_{45}A_{53})+A_{33}(A_{53}(A_{44}A_{45} + A_{45}A_{55}) + A_{33}A_{45}A_{53})$
$H_{104} = A_{44}(A_{44}(A_{44}^2 + A_{45}A_{54}) + A_{54}(A_{44}A_{45} + A_{45}A_{55})) + A_{54}(A_{45}(A_{44}^2 + A_{45}A_{54}) + A_{55}(A_{44}A_{45} + A_{45}A_{55}) + A_{25}A_{45}A_{52} + A_{35}A_{45}A_{53})$
$H_{105} = A_{45}(A_{44}(A_{44}^2 + A_{45}A_{54}) + A_{54}(A_{44}A_{45} + A_{45}A_{55})) + A_{55}(A_{45}(A_{44}^2 + A_{45}A_{54})+A_{55}(A_{44}A_{45}+A_{45}A_{55})+A_{25}A_{45}A_{52}+A_{35}A_{45}A_{53})+A_{25}(A_{52}(A_{44}A_{45}+A_{45}A_{55}) + A_{22}A_{45}A_{52}) + A_{35}(A_{53}(A_{44}A_{45} + A_{45}A_{55}) + A_{33}A_{45}A_{53})$

where A coefficients are defined in equations (7.23) to (7.35).

References

[1] Nieuwstadt M Van, Upadhyay D and Yuan F. "Diagnostics for Diesel Oxidation Catalysts". In *SAE Technical Paper 2005-01-3602*. SAE International, 2005. (cited in pp. 26, 64, and 164)

[2] Lepreux O., Creff Y. and Petit N. "Warm-up strategy for a Diesel Oxidation Catalyst". In *Control Conference (ECC), 2009 European*, pp. 3821–3826, 2009. (cited in p. 169)

[3] Yamamoto K, Takada K, Kusaka J, Kanno Y and Nagata M. "Influence of Diesel Post Injection Timing on HC Emissions and Catalytic Oxidation Performance". In *SAE Technical Paper 2006-01-3442*. SAE International, 2006. (cited in pp. 82 and 169)

[4] Sutjiono R, Tayal P, Zhou K and Meckl P. "Real-Time On-Board Indirect Light-Off Temperature Estimation as a Detection Technique of Diesel Oxidation Catalyst Effectiveness Level". In *SAE Technical Paper 2013-01-1517*. SAE International, 04 2013. (cited in pp. 26, 87, 138, and 175)

[5] Vitale G, Siebenbrunner P, Halser H, Bachler J and Pfahl U. "OBD Algorithms: Model-based Development and Calibration". In *SAE Technical Paper 2007-01-4222*. SAE International, 2007. (cited in pp. 8, 26, and 175)

[6] Schultz R and Meckl P H. "Light-Off Temperature Shift for Catalyzed Diesel Particulate Filter On-Board Diagnostics". In *SAE Technical Paper 2012-01-1248*. SAE International, 04 2012. (cited in pp. 26 and 176)

[7] Regulation EU Comission. *No 692/2008*. Official Journal of the European Union, 2008. (cited in pp. 7 and 179)

[8] Hsieh M F and Wang J. "An extended Kalman filter for ammonia coverage ratio and capacity estimations in the application of Diesel engine SCR control and onboard diagnosis". In *American Control Conference (ACC), 2010*, pp. 5874–5879. IEEE, 2010. (cited in pp. 33, 186, 191, and 192)

[9] Upadhyay D and Van Nieuwstadt M. "Model based analysis and control design of a urea-SCR deNOx aftertreatment system". *Journal of dynamic systems, measurement, and control*, Vol. 128 n^o 3, pp. 737–741, 2006. (cited in pp. 33, 186, 191, and 192)

[10] Cloudt R, Saenen J, Eijnden E van den and Rojer C. "Virtual Exhaust Line for Model-based Diesel Aftertreatment Development". In *SAE 2010 World Congress & Exhibition 2010-01-0888*. SAE International, apr 2010. (cited in pp. 31, 38, and 188)

[11] Guardiola C, Pla B, Piqueras P, Mora J and Lefebvre D. "Model-based passive and active diagnostics strategies for diesel oxidation catalysts". *Applied Thermal Engineering*, Vol. 110, pp. 962–971, 2017. (cited in pp. 26 and 188)

[12] Devarakonda M, Parker G, Johnson J H., Strots V and Santhanam S. "Model-Based Estimation and Control System Development in a Urea-SCR Aftertreatment System". *SAE International Journal of Fuels and Lubricants 2008-01-1324*, Vol. 1, pp. 646–661, apr 2008. (cited in pp. 32, 33, 191, and 192)

[13] Nova I, Lietti L and Tronconi E. "Transient response method applied to the kinetic analysis of the DeNO x-SCR reaction". *Chemical Engineering Science*, Vol. 56 n^o 4, pp. 1229–1237, 2001. (cited in pp. 152, 153, and 192)

Chapter 8

Conclusions and future work

Contents

8.1 Main contributions and conclusions

This dissertation has covered the development of diesel after-treatment models and diagnostics algorithms. While DOC and SCR are the after-treatment blocks focus of this dissertation, sensors measurements have also been assessed. For this purpose, the information is organized as indicated next along the text:

- The experimental behaviour of catalysts and sensors measurements has been the basis for the development of subsequent chapters. In this sense, the experimental characterization of catalysts with different ageing levels allows observing which and how emissions increase as the parts age.

Besides, the use of gas analyzers provides a wider view than the on-board sensors can offer, which combined with engine bench specific tests, enables the generation of modelling approaches and diagnosis concepts.

- Thermal models and temperatures estimation have been the basis about which further emissions species models and diagnostics algorithms are developed. The catalysts operation is mainly dominated by temperature, so that an analysis to explore the opportunities that the on-board measurements can offer is necessary.

- With the ageing process effect on emissions previously described, and the thermal part to feed the required temperatures modelled, the DOC and SCR models are focused on the ageing effect on emissions increase. As a result, a 0D control-oriented model has been presented for DOC, while 0D and 1D models have been presented for SCR. In both catalysts, the most relevant fact is the inclusion of an ageing parameter that allows varying from new to aged states.

- The presented diagnostics algorithms are based on the possibilities that the combination of catalysts ageing experimental behaviour, sensors measurements potential and models allow. On the other hand, the diagnostics algorithms must follow the regulation guidelines. Then, an algorithm for total failure or removal, in company with an indirect estimation of the catalyst efficiency through its LOT detection have been presented, while an observer for SCR ageing has been presented in combination with a urea quality indicator. On this last case, the urea quality indicator avoids associating low SCR efficiency to SCR ageing when the origin of the problem is rooted in poor quality of the urea or injection drift.

A detailed report of the conclusions that can be extracted from this disseration along the different chapters is presented next.

8.1.1 Experimental characterization of diesel catalysts

The experimental observation of DOC and SCR ageing has been assessed through a series of experiments performed to new and aged parts. The experimental differences due to catalysts ageing are next used as the key and the target for the development of models and diagnostics functions. The characteristics of some relevant measurements are also presented.

Sensors for DOC diagnostics The potential for DOC diagnostics of the up- and downstream λ and temperature sensors measurements has been assessed. On one hand, the upstream NTC temperature sensor is accurate in steady-state conditions. However, its dynamic response is compared with the measurement of a fast thermocouple, which manifest that the NTC sensor response is not able to capture the temperature signal bandwith of highly transient phases, as related works in literature also contemplate. In this sense, its slow response is due to its high thermal inertia, which is necessary for on-board robustness.

On the other hand, the pair of up- and downstream λ measurements of the NO_x sensors have been proved to be able for oxidation detection. First, the test in which the λ measurements are assessed is analyzed with gas analyzer measurements. A wider view with HC, CO and O_2 allows observing what happens in a specific test composed of post-injection pulses that start at a high temperature in which the DOC is oxidizing, and then the temperature decreases until a low temperature in which the DOC does not oxidize. Then, once the species concentrations are understood, the λ measurements show that its measurement is an intermediate value between the available oxygen and the actual λ as an oxygen excess indicator. In this sense, note that the oxygen excess takes into account the oxygen that would be necessary to oxidize the HC and CO species present in the exhaust gas.

Sensors for SCR diagnostics The up- and downstream NO_x and NH_3 signals are required for SCR diagnostics. In this case, the acquisition of downstream NO_x and NH_3 signals presented the problematic of the NO_x sensor cross-correlation with NH_3. As stated in [1], the cross-correlation factor is 0.63, although an on-purpose study has not been performed. In this sense, the use of the model presented in Chapter 6 allows determining that the use of a constant factor is proven to be not sufficient to separate the NH_3 signal from the NO_x sensor measurement.

DOC ageing The experimental study to observe the DOC functionalities and how ageing affects them has included a set of tests to observe the oxidation capacity, the light-off temperature, the HC and NO accumulation and the species slip. The specific tests were repeated for the new, the nominal, the aged, the DOC_{70} and the DOC_{40}. Then, the behaviour of new and aged parts has been assessed on the whole in transient regulation tests. As a result, the main functionalities affected are the LOT, the HC and NO accumulation and the species slip at cold conditions.

The LOT increases as the DOC ages, so Table 4.1 contains the results of the LOT identification tests for each catalyst. Then, the HC accumulation capacity test was done at cold conditions, in which the HC slip is modelled as a function of the HC accumulated in the catalyst. In this sense, aged catalysts are shown to be less able to retain HC and therefore its slip increases. With regards to NO accumulation, a dynamic test shows qualitatively the loss of capacity to retain NO. In this line, the NO to NO_2 conversion is also qualitatively shown during a dynamic warm phase, in which the average conversion is higher for a new part.

The application of regulation tests to new and aged DOCs have evidenced the effect of LOT on emissions. While the LOT is not achieved by the aged DOC during an NEDC until the extra-urban phase, the effect of LOT in a WLTC sensitively increase the emissions when T_{us} is lower than LOT.

SCR ageing First, a study of the slip dynamics has been done for the SCR by means of FFT to NO_x and NH_3 slip cases. In conclusion, the SCR acts as a low pass filter of the NH_3 slip, so while NO_x dynamics achieve higher frequencies, NH_3 dynamics are subjected to the slower temperature dynamics.

The ageing effect on SCR has been directly evaluated with the NO_x and NH_3 emissions increase, since ageing has a direct effect over these measured species. In this sense, the aged SCR has 40% more slip than a new part in order to have a similar efficiency of NO_x reduction. Although this part of the work do not really provide a novelty, it is relevant for later development of algoirithms.

8.1.2 Control-oriented thermal models and temperatures estimation

In order to estimate useful temperatures along the exhaust line for the subsequent presented algorithms, several approaches have been used, which used available signals in the ECU.

Fast DOC inlet temperature estimation A data fusion technique has been used to have a better dynamic response of the slow measurement of the NTC sensor. For this purpose, the use of an EKF allows combining a fast but non-necessarily precise model and an accurate but slow temperature sensor measurement. By using this temperature estimation, the energy entering into the DOC is better considered and the presence of short oxidation phases due to short temperature peaks can be identified.

Control-oriented 1D model The presented 1D thermal model has been able to reproduce the temperature distribution along the axial direction of the monolith, as well as the temperature sensor measurement. For this purpose, a novel control-oriented sensor model has been added to the model, which combines the heat losses to the surroundings. Then, different upstream temperature signals have been assessed in order to evaluate the model performance when reproducing the DOC downstream measured temperature. The error considered to calibrate the model was the maximum instantaneous value, since the presence of error peaks due to errors in dynamics is masked if using the averaged error. Results show that the use of fast measurements is not necessary to estimate the downstream temperature, being the error difference between the NTC sensor and the thermocouple in the downstream temperature estimation of 1°C, so that the on-board NTC sensor is a valid input.

Control-oriented 0D lumped model The presented 0D thermal model allows the reproduction of the DOC downstream temperature by means of energy and mass balances in combination with a variable delay that depends on the exhaust mass flow. As in the 1D model, this model contains a sensor model to reproduce the sensor measurement. The model has been validated in highly dynamic conditions, like the WLTC and the NEDC, as well as in high temperature steps, stressing the dynamics of the system. The 0D model presents a maximum peak error of 22°C, being 4°C higher than for the 1D and less demanding in terms of computational resources, therefore being still valid for on-board purposes.

Temperature estimation of oxidized post-injection pulses A model to estimate the temperature increase in steady-state conditions due to post-injection pulses has been developed in this dissertation. Specifically, the model can be used for the calibration of the diagnosis strategy that requires temperature increase roughly enough during active diagnostics.

8.1.3 Control-oriented models for diesel after-treatment catalysts

A control-oriented model for DOC and two control-oriented models for SCR have been presented in this dissertation. The main characteristic of the models is the inclusion of an ageing factor that allows varying from new to aged states. The models have been experimentally applied to a new and an

aged part in all cases. While the DOC model approach is fully developed in this work, the SCR model approach is based on available literature.

8.1.3.1 DOC control-oriented model including ageing

The DOC model aim is to estimate the HC and CO emissions increase due to ageing during normal driving conditions, whose approach is based on the experimental tests shown in Chapter 4. In this sense, the presence of extra excitations like high post-injections would require a more detailed heat release model. In the model, LOT and A_{eff} are the functions that depend on the ageing factor, being A_{eff} obtained from the calibration of DOCs with different ageing levels and LOT from the LOT identification tests. Then, the model has been validated in a WLTC for new and aged parts, presenting an efficiency error of 1.4% and 3.5% for the HC and CO, respectively, in the new catalyst, and 0% 8%, analogically, for the aged catalyst.

8.1.3.2 SCR control-oriented models including ageing

Both 1D and 0D SCR models presented in this dissertation rely on a physical approach, in which the ageing factor corresponds to the NH_3 accumulation capacity of the catalyst. Although this approach has been used in other works, the achieved accuracy of the model needs to be presented. In both cases, the model is calibrated to operate in temperature intervals out of the NH_3 oxidation and N_2O formation, i.e. below 400°C, for the sake of calibration simplification.

The models have been validated for a new and an aged part during 100min of transient conditions, in which the data of the new SCR comes from RDE, while the data of the aged SCR comes from WLTC repetitions in a raw. Being Ω_A the only difference in the calibrations, the achieved accuracy is similar, being below 6% in efficiency.

8.1.4 Diesel catalysts diagnostics

The diagnostics algorithms for DOC and SCR are based on the opportunities and limitations presented along the previous chapters.

8.1.4.1 DOC diagnosis

Diagnostics for total failure or removal The diagnostics strategy for total failure or removal detection is based on the exothermic reaction generated by the oxidable species from the engine raw emissions such as HC, CO and NO, but also on the exothermic reaction generated by fuel post-injections. Then, the diagnosis algorithm presented is able to discern whether a DOC is able to oxidize or not. For this purpose, the 0D passive DOC model, based on a non-impregnated DOC, is used.

Two thresholds of temperature increment, one lower and other higher, are set in order to evaluate the DOC state. Passive diagnosis uses the low threshold, set by the model accuracy, to have a low check. The high threshold is set to ensure 100% the state of the DOC: when post-injections are performed and the residuum overcomes the high threshold, the DOC is able to oxidize, but when the residuum do not overcome the low threshold, the DOC is not able to oxidize and it is considered faulty. The simplicity of the model allows to use it in ECU environment.

LOT estimation as a DOC efficiency indicator The LOT detection strategy uses the actual λ measurement of the NO_x sensors, which is an intermediate value between the oxygen concentration and the oxygen excess. However, the error that dynamic situations induce between upstream and downstream measurements, in company with sensors offsets, prevent its use for on-board use in dynamic conditions.

Therefore, the on-board method for LOT estimation is done during idle periods, since this engine operation point provides ideal steady-state conditions to avoid sensors offsets during the post-injection pulses and provides conditions in which the upstream temperature measurement is representative of the post-injection pulses oxidation, or no oxidation, into the DOC.

In the strategy of the Setup A, the λ measurements are used to determine if there is oxidation or not in the post-injection pulses. Next, the DOC upstream temperature is associated to the results of the post-injection pulses in order to generate a database. Then, when a long window of time has passed, the resulting database is used to determine temperature ranges of temperatures that include non-oxidation, undefined and an oxidation intervals. Finally, these ranges have to be evaluated over time to detect if the LOT increases.

8.1.4.2 SCR diagnosis

The presented OBD strategy combines an SCR ageing state observer and an indicator to parallely detect urea injection faults. The urea quality indicator avoids associating a decrease in SCR performance to ageing.

The ageing estimation is based on a 5 state EKF observer, in which Ω_A is the considered ageing parameter. The observability of the system is compared with other similar and relevant works available in literature. The introduction of the NO and NO_2 differentiation improves the reaction kinetics of the control-oriented model and therefore the accuracy of the observation. No extra excitation is required for the observer, which is able to converge in simulation from Ω_A=1 to an aged Ω in dynamic conditions like the WHTC. The convergence time required depends on the ageing state, being up to 14 WHTC, for values of Ω_A close to 1, the order of magnitude of time. Experimental validation with a new and an aged SCR is showed.

The developed urea quality indicator can be used in real time and it is independent from the ageing state. However, as the actual θ_{NH_3} needs to be estimated, it can limit its applicability. Its convergence time is in line with the OBD requirements for poor urea quality detection, being 400s the convergence time required. A simulation study on the dispersion that the downstream NO_x and NH_3 sensors would cause is also done.

8.2 Future work

The dissertation has a clear application-oriented goal, so it presents algorithms that can be embedded in on-board ECUs. In this sense, some of the algorithms shown are already implemented or can already be implemented in vehicles, although some others still require a further maturity step. Weaknesses, possible improvements and gaps between the results shown and the on-board implementation are next discussed.

Species measurements As neither HC nor CO sensors are available for on-board measurements, a gas analyzer has to be used instead. However, gas analyzer measurements induce a measurement delay. Besides, the HC are measured as total THC, in terms of CH_4, converting the wide variety of present HC chains into the simplest one, and therefore simplifying a more complex process. In this sense, the induced delay and the THC simplification may limit the DOC model accuracy.

On-board sensors measurements The diagnostics strategies fully rely on downstream sensors measurements. Therefore, it is important to assess their capacities and limitations in terms of accuracy, precision, cross-sensitivities, dynamic response and ageing effects. In this sense, NTC sensors and λ measurements are assessed for the required purposes. However, NO_x and NH_3 sensors still need a deeper characterization, since the correction of the cross-sensitivity with a constant is proven not to be sufficient.

Following the manufacturer indications, the NH_3 sensor requires the measurement of O_2, H_2O and pressure, which may not be available on-board, specially H_2O. Besides, its operation principle is based on the cross effects of O_2 and H_2O as a result of combustion in the exhaust gases. For this reason, the characterization of the sensor measurement is difficult to execute in controlled situations out of the exhaust line. However, in any case, a wide characterization of the NO_x and NH_3 sensor response in front of steps of NO_x and NH_3, in presence of different levels of O_2, H_2O, accounting also for dynamics, would be necessary for a deeper understanding of the sensors signals.

The use of an FTIR gas analyzer would be useful to isolate NO_x and NH_3 sensors measurements and compare with its accurate measurements. Then, NO_x dynamics should be evaluated with a fast Cambustion gas analyzer.

Engine-raw emissions models The use of catalysts models requires species concentrations as inputs. In the works presented, the inlet species, when required, are based on measurements that may not be available on-board, as the upstream HC, CO, the upstream NO_x sensor measurement, its separation into NO and NO_2 and the NH_3 downstream sensor measurement. For this reason, the development of reliable models is useful to feed a model that will improve as the inputs estimations improve.

Catalysts models When designing the approach of a model, the most relevant design factor is its future use. In this sense, the DOC model presented is able to estimate HC and CO slip in a determined range of engine operation conditions. Therefore, if the model is to be used for on-board purposes, a more robust approach could be of interest. In this sense, the model could be improved with a more detailed heat release, which should be able to reproduce high post-injection levels for DPF regeneration events. Besides, a desorption submodel that accounts for the accumulated HC slip could generalize more the model application.

On the other hand, as the purpose of the models presented is to include an ageing factor able to vary from new to aged states, an approach based

on reaction rates including this ageing factor approach like the one presented for SCR would be valuable for DOC. However, while the NH_3 accumulation capacity is the SCR ageing factor for modelling, as it is agreed in literature and it has been proven in this work, there is still not a unified accordance with regards to DOC. However, the methodology presented in this dissertation, in which the tuning parameters are calibrated for new and aged pieces, being then an ageing factor as a linear function of this tuned parameters, could be extrapolated to reaction rates-based DOC model.

The SCR model is simplified from models available in literature in order to operate in a determined range of engine operating conditions. In this sense, NH_3 oxidation and N_2O formation, which happen at higher temperatures than 400°C, should be included if the application is to be used on-board. In addition, the model calibration has been done following a manual procedure, in which the reaction rates parameters have been tuned in transient conditions. For this reason, a more detailed calibration procedure, including a wide discretization of steady-state measurement and transient steps could improve the model performance. However, this procedure is much more time and resources consuming. Finally, both 0D and 1D model integration is done by means of a quadratic method, so the use of a more efficient integration like the trapezoidal could reduce the computational resources required.

8.2.1 Catalysts diagnostics

The diagnostics algorithms for diesel after-treatment catalysts are a relevant part of this work. However, the exhaust line should be accounted on the whole, so that DPF and PNA or LNT should be included. For this reason, despite the work presented in this dissertation treats both DOC and SCR as isolated blocks, a general strategy that includes all after-treatment systems including blocks and sensors should be developed to be on-board implemented. In this sense, some of the methods described could be adapted for use in other blocks. E.g. the LNT could be diagnosed with a pair of up- and downstream NO_x sensors that account for its accumulation capacity and slip.

DOC diagnostics The presented methods for DOC diagnostics are suitable for on-board purposes. In this sense, both the algorithms for total failure or removal detection, as well as the algorithm for LOT detection as an indicator of the DOC ageing state could be implemented in vehicles. However, the DOC efficiency is estimated through the LOT detection as an indirect technique, so that the DOC model needs to be used to associate an emissions increase to

the LOT increase. In this sense, the effect of other ageing mechanisms like sulphur poisoning could not be taken into account.

SCR diagnostics The SCR system diagnostics is composed of an observer for SCR ageing based on a KF, as well as a urea quality indicator which avoids associating low SCR performance to ageing when the source is in poor urea quality. In this sense, this strategy is subjected to model performance for both the observer and the indicator. Therefore, the use of NH_3 oxidation and N_2O formation equations should be implemented for on-board purposes, and any model improvement would imply an increase of the strategy performance. On the other hand, in the case of the urea quality indicator, it is subjected to know the actual load state of the catalyst, which cannot be obtained as a measurement. For this reason, the regulation restriction of poor urea quality estimation in a 400s windows could not be accomplished. In addition, in order to generalize the model error and adapt it to different driving conditions, the torque is required, so that it requires this ECU estimation, which may limit the indicator applicability.

The SCR diagnostics strategy is also subjected to the sensors measurements. In this sense, the cross sensitivity of the NO_x sensor could limit the strategy performance. Some methods exist to separate the NO_x and NH_3 species concentrations from the NO_x sensor measurement. If the methods are not model-based, the ageing would not affect its performance. However, if the methods are model-based, an adaptive strategy should be developed in order to include the SCR ageing state. For this purpose, it is fundamental to separate the catalyst dynamics, since both the NO_x separation method and the ageing observer would be fed from the same NO_x sensor measurement. In this sense, the SCR ageing is a very slowly varying process, while the NO_x signal separation has to be done for each time step, which opens a door to combine this two dynamics using the same sensor measurement.

A similar case occurs with the urea quality indicator and the ageing observer. While the urea quality indicator may quickly vary if someone adds water into the urea tank, the injector can be slowly drifted over time. In this sense, as the indicator needs the actual estimation of the stored urea, which is provided by an SCR model, this estimation should include the ageing state of the catalyst. On the other hand, the KF based observer is observable with only the measurement of NO_x or NH_3, since it does not contemplate poor urea quality, which means that in case urea is good, the measurement of both sensors is redundant. For this reason, there is room for including a possible

equation that relates the urea quality with the SCR performance, and make the system require the measurement of both NO_x and NH_3.

In conclusion, all methods running in the ECU with regards to SCR rely on the downstream NO_x sensor measurement, and also on the NH_3 one if available. However, a proper time-based identification of dynamics could allow their implementation in parallel.

References

[1] Frobert A, Raux S, Creff Y and Jeudy E. "About Cross-Sensitivities of NOx Sensors in SCR Operation". In *SAE 2013 World Congress & Exhibition 2013-01-1512*. SAE International, apr 2013. (cited in pp. 100 and 211)

References

Alphabetic Index of Authors

A Morlang, U Neuhausen, K Klementiev and F Sc. "Bimetallic Pt Pd diesel oxidation catalysts: Structural characterisation and catalytic behaviour". *Applied Catalysis B: Environmental*, Vol. 60 n^o 3-4, pp. 191 – 199, 2005. (cited in p. 25)

Agency International Energy. "CO2 emissions from fuel Combustion". Technical report, OECD, 2017. (cited in p. 5)

Ahari H, Zammit M, Cattani L, Jacques J and Pauly T. "Cause and Effect of Reversible Deactivation of Diesel Oxidation Catalysts". In *SAE Technical Paper 2014-01-1518*. SAE International, 2014. (cited in pp. 26 and 27)

Alberer D. *Fast Oxygen Based Transient Diesel Engine Control*. PhD Thesis, Johannes Kepler Universitaet Linz, 2012. (cited in p. 34)

Alberer D. *Fast Oxygen Based Transient Diesel Engine Control*. Advances in mechatronics. Trauner, 2012. (cited in pp. 66 and 108)

Alberer D and del Re L. "Optimization of the transient Diesel engine operation". In *SAE Technical Paper 2009-24-0113*. Consiglio Nazionale delle Ricerche, 2009. (cited in pp. 64, 78, and 108)

Alkemade U G. and Schumann B. "Engines and exhaust after treatment systems for future automotive applications". *Solid State Ionics*, Vol. 177 n^o 26-32, pp. 2291 – 2296, 2006. (cited in pp. 6 and 41)

Arsie I, Flauti G, Pianese C, Rizzo G, Barberio C, Flora R, Serra G and Siviero C. "On-board diagnosis of SI engine catalyst efficiency: a confidence level analysis". In *International Workshop on Diagnostics in Automotive Engines and Vehicles, Fisciano, Italy*, 2002. (cited in p. 8)

Arsie I, Marra D, Pianese C and Sorrentino M. "Real-Time Estimation of Engine NOx Emissions via Recurrent Neural Networks". *IFAC Proceedings Volumes*, Vol. 43 n^o 7, pp. 228 – 233, 2010. 6th IFAC Symposium on Advances in Automotive Control. (cited in p. 42)

Arvajova A, Koci P, Schmeisser V and Weibel M. "The impact of CO and C3H6 pulses on PtOx reduction and NO oxidation in a diesel oxidation catalyst". *Applied Catalysis B: Environmental*, Vol. 181, pp. 644 – 650, 2016. (cited in p. 142)

B, J Cooper and J, E Thoss. "Role of NO in Diesel Particulate Emission Control". *Society of Automotive Engineers*, 1989. (cited in p. 29)

B J Cooper, W Evans and B Harrison. "Catalysis and Automotive Pollution Control". 1987. (cited in p. 29)

Bai S, Tang J, Wang G and Li G. "Soot loading estimation model and passive regeneration characteristics of DPF system for heavy-duty engine". *Applied Thermal Engineering*, Vol. 100, pp. 1292–1298, 2016. (cited in p. 29)

Bartley G J. "Identifying Limiters to Low Temperature Catalyst Activity". In *SAE Technical Paper 2015-01-1025*. SAE International, 2015. (cited in pp. 25, 87, and 139)

Bartley G J., Chadwell C J., Kostek T M. and Zhan R. "SCR Deactivation Kinetics for Model-Based Control and Accelerated Aging Applications". In *SAE Technical Paper 2012-01-1077*. SAE International, 04 2012. (cited in pp. 33, 102, and 151)

Birkhold F, Meingast U, Wassermann P and Deutschmann O. "Modeling and simulation of the injection of urea-water-solution for automotive SCR DeNOx-systems". *Applied Catalysis B: Environmental*, Vol. 70 n^o 1, pp. 119 – 127, 2007. (cited in p. 32)

Blanco-Rodriguez D., Vagnoni G. and Holderbaum B. "EU6 C-Segment Diesel vehicles, a challenging segment to meet RDE and WLTP requirements". *IFAC-PapersOnLine*, Vol. 49 n^o 11, pp. 649 – 656, 2016. 8th IFAC Symposium on Advances in Automotive Control AAC 2016. (cited in pp. 10 and 39)

Blanco-Rodriguez I.D. *Modelling and Observation of Exhaust Gas Concentrations for Diesel Engine Control*. PhD Thesis, Universitat Politecnica de Valencia, 2014. (cited in p. 34)

Boatas A, Agnes M, Peltier D and Dubuisson B. "OBD Using Statistical Pattern Recognition". In *SAE Technical Paper 2000-01-3104*. SAE International, 2000. (cited in pp. 8 and 26)

Bonfils A, Creff Y, Lepreux O and Petit N. "Closed-loop control of a SCR system using a NOx sensor cross-sensitive to NH3". *Journal of Process Control*, Vol. 24 n^o 2, pp. 368 – 378, 2014. (cited in p. 99)

Busca G, Lietti L, Ramis Go and Berti F. "Chemical and mechanistic aspects of the selective catalytic reduction of NOx by ammonia over oxide catalysts: A review". *Applied Catalysis B: Environmental*, Vol. 18 n^o 1, pp. 1 – 36, 1998. (cited in p. 153)

Cabello Galisteo F., Larese C., Mariscal R., López Granados M., Fierro J. L. G., Fernández-Ruiz R. and Furió M. "Deactivation on vehicle-aged diesel oxidation catalysts". *Topics in Catalysis*, Vol. 30 n^o 1, pp. 451–456, Jul 2004. (cited in p. 26)

Canova M, Midlam-Mohler S, Pisu P and Soliman A. "Model-based fault detection and isolation for a diesel lean NOx trap aftertreatment system". *Control Engineering Practice*, Vol. 18 n^o 11, pp. 1307 – 1317, 2010. Special Issue on Automotive Control Applications, 2008 IFAC World Congress. (cited in p. 30)

Cavataio G, Girard J, Patterson Joseph E, Montreuil C, Cheng Y and Lambert C K. "Laboratory Testing of Urea-SCR Formulations to Meet Tier 2 Bin 5 Emissions". In *SAE Technical Paper Series 2007-01-1575*. SAE International, 2007. (cited in p. 33)

Cavataio G, Jen H-W, Girard J W, Dobson D, Warner J R and Lambert C K. "Impact and prevention of ultra-low contamination of platinum group metals on SCR catalysts due to DOC design". *SAE International Journal of Fuels and Lubricants 2009-01-0627*, Vol. 2, pp. 204–216, 2009. (cited in p. 25)

Chan C Chue. "The state of the art of electric, hybrid, and fuel cell vehicles". *Proceedings of the IEEE*, Vol. 95 n^o 4, pp. 704–718, 2007. (cited in p. 4)

Chan CC, Wong YS, Bouscayrol Alain and Chen Keyu. "Powering sustainable mobility: roadmaps of electric, hybrid, and fuel cell vehicles". *Proceedings of the IEEE*, Vol. 97 n^o 4, pp. 603–607, 2009. (cited in p. 4)

Chatterjee D, Koci P, Schmeisser V, Marek M, Weibel M and Krutzsch B. "Modelling of a combined NOx storage and NH3-SCR catalytic system for Diesel exhaust gas aftertreatment". *Catalysis Today*, Vol. 151 n^o 3, pp. 395 – 409, 2010. Diesel emissions control catalysis. (cited in pp. 32 and 99)

Chen P. *Modeling, Estimation and Control of Integrated Diesel Engine and Aftertreatment Systems*. PhD Thesis, The Ohio State University, 2014. (cited in p. 40)

Chen P and Wang J. "Control-oriented modeling of thermal behaviors for a Diesel oxidation catalyst". In *American Control Conference (ACC), 2012*, pp. 4987–4992, 2012. (cited in p. 138)

Chen P and Wang J. "Nonlinear and adaptive control of NO/NO 2 ratio for improving selective catalytic reduction system performance". *Journal of the Franklin Institute*, Vol. 350 n^o 8, pp. 1992–2012, 2013. (cited in p. 24)

Chen P and Wang J. "Control-oriented model for integrated diesel engine and aftertreatment systems thermal management". *Control Engineering Practice*, Vol. 22, pp. 81–93, 2014. (cited in pp. 27, 110, 127, and 138)

Chen R and Wang X. "Model-Based Fault Diagnosis of Selective Catalytic Reduction Systems for Diesel Engines". *SAE Int. J. Passeng. Cars - Electron. Electr. Syst. 2014-01-0280*, Vol. 7, pp. 449–453, 04 2014. (cited in pp. 33 and 151)

Chi J N. "Control Challenges for Optimal NOx Conversion Efficiency from SCR Aftertreatment Systems". In *SAE World Congress & Exhibition 2009-01-0905*. SAE International, apr 2009. (cited in p. 32)

Chi John N. and DaCosta Herbert F. M. "Modeling and Control of a Urea-SCR Aftertreatment System". In *SAE 2005 World Congress & Exhibition 2005-01-0966*. SAE International, apr 2005. (cited in p. 32)

Chiang C-J, Stefanopoulou A G and Jankovic M. "Nonlinear observer-based control of load transitions in homogeneous charge compression ignition engines". *IEEE Transactions on Control Systems Technology*, Vol. 15 n^o 3, pp. 438–448, 2007. (cited in pp. 3 and 36)

Cloudt R, Saenen J, Eijnden E van den and Rojer C. "Virtual Exhaust Line for Model-based Diesel Aftertreatment Development". In *SAE 2010 World Congress & Exhibition 2010-01-0888*. SAE International, apr 2010. (cited in pp. 31, 38, and 188)

Colombo M, Nova I and Tronconi E. "A comparative study of the NH3-SCR reactions over a Cu-zeolite and a Fe-zeolite catalyst". *Catalysis Today*, Vol. 151 n^o 3, pp. 223 – 230, 2010. (cited in p. 32)

Colombo M, Nova I and Tronconi E. "Detailed kinetic modeling of the NH3-NO/NO2 SCR reactions over a commercial Cu-zeolite catalyst for Diesel exhausts after treatment". *Catalysis Today*, Vol. 197 n^o 1, pp. 243 – 255, 2012. (cited in p. 99)

Connolly FT and Rizzoni G. "Real time estimation of engine torque for the detection of engine misfires". *Journal of dynamic systems, measurement, and control*, Vol. 116 n^o 4, pp. 675–686, 1994. (cited in p. 109)

Daham B, Li H, Andrews G E., Ropkins K, Tate J E. and Bell M C. "Comparison of real world emissions in urban driving for EURO 1-4 vehicles using a PEMS". Technical report, SAE Technical Paper 2009-01-0941, 2009. (cited in p. 7)

Davis S., Diegel S. and Boundy R. *Transportation energy data book*. 2007. (cited in p. 5)

Del Re L, Allgöwer F, Glielmo L, Guardiola C and Kolmanovsky I. *Automotive model predictive control: models, methods and applications*, volume 402. Springer, 2010. (cited in pp. 66 and 108)

Delphi. "Worldwide emission standards". Technical report, Delphi, 2017. (cited in pp. 8 and 32)

Desantes J M and Payri F. *Motores de combustión interna alternativos*. 2011. (cited in p. 4)

Devarakonda M., Parker G., Johnson J. H. and Strots V. "Model-based control system design in a urea-SCR aftertreatment system based on NH3 sensor feedback". *International Journal of Automotive Technology*, Vol. 10 n^o 6, pp. 653, Dec 2009. (cited in p. 33)

Devarakonda M, Parker G, Johnson J H., Strots V and Santhanam S. "Model-Based Estimation and Control System Development in a Urea-SCR Aftertreatment System". *SAE International Journal of Fuels and Lubricants 2008-01-1324*, Vol. 1, pp. 646–661, apr 2008. (cited in pp. 32, 33, 191, and 192)

Dueker H, Friese KH and Haecker WD. "Ceramic aspects of the bosch lambda-sensor". Technical report, SAE Technical Paper 750223, 1975. (cited in p. 36)

Eijnden E v d, Cloudt R, Willems F and Heijden P v d. "Automated Model Fit Tool for SCR Control and OBD Development". In *SAE Technical Paper Series 2009-01-1285*. SAE International, apr 2009. (cited in pp. 8, 66, and 152)

El-Awar N, Geer D, Krellner T and Straub P. "Automotive temperature sensing". *Keystone Thermometrics Corporation Application Notes*, 1999. (cited in p. 35)

Emi M and Miura M. "Deterioration diagnosis of diesel particulate filter". 2007. US Patent 7,281,369. (cited in p. 10)

Englert N. "Fine particles and human health: a review of epidemiological studies". *Toxicology Letters*, Vol. 149 n^o 1, pp. 235 – 242, 2004. (cited in p. 5)

Eriksson L. "Mean Value Models for Exhaust System Temperatures". In *SAE Technical Paper 2002-01-0374*. SAE International, 2002. (cited in p. 110)

Feng T and Lue L. "The characteristics of ammonia storage and the development of model-based control for diesel engine urea-SCR system". *Journal of Industrial and Engineering Chemistry*, Vol. 28, pp. 97 – 109, 2015. (cited in p. 99)

Figura J, Kihas D, Pekar J, Uchanski M, Khaled N and Srinivasan S. "Automotive Selective Catalytic Reduction System Model-Based Estimators for On-ECU Implementation: A Brief Overview". In *SAE 2016 World Congress and Exhibition 2016-01-0972*. SAE International, apr 2016. (cited in p. 152)

Figura J, Pekar J, Krejza P, Mracek D, von Wissel D and Zhang T. "NO2/NOx Ratio and NH3 Storage Estimation of Automotive SCR Multi-Brick Systems". In *SAE Technical Paper 2017-01-0972*. SAE International, 2017. (cited in p. 99)

Franco V, Sánchez F P, German J and Mock P. "Real-world exhaust emissions from modern diesel cars". *communications*, Vol. 49 n^o 30, pp. 847129–102, 2014. (cited in p. 8)

Fritz N, Mathes W, Zuerbig J and Mueller R. "On-road demonstration of NOx emission control for diesel trucks with SINOx urea SCR system". Technical report, SAE Technical Paper 44716659, 1999. (cited in p. 30)

Frobert A, Creff Y, Lepreux O, Schmidt L and Raux S. "Generating Thermal Conditions to Regenerate a DPF: Impact of the Reductant on the Performances of Diesel Oxidation Catalysts". In *SAE Technical Paper 2009-01-1085*. SAE International, 04 2009. (cited in pp. 27 and 29)

Frobert A, Raux S, Creff Y and Jeudy E. "About Cross-Sensitivities of NOx Sensors in SCR Operation". In *SAE 2013 World Congress & Exhibition 2013-01-1512*. SAE International, apr 2013. (cited in pp. 100 and 211)

Galindo J, Luján JM, Climent H and Guardiola C. "Turbocharging system design of a sequentially turbocharged diesel engine by means of a wave action model". Technical report, SAE Technical Paper 2007-01-1564, 2007. (cited in p. 78)

Galindo J, Serrano JR, Guardiola C, Blanco-Rodriguez D and Cuadrado IG. "An on-engine method for dynamic characterisation of NOx concentration sensors". *Experimental Thermal and Fluid Science*, Vol. 35 n^o 3, pp. 470–476, 2011. (cited in p. 109)

Graziano B, Heuser B, Kremer F, Pischinger S and Rohs H. "The Oxidation Potential Number: An Index to Evaluate Inherent Soot Reduction in D.I. Diesel Spray Plumes". *SAE International Journal of Engines 2015-01-1934*, Vol. 9 n^o 1, pp. 222–236, sep 2015. (cited in p. 4)

Graziano B, Perez J Mora, Kremer F, Pischinger S, Reddemann MA, Kneer R, Heufer KA and Rohs H. "Virtual Fuel Approach: a new simulative methodology to analyse effects of fuel properties on mixture formation in compression igni-tion combustion". In *THIESEL Conference*, 2014. (cited in p. 4)

Grewe V, Dahlmann K, Matthes S and Steinbrecht W. "Attributing ozone to NOx emissions: Implications for climate mitigation measures". *Atmospheric Environment*, Vol. 59, pp. 102 – 107, 2012. (cited in p. 5)

Guan B, Zhan R, Lin H and Huang Z. "Review of state of the art technologies of selective catalytic reduction of NOx from diesel engine exhaust". *Applied Thermal Engineering*, Vol. 66 n^o 1, pp. 395–414, 2014. (cited in pp. 32 and 99)

Guardiola C, Climent H, Pla B and Blanco-Rodriguez D. "ECU-oriented models for NOx prediction. Part 2: adaptive estimation by using an NOx sensor". *Proceedings of the Institution of Mechanical Engineers, Part D: Journal of Automobile Engineering*, Vol. 229 n^o 10, pp. 1345–1360, 2015. (cited in pp. 66 and 108)

Guardiola C, Martín J, Pla B and Bares P. "Cycle by cycle NOx model for diesel engine control". *Applied Thermal Engineering*, Vol. 110, pp. 1011–1020, 2017. (cited in p. 42)

Guardiola C, Pla B, Blanco-Rodriguez D and Calendini P Olivier. "ECU-oriented models for NOx prediction. Part 1: a mean value engine model for NOx prediction". *Proceedings of the Institution of Mechanical Engineers, Part D: Journal of Automobile Engineering*, Vol. 229 n^o 8, pp. 992–1015, 2015. (cited in p. 108)

Guardiola C, Pla B, Blanco-Rodriguez D, Mazer A and Hayat O. "A bias correction method for fast fuel-to-air ratio estimation in diesel engines". *Proceedings of the Institution of Mechanical Engineers, Part D: Journal of Automobile Engineering*, Vol. 227 n^o 8, pp. 1099–1111, 2013. (cited in pp. 108 and 114)

Guardiola C., Pla B., Mora J. and Lefebvre D. "Control Oriented Model for Diesel Oxidation Catalyst Diagnosis". *IFAC-PapersOnLine*, Vol. 48 n^o 15, pp. 427 – 433, 2015. (cited in pp. 26, 27, 138, and 146)

Guardiola C, Pla B, Piqueras P, Mora J and Lefebvre D. "Model-based passive and active diagnostics strategies for diesel oxidation catalysts". *Applied Thermal Engineering*, Vol. 110, pp. 962–971, 2017. (cited in pp. 26 and 188)

Guzzella L and Onder C. *Introduction to modeling and control of internal combustion engine systems*. Springer Science & Business Media, 2009. (cited in p. 110)

Hagen G, Burger K, Wiegaertner S, Schoe Kamin D and Moos R. "A mixed potential based sensor that measures directly catalyst conversion a novel approach for catalyst on-board diagnostics". *Sensors and Actuators B: Chemical*, Vol. 217, pp. 158–164, 2015. (cited in pp. 8 and 39)

Han M. and Lee B. "Control oriented model of a lean NOx trap for the catalyst regeneration in a 2.2 L direct injection diesel engine". *International Journal of Automotive Technology*, Vol. 16 n^o 3, pp. 371–378, 2015. (cited in p. 30)

Haralampous O. A., Kandylas I. P., Koltsakis G. C. and Samaras Z. C. "Diesel particulate filter pressure drop Part 1: Modelling and experimental validation". *International Journal of Engine Research*, Vol. 5 n^o 2, pp. 149–162, 2004. (cited in p. 10)

Haralampous O. A., Kandylas I. P., Koltsakis G. C. and Samaras Z. C. "Diesel particulate filter pressure drop Part 2: On-board calculation of soot loading". *International Journal of Engine Research*, Vol. 5 n^o 2, pp. 163–173, 2004. (cited in p. 10)

Haugen F. *Discrete-time signals and systems*. Tech, 2005. (cited in p. 114)

Henry C, Currier N, Ottinger N, Yezerets A, Castagnola M, Chen H-Y and Hess H. "Decoupling the Interactions of Hydrocarbons and Oxides of Nitrogen Over Diesel Oxidation Catalysts". In *SAE 2011 World Congress & Exhibition 2011-01-1137*. SAE International, 2011. (cited in pp. 25 and 139)

Henry C, Gupta A, Currier N and Ruth M. "Advanced Technology Light Duty Diesel Aftertreatment System". Technical report, Cummins, 2012. (cited in p. 40)

Herman A, Wu M-C, Cabush D and Shost M. "Model Based Control of SCR Dosing and OBD Strategies with Feedback from NH3 Sensors". *SAE International Journal of Fuels and Lubricants 2009-01-0911*, Vol. 2 n^o 1, pp. 375–385, apr 2009. (cited in pp. 8 and 33)

Heuser B. "Tailor-Made Fuels from Biomass". Technical report, RWTH - Aachen, 2016. (cited in p. 4)

Heywood JB and others. *Internal combustion engine fundamentals*. Mcgraw-hill New York, 1988. (cited in pp. 5 and 22)

Hoepfner A and Roduner C A. "PM Sensor Based On-Board Diagnosis of Particulate Filter Efficiency". In *SAE Technical Paper 10.4271/*. SAE International, 2013. (cited in pp. 8, 29, and 39)

Hommen G, Kupper F and Seykens X. "Robust, Model-Based Urea Dosing Control for SCR Aftertreatment Systems using a Cross-Sensitive Tailpipe NOx Sensor". In *SAE Technical Paper Series 2017-01-0938*. SAE International, mar 2017. (cited in p. 138)

Hooftman N, Messagie M, Mierlo J Van and Coosemans T. "A review of the European passenger car regulations - Real driving emissions vs local air quality". *Renewable and Sustainable Energy Reviews*, Vol. 86, pp. 1 – 21, 2018. (cited in p. 7)

Hoppe F, Heuser B, Thewes M, Kremer F, Pischinger S, Dahmen M, Hechinger M and Marquardt W. "Tailor-made fuels for future engine concepts". *International Journal of Engine Research*, Vol. 17 n^o 1, pp. 16–27, 2016. (cited in p. 4)

HORIBA. "Horiba MEXA-7100DEGR Instruction Manual". Technical report, Horiba, 2011. (cited in p. 63)

Hsieh M. F. and Wang J. "Nonlinear model predictive control of lean NOx trap regenerations". In *Proceedings of the 48h IEEE Conference on Decision and Control (CDC) held jointly with 2009 28th Chinese Control Conference*, pp. 5182–5187, 2009. (cited in p. 30)

Hsieh M F and Wang J. "An extended Kalman filter for ammonia coverage ratio and capacity estimations in the application of Diesel engine SCR control and onboard diagnosis". In *American Control Conference (ACC), 2010*, pp. 5874–5879. IEEE, 2010. (cited in pp. 33, 186, 191, and 192)

Hsieh M F and Wang J. "An extended Kalman filter for NO x sensor ammonia cross-sensitivity elimination in selective catalytic reduction applications". In *American Control Conference (ACC), 2010*, pp. 3033–3038. IEEE, 2010. (cited in p. 33)

Husted H, Roth G, Nelson S, Hocken L, Fulks G and Racine D. "Sensing of Particulate Matter for On-Board Diagnosis of Particulate Filters". *SAE International Journal of Engines 2012-01-0372*, Vol. 5 n^o 2, pp. 235–247, apr 2012. (cited in pp. 29 and 39)

Jason S Moura, Fathy H K, Callaway D S and Stein J L. "A stochastic optimal control approach for power management in plug-in hybrid electric vehicles". *IEEE Transactions on control systems technology*, Vol. 19 n^o 3, pp. 545–555, 2011. (cited in p. 4)

Jen H-W, Girard J W., Cavataio G and Jagner M J. "Detection, Origin and Effect of Ultra-Low Platinum Contamination on Diesel-SCR Catalysts". *SAE Int. J. Fuels Lubr. 2008-01-2488*, pp. 1553–1559, 2008. (cited in p. 33)

Johannesson L, Murgovski N, Ebbesen S, Egardt B, Gelso E R and Hellgren J. "Including a battery state of health model in the HEV component sizing and optimal control problem". In *IFAC Advances in Automotive Control*, volume 7, pp. 398–403, 2013. (cited in p. 4)

Johansen K, Dahl S, Mogensen G, Pehrson S, Schramm Je and Ivarsson A. "Novel base metal-palladium catalytic diesel filter coating with NO2 reducing properties". Technical report, SAE Technical Paper 2007-01-1921, 2007. (cited in p. 25)

Johnson T. "Vehicular Emissions in Review". *SAE International Journal of Engines 2013-01-0538*, Vol. 6 n^o 2, pp. 699–715, apr 2013. (cited in pp. 24, 26, and 41)

Johnson T. "Vehicular Emissions in Review". *SAE Int. J. Engines 2014-01-1491*, Vol. 7, pp. 1207–1227, 2014. (cited in pp. 24, 25, and 39)

Johnson T and Joshi A. "Review of Vehicle Engine Efficiency and Emissions". In *WCX 17: SAE World Congress Experience 2017-01-0907*. SAE International, mar 2017. (cited in p. 8)

Johnson T V. "Diesel Emission Control in Review". In *SAE technical paper 2007-01-0233*. SAE International, 2007. (cited in pp. 6 and 28)

Johnson T V. "Diesel Emission Control in Review". *SAE Int. J. Fuels Lubr. 2008-01-0069*, pp. 68–81, 2008. (cited in p. 25)

Johnson TV. "Diesel Emission Control in Review". In *SAE 2001 World Congress 2001-01-0184*. SAE International, mar 2001. (cited in pp. 6 and 29)

Kalman RE. "A new approach to linear filtering and prediction problems". *Journal of basic Engineering*, Vol. 82 n^o 1, pp. 35–45, 1960. (cited in p. 115)

Kalman RE and Bucy RS. "New results in linear filtering and prediction theory". *Journal of basic engineering*, Vol. 83 n^o 1, pp. 95–108, 1961. (cited in p. 116)

Kamimoto T. "A review of soot sensors considered for on-board diagnostics application". *International Journal of Engine Research*, 2016. (cited in pp. 8 and 39)

Kampa M and Castanas E. "Human health effects of air pollution". *Environmental Pollution*, Vol. 151 n^o 2, pp. 362 – 367, 2008. (cited in p. 5)

Kang M, Wu Y and Shen T. "Logical control approach to fuel efficiency optimization for commuting vehicles". *International Journal of Automotive Technology*, Vol. 18 n^o 3, pp. 535–546, Jun 2017. (cited in p. 4)

Kar K, Roberts S, Stone R, Oldfield M and French B. "Instantaneous exhaust temperature measurements using thermocouple compensation techniques". *SAE SP 2004-01-1418*, pp. 169–190, 2004. (cited in pp. 80 and 108)

Katare S R., Patterson J E. and Laing P M. "Aged DOC is a Net Consumer of NO2: Analyses of Vehicle, Engine-dynamometer and Reactor Data". Technical Report 2007-01-3984, SAE Technical Paper 2007-01-3984, 2007. (cited in p. 26)

Kee R J., Hung P, Fleck B, Irwin G, Kenny R, Gaynor J and McLoone S. "Fast Response Exhaust Gas Temperature Measurement in IC Engines". In *SAE Technical Paper 2006-01-1319*. SAE International, 2006. (cited in p. 108)

Khair MK. "A Review of Diesel Particulate Filter Technologies". In *Future Transportation Technology Conference & Exposition 2003-01-2303*. SAE International, jun 2003. (cited in pp. 28 and 38)

Khosravi M, Abedi A, Hayes RE, Epling WS and Votsmeier M. "Kinetic modelling of Pt and Pt: Pd diesel oxidation catalysts". *Applied Catalysis B: Environmental*, Vol. 154, pp. 16–26, 2014. (cited in pp. 27 and 138)

Kim Y-D and Kim W-S. "Re-evaluation and Modeling of a Commercial Diesel Oxidation Catalyst". *Industrial & Engineering Chemistry Research*, Vol. 48 n^o 14, pp. 6579–6590, 2009. (cited in pp. 27 and 138)

Kim Y-W, Van Nieuwstadt M, Stewart G and Pekar Ja. "Model predictive control of DOC temperature during DPF regeneration". In *SAE Technical Paper 2014-01-1165*. SAE International, 2014. (cited in pp. 27, 29, and 138)

Kittelson DB. "Engines and nanoparticles: a review". *Journal of Aerosol Science*, Vol. 29 n^o 5, pp. 575 – 588, 1998. (cited in p. 5)

Koebel M, Elsener M and Kleemann M. "Urea-SCR: a promising technique to reduce NOx emissions from automotive diesel engines". *Catalysis today*, Vol. 59 n^o 3-4, pp. 335–345, 2000. (cited in p. 30)

Kolaczkowski S., Ye S., Yap Y., Robinson K. and Lukyanov D. "Transient experiments on a full-scale DOC Methodology and techniques to support modelling". *Catalysis Today*, Vol. 188 n^o 1, pp. 53 – 61, 2012. Modeling of Exhaust-Gas After-Treatment. (cited in p. 27)

Kong Y, Kozakiewicz T, Johnson R, Huffmeyer C, Huckaby J, Abel J, Baurley J and Duffield K. "Active DPF Regeneration for 2007 Diesel Engines". In *2005 SAE Commercial Vehicle Engineering Conference 2005-01-3509*. SAE International, nov 2005. (cited in p. 38)

Kryl D, Kocí P, Kubícek M, Marek M, Maunula T and Härkönen M. "Catalytic converters for automobile diesel engines with adsorption of hydrocarbons on zeolites". *Industrial & engineering chemistry research*, Vol. 44 n^o 25, pp. 9524–9534, 2005. (cited in pp. 26 and 138)

Ladommatos N, Abdelhalim S and Zhao H. "Control of oxides of nitrogen from diesel engines using diluents while minimising the impact on particulate pollutants". *Applied Thermal Engineering*, Vol. 18 n^o 11, pp. 963 – 980, 1998. (cited in p. 23)

Ladommatos N, Abdelhalim SM, Zhao Hua and Hu Z. "The dilution, chemical, and thermal effects of exhaust gas recirculation on diesel engine emissions-part 1: Effect of reducing inlet charge oxygen". Technical report, SAE Technical Paper 961165, 1996. (cited in p. 23)

Ladommatos N, Abdelhalim SM, Zhao Hua and Hu Z. "The dilution, chemical, and thermal effects of exhaust gas recirculation on diesel engine emissions-part 2: Effects of Carbon Dioxide". Technical report, SAE Technical Paper 961167, 1996. (cited in p. 23)

Ladommatos N, Abdelhalim SM, Zhao Hua and Hu Z. "The dilution, chemical, and thermal effects of exhaust gas recirculation on diesel engine emissions-part 3: Effects of water vapour". Technical report, SAE Technical Paper 971659, 1997. (cited in p. 23)

Ladommatos N, Abdelhalim SM, Zhao Hua and Hu Z. "The dilution, chemical, and thermal effects of exhaust gas recirculation on diesel engine emissions-part 4: Eects of Carbon Dioxide and Water Vapour". Technical report, SAE Technical Paper 971660, 1997. (cited in p. 23)

Ladommatos N, M. Abdelhalim S and Zhao H. "The Effects of Exhaust Gas Recirculation on Diesel Combustion and Emissions". Vol. 1, pp. 107–126, 02 2000. (cited in p. 23)

Ladommatos N, M. Abdelhalim S and Zhao H. "The Effects of Exhaust Gas Recirculation on Diesel Combustion and Emissions". Vol. 1, pp. 107–126, 02 2000. (cited in p. 23)

Ladommatos N, M Adelhalim S, Zhao Hua and Hu Z. "The effects of carbon dioxide in exhaust gas recirculation on diesel engine emissions". Vol. 212, pp. 25–42, 01 1998. (cited in p. 23)

Lee D and Rizzoni G. "Detection of partial misfire in IC engines using a measurement of crankshaft angular velocity". Technical report, SAE Technical Paper 951070, 1995. (cited in p. 109)

Lee J, Chu S, Cha J, Choi H and Min K. "Effect of the diesel injection strategy on the combustion and emissions of propane/diesel dual fuel premixed charge compression ignition engines". Vol. 93, pp. 1041–1052, 12 2015. (cited in p. 4)

Lepreux O., Creff Y. and Petit N. "Warm-up strategy for a Diesel Oxidation Catalyst". In *Control Conference (ECC), 2009 European*, pp. 3821–3826, 2009. (cited in p. 169)

Lepreux O, Creff Y and Petit N. "Model-based temperature control of a diesel oxidation catalyst". *Journal of Process Control*, Vol. 22 n^o 1, pp. 41 – 50, 2012. (cited in p. 27)

Li J, Szailer T, Watts A, Currier N and Yezerets A. "Investigation of the Impact of Real-World Aging on Diesel Oxidation Catalysts". *SAE Int. J. Engines 2012-01-1094*, Vol. 5, pp. 985–994, 04 2012. (cited in pp. 8, 26, and 87)

Lietti L, Nova I, Ramis G, DallAcqua L, Busca G, Giamello E, Forzatti P and Bregani F. "Characterization and Reactivity of V2O5-MoO3 TiO2 De-NOx SCR Catalysts". *Journal of Catalysis*, Vol. 187 n^o 2, pp. 419 – 435, 1999. (cited in p. 153)

López Hernández L. *Desarrollo de una metodología para la predicción y optimización de emisiones contaminantes y consumo en motores Diesel de automoción mediante redes neuronales artificiales*. PhD Thesis, 2004. (cited in p. 5)

Lu X, Han D and Huang Z. "Fuel design and management for the control of advanced compression-ignition combustion modes". *Progress in Energy and Combustion Science*, Vol. 37 n^o 6, pp. 741 – 783, 2011. (cited in p. 3)

Lukoil. "Global trends in oil and gas markets to 2025". Technical report, Lukoil, 2013. (cited in pp. 1, 2, and 4)

Lukoil. "Major trends global oil market to 2030". Technical report, Lukoil, 2015. (cited in p. 2)

M Klaus and T Helmut. *Handbook of diesel engines*. Springer-Verlag Berlin Heidelberg 2010, 2010. (cited in p. 34)

M Weibel, N Waldbuesser, R Wunsch, D Chatterjee, B Bandl-Konrad and B Krutzsch. "A Novel Approach to Catalysis for NO x Reduction in Diesel Exhaust Gas". *Topics in Catalysis*, 2009. (cited in p. 30)

M V Twigg. "Urea-SCR Technology for deNOx After Treatment of Diesel Exhausts". Technical report, Johnson Matthey Technol, 2015. (cited in p. 32)

Ma Y and Wang J. "Control of aged automotive selective catalytic reduction systems for consistent performances". *Journal of the Franklin Institute*, Vol. 354 n^o 18, pp. 8094 – 8116, 2017. (cited in p. 33)

Malanga M T, Allen, M P Das, N S Kotnis, A Mikulic, I Vosejpka and P C Majkowski. "Future Trends for DPF....SCR on-Filter (SCRF)". Technical report, DEER Conference, 2012. (cited in p. 40)

Mallamo F, Longhi S, Millo F and Rolando L. "Modeling of diesel oxidation catalysts for calibration and control purpose". *International Journal of Engine Research*, Vol. 15 n^o 8, pp. 965–979, 2014. (cited in pp. 27 and 143)

Maricq M. Matti. "Chemical characterization of particulate emissions from diesel engines: A review". *Journal of Aerosol Science*, Vol. 38 n^o 11, pp. 1079 – 1118, 2007. (cited in p. 5)

Marie-Luce D., Bliman P.-A., Di-Penta D. and Sorine M. "Reduced-Order Models for a LNT-SCR Diesel After-treatment Architecture with NO/NO2 Differentiation". *IFAC Proceedings Volumes*, Vol. 45 n^o 16, pp. 745 – 750, 2012. (cited in p. 33)

Marie-Luce D, Di-penta D, Bliman P-A and Sorine M. "Control-Oriented Modeling of a LNT-SCR Diesel After-Treatment Architecture". *SAE International Journal of Engines 2011-01-1307*, Vol. 4 n^o 1, pp. 1764–1775, apr 2011. (cited in p. 30)

Matsumoto A, Furui K, Ogiso M and Kidokoro T. "Model-Based OBD Logic Utilizing Adsorption and Desorption Model of NH3 in SCR Catalyst". In *SAE Technical Paper 2016-01-0960*. SAE International, 04 2016. (cited in pp. 8, 33, and 151)

Maunula T., Kallinen K., Savimaeki A. and Wolff T. "Durability Evaluations and Rapid Ageing Methods in Commercial Emission Catalyst Development for Diesel, Natural Gas and Gasoline Applications". *Topics in Catalysis*, Vol. 59 n^o 10-12, pp. 1049–1053, 2016. (cited in p. 33)

Maunula T, Kinnunen T and Iivonen M. "Design and Durability of Vanadium-SCR Catalyst Systems in Mobile Off-Road Applications". In *SAE 2011 World Congress & Exhibition 2011-01-1316*. SAE International, 2011. (cited in p. 33)

McKinley Thomas L. and Alleyne Andrew G. "Model Predictive Control: A Unified Approach for Urea-Based SCR Systems". *SAE International Journal of Fuels and Lubricants 2010-01-1184*, Vol. 3 n^o 1, pp. 673–689, apr 2010. (cited in p. 32)

Meisami-Azad M, Mohammadpour J, Grigoriadis K M and Harold M P. "An adaptive control strategy for urea-SCR aftertreatment system". In *American Control Conference (ACC), 2010*, pp. 3027–3032. IEEE, 2010. (cited in p. 32)

Michael J R. "ATP-LD; Cummins Next Generation Tier 2 Bin 2 Diesel Engine". Technical report, Cummins, 2014. (cited in p. 30)

Millo F, Rolando L, Mallamo F and Fuso R. "Development of an optimal strategy for the energy management of a range-extended electric vehicle with additional noise, vibration and harshness constraints". *Proceedings of the Institution of Mechanical Engineers, Part D: Journal of Automobile Engineering*, Vol. 227 n^o 1, pp. 4–16, 2013. (cited in p. 4)

Mock P. "2020–2030 CO2 standards for new cars and light-commercial vehicles in the European Union". In *ICCT*, pp. 1–19, 2017. (cited in pp. 7 and 8)

Mock P, Kuehlwein J, Tietge U, Franco V, bandivadekar A and German J. "The WLTP: How a new test procedure for cars will affect fuel consumption values in the EU". Technical report, The international council on clean trasnportation, 2014. (cited in p. 2)

Moos R. "A brief overview on automotive exhaust gas sensors based on electroceramics". *International Journal of Applied Ceramic Technology*, Vol. 2 n^o 5, pp. 401–413, 2005. (cited in pp. 9 and 36)

Moos R and Schoenauer D. "Recent Developments in the Field of Automotive Exhaust Gas Ammonia Sensing". *Sensor letters*, Vol. 6 n^o 6, pp. 821–825, 2008. (cited in p. 37)

Mrosek M, Sequenz H and Isermann R. "Identification of emission measurement dynamics for diesel engines". *IFAC proceedings volumes (IFAC-PapersOnline)*, Vol. 18, pp. 11839–11844, 2011. (cited in pp. 34 and 79)

Munguia N. *Lean NOx Trap Regeneration Control Strategy on a 1.9 L Turbocharged Diesel*. PhD Thesis, 2009. (cited in p. 30)

Naber D, Kufferath A, Krüger M, Maier R, Scherer S and Schumacher H. "Measures to fulfill real driving emission (RDE) with Diesel passenger cars". pp. 423–446, 2017. (cited in p. 7)

Nagar N, He X, Iyengar V, Acharya N, Kalinowski A, Kotrba A, Gardner T and Yetkin A. "Real Time Implementation of DOC-DPF Models on a Production-Intent ECU for Controls and Diagnostics of a PM Emission Control System". *SAE Int. J. Commer. Veh. 2009-01-2904*, Vol. 2, pp. 222–233, 10 2009. (cited in p. 29)

Nakane T., Ikeda M., Hori M., Bailey O. and Mussmann L. "Investigation of the Aging Behavior of Oxidation Catalysts Developed for Active DPF Regeneration Systems". In *SAE Technical Paper 2005-01-1759*. SAE International, 2005. (cited in p. 26)

Nieuwstadt M Van, Upadhyay D and Yuan F. "Diagnostics for Diesel Oxidation Catalysts". In *SAE Technical Paper 2005-01-3602*. SAE International, 2005. (cited in pp. 26, 64, and 164)

Ning J and Yan F. "Detection of Injected Urea Quantity and Correction for SCR Urea Dosing Control". In *SAE 2015 World Congress & Exhibition 2015-01-1038*. SAE International, apr 2015. (cited in pp. 32 and 33)

Nova I, Lietti L and Tronconi E. "Transient response method applied to the kinetic analysis of the DeNO x-SCR reaction". *Chemical Engineering Science*, Vol. 56 n^o 4, pp. 1229–1237, 2001. (cited in pp. 152, 153, and 192)

Nova I and Tronconi E. *Urea-SCR technology for deNOx after treatment of Diesel exhausts*. Springer, 2014. (cited in pp. 32 and 151)

Nuesch T, Ott T, Ebbesen S and Guzzella L. "Cost and fuel-optimal selection of HEV topologies using particle swarm optimization and dynamic programming". In *American Control Conference (ACC), 2012*, pp. 1302–1307. IEEE, 2012. (cited in p. 4)

Ochs T, Schittenhelm H, Genssle A and Kamp B. "Particulate Matter Sensor for On Board Diagnostics (OBD) of Diesel Particulate Filters (DPF)". *SAE International Journal*

of Fuels and Lubricants 2010-01-0307, Vol. 3 n^o 1, pp. 61–69, apr 2010. (cited in pp. 8 and 29)

Ogata K. *Modern control engineering*. Prentice Hall PTR, 2009. (cited in p. 109)

Organization World Health. "Review of evidence on health aspects of air pollution". Technical report, Regional office for Europe, 2013. (cited in p. 5)

Ostertag M. "Urea Reservoir Systems for Off-Highway and Heavy Duty Market". *CTI*, 2008. (cited in p. 32)

P Jones James C. and Muske Kenneth R. "Model-based OBD for Three-Way Catalyst Systems". In *2004-01-0639*. SAE International, 2004. (cited in p. 8)

Park S, Matsumoto T and Oda N. "Numerical Analysis of Turbocharger Response Delay Mechanism". In *SAE 2010 World Congress & Exhibition 2010-01-1226*. SAE International, apr 2010. (cited in p. 23)

Payri F, Guardiola C, Blanco-Rodriguez D, Mazer A and Cornette A. "Methodology for Design and Calibration of a Drift Compensation Method for Fuel-To-Air Ratio Estimation". In *SAE Technical Paper 2012-01-0717*. SAE International, 2012. (cited in p. 116)

Payri F, Luján JM, Guardiola C and Rizzoni G. "Injection diagnosis through common-rail pressure measurement". *Proceedings of the Institution of Mechanical Engineers, Part D: Journal of Automobile Engineering*, Vol. 220 n^o 3, pp. 347–357, 2006. (cited in pp. 78 and 109)

Payri F, Luján José M, Guardiola Carlos and Pla B. "A challenging future for the ic engine: new technologies and the control role". *Oil & Gas Science and Technology–Revue d´IFP Energies nouvelles*, Vol. 70 n^o 1, pp. 15–30, 2015. (cited in p. 4)

Pezzini A., Canova M., Onori S., Rizzoni G. and Soliman A. "A Methodology for Fault Diagnosis of Diesel NOx Aftertreatment Systems". *IFAC Proceedings Volumes*, Vol. 42 n^o 8, pp. 911 – 916, 2009. (cited in p. 33)

Piqueras P. *Contribucion al modelado termofluidodinamico de filtros de particulas diesel de flujo de pared*. PhD Thesis, Universitat Politecnica de Valencia, 2005. (cited in p. 10)

Pisu P., Canova M. and Soliman A. "Model-Based Fault Diagnosis of a NOx Aftertreatment System". *IFAC Proceedings Volumes*, Vol. 41 n^o 2, pp. 7072 – 7078, 2008. 17th IFAC World Congress. (cited in p. 30)

Pla B. *Análisis del Proceso de la Recirculación de los Gases de Escape de Baja Presión en Motores Diesel Sobrealimentados*. PhD thesis. Riunet, 2009. (cited in pp. 6 and 23)

Proakis G and Manolakis G. *Digital signal processing: principles, algorithms, and applications*. 1996. (cited in p. 114)

PwC. "Projected vehicle sales in China, the U.S. and the EU between 2017 and 2030.", 2017. (cited in p. 3)

Rafigh M. *Exhaust aftertreatment modeling for efficient calibration in diesel passenger car applications*. PhD Thesis, 20177. (cited in p. 27)

Regitz S and Collings N. "Study of cycle-by-cycle air-to-fuel ratio determined from the exhaust gas composition and a novel fast response device based on a wide band lambda sensor". Technical report, SAE Technical Paper 2008-01-2439, 2008. (cited in p. 36)

Regulation EU Comission. *No 715/2007*. Official Journal of the European Union, 2007. (cited in p. 7)

Regulation EU Comission. *No 692/2008*. Official Journal of the European Union, 2008. (cited in pp. 7 and 179)

Regulation EU Comission. *No 459/2012*. Official Journal of the European Union, 2012. (cited in p. 7)

Regulation EU Comission. *No 136/2014*. Official Journal of the European Union, 2014. (cited in p. 9)

Regulation EU Comission. *No 2016/427*. Official Journal of the European Union, 2016. (cited in p. 7)

Regulation EU Comission. *No 2017/1151*. Official Journal of the European Union, 2017. (cited in p. 7)

Reşitoğlu İbrahim A, Altinişik K and Keskin A. "The pollutant emissions from diesel-engine vehicles and exhaust aftertreatment systems". *Clean Technologies and Environmental Policy*, Vol. 17 n^o 1, pp. 15–27, 2015. (cited in p. 5)

Riegel J, Neumann H and Wiedenmann H-M. "Exhaust gas sensors for automotive emission control". *Solid State Ionics*, Vol. 152, pp. 783–800, 2002. (cited in pp. 8, 9, 34, and 138)

Ruetten O, Pischinger S, Kuepper C, Weinowski R, Gian D, Ignatov D, Betton W and Bahn M. "Catalyst Aging Method for Future Emissions Standard Requirements". In *SAE Technical Paper 2010-01-1272*. SAE International, 2010. (cited in pp. 8 and 26)

Russell April and Epling William S. "Diesel Oxidation Catalysts". *Catalysis Reviews*, Vol. 53 n^o 4, pp. 337–423, 2011. (cited in p. 25)

Sahner K, Fleischer M, Magori E, Meixner H, Deerberg J and Moos R. "HC-sensor for exhaust gases based on semiconducting doped SrTiO3 for On-Board Diagnosis". *Sensors and Actuators B: Chemical*, Vol. 114 n^o 2, pp. 861 – 868, 2006. (cited in pp. 8 and 39)

Sampara C S. *Global Reaction Kinetics for Oxidation and Storage in Diesel Oxidation Catalysts.* PhD Thesis, The University of Michigan, 2008. (cited in p. 27)

Sampara C S., Bissett E J. and Assanis D. "Hydrocarbon storage modeling for diesel oxidation catalysts". *Chemical Engineering Science*, Vol. 63, pp. 5179–5192, 2008. (cited in pp. 26, 88, and 140)

Sampara C S, Bissett E J and Chmielewski M. "Global kinetics for a commercial diesel oxidation catalyst with two exhaust hydrocarbons". *Industrial & Engineering Chemistry Research*, Vol. 47 n^o 2, pp. 311–322, 2008. (cited in pp. 25, 27, and 138)

Sampara C S, Bissett E J, Chmielewski M and Assanis D. "Global kinetics for platinum diesel oxidation catalysts". *Industrial & Engineering Chemistry Research*, Vol. 46 n^o 24, pp. 7993–8003, 2007. (cited in pp. 25, 27, and 138)

Schar C M, Onder Christopher H and Geering Hans P. "Control of an SCR catalytic converter system for a mobile heavy-duty application". *IEEE Transactions on Control Systems Technology*, Vol. 14 n^o 4, pp. 641–653, 2006. (cited in p. 32)

Schneider H., Tschudin S., Schneider M., Wokaun A. and Baiker A. "In Situ Diffuse Reflectance FTIR Study of the Selective Catalytic Reduction of NO by NH3 over Vanadia-Titania Aerogels". *Journal of Catalysis*, Vol. 147 n^o 1, pp. 5 – 14, 1994. (cited in p. 153)

Schnitzler J. "Particulate Matter and NOx Exhaust Aftertreatment Systems". *FEV Motorentechnik GmbH*, 2006. (cited in p. 40)

Schoenauer D, Nieder T, Wiesner K, Fleischer M and Moos R. "Investigation of the electrode effects in mixed potential type ammonia exhaust gas sensors". *Solid State Ionics*, Vol. 192 n^o 1, pp. 38 – 41, 2011. (cited in p. 38)

Schultz R and Meckl P H. "Light-Off Temperature Shift for Catalyzed Diesel Particulate Filter On-Board Diagnostics". In *SAE Technical Paper 2012-01-1248*. SAE International, 04 2012. (cited in pp. 26 and 176)

Serrao L, Onori S, Sciarretta A, Guezennec Y and Rizzoni G. "Optimal energy management of hybrid electric vehicles including battery aging". In *American Control Conference (ACC), 2011*, pp. 2125–2130. IEEE, 2011. (cited in p. 4)

Shost M, Noetzel J, Wu M-C, Sugiarto T, Bordewyk T, Fulks G and Fisher G B. "Monitoring, Feedback and Control of Urea SCR Dosing Systems for NOx Reduction: Utilizing an Embedded Model and Ammonia Sensing". In *SAE Technical Paper Series 2008-01-1325*. SAE International, 2008. (cited in p. 30)

Shost M, Noetzel J, Wu M-C, Sugiarto T, Bordewyk T, Fulks G and Fisher G B. "Monitoring, Feedback and Control of Urea SCR Dosing Systems for NOx Reduction: Utilizing an Embedded Model and Ammonia Sensing". In *SAE World Congress & Exhibition 2008-01-1325*. SAE International, apr 2008. (cited in pp. 33 and 100)

Simon D. "Kalman filtering, embedded systems programming". *Embedded. com*, 2001. (cited in p. 108)

Skaf Z, Aliyev T, Shead L and Steffen T. "The State of the Art in Selective Catalytic Reduction Control". In *SAE 2014 World Congress & Exhibition 2014-01-1533*. SAE International, 2014. (cited in pp. 32 and 100)

Song Q and Zhu G. "Model-based Closed-loop Control of Urea SCR Exhaust Aftertreatment System for Diesel Engine". In *SAE 2002 World Congress & Exhibition 2002-01-0287*. SAE International, mar 2002. (cited in pp. 30 and 99)

Stadlbauer S, Waschl H and del Re L. "NO/NO2 Ratio based NH3 Control of a SCR". In *SAE Technical Paper 2014-01-1565*. SAE International, apr 2014. (cited in p. 24)

Stadlbauer S, Waschl H, Schilling A and del Re L. "DOC Temperature Control for Low Temperature Operating Ranges with Post and Main Injection Actuation". In *SAE Technical Paper 2013-01-1580*. SAE International, 2013. (cited in pp. 29 and 87)

Stanglmaier Rudolf H. and Roberts Charles E. "Homogeneous Charge Compression Ignition (HCCI): Benefits, Compromises, and Future Engine Applications". In *International Fuels and Lubricants Meeting and Exposition 1999-01-3682*. SAE International, oct 1999. (cited in p. 3)

Steppan J, Henderson B, Johnson K, Yusuf Khan M., Diller T, Hall M, Lourdhusamy A, Allmendinger K and Matthews R D. "Comparison of an On-Board, Real-Time Electronic PM Sensor with Laboratory Instruments Using a 2009 Heavy-Duty Diesel Vehicle". In *SAE 2011 World Congress & Exhibition 2011-01-0627*. SAE International, apr 2011. (cited in p. 39)

Surenahalli H Shankar, Parker G and Johnson J H. "Extended Kalman Filter to Estimate NO, NO2, Hydrocarbon and Temperatures in a DOC during Active Regeneration and Under Steady State Conditions". In *SAE Technical Paper 2015-01-1059*. SAE International, 2015. (cited in p. 27)

Surenahalli H.S., Parker G.G., Johnson J.H. and Devarakonda M.N. "A Kalman Filter estimator for a Diesel Oxidation Catalyst during active regeneration of a CPF". In *American Control Conference (ACC), 2012*, pp. 4969–4974, 2012. (cited in p. 27)

Sutjiono R, Tayal P, Zhou K and Meckl P. "Real-Time On-Board Indirect Light-Off Temperature Estimation as a Detection Technique of Diesel Oxidation Catalyst Effectiveness Level". In *SAE Technical Paper 2013-01-1517*. SAE International, 04 2013. (cited in pp. 26, 87, 138, and 175)

Tanaka Y, Hihara T, Nagata M, Azuma N and Ueno A. "Modeling of diesel oxidation catalyst". *Industrial & engineering chemistry research*, Vol. 44 n^o 22, pp. 8205–8212, 2005. (cited in pp. 27 and 138)

Theis J R., Dearth M and McCabe R. "LNT+SCR Catalyst Systems Optimized for NOx Conversion on Diesel Applications". In *SAE 2011 World Congress & Exhibition 2011-01-0305*. SAE International, apr 2011. (cited in p. 40)

Thomas C.E. "Fuel cell and battery electric vehicles compared". *International Journal of Hydrogen Energy*, Vol. 34 n^o 15, pp. 6005 – 6020, 2009. (cited in p. 4)

Thomas C.E. Sandy. "Transportation options in a carbon-constrained world: Hybrids, plug-in hybrids, biofuels, fuel cell electric vehicles, and battery electric vehicles". *International Journal of Hydrogen Energy*, Vol. 34 n^o 23, pp. 9279 – 9296, 2009. (cited in p. 4)

Thomas C.E. Sandy. "How green are electric vehicles?". *International Journal of Hydrogen Energy*, Vol. 37 n^o 7, pp. 6053 – 6062, 2012. XII International Symposium on Polymer Electrolytes: New Materials for Application in Proton Exchange Membrane Fuel Cells. (cited in p. 4)

Tobias P, Martensson P, Goeras A, Lundstroem I and Spetz AL. "Moving gas outlets for the evaluation of fast gas sensors". *Sensors and Actuators B: Chemical*, Vol. 58 n^o 1, pp. 389 – 393, 1999. (cited in p. 9)

Tourlonias P and Koltsakis G. "Model-based comparative study of Euro 6 diesel aftertreatment concepts, focusing on fuel consumption". *International Journal of Engine Research*, Vol. 12 n^o 3, pp. 238–251, 2011. (cited in pp. 40 and 139)

Tschanz F, Amstutz A, Onder C H. and Guzzella L. "Feedback control of particulate matter and nitrogen oxide emissions in diesel engines". *Control Engineering Practice*, Vol. 21 n^o 12, pp. 1809 – 1820, 2013. (cited in p. 24)

Twigg M V. "Progress and future challenges in controlling automotive exhaust gas emissions". *Applied Catalysis B: Environmental*, Vol. 70 n^o 1, pp. 2 – 15, 2007. (cited in p. 39)

Twigg M V. "Cleaning the Air We Breathe - Controlling Diesel Particulate Emissions from Passenger Cars". *Emission Control Technologies*, 2009. (cited in p. 40)

Twigg M.V. "Advanced integrated exhaust aftertreatment systems and the mechanisms of {NOx} emissions control". In IMechE, editor, *Internal Combustion Engines: Performance, Fuel Economy and Emissions*, pp. 219 – 229. Woodhead Publishing, 2013. (cited in pp. 32 and 40)

Upadhyay D and Van Nieuwstadt M. "Modeling of urea SCR catalyst with automotive applications". 2002. (cited in pp. 33 and 156)

Upadhyay D and Van Nieuwstadt M. "Model based analysis and control design of a urea-SCR deNOx aftertreatment system". *Journal of dynamic systems, measurement, and control*, Vol. 128 n^o 3, pp. 737–741, 2006. (cited in pp. 33, 186, 191, and 192)

van Helden R, Verbeek R, Willems F and van der Welle R. "Optimization of Urea SCR deNOx Systems for HD Diesel Engines". In *SAE Technical Paper Series 2004-01-0154*. SAE International, mar 2004. (cited in pp. 32 and 38)

Van Nieuwstadt M. "Pressure sensor diagnosis via a computer". 2005. US Patent 6,947,831. (cited in p. 10)

Van Nieuwstadt MJ and Trudell DF. "Diagnostics for diesel particulate filters". *SAE Technical Papers 2004-01-1422*, 2004. (cited in p. 10)

Vitale G, Siebenbrunner P, Halser H, Bachler J and Pfahl U. "OBD Algorithms: Model-based Development and Calibration". In *SAE Technical Paper 2007-01-4222*. SAE International, 2007. (cited in pp. 8, 26, and 175)

Walker AP. "Controlling particulate emissions from diesel vehicles". *Topics in Catalysis*, Vol. 28, pp. 165–170, 2004. (cited in p. 39)

Wang D Y, Yao S, Shost M, Yoo J-H, Cabush D, Racine D, Cloudt R and Willems F. "Ammonia Sensor for Closed-Loop SCR Control". *SAE International Journal of Passenger Cars - Electronic and Electrical Systems 2008-01-0919*, Vol. 1, pp. 323–333, apr 2008. (cited in pp. 9, 38, 99, and 138)

Wang Y-Y, Sun Y, Chang C-F and Hu Y. "Model-Based Fault Detection and Fault-Tolerant Control of SCR Urea Injection Systems". *IEEE Transactions on Vehicular Technology*, Vol. 65 n^o 6, pp. 4645–4654, 2016. (cited in p. 33)

Weiss Martin, Bonnel Pierre, KÃ¼hlwein JÃ¶rg, Provenza Alessio, Lambrecht Udo, Alessandrini Stefano, Carriero Massimo, Colombo Rinaldo, Forni Fausto, Lanappe Gaston, Lijour Philippe Le, Manfredi Urbano, Montigny Francois and Sculati Mirco. "Will Euro 6 reduce the NOx emissions of new diesel cars? - Insights from on-road tests with Portable Emissions Measurement Systems (PEMS)". *Atmospheric Environment*, Vol. 62, pp. 657 – 665, 2012. (cited in p. 7)

Wiebenga M H., Kim C Hwan, Schmieg S J., Oh S H., Brown D B., Kim D Heui, Lee J-H and Peden C H.F. "Deactivation mechanisms of Pt/Pd-based diesel oxidation catalysts". *Catalysis Today*, Vol. 184 n^o 1, pp. 197 – 204, 2012. Catalytic Control of Lean-Burn Engine Exhaust Emissions. (cited in p. 26)

Wiegaertner S, Hagen G, Kita J, Reitmeier W, Hien M, Grass P and Moos R. "Thermoelectric hydrocarbon sensor in thick-film technology for on-board-diagnostics of a diesel oxidation catalyst". *Sensors and Actuators B: Chemical*, Vol. 214, pp. 234–240, 2015. (cited in p. 39)

Willems F. and Cloudt R. "Experimental Demonstration of a New Model-Based SCR Control Strategy for Cleaner Heavy-Duty Diesel Engines". *IEEE Transactions on Control Systems Technology*, Vol. 19 n^o 5, pp. 1305–1313, 2011. (cited in pp. 66, 138, 151, and 152)

Willems F, Cloudt R, van den Eijnden E, van Genderen M, Verbeek R, de Jager B, Boomsma W and van den Heuvel I. "Is Closed-Loop SCR Control Required to Meet Future Emission Targets?". In *SAE Technical Paper Series 2007-01-1574*. SAE International, apr 2007. (cited in pp. 8, 33, 34, 37, and 99)

Willems F, Mentink P, Kupper F and Van den Eijnden E. "Integrated emission management for cost optimal EGR-SCR balancing in diesels". *IFAC Proceedings Volumes*, Vol. 46 n^o 21, pp. 711–716, 2013. (cited in pp. 24 and 66)

Wu C-W, Chen R-H, Pu J-Y and Lin T-Hui. "The influence of air-fuel ratio on engine performance and pollutant emission of an SI engine using ethanol-gasoline-blended fuels". *Atmospheric Environment*, Vol. 38 n^o 40, pp. 7093 – 7100, 2004. (cited in p. 5)

Wu Ming-Cheng and Micheli Adolph L. "Calorimetric hydrocarbon sensor for automotive exhaust applications". *Sensors and Actuators B: Chemical*, Vol. 100 n^o 3, pp. 291–297, 2004. (cited in p. 39)

Xie H, Stobart R, Tunestal P, Eriksson L, Huang Y and Leteinturier P. "Future Engine Control Enabling Environment Friendly Vehicle". In *SAE 2011 World Congress & Exhibition 2011-01-0697*. SAE International, apr 2011. (cited in p. 4)

Xu F., Toyoda M., Yasui Y., Matsunaga H., Kato A. and Shen T. "Optimal control design for lean NOx trap regeneration in diesel engines". In *2017 56th Annual Conference of the Society of Instrument and Control Engineers of Japan (SICE)*, pp. 349–352, 2017. (cited in p. 30)

Yamada H, Misawa K, Suzuki D, Tanaka K, Matsumoto J, Fujii M and Tanaka K. "Detailed analysis of diesel vehicle exhaust emissions: Nitrogen oxides, hydrocarbons and particulate size distributions". *Proceedings of the Combustion Institute*, Vol. 33 n^o 2, pp. 2895 – 2902, 2011. (cited in p. 5)

Yamamoto K, Takada K, Kusaka J, Kanno Y and Nagata M. "Influence of Diesel Post Injection Timing on HC Emissions and Catalytic Oxidation Performance". In *SAE Technical Paper 2006-01-3442*. SAE International, 2006. (cited in pp. 82 and 169)

Yang H and Chimner C. "Integration of Reformer Model Based Estimation, Control, and Diagnostics for Diesel LNT Based Aftertreatment Systems". *SAE International Journal of Engines 2010-01-0569*, Vol. 3 n^o 1, pp. 282–295, apr 2010. (cited in p. 30)

Yang L, Franco V, Campestrini A, German J and Mock P. "NOx control technologies for Euro 6 diesel passenger cars". *Int. Council Clean Transportation, white paper*, pp. 1–22, 2015. (cited in pp. 29 and 30)

Ye S, Yap Y H., Kolaczkowski S T., Robinson K and Lukyanov D. "Catalyst light-off experiments on a diesel oxidation catalyst connected to a diesel engine-methodology and techniques". *Chemical Engineering Research and Design*, Vol. 90 n^o 6, pp. 834 – 845, 2012. (cited in pp. 25, 84, 87, and 146)

Yong-Wha K and Van Nieuwstadt M. "Threshold Monitoring of Urea SCR Systems". In *SAE 2006 Commercial Vehicle Engineering Congress & Exhibition 2006-01-3548*. SAE International, oct 2006. (cited in pp. 33 and 37)

Yu Wang D, Yao S, Cabush D and Racine D. "Ammonia Sensor For SCR NOx Reduction". Technical report, DELPHI, 2007. (cited in pp. 38 and 99)

Yuan X, Liu H and Gao Y. "Diesel engine SCR control: current development and future challenges". *Emission Control Science and Technology*, Vol. 1 n^o 2, pp. 121–133, 2015. (cited in pp. 32 and 100)

Zehni A, Saray R K and Poorghasemi K. "Numerical comparison of PCCI combustion and emission of diesel and biodiesel fuels at low load conditions using 3D-CFD models coupled with chemical kinetics". *Applied Thermal Engineering*, Vol. 110, pp. 1483 – 1499, 2017. (cited in p. 4)

Zervas E. "Development of an indicator for the emission control of diesel passenger cars". *Applied Thermal Engineering*, Vol. 28 n^o 11, pp. 1437–1442, 2008. (cited in p. 72)

Zhan R, Li W, Eakle S T. and Weber P. "Development of a Novel Device to Improve Urea Evaporation, Mixing and Distribution to Enhance SCR Performance". In *SAE 2010 World Congress & Exhibition 2010-01-1185*. SAE International, apr 2010. (cited in p. 32)

Zhao D, Liu C, Stobart R, Deng J, Winward E and Dong G. "An explicit model predictive control framework for turbocharged diesel engines". *IEEE Transactions on Industrial Electronics*, Vol. 61 n^o 7, pp. 3540–3552, 2014. (cited in p. 24)

Zheng M and Banerjee S. "Diesel oxidation catalyst and particulate filter modeling in active Flow configurations". *Applied Thermal Engineering*, Vol. 29 n^o 14-15, pp. 3021 – 3035, 2009. (cited in p. 27)